DOCTOR OF PHILOSOPHY

The p97 cofactors UBXN7 and UBXN8 interact with and modulate the function of cullin-RING complexes and Fanconi anaemia proteins FANCD2/FANCI, respectively

Bandau, Susanne

Award date:
2014

DOCTOR OF PHILOSOPHY

The p97 cofactors UBXN7 and UBXN8 interact with and modulate the function of cullin-RING complexes and Fanconi anaemia proteins FANCD2/FANCI, respectively

Susanne Bandau

2014

University of Dundee

The p97 cofactors UBXN7 and UBXN8 interact with and modulate the function of cullin-RING complexes and Fanconi anaemia proteins FANCD2/FANCI, respectively

Susanne Bandau

A thesis submitted for the degree of Doctor of Philosophy
University of Dundee

May 2014

I. Table of Contents

II. List of Figures

III. List of Tables

IV. List of Publications

BANDAU, S., KNEBEL, A., GAGE, Z. O., WOOD, N. T. & ALEXANDRU, G. 2012. UBXN7 docks on neddylated cullin complexes using its UIM motif and causes HIF1alpha accumulation. *BMC biology,* 10**,** 36.

V. Abbreviations

3D-SIM	Three-dimensional structured illumination microscopy
aa	Amino acid
ACN	Acetonitrile
ADP	Adenosindiphosphate
AEBSF	4-(2-Amino-ethyl) benzenesulfonyl
ALS	Amyotropic lateral sclerosis
AML	Acute myelogenous leukemia
Amp	Ampicillin
ATP	Adenosine 5′-triphosphate
ATP	Adenosintriphosphate
ATR	Ataxia-techangiectasia and Rad3-related
BS1	Binding site 1
BSA	Bovine serum albumin
cm	Centimeter
CRL	Cullin-RING E3 ligase
CSN	COP9 signalosome
CUE	coupling of ubiquitin conjugation to endoplasmic reticulum degradation
DAPI	4’,6-Diamidino-2-phenylindole dihydrochloride
DBD	DNA binding domain
DEB	Diepoxybutane
DMP	Dimethyl pimelimidate
DMSO	Dimethyl sulphoxide
DNA	Deoxyribonucleic acid
DSB	Double-strand break
DSTT	Division of Signal Transduction and Therapy
DTT	Dithiothreitol
EB	Elution buffer
ECL	Enhanced chemiluminescence
EDTA	Ethylene diamine tetraacetic acid
EGTA	Ethylene glycol tetraacetic acid
ER	Endoplasmatic reticulum
ERAD	Endoplasmatic reticulum-associated degradation
FA	Fanconi anaemia
FACS	Fluorescence-activated cell sorting
FBS	Fetal bovine serum
GSH	Glutathione Sepharose
h	Hour
HBV	Hepatitis B virus
HCC	Hepatocellular carcinoma
HCl	Hydrogen chloride
HECT	Homologous to E6-AP carboxyl terminus
HEPES	N-2-hydroxyethylpiperazine-N-2-ethane sulfonic acid
HR	Homologous recombination
HRP	Horseradish peroxidase
HU	Hydroxyurea
IBMPFD	Inclusion body myopathy with early-onset Paget disease and Frontotemporal dementia
ICL	Interstrand Crosslinks

ID	FANCD2/FANCI complex
IP	Immunoprecipitation
IPTG	Isopropyl β-D-thiogalactopyranoside
IR	Ionizing radiation
kbp	kilo-basepair
KCl	Potassium chloride
kDa	Kilo-dalton
KOAc	Potassium acetate
KOH	Potassium hydroxide
LB	Luria Bertani
Lys	Lysine
M	Molar
mA	Milliamp
MALS	Multi angle light scattering
MEM	Minimum Essential Medium
$Mg(OAc)_2$	Magnesium acetate
$MgCl_2$	Magnesium chloride
min	Minute
ml	Milliliter
mm	Millimeter
MMC	Mitomycin C
mRNA	Messenger ribonucleic acid
MS	Mass spectrometry
MudPIT	Multidimensional Protein Identification Technology
NA	Numerical aperture
NaCl	Sodium chloride
NaOH	Sodium hydroxide
ng	Nanogramm
nm	Nanometer
non-Ub	Non-ubiquitylated
NPC	Nuclear core complex
NS	Not significant
OD	Optical density
OTF	Optical transfer functions
PBS	Phosphate buffered serum
PIPES	Piperazine-N,N′-bis(2-ethanesulfonic acid)
PMSF	Phenylmethanesulphonylfluoride
PPAD	Protein Production and Assay Development Team
PUB	PNGase/UBA or UBX
RING	Really Interesting New Gene
rpm	Rounds per minute
RT	Room temperature
SCC	Squamous cell carcinoma
SDS	Sodium dodecyl sulphate
SEC	Size-exclusion chromatography
SEP	Shp, eyes-closed
siRNA	Small interfering RNA
TAE	Tris-acetate-EDTA
TBS	Tris-buffered saline
TEV	Tobacco etch virus

TFA	Trifluoroacetic acid
ThF	Thioredoxin-like fold
TLS	Translesion DNA synthesis
Tris	Tris(hydroxymethyl)aminomethane
U	Unit
UAS	Ubiquitin-associating domain
Ub	Ubiquitylated
UBA	Ubiquitin-associating domain
UBL	Ubiquitin-like
UBX	Regulatory X domain
UIM	Ubiquitin-interaction motif
UPS	Ubiquitin-proteasome system
UV	Ultraviolet
V	Volt
VBM	VCP-binding motif
VIM	VCP-interaction motif
µg	Microgram
µl	Microliter
µM	Micromolar

VI. Declarations

I declare that the following thesis is based on the results of investigations conducted by myself, and that this thesis is of my own composition. Work other than my own is clearly indicated in the text by reference to the relevant researchers or to their publications. This dissertation has not in whole, or in part, been previously submitted for a higher degree.

Susanne Bandau

I certify that Susanne Bandau has spent the equivalent of at least nine terms in research work at the School of Life Sciences, University of Dundee, and that she has fulfilled the conditions of the Ordinance General No. 14 of the University of Dundee and is qualified to submit the accompanying thesis in application for the degree of Doctor of Philosophy.

Dr. Gabriela Alexandru

VII. Acknowledgements

I would like to thank my supervisor Dr. Gabriela Alexandru for giving me the opportunity to work in her laboratory and her help and advice over the last few years.

I also want to thank the two PostDocs I worked with during my PhD. Dr. Flavia Scialpi for her outstanding help at the beginning of my PhD and her support as good friend before and after leaving the lab. Dr. Yorann Baron for his great help and advice during my PhD, and all the discussion we had that kept me going.

I am also grateful to everyone in the DSTT for the reagents provided, in particular a big thank you to Melanie Wrightman and Nicola Wood for the cloning and Dr. Axel Knebel + team for the protein production. I would also like to thank the support staff of the microscope facility, Dr. Rosie Clarke and Arlene Whigham for the FACS analysis and Dr. Patrick Pedrioli's group as well as Dr. Matthias Trost's group for the mass spectrometry analysis. And of course a big thanks to all the MRC-PPU support staff that makes our life in the lab so much easier every day.

A special thanks to my colleagues from SCILLS for their good advises in the seminars and good scientific discussions in the last 4 years. In particular, a big thank you to Alejandro for his enthusiasm for science, support with my complicated project and great help in microscopy.

I would like to convey my deepest thanks to my family for their love and support throughout my life. Without them I would not be where I am now.

Last but not least and already part of my family, I would like to thank my fiancé Subbu who is definitely the best thing that happened to me in Dundee. Without his endless

support, encouragement, patience and love, I would have not finished this PhD. That's for you PAB!!

VIII. Summary

The ATPase p97 plays a role in diverse cellular activities such as cell cycle progression, membrane fusion, DNA repair and ubiquitin-dependent protein degradation (including endoplasmic reticulum-associated protein degradation, ERAD). The functional diversity of p97 is achieved by its association with a large number of cofactors including the 13 human UBX-domain containing proteins. My PhD projects focused on two of the UBX-domain proteins, UBXN7 and UBXN8.

Among human UBA-UBX proteins, UBXN7 is the most proficient in interacting with CRL (cullin-RING E3 ligase) subunits, in particular CUL2, and it was assumed that these interactions were indirect, mediated by ubiquitylated substrates. However, we show that UBXN7 interaction with CUL2 is independent of ubiquitin- and substrate binding. Instead, it involves the direct docking of the ubiquitin interaction motif (UIM) in UBXN7 onto the neddylated cullin. Furthermore, we found that UBXN7 overexpression keeps the E3 ligase CUL2 (a member of the CRL2 complex) in its neddylated form and causes the accumulation of non-ubiquitylated HIF1α (CRL2 substrate). Both effects are strictly UIM-dependent and occur only when UBXN7 contains an intact UIM. We also show that HIF1α carrying long ubiquitin-chains can interact with an alternative ubiquitin-binding protein, which is independent from p97's segregase activity. We therefore propose that UBXN7 negatively regulates the ubiquitin-ligase activity of CRL2 by sequestering CUL2 in its neddylated form and that this might prevent recruitment of ubiquitin-receptors other than p97 to HIF1α.

The mass spectrometry analysis of Flag-UBXN8 immunoprecipitates identified several DNA damage-related proteins, including the Fanconi anaemia proteins FANCD2 and

FANCI. I could show that homodimeric UBXN8 interacts directly with non-ubiquitylated FANCD2 and FANCI. The direct binding of UBXN8 to the non-ubiquitylated FA proteins supports the notion that UBX-only proteins interact with substrates in an ubiquitin-independent manner. Furthermore, FANCD2 and FANCI are released from UBXN8 upon DNA damage, that in case of FANCI requires p97 binding to UBXN8.

My data indicate that UBXN8 acts as a negative regulator in the DNA damage response, because UBXN8 silenced cells show increased resistance to ICL-inducing agents. This phenotype was supported by my finding that UBXN8 silenced cells have increased levels of FANCD2 and FANCI mono-ubiquitylation as well as increased dimer formation and FANCD2 foci formation in the presence and absence of DNA damage. UBXN8 overexpression had the opposite effect on FANCD2 and FANCI modification and dimerization. I therefore propose that UBXN8 has an inhibitory effect on FANCD2 and FANCI that may prevent their ectopic activation in the absence of DNA damage.

Chapter 1

1. Introduction

1.1 The ATPase p97

The ATP-dependent molecular chaperone p97 is an essential protein, and is evolutionarily conserved from archaebacteria to mammals. As an ATPase, p97 uses the energy derived from ATP hydrolysis to unfold proteins, or to dissociate proteins from large cellular structures such as chromatin or the endoplasmic reticulum (ER) membrane (White and Lauring, 2007). It is involved in a wide variety of cellular processes ranging from cell cycle regulation and DNA damage repair, to membrane fusion and ubiquitin-dependent protein degradation (including endoplasmic reticulum-associated protein degradation, ERAD) (Ye, 2006, Haines, 2010a).

The functional diversity of p97 is achieved by its association with a large number of cofactors. Their interaction with p97 is mediated through conserved p97 binding domains/motifs such as the UBX (ubiquitin regulatory X) domain, BS1 (binding site 1) sequence, VCP-binding motif (VBM), PUB (PNGase/UBA or UBX) domain, and VCP-interacting motif (VIM) (Yeung et al., 2008). Some of these cofactors contain additional ubiquitin-binding motifs that allow simultaneous binding with p97 and ubiquitylated substrates (Buchberger, 2002, Alexandru et al., 2008, Meyer et al., 2002).

Based on their biological roles, these cofactors can be classified in two main groups: substrate-recruiting cofactors, and substrate-processing cofactors (Jentsch and Rumpf, 2007).

The substrate-recruiting cofactors (such as UBX-domain proteins, UFD1 and NPL4) bind protein substrates, either directly or via modifications (most commonly ubiquitylation), and thereby mediate the interactions of p97 with its substrates (Madsen et al., 2009, Jentsch and Rumpf, 2007).

The group of substrate-processing cofactors includes E3 enzymes (HRD1, gp78), E4 enzymes (E4B) and deubiquitylation enzymes (e.g. VCIP135) that control the degree of ubiquitylation of the bound substrates by either promoting polyubiquitylation or deubiquitylation (Madsen et al., 2009, Jentsch and Rumpf, 2007).

It has been shown that some of these cofactors (e.g. UBXN7, NPL4, UFD1) can coexist in the same p97 complex (Alexandru et al., 2008), whereas other cofactors (e.g., UFD1 versus p47) compete for the same docking site on p97 N-termini (Schuberth and Buchberger, 2008).

1.1.1 Domains and structure of p97

Irrespective of its bound cofactors, p97 is believed to convert the energy derived from ATP hydrolysis into mechanical force to disassemble protein complexes or segregate proteins from intracellular structures such as the chromatin or the ER membrane.

The p97 protomer consists of an N-terminal region that functions as adaptor protein binding domain, two tandem AAA ATPase domains D1 and D2, separated by a D1–D2 linker region, and a disordered C-terminal region (Huyton et al., 2003, Zhang et al., 2000) (Figure 1.1). Each D1 and D2 domain contains a signature nucleotide-binding Walker A and B motif, and a second region of homology (SRH) region that play a critical roles in mediating ATP binding and hydrolysis (Ogura et al., 2004, Song et al., 2003). In cells, p97 acts as a hexamer, with the D1 and D2 domains stacked in a 'head-to-tail' fashion forming a hexameric double ring (Huyton et al., 2003). The D1 domain

is a degenerate ATPase domain that is responsible for the stability of the hexameric state (Wang et al., 2003), whereas the D2 domain is the major ATPase domain of p97 that facilitates the ATP hydrolysis and generates the main driving force (Song et al., 2003). Mutations in D2, that abrogate ATP binding or hydrolysis through the D2 domain, result in dominant-negative variants that bind, but cannot release substrates (Song et al., 2003). During ATP hydrolysis, both the D1 and D2, as well as the N-terminal domain, experience dramatic conformational changes (DeLaBarre and Brunger, 2005). The rings formed by D1 and D2 rotate with respect to each other, and the sizes of their axial openings fluctuate (Yeung et al., 2014). Although ATP hydrolysis is carried out mainly by the D2 domain recent studies have shown that the interplay of conformational changes between the rings and mobility of the N-terminal domain is important for efficient ATPase activity (Niwa et al., 2012). Furthermore, the D2 domain as major ATPase domain and the N-domain as principal substrate binding domain reside at opposite ends of the proteins. Hence, the ATP hydrolysis-induced motion must be transmitted trough the length of the entire molecule.

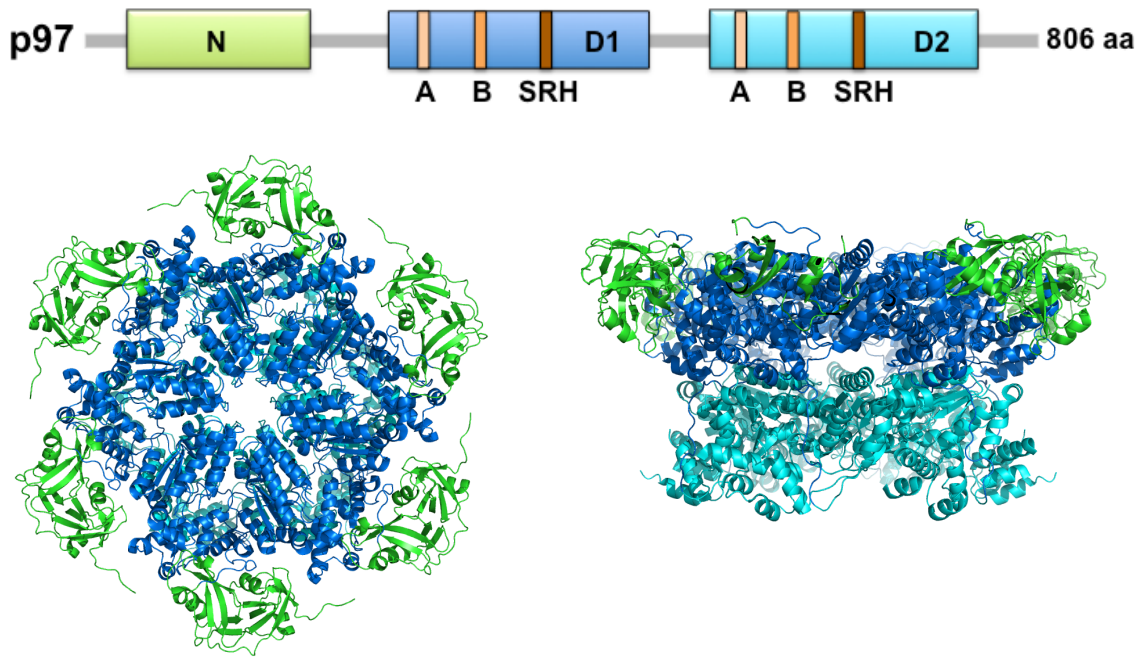

Figure 1.1: The hexameric ATPase p97

Top: Schematic showing the domains of p97 (N: N-terminus; D1: ATPase D1; D2: ATPase D2), the Walker A and B motifs within the ATPase domains and the second region of homology (SRH).

Bottom: Structure of p97 shown in two orientations (*left*: top view and *right*: side view). N-terminus (green), ATPase D1 (dark blue), ATPase D2 (light blue). The cartoon representation of the p97 hexamer was drawn using the PDB 1R7R in Pymol.

1.1.2 Mammalian p97 interacts with multiple UBX domain-containing cofactors

UBX-domain proteins represent the largest group of p97 cofactors (13 members in human) that interact directly with p97 via their UBX domains (Alexandru et al., 2008, Dreveny et al., 2004, Schuberth and Buchberger, 2008, Liang et al., 2006) (Figure 1.2).

Five of the UBX-domain proteins, the UBA–UBX proteins (UBXN7, UBXD8, FAF1, SAKS1, p47) contain an additional N-terminal UBA (ubiquitin-associated) domain, which enables them to bind ubiquitylated proteins (Alexandru et al., 2008). UBA–UBX cofactors can interact with a large spectrum of substrates carrying a ubiquitin modification, therefore they function as substrate-binding adaptors for p97 (Schuberth and Buchberger, 2008).

The remaining eight UBX-only proteins (p37, UBXN2A, UBXN4, UBXN8, UBXN6, UBXN10, UBXN11, ASPL) lack the UBA domain and the ability to bind ubiquitin, which might limit their substrate specificity. Furthermore, the expression of several UBX-only proteins is tissue-dependent and therefore their function might be restricted to specific cell types (Yamabe et al., 1997, Carim-Todd et al., 2001).

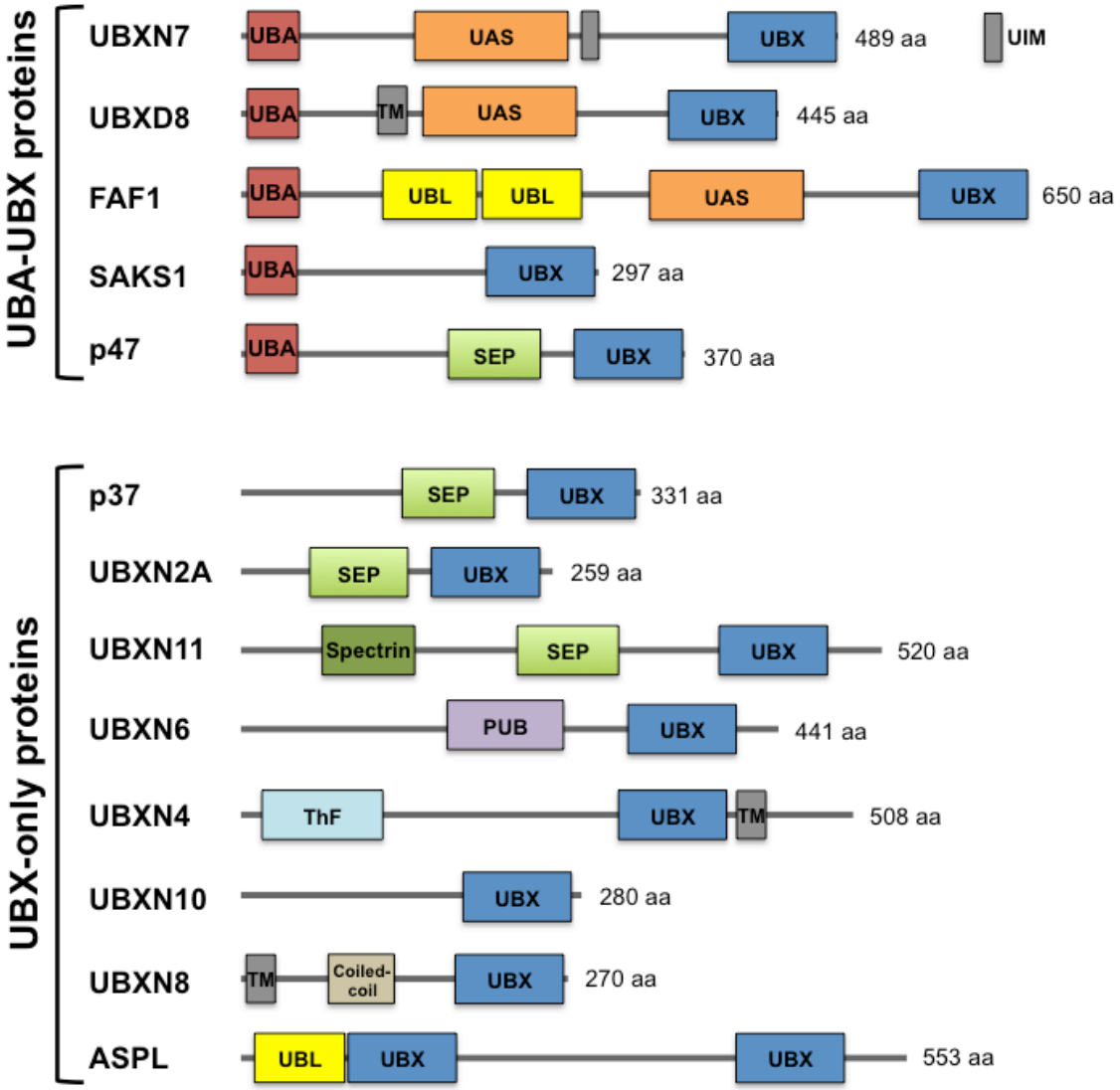

Figure 1.2: **The 13 UBX-domain cofactors of p97 in mammalian cells**
Schematics show the 13 human UBX-domain proteins and their various domains. UBX: Regulatory X domain; UBA: ubiquitin-associated domain; UAS: ubiquitin-associating domain; UIM: ubiquitin-interaction motif; UBL: ubiquitin-like; SEP: Shp, eyes-closed, p47; TM: transmembrane domain; PUB: PNGase/UBA or UBX; ThF: Thioredoxin-like fold

1.1.3 p97 and its diverse functions in the cell

As already mentioned, p97 is involved in a wide variety of cellular processes. In this subchapter, I tried to list some of the functions that have been assigned to p97.

Endoplasmic reticulum-associated protein degradation

The role of p97 in the endoplasmic reticulum-associated protein degradation (ERAD) is the best-described function of p97 in proteolysis. The ERAD pathway mediates the degradation of misfolded or misassembled proteins at the ER. These proteins are retro-translocated from the ER lumen into the cytoplasm to facilitate their ubiquitylation and ubiquitin-dependent protein degradation via the proteasome (Vembar and Brodsky, 2008, Ye, 2006, Liu and Ye, 2012).

The first step of the ERAD pathway is the recognition of the misfolded or unassembled polypeptides by ER chaperones that target these proteins to a retro-translocation complex in the membrane (Liu and Ye, 2012). This retro-translocation complex comprises of at least one E3 ubiquitin ligase (for example HRD1 or gp78 in mammals (Kikkert et al., 2004, Fang et al., 2001)) that ubiquitylates the substrate emerging from the ER membrane at the cytoplasmic side. The retro-translocation of the targeted polypeptides to the cytoplasm requires the p97–UFD1–NPL4 complex (Ye et al., 2003) that is recruited to the ER through ER membrane proteins such as UBXD8 and UBXD2 (Liang et al., 2006, Olzmann et al., 2013). The recognition of the polypeptide by p97 in the cytoplasm is mediated by the ubiquitin-binding motif in UFD1 that binds the ubiquitin chains attached to the polypeptide (Ye et al., 2003, Park et al., 2005). The energy derived from ATP hydrolysis by p97 generates the driving force to pull the substrate into the cytoplasm (Ye et al., 2003). The substrate is then delivered to the 26S proteasome for ubiquitin-dependent protein degradation (Raasi and Wolf, 2007).

The ubiquitin-dependent degradation of outer mitochondrial membrane-associated proteins also requires p97 and follows a similar mechanism as described for ERAD (Taylor and Rutter, 2011). Upon mitochondrial stress, VMS1 recruits p97 and NPL4 to

the mitochondrial membrane where it retro-translocates ubiquitylated substrates into the cytoplasm (Xu et al., 2011, Heo et al., 2010). The E3 ligase Parkin binds to the outer mitochondrial membrane and ubiquitylates the emerging substrates at the cytoplasmic side (Narendra et al., 2008). After the retro-translocation into the cytoplasm, the ubiquitylated proteins are targeted for proteasome-dependent degradation (Taylor and Rutter, 2011).

Autophagy

Autophagy is an intracellular degradation system that eliminates protein aggregates and organelles by the lysosome.

The role of p97 in autophagy has been first described in the context of IBMPFD (inclusion body myopathy associated with Paget's disease of the bone and fronto-temporal dementia), in which mutations in p97 lead to the accumulation of protein aggregates caused by defective autophagy (Ju et al., 2009, Tresse et al., 2010).

Autophagy is mediated by the autophagosome that engulfs cellular components and subsequently fuses with the lysosome (forms autolysosome) for their degradation. (Mizushima, 2007). The autophagosome maturation, a process including autophagosome-lysosome fusion and autolysosome formation, requires p97. Hence, the expression of disease-causing p97 mutants results in the accumulation of autophagosomes (Ju et al., 2009). Furthermore, the majority of accumulated autophagosomes contain ubiquitin conjugates, suggesting that p97 may be required for the autophagic degradation of ubiquitylated substrates (Tresse et al., 2010)

Membrane fusion

During mitosis, p97 is described to be involved in the reformation of the endoplasmic reticulum, the Golgi complex (Uchiyama and Kondo, 2005) and the nuclear envelope (Hetzer et al., 2001). In mammalian cells, the three organelles are fragmented into vesicles at the onset of mitosis and reassembled at the end of mitosis to allow the formation of new organelles in the daughter cells.

The reassembling of the ER and the Golgi requires membrane fusion that is mediated by p97 together with its co-factors p47 and VCP135 (Uchiyama et al., 2002, Kondo et al., 1997, Uchiyama and Kondo, 2005). Furthermore, another membrane fusion pathway that involves the p97–p37 complex is required for Golgi and ER maintenance during interphase and their re-assembly at the end of mitosis (Uchiyama et al., 2006).

The nuclear envelope formation requires the re-assembly of a tubular network on the chromatin surface resulting in a closed envelope, which then expands (Guettinger et al., 2009). p97 is involved in two steps of the nuclear envelope re-assembly: sealing of the nuclear envelope (mediated by p97–UFD1–NPL4) and nuclear growth (mediated by p97–p47) (Hetzer et al., 2001).

Chromatin-associated functions of p97 in the DNA-damage response

Recent publications have identified the p97–UFD1–NPL4 complex as an essential factor in the ubiquitin-dependent DNA damage response, highlighting its importance in guarding genome stability (Meerang et al., 2011, Dantuma and Hoppe, 2012).

The ubiquitin ligases RNF8 and RNF168 are recruited to DNA double-strand breaks (DSBs) and assemble ubiquitin chains at sites of DNA damage (Mailand et al., 2007, Huen et al., 2007). This results in recruitment of DNA damage repair proteins such as BRCA1, RAD18, and 53BP1 that are required to facilitate DNA repair (Mailand et al.,

2007, Huen et al., 2007). Recent publications show that RNF8-mediated ubiquitylation triggers recruitment of p97 and its cofactors UFD1–NPL4 to DSBs (Ramadan, 2012, Meerang et al., 2011). Inhibiting the p97–UFD1–NPL4 function resulted in prolonged accumulation of K48 ubiquitin conjugates and defective recruitment of BRCA1, RAD51, and 53BP1 to DSBs (Meerang et al., 2011).

Furthermore, recent publications have shown that RNF8-mediated recruitment of p97 to DNA damage sites results in removal of the K48-conjugated substrate proteins, such as L3MBTL1 (Acs et al., 2011) or the TLS (Translesion DNA synthesis) polymerase Pol η (Davis et al., 2012). Substrate removal from the DNA damage site then allows proper assembly of downstream signalling factors, including Rad51, BRCA1 and 53BP1 (Acs et al., 2011) (Meerang et al., 2011). Furthermore, the depletion of p97, UFD1 and NPL4 in mammalian cells and worms leads to hypersensitivity to DSB-inducing agents, consistent with a role for this complex in the cellular response to DNA damage (Meerang et al., 2011, Acs et al., 2011).

1.1.4 The role of p97 and its UBX-domain cofactors in health and disease

The involvement of p97 in a wide variety of cellular processes suggests that it plays an important role in health and disease. Indeed, p97 has been implicated in the direct regulation of several cancer-relevant proteins, such as HIF1α (Alexandru et al., 2008), IκBα (Dai et al., 1998), Aurora B (Ramadan et al., 2007), and NF1 (Phan et al., 2010). Furthermore, elevated levels of p97 have been reported in a number of human malignancies including cancers of breast, liver, lung, pancreas, ovary, and colon, often with aggressive and poor outcomes (Yamamoto et al., 2005, Yamamoto et al., 2003, Valle et al., 2011, Yamamoto et al., 2004). A possible explanation for the increased p97 levels in malignant cells could be the protein damage-induced stress signals that are

elevated in cancer cells. The induction of elevated p97 levels could help in the clearance of abundant, misfolded/aggregate-prone, and potentially toxic proteins from malignant cells and facilitate their survival (Haines, 2010b).

Mutations in human p97 have been identified in neurodegenerative diseases such as IBMPFD (patient develop frontotemporal dementia) (Watts et al., 2004) and amyotrophic lateral sclerosis (ALS, degeneration of motor neurons) (Johnson et al., 2010). The majority of mutations are located within or close to the N- and D1-domains. These domains are required for the transmission of the conformational changes derived from ATP hydrolysis to the co-factors and/or substrate proteins (Tang et al., 2010, Halawani et al., 2009, Fernandez-Saiz and Buchberger, 2010). Hence, mutations affecting these domains cause impaired autophagy and degradation of ERAD substrates (Weihl et al., 2006, Ju et al., 2009).

Furthermore, altered expression levels of the p97 cofactor FAF1 and ASPL (UBXD9) have been reported in tumour cells. FAF1 down-regulation has been shown in gastric cancers (Bjorling-Poulsen et al., 2003) and in malignant mesothelioma cell lines and primary tumours (Altomare et al., 2009), suggesting that FAF1 is likely to be involved in cancer progression. The underlying mechanism is not clear.

The expression of the UBX-only cofactor ASPL is altered in the rare and unusual cancer, alveolar soft part sarcoma, that is caused by translocation between chromosomes X and 17 (Kuroda et al., 2012). The translocations involving ASPL result in the replacement of the amino terminal region of transcription factor TFE3 with the amino terminal half of ASPL (Ladanyi et al., 2001, Argani et al., 2001). How the translocation affects the activity of both proteins is not clear.

1.2 The p97 co-factor UBXN7

1.2.1 The p97 co-factor UBXN7 and its domains

UBXN7 (also known as UBXD7) is one of the five UBA–UBX proteins in mammalian cells that binds p97 via its UBX domain and ubiquitylated substrates via its UBA domain (Alexandru et al., 2008). In addition to the UBA domain at its N-terminus and the UBX domain at its C-terminus, UBXN7 harbours an UAS domain and an ubiquitin interaction motif (UIM) in the middle of its sequence (Figure 1.3). Studies on UBA and UIM domains from various proteins have shown that these modules are capable of interacting with mono- and poly-ubiquitin chains (Hicke et al., 2005). Additionally, *in vitro* studies have illustrated that, for example, the UIM of HRS and the UBA domain of NUB1 can also interact with the ubiquitin-like modifier NEDD8 (Oved et al., 2006, Tanaka et al., 2003). NEDD8 exhibits a similar hydrophobic surface to the one that allows ubiquitin to interact with ubiquitin binding domains (Whitby et al., 1998). Whereas the UBA domain of UBXN7 binds ubiquitylated substrates, the role of the UIM is yet to be discovered. The function of the UBXN7 UAS domain is also unknown, but a recent study suggests that the UAS domain in the UBA–UBX proteins UBXD8 or FAF1 mediates their polymerization upon interaction with long-chain unsaturated fatty acids (Kim et al., 2013).

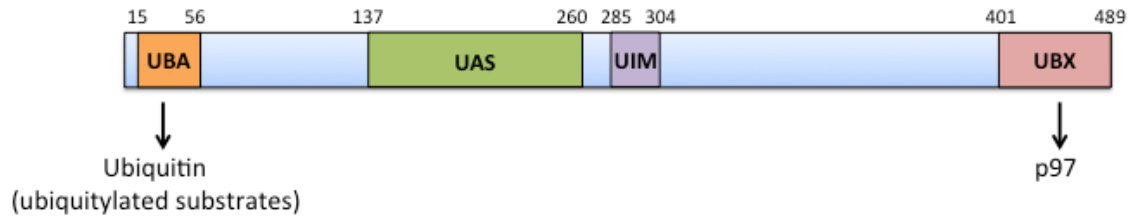

Figure 1.3: **Schematic representation of human UBXN7 highlighting its various domains including reported protein-interactions**
UBA: ubiquitin-associated domain; UAS; UIM: ubiquitin-interaction motif; UBX: Ubiquitin regulatory X

1.2.1 UBXN7 is the UBA–UBX protein that shows the most extensive interaction with cullin-RING E3 ligase subunits

The study performed by Alexandru et al. (2008) not only revealed that p97 interacts with all 13 mammalian UBX-domain proteins, but also that five of the UBA–UBX proteins (UBXN7, UBXD8, FAF1, SAKS1, p47) interact with a large variety of E3 ubiquitin ligases (Alexandru et al., 2008). The comparative MudPIT (Multidimensional Protein Identification Technology) analysis of Flag-(UBA–UBX) protein immunoprecipitates identified multiple components of cullin-RING E3 ligase complexes as well as single subunit RING- and HECT-domain E3s. Notably, among the UBA–UBX proteins, UBXN7 is the most proficient to interact with CRL subunits (Alexandru et al., 2008).

1.2.2 The cullin-RING E3 ligase complex

The cullin-RING E3 ligase complexes (CRLs) are conserved from yeast to humans. They comprise the largest group of ubiquitin ligases and mediate the ubiquitylation of numerous protein substrates, which are subsequently targeted for proteasomal degradation. By controlling the stability of various key regulators, CRLs influence many cellular and biological processes, such as gene expression, cell cycle progression, DNA damage response, or cell signalling (Kamura et al., 2000, Bloom et al., 2003, Karin and Ben-Neriah, 2000, Sato et al., 2012a).

The CRLs are multi-subunit complexes assembled by three core components – a cullin, a RING finger protein, and (except for CUL3-based CRLs) a cullin-specific adaptor protein (Deshaies and Joazeiro, 2009) (Figure 1.4). Humans express seven cullins (CUL1, 2, 3, 4A, 4B, 5 and 7), each acting as scaffold for ubiquitin ligases (E3). The C-terminus of the cullin binds the RING-finger protein that facilitates the direct transfer of

the ubiquitin from an ubiquitin-conjugated E2 enzyme to lysine residues on the target substrate. The N-terminus of the cullin binds cullin-specific adaptors. These adaptors bind interchangeable substrate specific receptors, which in turn recruit substrates for ubiquitylation (Figure 1.4A). For instance, within the CRL2 complex, Cullin 2 (CUL2) acts as a scaffold that binds, with its C-terminus, the RING-finger protein RBX1 and, with its N-terminus, the adaptor complex Elongin B/C (Kamura et al., 1999). Elongin C directly binds the substrate receptor VHL, which in turn recruits the substrate for ubiquitylation (Stebbins et al., 1999, Ivan and Kaelin, 2001).

Ubiquitylation of a substrate is initiated by the slow transfer of a ubiquitin molecule to a lysine in the substrate, this is proposed to have a proofreading function (Petroski and Deshaies, 2005) (Figure 1.4A). The attachment of this first ubiquitin is then followed by rapid elongation of the ubiquitin chain (Saha and Deshaies, 2008). The poly-ubiquitylated proteins are subsequently targeted for degradation by the 26S proteasome (Figure 1.4B).

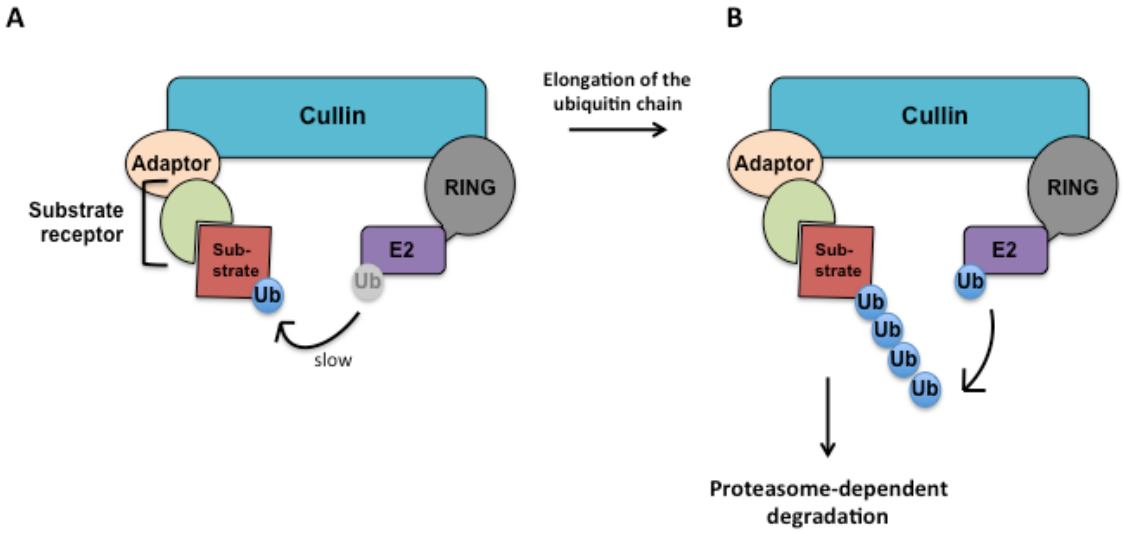

Figure 1.4: **CRL complexes mediate proteasome-dependent degradation**

A) The general CRL complex is assembled by a RING finger protein (RING), a cullin, and a cullin-specific adaptor (Adaptor). The RING finger protein binds an ubiquitin-conjugated E2-enzyme (E2) and facilitates the direct transfer of ubiquitin to the substrate. The adaptor binds interchangeable substrate receptors, which in turn recruit substrates for ubiquitylation. The

slow transfer of the first ubiquitin molecule initiates substrate ubiquitylation. B) After the initial ubiquitylation, rapid elongation of the ubiquitin chain and proteasome-dependent degradation of the substrate follows.

1.2.2.1 Regulation of the CRL complexes

The activation of the CRLs is achieved through the post-translational modification of a conserved C-terminal lysine residue in cullins with the ubiquitin-like modifier NEDD8 (Pan et al., 2004, Osaka et al., 1998, Duda et al., 2008). Early modelling studies have shown an approximately 50Å gap between the catalytic cysteine of the RBX1-bound E2 and the substrate conjugation site (Zheng et al., 2002b) (Figure 1.5A). The NEDD8 conjugation induces a conformational flexibility of the RING domain (Duda et al., 2008, Boh et al., 2011) (Figure 1.5B). This flexibility allows positioning of the RING-domain and its bound activated-E2 enzyme in close proximity to the acceptor lysine of the substrate, thus stimulating the transfer of the ubiquitin molecule (Saha and Deshaies, 2008, Duda et al., 2008).

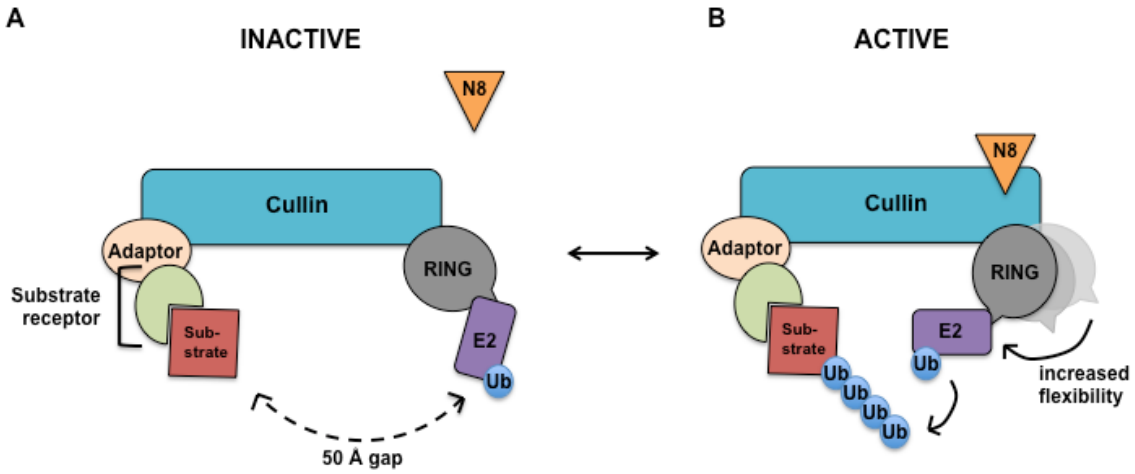

Figure 1.5: **NEDD8 conjugation promotes the activation of cullin-RING ligases by inducing conformational flexibility of the RING domain**
A) The assembled but unmodified CRLs show an approximately 50Å gap between the catalytic cysteine of the RBX1-bound E2 and the substrate.
B) Duda et al. (2008) showed that NEDD8 conjugation on the cullin induces the conformational flexibility of the RING domain. This allows the positioning of the RING-domain and its bound activated-E2 enzyme in close proximity to the acceptor lysine of the substrate, thus stimulating the transfer of the ubiquitin molecule.

Cycles of neddylation and deneddylation play a crucial part in the dynamic regulation of CRLs (Wu et al., 2005, Bosu and Kipreos, 2008). Neddylation of the CRLs is performed by the cullin-directed Nedd8 E3 ligase, DCN1. The RING subunit of the CRL complex allows DCN1 to bring the E2-conjugating enzyme specific for NEDD8 and the cullin in close proximity (Kurz et al., 2008, Kurz et al., 2005, Scott et al., 2010). Deneddylation of the CRLs is mediated by the COP9 signalosome (CSN), an eight-subunit (CSN1–CSN8) complex with CSN5 acting as isopeptidase (Cope et al., 2002, Lyapina et al., 2001). CSN binds neddylated-CRLs for NEDD8-deconjugation, but is also shown to bind unneddylated-CRLs to keep them in a low activity conformation (Emberley et al., 2012). This suggests a model where CSN binds neddylated CRLs, removes the neddylation and keeps CRLs in an assembled but inactive state (Figure 1.6). Furthermore, *in vitro* data show that the addition of ligand (cyclin E peptides) for the substrate receptor relieves CSN from the CRLs (Emberley et al., 2012). This is supported by structural studies showing CSN subunits (CSN1/CSN3) engaging the substrate receptor Skp2/Csk1 of the CUL1 $SCF^{Skp2/Csk1}$ ligase (Enchev et al., 2012). The competition between substrate and CSN binding suggests a potential mechanism to control the assembly of CRLs, however this needs further proof *in vivo*.

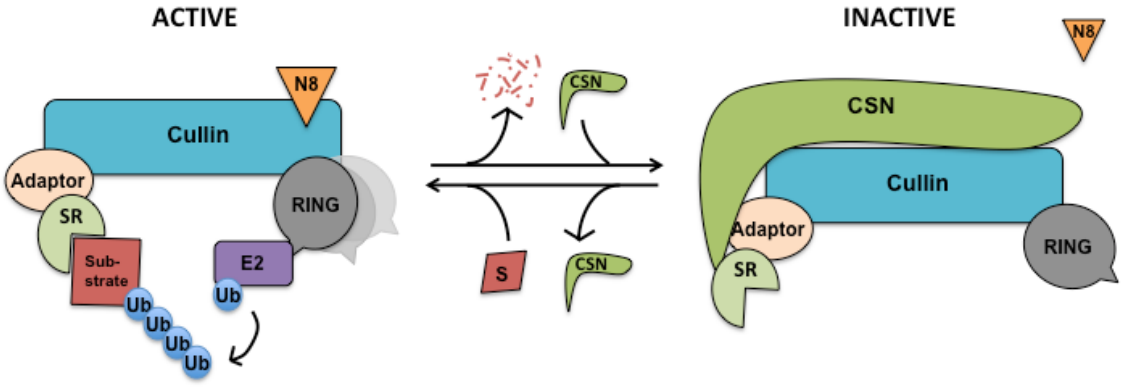

Figure 1.6: The COP9 signalosome deneddylates cullin-E3 ligases and maintains them in a low activity state

Upon substrate depletion, the COP9 signalosome (CSN) binds and deneddylates CRLs. The CSN stays associated with the assembled CRL complexes and maintains them in a low activity conformation. Structural and *in vitro* studies suggest that the increase of available substrate can trigger the release of the CSN from CRLs, which would allow their activation through NEDD8 conjugation. (SR: substrate receptor)

Another CRL regulator is the protein CAND1 (cullin-associated-Nedd8-dissociated-1) that interacts with CRLs at the N-terminus, where it competes with the substrate adaptor for binding, and at the C-terminus, where it masks the neddylation site (Goldenberg et al., 2004). Thus, CAND1 interaction with the cullin is mutually exclusive with substrate adaptor binding and neddylation (Liu et al., 2002, Zheng et al., 2002a). Initially, CAND1 was described to sequester CRLs, thereby causing the inhibition of ligase assembly and activation (Goldenberg et al., 2004). However, it has become evident that CAND1 is actually required for CRL activity, by allowing substrate adaptor exchange and, consequently, the formation of other specific CRL complexes (Bosu and Kipreos, 2008, Zemla et al., 2013, Pierce et al., 2013) (Figure 1.7).

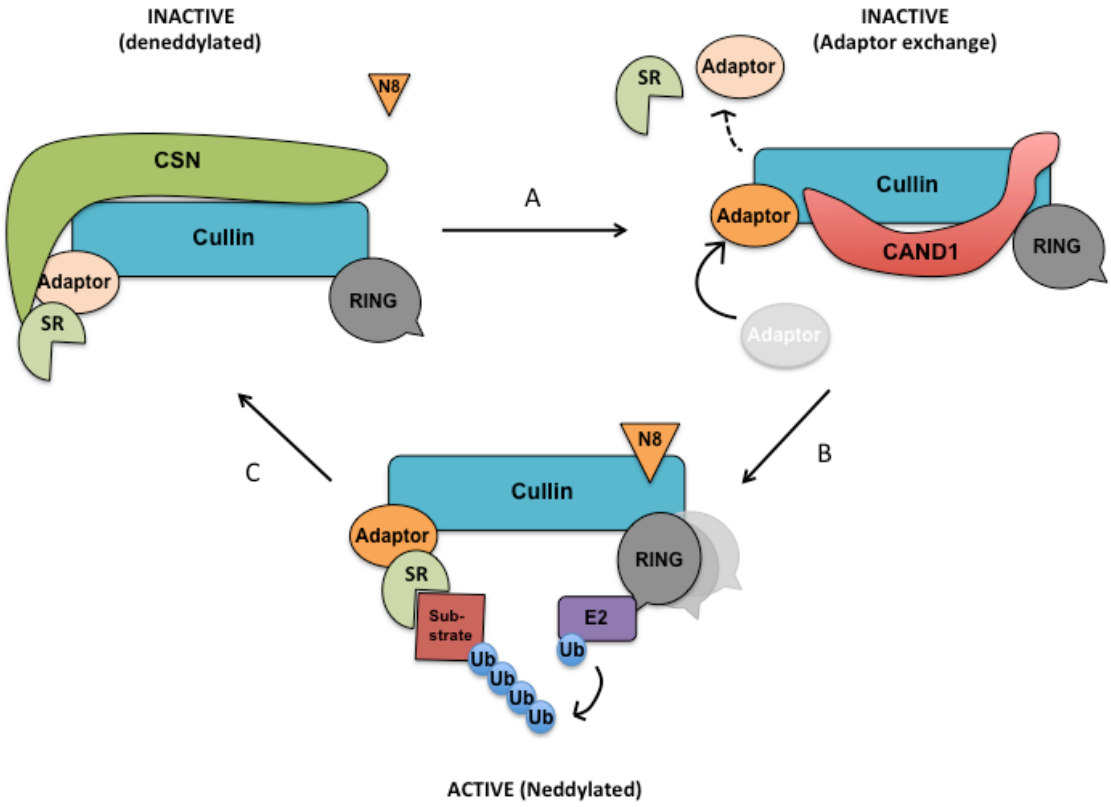

Figure 1.7: CAND1 is required for the adaptor exchange on the CRLs

This model is based on the proposed role of CAND1 as adaptor exchange factor.
A) The COP9-signalosome deneddylates CRLs and dissociates from the complex to allow CAND1 binding. The binding of CAND1 leads to dissociation of the cullin-specific adaptor and allows the association of a pre-existing or newly synthesized adaptor.
B) After the adaptor exchange, CAND1 is released, allowing CRLs activation through NEDD8 conjugation and the subsequent degradation of the substrate.
C) Upon substrate depletion, the COP9 signalosome (CSN) binds and deneddylates CRLs.

1.2.3 UBXN7 links p97 to the ubiquitin ligase CUL2/VHL and its substrate hypoxia-inducible factor 1alpha (HIF1α)

The mass spectrometry analysis of the five UBA–UBX proteins revealed their interaction with a large variety of ubiquitin E3 ligases. Among human UBA–UBX proteins, UBXN7 is the most proficient in interacting with CRL subunits (Alexandru et al., 2008).

The mass spectrometry analysis identified all CRL2 complex components in Flag-UBXN7 immunoprecipitates: CUL2, RBX1, Elongin B/C and VHL. The Western blot

analysis of Flag-UBXN7 immunoprecipitates revealed that UBXN7 has a remarkable ability to bind CUL2. Furthermore, brief inhibition of the proteasome did not affect this binding, suggesting that substrate binding does not regulate the interaction between UBXN7 and CUL2. In contrast, the substrate receptor VHL was only detectable upon proteasome inhibition (Alexandru et al., 2008).

Upon proteasome inhibition, Flag-UBXN7 also co-immunoprecipitates the most prominent CRL2 substrate HIF1α (Alexandru et al., 2008). HIF1α is part of a heterodimeric transcription factor (consisting of HIF1α and HIF1β) that is essential during hypoxia for triggering the expression of specific proteins required to counteract hypoxic stress (Wang et al., 1995, Jiang et al., 1996). Under normoxia conditions, HIF1α is hydroxylated, recognized by the CUL2/VHL ubiquitin ligase, and subsequently degraded by the proteasome. However, HIF1β appears to be constitutively stable (Ivan and Kaelin, 2001, Maxwell et al., 1999).

By investigating further the interaction between UBXN7, p97 and the CRL2 complex, including its substrate HIF1α, Alexandru et al. could demonstrate the following main points:

1) Treatment with p97 siRNA did not alter the interaction between UBXN7 and CUL2, indicating that this interaction does not depend on p97.

2) Myc-p97 immunoprecipitation showed diminished CUL2- and HIF1α-binding to myc-p97 in UBXN7-silenced cells, suggesting that UBXN7 mediates p97 interaction with CUL2 and its substrate HIF1α (Figure 1.8).

3) Silencing of p97 caused HIF1α accumulation, an effect that was more pronounced after proteasome inhibition, which introduces HIF1α as a novel p97 substrate.

4) Upon proteasome inhibition, UBXN7 and p97 interact mainly with ubiquitylated HIF1α, suggesting UBXN7 and p97 may participate in HIF1α degradation via the ubiquitin-proteasome system (UPS) (Figure 1.8).

5) UBXN7 silencing causes a reduction in HIF1α levels, a paradoxical observation, considering that silencing of p97 leads to HIF1α accumulation. This result might indicate that UBXN7 involvement in HIF1α degradation is more complex than initially anticipated.

Taken together, Alexandru et al. could establish that UBXN7 is the substrate-binding adaptor for HIF1α whose degradation requires p97, thereby expanding p97 function beyond ERAD (Figure 1.8).

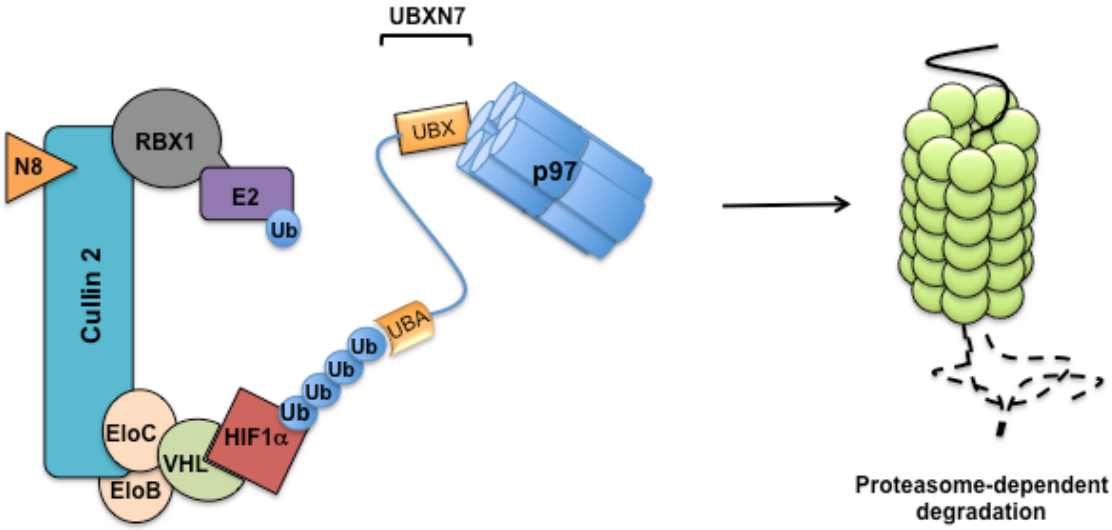

Figure 1.8: UBXN7 recruits p97 to the ubiquitin ligase CUL2/VHL and its substrate HIF1α
This model summarizes some of the findings obtained by Alexandru et al, 2008: The interaction between UBXN7 and CUL2 does not depend on p97. p97 is recruited to the CRL2 complex via UBXN7, which mediates interaction with CRL2 substrate HIF1α. Since UBXN7 and p97 interact mainly with ubiquitylated HIF1α upon proteasome inhibition, this suggests they may participate in HIF1α degradation via the ubiquitin-proteasome system.

1.3 The p97 co-factor UBXN8

1.3.1 UBXN8 interacts with p97 via its UBX domain

UBXN8, also called UBXD6 and REP8, is conserved in vertebrates, but not present in lower eukaryotes. Full-length UBXN8 has a molecular weight of 30.5 kDa (Yamabe et al., 1997) and contains a transmembrane domain at the N-terminus, followed by a predicted coiled-coil region, and a UBX domain at the C-terminus (Figure 1.9). The transmembrane domain anchors UBXN8 at the ER membrane, while the UBX domain mediates its interaction with the N-terminus of p97 (Madsen et al., 2011). The function of the coiled-coil domain is currently unknown. As one of the UBX-only p97 co-factors, UBXN8 lacks the UBA domain and cannot bind ubiquitin directly. The interaction between UBXN8 and other proteins must therefore be mediated in a different manner.

Based on alternative splicing, two additional UBXN8 isoforms are predicted: Isoform 2 that lacks a region between the coiled-coil region and the UBX domain, and isoform 3 that lacks the transmembrane domain (Figure 1.9).

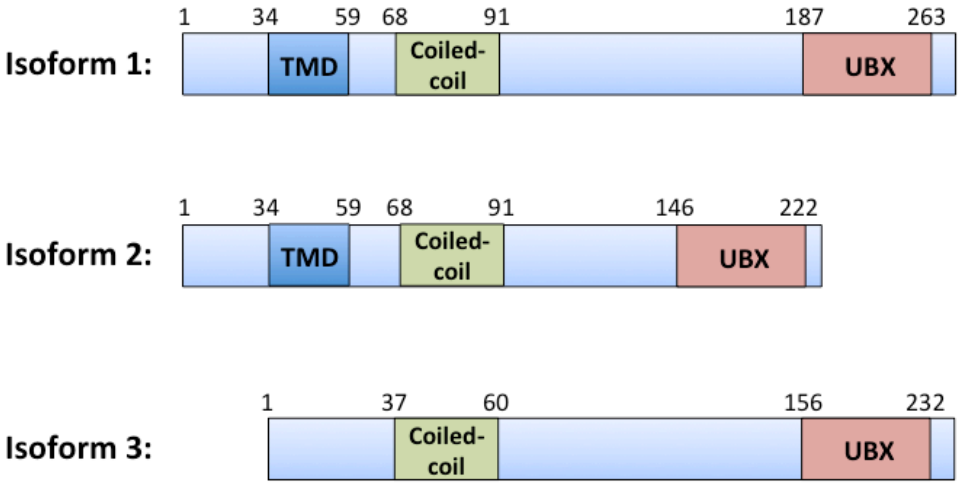

Figure 1.9: Schematic representation of the three predicted UBXN8 isoforms
Based on alternative splicing, three isoforms are predicted for UBXN8 with isoform 1 representing full-length UBXN8.
TMD: Transmenbrane domain; UBX: Ubiquitin regulatory X

1.3.2 UBXN8 is highly expressed in reproductive tissues

As mentioned before, the expression of several UBX-only proteins is tissue dependent (Yamabe et al., 1997, Carim-Todd et al., 2001). This is also true for UBXN8, whose mRNA, as well as protein levels are highly increased in the reproductive tissues: testes and ovaries (Yamabe et al., 1997, Madsen et al., 2011).

In testes, the *UBXN8* mRNA expression was studied in more detail, and revealed that the high levels of *UBXN8* expression are caused by its up-regulated expression in the post-meiotic, round spermatids (Madsen et al., 2011). Furthermore, *in situ* hybridisation experiments with developing germ cells in adult testes showed that the up-regulation of *UBXN8* expression is specific during the late stages of round spermatid differentiation. The early stages of round spermatid differentiation, and the elongated spermatids, showed low to undetectable *UBXN8* expression (Madsen et al., 2011).

In ovaries, *UBXN8* mRNA is abundant in somatic granulosa cells that surround the oocyte in the developing follicles (Madsen et al., 2011). The high UBXN8 expression within somatic cells in ovaries is in contrast to its high expression within germ cells in testis. This might indicate that there is no common UBXN8 expression cell lineage in male and female gonads (Madsen et al., 2011).

1.3.3 UBXN8 is an ER membrane protein and is implicated in ERAD

UBXN8 subcellular localisation, its membrane topology and its role in ERAD were studied in more detail in cancer cells (Madsen et al., 2011).

In HeLa cells, UBXN8-GFP localises at the ER membrane with the C-terminal UBX domain facing into the cytoplasm. By binding p97 via its UBX domain, UBXN8 tethers p97 at the ER membrane. Accordingly, the amount of ER-associated p97 is reduced in UBXN8 siRNA treated cells (Madsen et al., 2011).

Furthermore, the data presented by Madsen et al. indicate that UBXN8 participates in ERAD. They show that the degradation of the ERAD substrates TCRα and CD3δ is slightly reduced in melanoma cells (MelJuSo) treated with UBXN8 siRNA. In contrast, the degradation of the cytoplasmic model substrate ubiquitin-G76V-YFP is not affected by UBXN8 silencing, suggesting that UBXN8 specifically targets ER-derived proteasome substrates (Madsen et al., 2011).

1.3.4 UBXN8, a tumour suppressor gene candidate

A recent publication from Li et al. (2014) identified host genes frequently targeted for hepatitis B virus (HBV) integration, and revealed that *UBXN8* is one of the recurrent candidate genes (Li et al., 2014). The integration of HBV DNA into the genome of hepatocytes is one of the major causes of hepatocarcinogenesis (Shafritz et al., 1981), which is the third leading cause of global cancer death (Forner et al., 2012). The identification of host genes targeted by HBV integration could be therefore important to understand the process of carcinogenesis associated with HBV integration.

In hepatocellular carcinoma (HCC) tissues, expression of *UBXN8* was shown to be significantly down-regulated compared to non-tumorous tissue, particularly in the HCC tissue with the HBV integration within the intron of *UBXN8* (Li et al., 2014). The function of UBXN8 in the process of carcinogenesis was evaluated by overexpressing UBXN8 in various HCC cell lines. In the HCC cell lines carrying the wild type *TP53* gene, ectopic expression of UBXN8 slowed proliferation and induced G1/S transition retardation. Furthermore, the UBXN8 overexpression was shown to cause increased p53 and $p21^{WAF1/CIP1}$ levels accompanied by decreased cyclin D1 levels (Li et al., 2014).

TP53 encodes for the tumour suppressor protein p53, which is inactivated in many human cancers (Kern et al., 1991). p53 up-regulates the expression of other genes, such

as the G1 cyclin-dependent kinase inhibitor $p21^{WAF1/CIP1}$ leading to cell cycle arrest (Gartel and Radhakrishnan, 2005, el-Deiry et al., 1994). Therefore, the data from Li et al. suggest that UBXN8 overexpression might negatively regulate cell cycle progression by inducing a delay in the G1/S transition via a $p53/p21^{WAF1/CIP1}$ -dependent mechanism. Cyclin D1 drives the G1/S transition (Resnitzky and Reed, 1995) and its reduction would also promote the G1 arrest. Because the effects caused by UBXN8 overexpression were not observed for HCC cell lines harbouring mutated *TP53,* the function of UBXN8 seems to be p53-dependent (Li et al., 2014).

1.3.5 Fanconi Anaemia

The analysis of Flag-UBXN8 immunoprecipitates by mass spectrometry identified the Fanconi anaemia (FA) key proteins, FANCD2 and FANCI, as UBXN8 interaction partners (unpublished results by Gabriela Alexandru). This interaction links UBXN8 to the rare genetic disease FA, which can be caused by mutations in any of the currently known 15 FA genes, resulting in defective DNA crosslink repair (Moldovan and D'Andrea, 2009, Kitao and Takata, 2011, Kim and D'Andrea, 2012). DNA interstrand crosslinks (ICL) are very toxic lesions that covalently link both strands of the DNA helix, thereby blocking replication (resulting in stalled replication forks) and transcription (Scharer, 2005, Noll et al., 2006). They can be caused by byproducts of metabolism (e.g. malondialdehyde produced during lipid peroxidation) (Niedernhofer et al., 2003), cellular metabolites (e.g. activated oestrogens) (Dai and Lui, 2000), or bi-functional crosslinking agents (e.g. cisplatin, mitomycin C) (Noll et al., 2006, Scharer, 2005). Because the FA pathway plays a major role in removing these crosslinks, FA proteins are required for maintaining genome stability and preventing cancer (Kee and D'Andrea, 2010).

FA is a rare autosomal or X-linked recessive disorder characterized by progressive bone marrow failure, multiple congenital abnormalities, and cancer predisposition (Kee and D'Andrea, 2012). Although FA is a rare disease, the FA pathway provides an attractive model for studying DNA repair, cancer progression, and the role of ubiquitin signalling (Moldovan and D'Andrea, 2009).

Clinically, FA is very heterogeneous. Most FA patients develop anaemia as a consequence of bone marrow failure during childhood (Kim and D'Andrea, 2012). Later in life, individuals with FA are at high risk of developing cancer, especially acute myelogenous leukaemia (AML), squamous cell carcinoma (SCC) of the head and neck, and hepatocellular carcinoma (HCC) (Bakker et al., 2013).

Genetically, FA is caused by mutations in any of the 15 currently known FA genes (*FANCA*, *-B*, *-C*, *-D1* (*BRCA2*), *D2*, *-E*, *-F*, *-G*, *-I*, *-J (BACH1)*, *-L*, *-M*, *-N*, *-O* (*RAD51C),* and *-P (SLX4)*) coding for proteins that function together in the FA pathway (Kim and D'Andrea, 2012, Kee and D'Andrea, 2012). Approximately 85% of FA patients are defective in one of the most common disease-causing genes *FANCA*, *FANCC* or *FANCG* (Auerbach, 2009). Mutations in FANCD2 and FANCI account for approximately 3% of the mutations found in FA patients (Auerbach, 2009). To date, some patients still remain unassigned, which indicates the possibility that there are FA genes still to be identified.

The FA pathway is a DNA repair pathway, which is essential to resolve ICLs encountered during replication. Accordingly, FA patient-derived cells are hypersensitive to DNA interstrand crosslink-inducing agents, such as mitomycin C (MMC), cisplatin and diepoxybutane (DEB), resulting in a dramatic increase in chromosomal aberrations (including translocations and radial chromosomes). The hypersensitivity of FA cells to ICL-inducing agents and the consequential increase of

chromosomal aberrations provide a cellular marker to diagnose FA in the context of chromosomal breakage tests (Auerbach and Wolman, 1976).

1.3.5.1 The Fanconi anaemia pathway and its key players

The FA pathway consists of three types of member proteins: the FA core complex, the FA FANCD2/I (ID) complex and downstream members that facilitate the ICL repair.

The FA core complex contains eight FA proteins (FANCA, -B, -C, -E, -F, -G, -L, -M) and forms a multi-subunit ubiquitin E3 ligase complex (Kim and D'Andrea, 2012). The DNA lesion is recognised by FANCM that forms a heterodimer with the FA-associated protein FAAP24 and binds DNA directly (Ciccia et al., 2007) (Figure 1.10). The stable association of FANCM with chromatin is further maintained through its binding to the histone fold-containing proteins, MHF1 and MHF2 (Singh et al., 2010, Yan et al., 2010). The heterodimer FANCM/FAAP24 has multiple roles in pathway activation by recognising the DNA lesion and recruiting the FA core complex, stabilizing the stalled replication fork, and initiating the ATR-mediated checkpoint signalling (FA pathway independent) (Ciccia et al., 2007, Collis et al., 2008, Schwab et al., 2010). The association of FANCM with other FA core complex members is mediated by its interaction with FANCF (Deans and West, 2009) (Figure 1.10).

The FA core complex subunit FANCL acts as E3 ubiquitin ligase and catalyses mono-ubiquitylation of FANCD2 and FANCI together with UBE2T as an E2 enzyme (Cole et al., 2010, Machida et al., 2006, Hodson et al., 2014) (Figure 1.10). Mono-ubiquitylation of the two FA proteins by the FA core complex is considered to be the key regulatory step in the FA pathway. In human cells, FANCL/UBE2T conjugates a single ubiquitin moiety to Lys561 of human FANCD2 and Lys523 of human FANCI (Garcia-Higuera et al., 2001, Smogorzewska et al., 2007). The modifications on FANCD2 and FANCI and

their regulatory function will be discussed in more detail below. The E3 ligase FANCL is the only member of the FA core complex that is conserved in lower multicellular eukaryotes (together with FANCD2 and FANCI) and is able to mono-ubiquitylate its substrates *in vitro* in the absence of the other subunits of the complex (Alpi et al., 2008). Although the mono-ubiquitylation event *in vitro* requires only FANCL, it is clear from patient mutations that all members of the FA core complex are required *in vivo*. Certain multicellular animals such as flies and worms seem to lack the majority of FA core complex proteins (Marek and Bale, 2006, Patel and Joenje, 2007, Collis et al., 2006, Lee et al., 2013). Lower eukaryotes might therefore exhibit a simplified FA pathway, where the ubiquitin-activating enzyme E1, Ube2t, FANCL, and FANCI may be sufficient for FANCD2 mono-ubiquitylation.

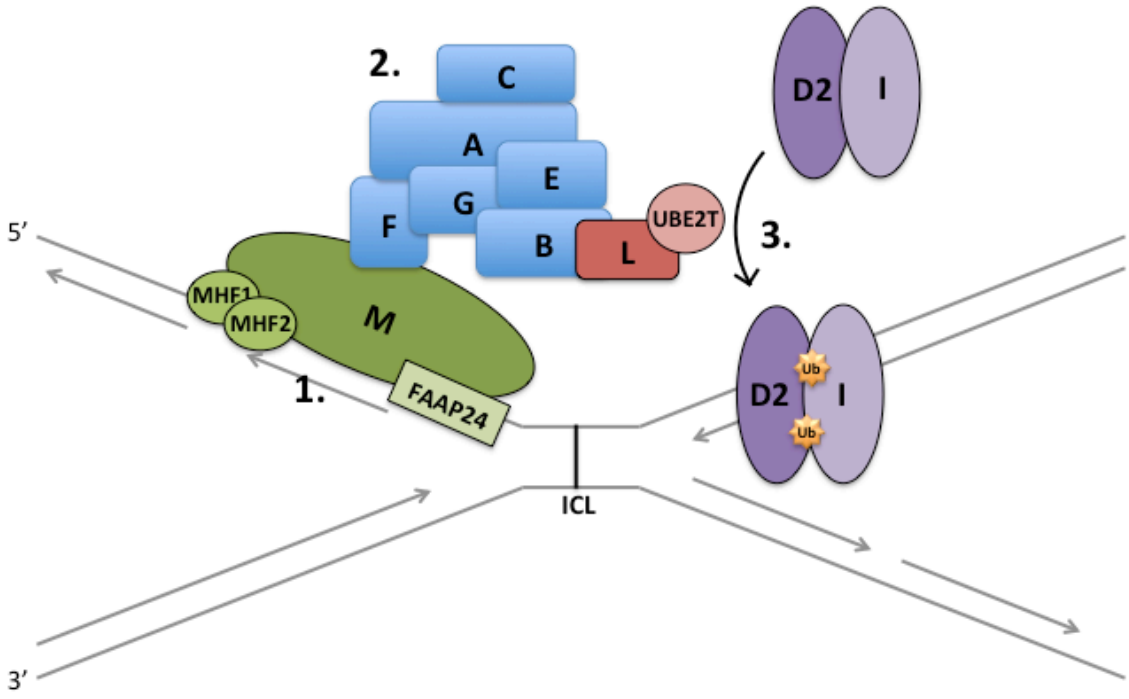

Figure 1.10: Schematic representation showing the activation of the FA pathway

ICLs can occur naturally or by ICL-inducing agents such as MMC or cisplatin. During S-phase, replication forks converge from different directions and stall on the DNA ICL that covalently links the two strands of DNA.

1) The DNA lesion is recognised by FANCM that forms a heterodimer with the FA-associated protein FAAP24. Additionally, FANCM binds the histone fold-containing proteins, MHF1 and MHF2 that stably associate FANCM with chromatin.

2) FANCM recruits the FA core complex to the DNA through its interaction with FANCF. FA core complex subunit FANCL acts as E3 ubiquitin ligase.
3) FANCD2 and FANCI are recruited to the DNA lesion and are mono-ubiquitylated by FANCL together with UBE2T as an E2 enzyme.

The FA pathway orchestrates the coordinated action of three critical DNA repair processes: nucleolytic incision, translesion DNA synthesis (TLS), and homologous recombination (HR); and facilitates the ICL repair in S-phase (Kim and D'Andrea, 2012).

After the modification of the ID complex, mono-ubiquitylated FANCD2 recruits the nucleases FAN1 (FA-associated nuclease 1) and FANCP (SLX4) to the ICL lesion in order to initiate nucleolytic incision (MacKay et al., 2010, Yamamoto et al., 2011) (Figure 1.11). Both nucleases harbour the UBZ4 (ubiquitin binding zinc finger 4) domain, which is an ubiquitin-binding domain specifically recognising the ubiquitin-modification on FANCD2 (Yamamoto et al., 2011, MacKay et al., 2010).

FANCP acts as a scaffold for multiple nucleases that are required for ICL repair and HR, and it recruits the heterodimeric nucleases MUS81-EME1 and XFP-ERCC1 (Fekairi et al., 2009) (Figure 1.11, [1]). These structure-specific endonucleases promote incisions flanking the region of the ICL, which unhook the ICL (Hanada et al., 2006, Niedernhofer et al., 2004). Polymerases of the translesion DNA synthesis then bypass the lesion and extend the leading strand (Ho et al., 2011, Waters et al., 2009) (Figure 1.11, [2]).

Furthermore, the ICL unhooking creates a DSB in the other sister chromatid (Figure 1.11, [3]). Homologous recombination resolves the DSB by using the homologous template restored by TLS. The repair of the DSB by homologous recombination involves the loading of RAD51 onto the DNA lesion, and the RAD51-mediated strand invasion of the sister chromatid strands (Krejci et al., 2012). The downstream FA

proteins FANCD1, -J, -N and –O are required for these processes. FANCD1 (BRCA2) interacts with RAD51 and promotes its loading to single-strand DNA (Jensen et al., 2010, Subramanyam et al., 2013). FANCN (PALP2) binds FANCD1 and regulates its intranuclear localisation and stability (Xia et al., 2006). FANCJ works downstream of RAD51 and dissociates RAD51 from single-strand DNA in order to allow the completion of HR repair (Litman et al., 2005, Sommers et al., 2009, Wu et al., 2010). FANCO (RAD51C) is also required for RAD51 loading, and for resolving Holliday junction intermediates at a later step of HR (Liu et al., 2007, French et al., 2002).

After finishing DNA repair, mono-ubiquitylated FANCD2 and FANCI are de-ubiquitylated by the deubiquitylating enzyme USP1 (Nijman et al., 2005) (Figure 1.11, [4]). USP1 forms a heterodimeric complex with UAF1 that acts as an activator of USP1, by stimulating its activity towards the substrate (Cohn et al., 2007). Under normal conditions, the USP1/UAF1 complex keeps FANCD2 ubiquitylation in check. Upon DNA damage, the expression of *USP1* is turned off, while the remaining USP1 protein is degraded by the proteasome (Huang et al., 2006). These two mechanisms of USP1 repression allow the accumulation of mono-ubiquitylated FANCD2 and FANCI.

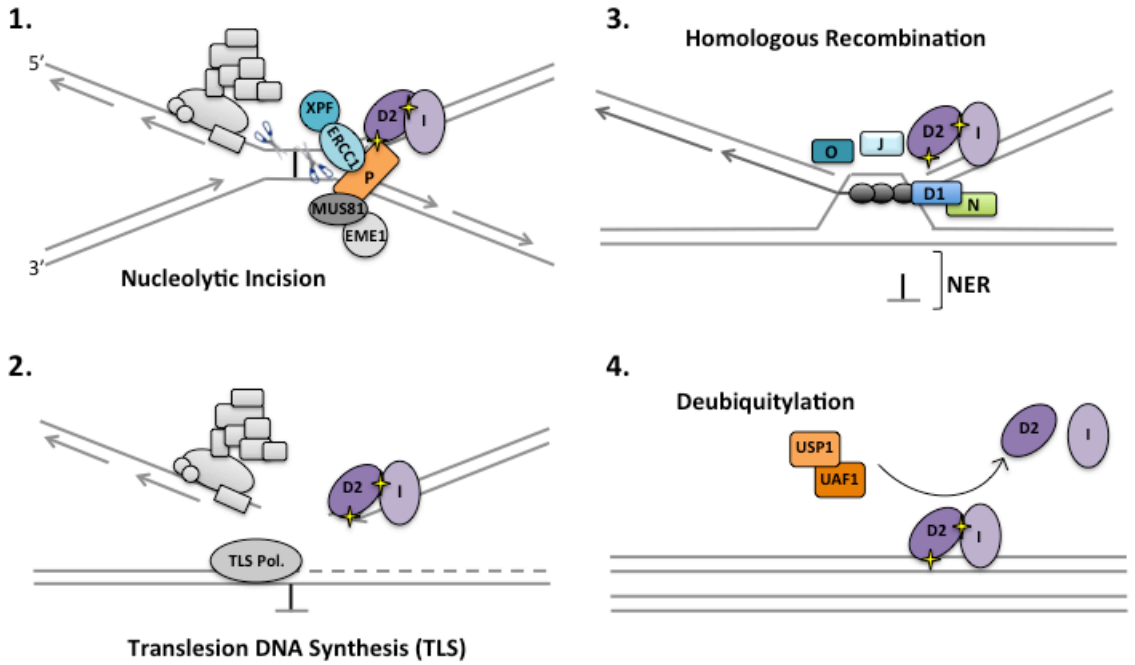

Figure 1.11: Schematic representation of replication-dependent ICL repair after FANCD2/I activation

1. Mono-ubiquitylated FANCD2 recruits FANCP (SLX4) to the ICL lesion in order to initiate nucleolytic incision. FANCP recruits the heterodimeric nucleases MUS81-EME1 and XFP–ERCC1. These structure-specific endonucleases promote incisions flanking the region of the ICL, which unhook the ICL.
2. Polymerases of the translesion DNA synthesis then bypass the lesion and extend the leading strand.
3. The ICL unhooking creates a double-strand break (DSB) in the other sister chromatid. Homologous recombination (HR) resolves the DSB by using the homologous template restored by TLS. RAD51 is loaded onto the DNA lesion (dark cycles) and mediates strand invasion of the sister chromatid strands. The downstream FA proteins FANCD1, -J, -N and -O are required for these processes. Nucleotide excision repair (NER) excises the remaining adducts.
4. At the end of DNA repair, mono-ubiquitylated FANCD2 and FANCI are de-ubiquitylated by the deubiquitylating enzyme USP1 that forms a heterodimeric complex with UAF1.

1.3.5.2 Regulation of FANCD2 and FANCI through phosphorylation and ubiquitylation

FANCD2 and FANCI form the ID complex that is associated with chromatin in response to DNA damage. Both FA proteins are mono-ubiquitylated and phosphorylated to regulate their activity (Ishiai et al., 2008, Zhi et al., 2009, Smogorzewska et al., 2007, Garcia-Higuera et al., 2001).

Stalled replication forks at the site of DNA damage lead to the activation of the S-phase checkpoint mediated by the protein kinase ATR (ATM and Rad3-related) (Cimprich and Cortez, 2008). ATR is recruited to RPA-coated single strand DNA that is exposed at the site of DNA damage during replication. ATR then phosphorylates numerous proteins involved in checkpoint function and DNA repair (Andreassen et al., 2004, Zou and Elledge, 2003).

Several FA proteins are phosphorylated by ATR in response to DNA damage, including FANCD2 and FANCI, which leads to S-phase dependent activation of the FA pathway (Andreassen et al., 2004, Qiao et al., 2004, Wang et al., 2007, Ishiai et al., 2008).

The phosphorylation of FANCD2 at the residues Ser331, Ser717 and Thr691 was shown to promote FANCD2 ubiquitylation and resistance to ICL-inducing agents (Ho et al., 2006, Zhi et al., 2009, Andreassen et al., 2004).

The ATR-mediated phosphorylation of a S/TQ cluster in FANCI close to the ubiquitylation site is essential for FANCD2 mono-ubiquitylation and the localization of FANCD2 and FANCI to nuclear foci (Ishiai et al., 2008, Shigechi et al., 2012). Mimicking phosphorylation at six S/TQ sites in chicken FANCI is sufficient to induce FANCD2 mono-ubiquitylation and efficient repair, even in the absence of FANCD2 or core complex phosphorylation through ATM/ATR inhibition. (Ishiai et al., 2008). The phosphorylation of FANCI is therefore described as the molecular switch that turns on the FA pathway (Ishiai et al., 2008).

The formation of foci and the mono-ubiquitylation of FANCD2 and FANCI are key regulatory steps for the activation of the FA pathway. In mammalian cells, mono-ubiquitylation on FANCI is required for FANCD2 mono-ubiquitylation and foci formation. Reciprocally, FANCD2 mono-ubiquitylation is required for FANCI mono-

ubiquitylation (Smogorzewska et al., 2007). The interdependent nature of FANCD2 and FANCI mono-ubiquitylation was also shown *in vitro* in ubiquitylation assays using the ID complex containing either FANCD2 K561R or FANCI K523R (Longerich et al., 2014). In contrast, in chicken cells, the mono-ubiquitylation of FANCI is described to be dispensable for resistance to ICLs, indicating regulatory and functional differences between chicken and human FANCI (Ishiai et al., 2008).

Although the mono-ubiquitylations of FANCD2 and FANCI within the ID complex are interdependent, they are described to serve different purposes. While FANCD2 mono-ubiquitylation is essential for the recruitment of downstream repair proteins to the DNA damage site (MacKay et al., 2010, Yamamoto et al., 2011), FANCI mono-ubiquitylation is described to promote the stability of the FANCD2/I heterodimer by interacting with the CUE (coupling of ubiquitin conjugation to endoplasmic reticulum degradation)-domain in FANCD2 (Rego et al., 2012). The mutations of the ubiquitylation sites in FANCD2 or FANCI result in defective ICL repair (Smogorzewska et al., 2007, Garcia-Higuera et al., 2001).

The crystal structure of the mouse ID-complex revealed that both FANCD2 and FANCI fold into a saxophone-like structure, and they interact along a ~560 residue-long region within this shape (Joo et al., 2011). The mono-ubiquitylation and phosphorylation sites of FANCD2 and FANCI are imbedded in the interface of the ID complex. Although conjugated ubiquitin to these lysine residues does not cause steric hindrance with the surrounding residues in the ID complex, the access for the ubiquitin-conjugating (E2) enzyme to the lysine residue is occluded. Therefore, the crystal structure of the ID complex suggests that the mono-ubiquitylation of FANCD2 and FANCI either happens on the monomeric proteins followed by their dimerization, or that the ID complex has to

undergo a conformational change to allow access to the ubiquitylation sites (Joo et al., 2011). Since both FA protein, FANCD2 and FANCI, possess DNA binding activity, it has been suggested that binding of the ID complex to DNA might facilitate the required conformational change (Joo et al., 2011, Yuan et al., 2009, Longerich et al., 2009).

This was confirmed in recent publications with human or chicken FANCD2 and FANCI proteins, showing that DNA ligands (double-strand DNA or single-strand DNA with secondary structures) indeed stimulate the mono-ubiquitylation of FANCD2 and FANCI in the context of the ID complex, *in vitro* (Longerich et al., 2014, Sato et al., 2012b). The mono-ubiquitylation of FANCD2 induced by DNA is stronger than that of FANCI, which was only modestly modified. Furthermore, reduced DNA binding activity of FANCI leads to decreased mono-ubiquitylation of FANCD2, even in the presence of DNA, suggesting that DNA binding of FANCI is required for FANCD2 mono-ubiquitylation (Longerich et al., 2014). The described ubiquitylation assays are performed with human UBE1, UBE2T and FANCL only. Therefore, it is likely that other components of the FA core complex and/or post-translational modifications on FANCD2 and/or FANCI are required for increased FANCI mono-ubiquitylation within the ID complex in cells. However, in the absence of FANCD2, mono-ubiquitylation of FANCI was greatly enhanced by various types of DNA (poor mono-ubiquitylation without DNA) (Longerich et al., 2014). This indicates that mono-ubiquitylation of monomeric FANCI is DNA stimulated as well, but that within the ID complex, FANCI mono-ubiquitylation is attenuated relative to free FANCI (Longerich et al., 2014).

1.4 Aim of the thesis

The diverse cellular functions of p97 are determined through its binding to a large number of different co-factors, that in turn recruit substrates to p97. The largest family

of p97 co-factors are the UBX-domain proteins that can be classified into two subgroups: UBA-UBX proteins and UBX-only proteins (Alexandru et al., 2008). The UBA-UBX proteins have ubiquitin-binding capabilities and facilitate p97 function as an ubiquitin-receptor, while UBX-only proteins appear to direct p97 to ubiquitin-independent functions. The identification of specific cellular targets for the UBX-domain proteins will help to define the subset of p97 functions they regulate and can help us to understand the role of p97 at the molecular level.

In this thesis, I describe two projects, one focussing on the UBA-UBX protein UBXN7 and the other on the UBX-only protein UBXN8.

Among human UBA-UBX proteins, UBXN7 is the most proficient in interacting with CRL subunits, in particular CUL2, and it was assumed that these interactions were indirect, mediated by their ubiquitylated substrates (Alexandru et al., 2008). The aim of this project was to determine whether UBXN7 interaction with cullins is direct or mediated by its ubiquitylated targets bound to the UBA domain.

My main project was initiated by results obtained in the MS analysis of Flag-UBXN8 immunoprecipitates that identified the two key FA proteins FANCD2 and FANCI as potential UBXN8 interaction partners (unpublished results by Gabriela Alexandru). The identification of both FA proteins may link UBXN8 to the rare genetic disease FA, which is caused by defective ICL repair. The aim of this project was to investigate the interaction between UBXN8 and the FA proteins FANCD2 and FANCI, to shed light on the functional relevance of these interactions, as well as gain a better understanding of the role of UBXN8 in the DNA damage response.

Chapter 2

2. Materials and Methods

2.1 Materials

2.1.1 Instruments

The pipettes and pipetting aid were from Gilson. The Thermomixer/shakers and multipipette® steam were from Eppendorf. The pH meters and electrodes were from VWR. The incubators for incubating bacteria's were from Binder. Tissue culture class II safety cabinets were from Medical Air Technology. CO_2 incubators were from Mackay and Lynn. Centrifuge tubes, rotors and centrifuges were from Beckmann. The NanoDrop used to measure DNA concentrations was the Nano Vue Plus from GE Healthcare. The UV/Visible Spetrophotometer for measuring protein concentrations was the UltroSpec 2100 *pro* from Amersham Bioscience. The Electrophorese Power Supply used for DNA gel-electrophoresis was from Thermo. The Power Supplies used for running polyacrylamide gels were from Amersham Bioscience and BioRad. The X-Cell SureLock Mini-cell electrophoresis systems were from Invitrogen. The Mini Trans-Blot cell was from BioRad. Stained polyacryamid gels were dried with the DryEase Mini-Gel Drying system from Invitrogen. The SpeedVac, rotator with Clips (used to incubate IPs) as well as the microcentrifuges Heraeus Pico or Fresco 17 were from Thermo Scientific. The mini orbital shaker was from Bibby Scientific and Vortex-Genie® 2 was purchased from Scientific Industries. The Konica automatic film processor was from Konica Corporation. The LiCOR odyssey infrared imaging system was from LiCOR biosciences (Cambridge, UK). The mass spectrometry samples were acquired on an LTQ Orbitrap Velos mass spectrometer (Thermo Scientific). The FACS

analyses were performed with FACSCalibur flow cytometer (BD Biosciences). The microscopes used in immunofluorescence experiments were the DeltaVision Spectris and the DeltaVision OMX Blaze (GE Healthcare).

2.1.2 Commercial chemicals

Table 2.1 enlist the reagents used in this thesis and their supplier

Table 2.1: Commercial chemicals

Product name	**Supplier**
4-(2-Amino-ethyl) benzenesulfonyl (AEBSF) 4',6-Diamidino-2-phenylindole dihydrochloride (DAPI) Adenosine 5′-triphosphate (ATP) Anti-FLAG-agarose Benzamidine Benzonase Bovine serum albumin (BSA) Bromophenol blue Cisplatin Dimethyl pimelimidate (DMP) Dimethyl sulphoxide (DMSO) Ethanolamine Ethidium bromide Ethylene glycol tetraacetic acid (EGTA) Ethylene diamine tetraacetic acid (EDTA) Hydroxyurea Iodoacetamide Kodak BioMax MR film Magnesium chloride ($MgCl_2$) Mitomycin C (MMC) Nocodazole Phenylmethanesulphonylfluoride (PMSF) Piperazine-N,N′-bis(2-ethanesulfonic acid) (PIPES) Ponceau S Protein-A agarose Ribonuclease A Sodium chloride Sodium dodecyl sulphate (SDS) Sodium tetraborate Thymidine	Sigma Aldrich

Triethylammonium bicarbonate Triton-X-100 Tween-20 Urea β-mercaptoethanol	
Sodium chloride (NaCl) Tris(hydroxymethyl)aminomethane (Tris-HCl) Glycerol Ethanol Sucrose Giemsa staining solution Sodium hydroxide (NaOH) Potassium hydroxide (KOH) Potassium chloride (NaCl)	VWR
Lipofectamin RNAiMax NuPAGE Tris-Acetate running buffer (20X) NuPAGE transfer buffer Propidium Iodid Agarose Precast 4-20% and 8% Novex Tris-Glycine gels 3-8% NuPAGE Tris-Acetate gels	Invitrogen
Bio-Rad Protein Assay Horseradish peroxidase (HRP)-conjugated secondary antibodies Micro Bio-Spin Chromatography columns Precision Plus Protein all blue Standards	BioRad
5x siRNA buffer RNAse free water	Dharmacon
Endoproteinase Lys-c (Sequencing grade) Protease inhibitor cocktail tablets Trypsin (modified, sequencing grade)	Roche
Hyperfilm MP Protein A-agarose	GE Healthcare
Instant Blue staining solution	Expedion
Coomassie protein assay reagent (Bradford reagent)	Pierce
Protran BA nitrocellulose membrane (pore size - 0.45µm and 0.20µm)	Schleicher and Schuell
HA-Ubiquitin	Boston Biochem
Plasmid MiniPrep Kit	Qiagen
The Maxi Pep kit	Machery&Nagel
3MM chromatography paper	Whatman
Dithiothreitol (DTT) N-2-hydroxyethylpiperazine-N-2-ethane sulfonic acid (HEPES)	Formidium
16% Formaldehyd Solution	Thermo Scientific

Western Lightning® Plus-Enhanced chemiluminescence (ECL)	Perkin Elmer
DNA ladder (1 kbp)	Biolabs
TransIT-LT1 transfection reagent	Mirus
MG132 (Proteasome inhibitor)	Enzo
Hydromount (mounting media) Potassium acetate	Fisher Scientific
NP-40	Calbiochem

2.1.3 Tissue culture reagents

McCoy's 5A medium, Minimum Essential Medium (MEM)-medium, Leibovitz's medium (for Live cell imaging), OptiMEM reduced serum media, Fetal bovine serum (FBS), tissue culture grade Dulbecco's phosphate buffered serum (PBS), Trypsin/EDTA solution, L-glutamine and sodium pyruvate were from GIBCO. Hygromycin, Penicillin/Streptomycin solution, Blasticidin and Zeocin were purchased from Invitrogen. Six-well plates, cell culture dishes and cryovials were from Corning Incorporated. Tetracycline was purchased from Bioline. As transfection reagents were used TransIT-LT1 fom Mirus and Lipofectamin RNAiMax from Invitrogen.

2.1.4 In-house reagents

Luria Bertani (LB) broth and LB agar plates supplemented with 200 μg/ml ampicillin as well as 10x Tris-buffered saline (TBS), 10x PBS and 50x Tris-acetate-EDTA (TAE) buffer were supplied by the University of Dundee media kitchen facility. The protein purification of recombinant human Flag-UBXN8, *Xenopus lavis* Flag-FANCI wild-type, *Xenopus lavis* Flag-FANCI S556D S559D S565D S596D, human UBA1 and UBE2T were carried out by the Protein Production and Assay Development (PPAD) team.

2.1.5 Plasmids

The plasmids used in this thesis are described in Table 2.2. Plasmids were constructed by Nicola Wood and Melanie Wightman (Cloning Team, DSTT, University of Dundee). The correctness of the construct sequences were verified by the DNA Sequencing Service (University of Dundee).

Table 2.2: Plasmids

DU Number	Expressed	Vector
DU20791	FLAG-UBXN8 isoform 1	pCMV
DU21722	FLAG-UBXN8 P238G	pCMV
DU20792	FLAG-UBXN8 isoform 2	pCMV
DU20793	FLAG-UBXN8 isoform 3	pCMV
DU22873	UBXN8-FLAG	pCMV
DU22749	HA-UBXN8	pCMV5D
DU22822	mCherry-UBXN8	pCMV5D
DU22439	FLAG-UBXN8 Iso1 Del aa 67-91	pCMV
DU22393	FLAG-UBXN8 isoform1	pcDNA5 FRT/TO
DU22394	FLAG-UBXN8 (P238G) isoform 1	pcDNA5 FRT/TO
DU22416	FLAG-UBXN8 isoform 3	pcNDA5 FRT/TO
DU24190	GST-TEV-Flag-UBXN8 aa92-270 (end)	pGEX
DU22438	GST-TEV-Flag-UBXN8 aa67-270 (end)	pGEX
DU20778	GST-UBXN8 isoform 1 67-270)	pGEX
DU20767	6His-UBXN8 67-270	pET
DU33156	FLAG-FANCI	pcDNA5-FRT/TO
DU24038	FLAG-FANCI R1285Q	pcDNA5-FRT/TO
DU33181	FLAG-FANCI K523R	pcDNA5-FRT/TO
DU33165	GFP-FANCI	pcDNA5-FRT/TO
DU22475	FLAG-FANCI S556D/S559D/S565D/S596D	pcDNA5-FRT/TO
DU22465	FLAG-FANCI S556A/S559A/S565A/S596A	pcDNA5-FRT/TO
DU22489	FLAG-FANCI S556D/S559D/S565D/S596D/S617D/S629D	pcDNA5-FRT/TO
DU22471	FLAG-FANCI S556A/S559A/S565A/S596A/S617A/S629A	pcDNA5 FRT/TO
DU22668	FLAG-FANCI K523R S556D S559D S565D S596D	pcDNA5 FRT/TO
DU22654	FLAG-FANCI K523R S556A S559A S565A S596A	pcDNA5 FRT/TO
DU22790	FLAG-FANCI K898E K980E	pcDNA5- FRT/TO
DU22791	FLAG-FANCI S556D S559D S565D S596D K898E K980E	pcDNA5- FRT/TO
DU22615	GST-Tev-FANCI	pGEX
DU22631	GST-Tev-FANCI S556D S559D S565D S596D	pGEX
DU22632	GST-Tev-FANCI S556A S559A S565A S596A	pGEX
DU22648	GST TEV FANCI	pGEX
DU22652	GST FANCI S556D S559D S565D S596D	pGEX
DU22653	GST TEV FANCI S556A S559A S565A S596A	pGEX
DU33428	GST-FANCI	pFB
DU25063	FLAG-FANCI (Xenopus)	pFastBac
DU25094	FLAG-FANCI S557A S560A S566A S597A (Xenopus)	pFB
DU25095	FLAG-FANCI S557D S560D S566D S597D (Xenopus)	pFB
DU20249	FLAG UBXD7	pCMV5
DU20281	FLAG UBXD7 (No ATG)	pCMV5
DU20293	FLAG UBXD7 P459G	pCMV5

DU21457	FLAG UBXD7 S297A (No ATG)	pCMV5
DU21458	FLAG UBXD7 A293Q (No ATG)	pCMV5
DU21459	FLAG UBXD7 S297H (No ATG)	pCMV5
DU20294	FLAG UBXD7 del UBA Domain	pCMV5
DU20296	FLAG UBXD7 del UAS Domain	pCMV5
DU20297	FLAG UBXD7 del UIM Domain	pCMV5
DU20258	FLAG CUL2	pCMV5
DU20288	FLAG CUL2 K689R	pCMV5
DU20291	FLAG CUL2 K719R	pCMV5
DU21544	FLAG-RAD23B	pCMV5

2.1.6 Small interfering (si) RNA oligos

All small interfering RNA oligos used in this thesis were purchased from Dharmacon. The sequences are listed in Table 2.3.

Table 2.3: Small interfering RNA oligos

Target protein	siRNA name	siRNA target sequence (5'-3')
UBXN8	UBXN8 ♯1	UUGACUGGAUGACGAGAAC
UBXN8	UBXN8 ♯2	AACUGAUGUUUGCGAUUUA
FANCI	FANCI	siGENOME SMARTpool
FANCD2	FANCD2	siGENOME SMARTpool
UBE2T	UBE2T	siGENOME SMARTpool
FAN1	FAN1-1	GUAAGGCUCUUUCAACGUA
Luciferase	Luc	CAUUCUAUCCUCUAGAGGAUG

2.1.7 Antibodies

Table 2.4 lists the source and catalogue numbers of all antibodies used in this thesis. In-house rabbit or sheep polyclonal antibodies were produced by the Division of Signal Transduction Therapy (DSTT, University of Dundee). Antisera were raised in sheep or rabbit by Diagnostics Scotland (Carluke - Lanarkshire, UK). All in-house antibodies were affinity purified on CH-Sepharose covalently coupled to the corresponding antigen.

The two anti-UBXN8 polyclonal antibodies were raised in rabbits using bacterially-expressed UBXN8 (amino acids 67-270). The anti-FANCD2 polyclonal antibodies were

raised in sheep using bacterially-expressed full-length FANCD2.

Table 2.4: Antibodies

Antibody	Catalogue No.	Source	Species
FK1 poly-Ubiquitin	BML-PW8805	BIOMOL (ENZO)	mouse
FK2 mono-poly Ubiquitin	BML-PW8810	BIOMOL (ENZO)	mouse
Flag M2	F3165	Sigma	mouse
p97	10R-P104A	Fitzgerald	mouse
Tubulin	T6199	Sigma	mouse
UFD1L	611642	BD	mouse
FANCD2	NB100-182	Novus	rabbit
FANCI	A301-254A	Bethyl	rabbit
FITC donkey anti-mouse IgG	751-095-151	Jackson Immuno Research	
Rhodamine Red donkey anti-rabbit IgG	711-296-152	Jackson Immuno Research	
Alexa Fluor® 594 Chicken Anti-Rabbit IgG (H+L)	A21442	Invitrogen	
Alexa Fluor® 488 Chicken Anti-Rabbit IgG (H+L)	A21441	Invitrogen	
CUL2	51-1800	Invitrogen	rabbit
Nedd8	341400	Invitrogen	rabbit
UBXN7		courtesy of Millipore	rabbit
UBXN8	R2823	DSTT	rabbit
UBXN8	R2824	DSTT	rabbit
FANCD2	S099D (3. Bleed)	DSTT	sheep
FAN1	S420C (4. Bleed)	DSTT	sheep
Elongin C	610760	BD Transduction Laboratories	mouse
VHL	sc-5575	Santa Cruz Biotechnology	rabbit
RBX1	PIPA529149	Thermo	rabbit
HIF1α	NB100-449	Novus	rabbit

2.1.8 Proteins

The proteins used in this thesis as well as the sources are described in Table 2.5.

Table 2.5: Proteins

Protein	Source
Human Flag-UBXN8 (62 – 260aa)	PPAD
Murine FANCD2	provided by KJ Patel Laboratory
Murine FANCI	provided by KJ Patel Laboratory
Xenopus lavis Flag-FANCI wild-type	PPAD
Xenopus lavis Flag-FANCI S557D S560D S566D S597D	PPAD
Xenopus lavis Flag-FANCD2 wild-type	provided by Helen Warden laboratory

Xenopus Tropicalis FANCL	provided by Helen Warden laboratory
Human UBE2T	PPAD
Human UBE1	PPAD
HA-Ubiquitin	Boston Biochem

PPAD: Protein Production and Assay Development in the ubiquitylation system

2.1.9 Buffers and solutions

The following buffers were used in this thesis:

- **IP lysisbuffer (milder to preserve protein-protein interactions):** 50 mM HEPES/KOH pH 7.2, 5 mM $Mg(OAc)_2$, 70 mM KOAc, 0.2% Triton X-100, 10% Glycerol, 0.2 mM EDTA (add fresh protease inhibitors and 750 Units (U)/ml benzonase)
- **Extracts lysisbuffer (stronger – mainly used for extracts):** 50 mM HEPES (pH 7.2), 400 mM NaCl, 1% NP-40, 0.2 mM EDTA, 10% Glycerol (add fresh protease inhibitors)
- **CSK buffer (pre-extraction for immunofluorescence microscopy):** 100 mM NaCl, 300 mM Sucrose, 10 mM PIPES pH7, 3 mM $MgCl_2$, 1 mM EGTA (add fresh 0.5% Triton X-100 and protease inhibitors)
- ***In vitro* binding buffer:** 50 mM HEPES/KOH, pH 7.5, 60 mM KOAc, 5 mM $MgCl_2$, 5 % glycerol, 0.1 % Triton X-100
- ***In vitro* ubiquitylation buffer:** 50 mM Tris pH 7, 100 mM KCl, 2 mM $MgCl_2$, 2 mM ATP and 0.5 mM DTT
- **3x SDS Sample Buffer:** 187.5 mM Tris-HCl (pH 6.8), 6% SDS, 30% Glycerol, Bromphenolblue
- **10x SDS Running Buffer :** 250 mM Tris-HCl, 1.92 M glycine, 0.1% (w/v) SDS
- **25x Novex® Tris-Glycine Transfer Buffer:** 300 mM Tris-Base (pH 8.3), 2.4 M glycine

- **6x DNA gel loading dye:** 75% Glycerol, Bromphenolblue
- **Tris buffered saline (TBS):** 50 mM Tris/HCl pH 7.6, 150 mM NaCl
- **Phosphate-buffered saline (PBS) (1x):** 137 mM NaCl, 2.7 mM KCl, 4.3 mM Na_2HPO_4, 1.47 mM KH_2PO_4. Final pH was adjusted to pH 7.4
- **TBS-Tween Buffer:** 1x TBS, 0.2% (v/v) Tween
- **Blocking Buffer:** 5% milk or 1% BSA in 1x TBS, 0.1% (v/v) Tween
- **Staining Solution for FACS sample:** 1% FBS/PBS with 50 μg/ml propidium iodide, 50 μg/ml ribonuclease A
- **Fixing Solution for Silver Staining:** 30% ethanol, 10% acetic acid

2.2 Methods

2.2.1 Molecular Biology Methods

2.2.1.1 Transformation of Escherichia coli cells

Competent *Escherichia coli* (*E. coli*) DH5α cells were obtained from the DSTT and stored at -80°C. For the transfection, 30 µl aliquots were thawed on ice and mixed with approximately 100 ng plasmid DNA. The cells were incubated on ice for 10 min. To facilitate the uptake of DNA, cells were heat-shocked at 42°C for 1 min and were placed back on ice for 1 min. Finally, the cells were diluted with 1 ml LB medium and 50–100 µl streaked onto LB agar plates containing 200 µg/ml ampicillin. Plates were then incubated overnight at 37°C to allow colony growth.

2.2.1.2 Preparation of plasmid DNA from bacteria

To prepare small amounts of plasmid DNA in microgram quantities (termed 'mini-prep'), *E. coli* DH5α cells were transformed with plasmid DNA, and a single colony was inoculated in LB/ ampicillin (5 ml). The transformed cells were grown in LB media containing appropriate antibiotics to stationary phase by incubation at 37°C overnight in a shaking incubator. The cells were harvested by centrifugation (4000 rpm, 15min) and the plasmid DNA purified using the Qiagen plasmid MiniPrep kit according to the manufacturer's instructions. The DNA was eluted in elution buffer (EB) (60 µl) and the typical yield achieved was around 30 µg of plasmid DNA.

To prepare larger quantities of plasmid DNA, transformed *E. coli* DH5α were cultured in 300 ml LB containing 200 µg/ml ampicillin at 37°C while shaking at 200 rpm overnight. Cells were pelleted by centrifugation at 4000 rpm for 15 min. Plasmid DNA

was purified using the NucleoBond Xtra Maxi Plus Kit (Machery-Nagel) according to the manufacturer's instructions. Overnight cultures of 300 ml typically yielded 1.5–2 mg of plasmid DNA.

2.2.1.3 Determination of DNA concentration

The absorbance of DNA in EB buffer was measured via NanoDrop using the $OD_{260/280}$ of EB buffer as zero. The integrity of plasmid DNA was assessed by agarose gel electrophoresis.

2.2.1.4 DNA agarose gels

The size and the purity of plasmids were verified by agarose gels electrophoresis (1% agarose) containing ethidium bromide (0.2 μg/ml). The gels were placed in an agarose gel tank filled with 1x TAE running buffer. The plasmid DNA was mixed with DNA loading dye (1x) and loaded onto the agarose gel. The Quick load DNA ladder (1kbp) from BioLabs was used as a standard. Gels were run at 100 V for approximately 30 min. DNA/ethidium bromide complexes were visualised using a UV transilluminator.

2.2.1.5 DNA sequencing

Sequencing of plasmid DNA was performed by The Sequencing Service, School of Life Sciences, University of Dundee, using DYEnamic ET terminator chemistry (Amersham Pharmacia Biotech) on Applied Biosystems automated DNA sequencers.

2.2.2 Mammalian Cell Culture

2.2.2.1 Cell culture

All procedures were carried out under aseptic conditions meeting biological safety category 2. The media and buffers used for mammalian cell culture were pre-warmed to 37ºC prior to use. Cells were cultured and maintained at 37ºC in a 5% CO_2 water-saturated incubator. For the routine maintenance of the different cell lines, cells were grown until 80-90% confluency, washed with sterile PBS, detached with Trypsin/EDTA (3 min at 37ºC) and transferred into fresh plates.

HeLa cells were maintained in MEM containing 10% fetal bovine serum, 1% penicillin/streptomycin, 1% L-glutamine, and 1% sodium pyruvate. U2OS cells were maintained in McCoy's 5A medium containing 10% fetal bovine serum, 1% penicillin/streptomycin, and 1% L-glutamine.

2.2.2.2 Cell counting using a haemocytometer

Cells were detached with Trypsin/EDTA as described before and pelleted by centrifugation at 1000 rpm for 4 min. The cell pellet was re-suspended in growth media. To differentiate between cells that are alive or dead, 50 µl of cell suspension was added to 50 µl of trypan-blue, and 10 µl of this mixture was placed on a haemocytometer. Cells within a 1 mm^2 area, delimited by a double line (9 small squares) were counted. Four 1 mm^2 areas were counted. Cells stained by trypan-blue represented dead cells and were not counted. The counted cell number was divided by the number of counted areas and multiplied by the dilution factor and 10^4, providing the total number of cells per ml.

2.2.2.3 Freezing / thawing cells

Cells (approximately 70% confluent) were detached with Trypsin/EDTA and pelleted by centrifugation at 1000 rpm for 4 min. The supernatant was aspirated and the cells were resuspended in growth media supplemented with 10% DMSO. Aliquots of cell suspension (1 ml) were transferred into 1.5 ml cryogenic screw top vials (Corning) and stored at -80°C in an insulated box for 24h, before transfer to the liquid nitrogen cell freezer.

Cells were thawed in a 37°C water bath, plated into fresh growth medium and allowed to adhere overnight prior to medium change.

2.2.2.4 Plasmid transfection of mammalian cells

Transient transfection of HeLa and U2OS cells was performed using TransIT-LT1 according to the manufacturer's instructions. Cells were grown to 50-60% confluency for transfection. For the transfection of cells growing in a 15 cm dish, 20 µl TransIT-LT1 were diluted in 3 ml OptiMEM and incubated for 10 min. Then 10 µg plasmid was added, mixed and incubated for an additional 20 min at RT before the transfection mix was evenly distributed into the 15 cm dish containing 20 ml media without antibiotics. After 24h, cells were further treated with e.g. cisplatin or harvest post plasmid transfection.

2.2.2.5 siRNA transfection of mammalian cells

The siRNA oligonucleotides were purchased from Dharmacon and 5 nM siRNA/plate transfected into HeLa cells using Lipofectamine RNAiMax (Invitrogen) according to the manufacturer's instructions. The cells were lysed 48 - 72 h after siRNA transfection.

2.2.2.6 Generation of stable cell lines

To ensure low-level uniform expression of recombinant proteins, manufacturer's instructions (Invitrogen) were followed to generate stable cell lines that express FLAG-tagged forms of proteins (cDNA subcloned into pcDNA5-FRT/TO plasmid) in a tetracycline inducible manner. Flp-In T-Rex U2OS host cells containing integrated FRT recombination site sequences and Tet repressor were co-transfected with 9 μg of pOG44 plasmid (which constitutively expresses the Flp recombinase) and 1 μg of pcDNA5-FRT/TO vector containing a hygromycin resistance gene for selection of the gene of interest with FLAG tag under the control of a tetracycline-regulated promoter. Cells were selected for hygromycin and blasticidin resistance two days after transfection by adding new medium containing hygromycin (100 μg/ml) and blasticidin (15 μg/ml). To have a cell population with homogneous expression, the cells were colony purified. For this purpose, the cells were seeded in a low density and grown for 8 days to allow colony formation. The colonies were then trypsinized and expanded. The homogenous expression of the integrated gene was validated by microscopy. Expression of the protein was induced with tetracycline for 12-24 hours.

2.2.2.7 Cell treatment with genotoxins

Cells were treated with a variety of genotoxins at a range of concentrations as indicated. Cisplatin and MG132 were dissolved in DMSO to make 33.3 mM and 20 μM stock solutions, respectively. MMC was dissolved in Milli-Q water to make a 0.5 mg/ml stock solution. All three drugs were stored at -80^{o}C. Stock solutions of thymidine, hydroxyurea or nocodazole were made fresh in water.

Cells were treated with 1 μM MMC for 24h, 3 μM cisplatin for 24h, 1 mM Hydroxyurea for 24h, 10 μM MG132 for 2h, 2.5 mM thymidine for 24h, or 40 ng/ml nocodazole for 12h, unless indicated otherwise.

2.2.2.8 Preparation of protein extracts from mammalian cells

Cells were detached with Trypsin/EDTA, pelleted by centrifugation at 1000 rpm for 4 min and washed twice with cold 1x PBS. The cell pellet was resuspend in lysis buffer containing protease inhibitors. The experiments performed for the UBXN8 project, 750 U/ml benzonase was freshly added to the lysis buffer to allow the efficient extraction of DNA-bound proteins. The lysis was performed for 30 min on the rotator at 4°C. The lysate was centrifuged at 13 000 rpm for 10 min to pellet the debris. The supernatant was either used for immunoprecipitations or 3x SDS sample buffer was added to denature the protein. In case of the UBXN7 experiments, the samples were incubated 20 min at 37°C prior loading on the polyacrylamide gel. For the UBXN8 project, the samples were incubated 5–10 min at 70°C prior loading.

2.2.3 Protein Biochemistry

2.2.3.1 Recombinant protein expression and purification

The Protein Production and Assay Development Team (PPAD) produced the various recombinant proteins in bacteria, as follows.

Expression vectors for full length, UBA- or UIM-deleted UBXN7 were transformed into BL21 DE3 cells. Overnight cultures were grown in LB medium (1% tryptone, 0.5% yeast extract, 1% NaCl) supplemented with carbenicillin. Autoinduction medium was inoculated and the cells were left to grow at 37°C until the OD_{600} reached about 1.5.

The temperature was then dropped to 15°C and the cells were left for about 16 hours to express the protein. The cells were collected by centrifugation and resuspended in 50 mM Tris-HCl pH 7.5, 250 mM NaCl, 0.4% Triton X-100, 0.1 mM EDTA, 0.1 mM EGTA, 1 mM DTT and protease inhibitors. The suspension was sonicated and the insoluble material was pelleted by centrifugation at 4°C, 28,000 g for 20 min. The supernatant was incubated with Glutathione (GSH)-sepharose for one hour. The sepharose was washed four times and UBXN7 was recovered upon cleavage with Tobacco etch virus (TEV) protease. The proteins were further purified by chromatography over a Superdex 75 column after which protein purity exceeded 90%.
The dual expression vector encoding GST-CUL2/HIS6-RBX1 was used to generate recombinant baculoviruses using the Bac-to-Bac system (Invitrogen) following the manufacturer's protocol. These baculoviruses were used to infect Spodoptera frugiperda 21 cells (1.5 ×106/ml) at a multiplicity of infection of 5 and the infected cells were harvested 48 hours post-infection. GST-CUL2/RBX1 was purified on GSH-Sepharose and dialysed into 50 mM Tris-HCl pH 7.5, 0.1 mM EGTA, 150 mM NaCl, 270 mM sucrose, 0.03% Brij-35, 0.1% 2-mercaptoethanol, 1 mM benzamidine, 0.1 mM PMSF.

BL21 cells were transformed with pGEX-TEV-FLAG-UBXN8 (67-270) DU22438. A clone was picked and grown overnight, in LB medium supplemented with 50µg/ml carbenicillin. Two litre cultures were set up and grown to OD_{600}= 0.6. Expression was induced by supplementing the medium with 0.5 mM IPTG (Isopropyl β-D-thiogalactopyranoside) and further grown for 16h at 15ºC. The cells were collected by sedimentation for 15 min at 4ºC in a Beckmann J6 centrifuge. The cells were resuspened in the buffer: 50 mM Tris/HCl pH 7.5, 250 mM NaCl, 0.5% Triton, 0.5 mM EDTA, 0.5 mM EGTA, 1 mM Pefabloc, 10 µg/ml Leupeptin, 1 mM DTT. The lysate

was sonicated and insoluble material was removed by centrifugation for 20 min at 40000 x g. The supernatant was incubated with 2 ml GSH-Sepharose for 1h at 4ºC and then washed 5 times with 12 ml 50 mM Tris/HCl pH 7.5; 250mM NaCl; 0.5% Triton; 1mM DTT. The GSH beads were incubated with 150 ug of TEV-protease for 2 hours at room temperature in 50 mM HEPES pH 7.5, 150 mM NaCl, 10 % glycerol, 1 mM DTT. The beads were washed 3 times with 1 ml of ubiquigent buffer + 0.03% Brij-35 to collect all cleaved material. This gave 5.5 ml at 2.4 mg/ml (13.2 mg). The protein was incubated for a further hour with 1 ml GSH beads to deplete the eluate of partially cleaved material and other contaminants. This gave 5.5 ml at 2.2 mg/ml (12.1 mg). The protein was left on ice over night. The following morning, it was slowly concentrated down to 2.1 ml using a 10 kDa MWCO filter. There was slight precipitation, but this was centrifuged into a small pellet and the sample was chromatographed on a SD75 column, which had been pre-equilibrated with 50 mM HEPES, pH 7.5, 150 mM NaCl, 10% glycerol, 0.03% Brij-35, 1 mM DTT. There were 2 peaks one with an apex at 50.5 ml and a second with an apex at 65 ml, the latter of which is dimerised UBXN8. Each peak was pooled and vialed separately.

Xenopus Flag-FANCI wild type and the phospho-mimicking mutant 4SD (S557D S560D S566D S597D) were expressed in insect express SF21 cells (Invitrogen) using the Sf900II virus (Invitrogen). Cells were collected by centrifugation at 3500 rpm for 15 min. The sediment was resuspended in 25 ml of 50 mM HEPES, pH 7.4, 150 mM NaCl, 0.1 mM EDTA, 0.1 mM EGTA, 0.2% Triton. After lysis, the cell suspension was diluted to 80 ml and spun at 40 000 x g for 20 min. Clarified lysate was incubated with 500 µl of pre-equilibrated anti-FLAG-M2 affinity gel for 1.5 h at 4ºC. Resin was washed 3 times with 12 ml of 50 mM HEPES, pH 7.5, 500 mM NaCl, 0.03% Brij-35

and twice with 50 mM HEPES, 150 mM NaCl, 0.03% Brij-35. The pulldown was repeated with fresh resin, because the protein yield was somewhat low, due to restricted resin capacity. Bound protein was eluted using 3 x 500 µl of FLAG peptide (100 µg/ml) in 50 mM HEPES pH 7.5, 150 mM NaCl, 0.03% Brij-35. The first elution was 1.2 h and the other elution 30 min. All protein was recovered with three elutions and the subsequent elutions diluted the prep to 0.11 mg/ml.

2.2.3.2 Determination of protein concentrations

Protein concentrations were measured by the Bradford method (Bradford, 1976). A standard curve was prepared according to the manufacturer's protocol, by adding increasing amounts of BSA (0.5, 1, 2, 3, 4, 6, 8 and 10 µg) to a final volume of 1 ml Bradford reagent. The mixture was allowed to stand at room temperature for 5 min. The optical density of the standards was measured at 595 nm (OD_{595}) in 1.5 ml plastic cuvettes against a reference cuvette containing Bradford reagent only. This was used to construct a standard curve that was employed to determine protein concentrations of cell lysates. On average the linear range of protein Bradford measurements lies between OD_{595} 0.1 and OD_{595} 0.3.

2.2.3.3 Size exclusion chromatography and multi angle light scattering

Size exclusion chromatography and multi-angle light scattering (SEC–MALS) experiments were performed on a Dionex Ultimate 3000 HPLC system with an inline Wyatt miniDAWN TREOS MALS detector and Optilab T-rEX refractive index detector. 50uLs of 2 mg/mL of protein was injected into Superdex S75 CL 10/300 (GE Healthcare) column. Buffer conditions were 40mM Tris pH 7.5 and 150mM sodium

chloride. Molar masses spanning elution peaks were calculated with ASTRA v6.0.0.108 (Wyatt).

2.2.3.4 Covalent coupling of antibodies to Protein A Sepharose

Protein A-Sepharose [500 µl] was incubated with 200 µg anti-UBXN7 antibody for 2 h at room temperature to allow the antibodies to bind protein A (non-covalently). After washing with 10 ml 1x PBS and 10 ml 0.2 M Na-borate pH 9, the beads were incubated with 5 ml of 20 mM DMP (in Na-borate pH 9) to crosslink the antibody to protein A. The reaction was stopped after 30 min by washing the beads twice with 10 ml of 0.2 M ethanolamine pH 8. The beads were then incubated 2h with 5 ml 0.2 M ethanolamine pH 8. After incubation, the beads were briefly washed with 100 mM glycine pH 2.8 to remove the antibody that is not covalently bound, followed by three washes with 10 ml 50 mM Na-borate pH 9 to equilibrate the pH and two washes with 10 ml 1x PBS. The beads were resuspended in PBS with 0.02% sodium azide and stored at 4°C. The efficiency of the coupling was investigated by silver staining.

2.2.3.5 Immunoprecipitation

For immunoprecipitation experiments, the cells were lysed in IP lysis buffer containing 50 mM HEPES/KOH (pH 7.5), 5 mM $Mg(OAc)_2$, 70 mM KOAc, 0.2% Triton X-100, 10% glycerol, 0.2 mM EDTA and protease inhibitors. To pull down Flag-tagged proteins, 60 µl anti-Flag M2 agarose (Sigma) 50% slurry was added to 2–3 mg total cell lysate and incubated for 2 h at 4°C. To pull down endogenous UBXN7, 60 µl anti-UBXN7 beads were added to the lysis buffer and incubated for 2h at 4°C. To pull down endogenous FANCD2, 1 µg anti-FANCD2 antibody (S099D, 3. Bleed) was added to 1

mg lysate and incubated for 90 min at the rotator at 4°C. 70 µl Protein-A Sepharose beads (50% slurry) were added to the antibody-lysate mix and were incubated for additional 1h at 4°C.

After incubating the beads with the lysate, the beads were washed three times with lysis buffer. The beads were then transferred to a Spin Chromatography column (BioRad). The column was closed and the beads incubated with 60 µl 3x SDS-Sample buffer for 10 min at room temperature. The column was opened after incubation and the eluates collected by centrifugation. 4 µl β-mercaptoethanol was added to the samples, which were then heated at 70°C for 10 min before loaded on the gel.

2.2.3.6 Separation of proteins by sodium dodecyl sulphate (SDS)-polyacrylamide gel electrophoresis (PAGE)

Protein samples were denatured in SDS sample buffer (1x) and β-mercaptoethanol (2% (v/v)). Samples were boiled at 70°C for 5-10 min before loading onto polyacrylamide gels.

For FANCD2-detection, the samples were separated in NuPAGE 3-8% Tris-Acetate pre-cast gels in 1x Tris-Acetate running buffer. To allow the separation of the modified and unmodified form of FANCD2, the gels were run for 30 min at 80V followed by 2h at 160V. For FANCI detection, the samples were separated in Novex 4-20% Tris-Glycine pre-cast gels in 1x Novex Tris-Glycine runing Buffer. To allow the separation of the modified and unmodified form of FANCI, the gels were run at constant 24 mA current for 2h 15min. The detection of the other proteins was performed using Novex 4-20% or 8% Tris-Glycine gels, which were run at 24 mA for 1h 30min.

2.2.3.7 Staining of protein gels

Coomassie

To visualize proteins after SDS-PAGE, gels were stained in Coomassie stain for 60 min at room temperature with continual agitation on a rocking platform.

Silver staining

Silver staining was performed using Pierce Silver Stain Kit following the manufacture's protocol. The gel was stored in ultrapure water or dried using the DryEase Mini-Gel Drying system (Invitrogen).

2.2.3.8 Transfer of proteins to nitrocellulose membrane

Protein gels were assembled into a gel-membrane sandwich as described in the manufacturer's protocol. Nitrocellulose membrane was placed on a gel, this assembly was placed between two pieces of filter paper (3MM), and this structure placed between two sponges. All components were pre-soaked in transfer buffer. This assembly was placed into a BioRad cell-tank filled with transfer buffer, and proteins were transferred to nitrocellulose at 150 mA for 2h.

2.2.3.9 Immunoblotting

The nitrocellulose membranes were blocked in TBS-T containing skimmed milk (5% (w/v)) for 45 min at room temperature. Primary antibodies were diluted in TBS-T containing 5% (w/v) skimmed milk, and incubated with the membrane for 1h or o/n. After the incubation with the primary antibodies, membranes were washed, and incubated with secondary antibodies conjugated to HRP for 45 min at room temperature. All secondary antibodies were used at 1:3000 dilutions in TBS-T

containing 5% (w/v) skimmed milk. After washing three times for 10 min with TBS-T, membranes were developed with ECL reagent. The membrane was covered with a clean piece of polythene roll and placed into a film cassette. The membrane was then exposed to Kodak BioRad films (strong signals) or Amersham Hyperfilm^{TM} ECL films (weak signals) and developed in an automatic processor.

2.2.4 In vitro Assays

2.2.4.1 In vitro binding assays

The *in vitro* binding assays were performed with recombinant Flag-UBXN8 (62-270aa) and murine FANCD2 and FANCI (provided by Michael Hodskinson/KJ Patel Laboratory). The binding assay was performed in 400 µl *in vitro* binding buffer. For the assays, fixed amounts of Flag-UBXN8 were incubated with increasing molar ratios of monomeric FANCD2 or FANCI. 0.1 µM Flag-UBXN8 was incubated with 0.01 µM, 0.025 µM, 0.05 µM and 0.1 µM monomeric murine FANCD2 or FANCI. 20 µl sample were taken as input, diluted with 20 µl buffer and 20 µl 3x SDS sample buffer. 20 µl anti-Flag beads (50% slurry) were added 30 min after adding Flag-UBXN8 and the protein-beads mix was incubated for an additional one hour. 20 µl sample were taken to determine efficiency of the immunoprecipitation and were processed as the input sample described before. The beads were washed 3x with 1 ml *in vitro* binding buffer and Flag-UBXN8 eluted from the beads using 60 µl 3x SDS Sample buffer. All samples were heated at 70°C before loading on the gel.

2.2.4.2 In vitro ubiquitylation assays

The ubiquitylation assay was performed to study the mono-ubiquitylation of FANCD2 and FANCI in the presence of Flag-UBXN8.

The 25 µl reactions were performed in reaction buffer 50 mM Tris pH 7, 100 mM KCl, 2 mM $MgCl_2$, 2 mM ATP and 0.5 mM DTT. The following proteins were included in the assay: 13 nM UBE1, 640 nM human UBE2T, 5.6 µM HA-ubiquitin (Boston Biochem), 1.5 µM *Xenopus Tropicalis* FANCL, 0.2 µM *Xenopus lavis* Flag-FANCD2 and/or 0.2 µM *Xenopus lavis* Flag-FANCI. When indicated 0.5, 2 or 4 µM human Flag-UBXN8 was added to the reaction. The reactions were incubated at 25°C for 90 min and then stopped by adding 12.5 µl 3x SDS Sample buffer containing β-mercaptoethanol. 5 µl of each sample were analysed by Western Blot. The immunoblotting was performed using anti-HA and anti-Flag antibodies.

2.2.5 Mass Spectrometry

2.2.5.1 Sample preparation

For the Mass Spectrometry (MS) analysis, the immunorecipitations were performed as described in section 2.2.3.4 with small changes. After washing the beads three times with lysis buffer, the beads were washed an additional two times with 100 mM Tris-HCl, pH 8.5. Bound-proteins were eluted by incubating the beads with 8 M Urea (saturated) in 100 mM Tris-HCl, pH 8.5 for 15 min at 37°C.

<u>Trypsin-digestion in solution</u>

The eluted proteins (40 µl) were reduced by incubating with 3 mM TCEP for 20 min and then alkylated with 11 mM iodoacetamide for 15 min. Both incubations were

performed at room temperature and in the dark. The samples were pre-digested with 0.1 µg Lys-C for 4 h at 37°C. The Samples were then diluted to the final concentration of 2 M urea by adding 100 mM Tris-HCl, pH 8.5. To enhance trypsin activity 100 mM $CaCl_2$ was added to a final concentration of 1 mM $CaCl_2$ and then 0.5 µg/µl trypsin added. Trypsin-digestion was performed at 37°C for 16h. The digested peptides were acidified to pH < 3 using 1% trifluoroacetic acid (TFA) and then purified using C18 Silicia microspin columns. The peptides were eluted in 0.1% TFA, 50% acetonitrile (ACN), dried in Speed-Vac and stored at -80°C till required.

In-gel trypsin digestion

The protein bands were excised from the silver stained gel using a sterile scalpel. The protein bands were destained using the 'Silver Stain Kit' from Pierce following the manufacture's protocol. Once colourless, the gel pieces were shrunk with 0.3 ml ACN for 15 min, the ACN was then removed and were dried using a Speed-Vac. Gel pieces were then swollen in 30 µl 25 mM Triethylammonium bicarbonate containing 5 µg/ml trypsin and incubated over-night at 30^{o}C on a shaker. After 14h an equivalent volume of ACN was added to the digest and incubated for a further 15 min. The supernatants were transferred to a clean tube, frozen using dry ice and concentrated to dryness by Speed Vac. Meanwhile 100 µl 50% ACN/2.5% formic acid was added to the gel pieces. This second extraction was combined with the dried first extract. The samples were stored at -20^{o}C.

2.2.5.2 Mass Spectrometry analysis

Patrick Pedrioli's group performed the MS analysis for the samples that were trypsin-digested in solution. The dried pellets were resuspended in 20 µl 0.1% (v/v) TFA and separated on a Dionex UltiMate 3000 LC system (Thermo Scientific) using a 25 cm

column packed with 3 mm Magic C18 material (Michrom Bioresource). Mass spectra were acquired on an LTQ Orbitrap Velos mass spectrometer (Thermo Scentific) operating in data-dependent mode. After conversion to mzXML the raw data were searched using Comet against version 3.87 of the IPI human protein database using static carboxamidomethylation of cysteine residues, variable oxidation of methionine residues and accounting for up to 2 missed tryptic cleavages.

Matthias Trost's group performed the MS analysis for the samples that were in-gel trypsin digested. The MS analysis was performed by LC-MS-MS using a linear ion trap-orbitrap hybrid mass spectrometer (Orbitrap-Classic, Thermo) equipped with a nanoelectrospray ion source (Thermo) and coupled to a Proxeon EASY-nLC system. Peptides were injected onto a Thermo (Part No. 160321) Acclaim PepMap100 reverse phase C_{18} 3 μm column, 75 μm x 15 cm, with a flow of 300 nl/min and eluted with a 30 min linear gradient of 95% solvent A (2% ACN, 0.1% formic acid in H_2O) to 40% solvent B (90% acetonitrile, 0.08% formic acid in H_2O), followed by a rise to 80%B at 32min. The instrument was operated with the "lock mass" option to improve the mass accuracy of precursor ions and data were acquired in the data-dependent mode, automatically switching between MS and MS-MS acquisition. Full scan spectra (m/z 340-1800) were acquired in the orbitrap with resolution R = 60,000 at m/z 400 (after accumulation to an FTMS Full AGC Target; 1,000,000; MSn AGC Target; 100,000). The 5 most intense ions, above a specified minimum signal threshold (5,000), based upon a low resolution (R = 15,000) preview of the survey scan, were fragmented by collision induced dissociation and recorded in the linear ion trap (Full AGC Target; 30,000. MSn AGC Target; 5,000).

2.2.6 Other methods

2.2.6.1 Measurement of genotoxin hypersensitivity of mammalian cells by clonogenic survival assay

U2OS cells grown in 10 cm dishes were transfected with the indicated siRNA duplexes according to the protocol described in 2.2.2.1. After 48 h cells were counted using a haemocytometer and seeded into new 10 cm^2 dishes at approximately 2000 - 4000 cells per dish. Cells were allowed to adhere to the dish for a minimum of 8h before they were treated with the DNA damage-inducing agent cisplatin or MMC. Cells were incubated with the drugs for 24h before the media was exchanged with fresh drug free media. The cells were then incubated for 10 days to allow colony formation of surviving cells. To count the colonies, the media was removed and the cells were dried overnight. The following day, the cells were fixed and stained with 2% Giemsa (in methanol) and washed with tap water. Colonies of more than 50 cells were counted.

2.2.6.2 Cell cycle analysis by flow cytometry

Cells were harvested using standard trypsinisation, washed once in PBS and resuspended in ice-cold 70% (v/v) ethanol while vortexing. Samples were then stored at -20°C until required. To prepare samples further for the cell cycle analysis by flow cytometry, samples were brought to room temperature and washed twice in PBS with 1% (w/v) FBS. After washing, the cells were resuspended in 300–500 µl PBS containing 1% (w/v) FBS, 50 µg/ml propidium iodide, and 50 µg/ml ribonuclease A. Samples were then incubated at room temperature for 20 min in the dark. The DNA content of cells was quantified on the basis of propidium iodide fluorescence using a FACSCalibur flow cytometer (BD Biosciences) and CellQuest software for data

acquisition. Red fluorescence (585±42 nm) was acquired on a linear scale, and pulse width analysis was used to exclude doublets. Cell cycle distribution was determined by applying the Watson (pragmatic) model for cell cycle distribution using FlowJo software (Tree Star Inc.).

2.2.6.3 Immunoflourescence microscopy

Cells were grown on sterile coverslips in 6-well plates. For FANCD2 immunostaining, the cells were fixed with 2% Paraformaldehyde for 10 min and permeabilized with 0.2% Triton X-100 for 10 min. For Flag-UBXN8 and Flag-UBXN7 immunostaining, the cells were fixed with ice-cold methanol at -20°C for at least 8 min. After fixation/permeablisation, cells were blocked in 3% BSA/PBS for 30 min at room temperature and subsequently incubated with primary antibodies: 1:300 mouse M2 anti-Flag primary antibody, 1:5000 anti-Lamin B1, or 1:1000 anti-FANCD2 (in 3% BSA/PBS) for 1hr at room temperature. After washing with 1x PBS, cells were incubated with the secondary antibody for 45 min at room temperature. In case of co-immunostaining, the cells were incubated with the first primary and secondary followed by the second primary and secondary. The cell nuclei were stained with DAPI. The coverslips were mounted onto glass slide using Hydromount mounting media.

Images were obtained with a DeltaVision Spectris microscope (Applied Precision), using a CoolSNAP HQ camera (Roper) and a 60x 1.4 numerical aperture (NA) objective (Olympus). SoftWoRx software (Applied Precision) was used for acquisition and deconvolution.

3D-SIM images were acquired on a DeltaVision OMX Blaze (GE Healthcare) fitted with an Olympus PlanApo N 60x 1.42 NA oil objective. Laser light from solid state

lasers (405, 488 and 564nm), shuttered by high-speed tilt mirrors and coupled into a broadband single mode optical fibre was split into three beams. 3D interference pattern in the sample plane are generated by focusing of the beams onto the back focal plane of the objective lens. Striped illumination patters are shifted by five phase steps and rotated by 3 angles (-60˚, 0˚ and +60˚), providing a set of 15 images per unprocessed z-section.

Interference patterns were phase shifted by directing the outer two beams through a separate pair of windows with individual tilt control. Phase of the interference pattern at the sample plane was shifted due to the change in the path length for the respective outer beam, while lateral refractive beam translation was canceled by tilting a given window pair in complementary directions. Angles of pattern orientation were shifted by a tilt mirror, directing the three beams pattern to one of three mirror clusters; the beam pattern from each of the three rotation paths was redirected back to a common exit path by reflecting a second time from the tilt mirror.

Exposure times were typically between 100 and 200 ms, and the power of each laser was adjusted to achieve optimal intensities of between 1,000 and 3,000 counts in a raw image of 15-bit dynamic range of Edge sCMOS camera (PCO AG, Germany). The lowest possible laser power was chosen for each channel to minimize photo bleaching. Unprocessed image stacks were composed of 15 images per z-section (five phase-shifted images per each of three interference pattern angles). The microscope was routinely calibrated by measuring of channel specific optical transfer functions (OTFs) to optimise lateral and axial image resolution (channel dependent and typically ~120 and ~300nm, resp.). Super-resolution three-dimensional image stacks were reconstructed with SoftWoRx 6.0 (GE) using channel specific OTFs and Wiener filter setting of 0.002 (0.005 for the DAPI channel) to generate a super-resolution three-

dimensional image stack. Images from the different colour channels, recorded on separate cameras, were registered with SoftWorx 6.0 alignment tool (GE), based on alignment parameters obtained from calibration measurements with 100nm-diameter TetraSpeck beads (Life Technologies).

Chapter 3

3. UBXN7 docks on neddylated cullin complexes using its UIM and causes HIF1α accumulation (Bandau et al., 2012)

3.1 Introduction

The proteins from the UBA–UBX family interact with ubiquitylated proteins via their UBA domain and with p97 via their UBX domain, thereby acting as substrate-binding adaptor for the p97 ATPase (Alexandru et al., 2008).

Alexandru et al. (2008) established that the UBA-UBX protein UBXN7 mediates the interaction between p97 and the transcription factor HIF1α that is continuously expressed and is actively targeted for ubiquitin-mediated degradation through the CRL2 complex during normoxia. Furthermore, the MS analysis of UBA-UBX protein immunoprecipitates showed that they interact with a multitude of E3 ubiquitin ligases. Among human UBA-UBX proteins, UBXN7 is the most proficient in interacting with CRL subunits, in particular CUL2. It was shown that the interaction between UBXN7 and CUL2 does not depend on p97. Therefore, the aim of this project was to determine whether UBXN7 interaction with cullins is direct or mediated by its ubiquitylated targets bound to the UBA domain.

3.2. Results

3.2.1 Endogenous UBXN7 stably interacts with the core subunits of the CRL2 complex

As described in the introduction, all core CRL2 subunits (CUL2, elongin B/C, RBX1 and VHL) have been identified in Flag-UBXN7 immunoprecipitates by mass spectrometry (Alexandru et al., 2008). The Flag-UBXN7 interactions with CUL2, VHL and the CRL2 substrate HIF1α were analysed further by Western blotting. The UBXN7 binding to CUL2 was unaffected by inhibition of the proteasome suggesting a substrate independent regulation. In contrast, the UBXN7 interaction with VHL and HIF1α was only be observed upon brief proteasome inhibition. The interaction between UBXN7 and the remaining CRL2 complex component was not analysed further (Alexandru et al., 2008).

To confirm the interactions between the endogenous UBXN7 and all CRL2 subunits including its substrate HIF1α, endogenous UBXN7 was immunoprecipitated from HeLa cells using UBXN7-specific antibodies. The cells were grown in the presence or absence of proteasome inhibition (10 μM MG132, 2h), to allow the detection of VHL and the CRL2 substrate HIF1α (constitutively degraded under normoxia conditions).

Endogenous UBXN7 effectively co-immunoprecipitated CUL2, elongin C and RBX1, which constitute the core CRL2 complex (Figure 3.1). Consistent with the results obtained upon UBXN7 overexpression, endogenous UBXN7 interacts with VHL and polyubiquitylated-HIF1α only upon brief inhibition of the proteasome. Thus, the results suggest that the UBXN7 interactions with CUL2, elongin C and RBX1, which constitute the core CRL2 complex, are more stable compared to the UBXN7 interaction

with VHL and HIF1α, which seem to be more transient and can only be captured after proteasome inhibition.

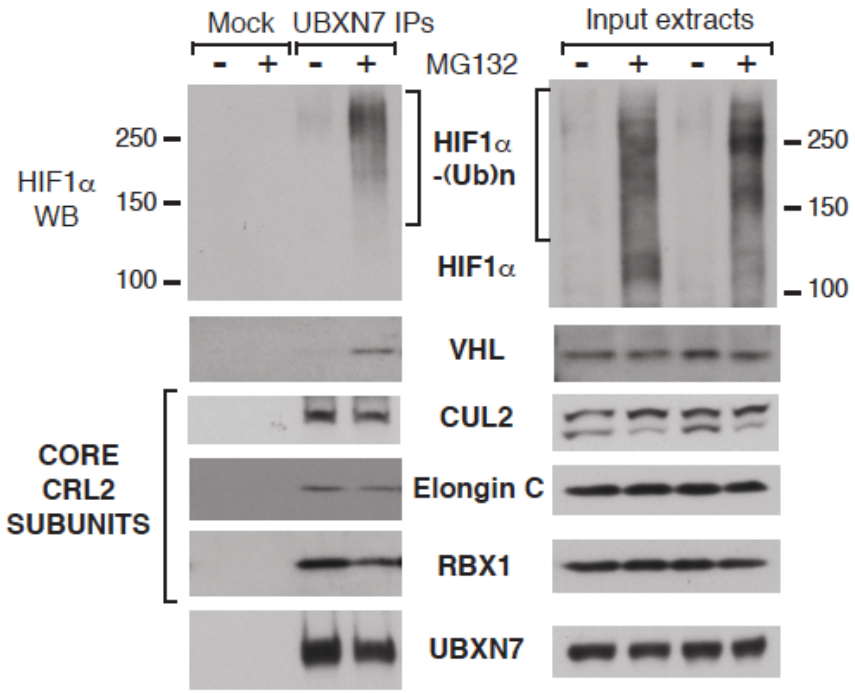

Figure 3.1: UBXN7 stably interacts with the core subunits of the CRL2 complex
Endogenous UBXN7 was immunoprecipitated from HeLa cells untreated or treated with 10 μM MG132 for 2h. Endogenous UBXN7 co-immunoprecipitated CUL2, elongin C and RBX1 from cells grown in the presence and absence of MG132, whereas VHL and HIF1α are only detected upon inhibition of the proteasome.

3.2.2 Active ubiquitylation is not necessary for UBXN7 interaction with CUL2

To test the assumption that the UBXN7 interaction with CUL2 is mediated by ubiquitylated substrates, Flag-UBXN7 was immunoprecipitated from A31N–ts20 cells (performed by Gabriela Alexandru). These mouse embryo fibroblasts are thermosensitive for ubiquitin-E1, leading to the inhibition of the initial step in the protein-ubiquitylation cascade when grown at the non-permissive temperature (Salvat et al., 2000).

Growth of the cells at 39°C led to a dramatic reduction of ubiquitylated protein levels (including HIF1α) compared to control cells grown at 35°C (Figure 3.2, right panel). Although ubiquitin binding to Flag-UBXN7 was drastically reduced, its binding to CUL2 was not affected (Figure 3.2, left panel), demonstrating that UBXN7 interaction with CUL2 is not mediated by ubiquitylated CRL2 substrates.

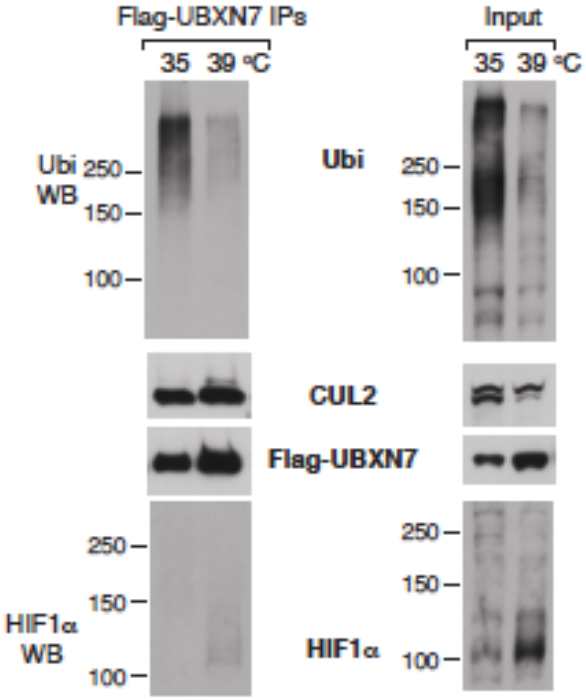

Figure 3.2: CUL2 interaction is independent of ubiquitin-binding

Flag-UBXN7 was immunoprecipitated from A31N–ts20 cells (mouse embryo fibroblasts) that are thermosensitive for the ubiquitin-E1. The cells were grown at the indicated temperatures for 20h and Flag-UBXN7 was immunoprecipitated using anti-Flag beads. Upon growth at 39°C, the protein ubiquitylation was drastically reduced compared to control cells (right panel). Although the ubiquitin binding to Flag-UBXN7 is clearly reduced, it did not affect binding to CUL2 (left panel).

3.2.3 Cullin-neddylation is required for the interaction with UBXN7

Interestingly, the Western blot analysis of protein extracts obtained from HeLa cells overexpressing Flag-UBXN7 revealed a clear up-shift of CUL2 to a slower migrating form (Figure 3.3, compare lanes 1 and 3). The inhibition of neddylation using the

chemical inhibitor of the NEDD8-E1 (Brownell et al., 2010) further confirmed that the slower migrating form is neddylated CUL2 (data not shown).

Furthermore, the comparison of protein extracts before and after Flag-UBXN7 immunoprecipitation showed that mainly neddylated CUL2 was depleted from the extracts (Figure 3.3, compare lane 3 and 4), indicating that Flag-UBXN7 preferentially interacts with the neddylated form of CUL2 (Experiments performed by Gabriela Alexandru).

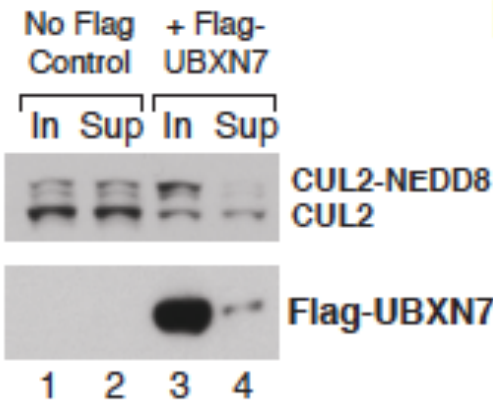

Figure 3.3: Flag-UBXN7 preferentially interacts with neddylated-CUL2
Protein extracts retained from HeLa cells overexpressing Flag-UBXN7 were compared before (In) and after (Sup) Flag-UBXN7 immunoprecipitation.

To investigate if CUL2 neddylation is required for the interaction between UBXN7 and CUL2, two neddylation-defective CUL2 mutants, K689R and K719R, were created. Lys689 is the site of NEDD8 conjugation in human CUL2, and mutating this residue to arginine abolishes neddylation (Wada et al., 1999). Lys719 is a conserved residue among cullins, and its equivalent in yeast, Cdc53, is part of the interaction surface with DCN1 (Kurz et al., 2008, Wada et al., 1999).

The CUL2 neddylation was completely abolished in the K689R mutant, and partially defective in the K719R mutant, as shown in an anti-NEDD8 Western blot (Figure 3.4). However, both mutations did not affect CUL2 interaction with RBX1. Interestingly, the loss of neddylation on CUL2 correlated with its ability to bind UBXN7. The UBXN7

binding was completely abolished in the K689R mutant and strongly reduced in the K719R mutant. Thus neddylation was required for CUL2 interaction with UBXN7.

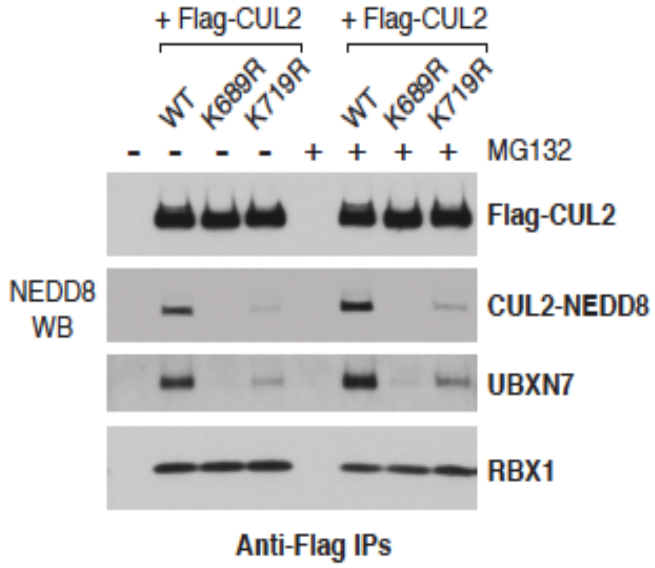

Figure 3.4: Neddylation of CUL2 isrequired for its interaction with UBXN7
Flag-CUL2 wild type and two neddylation-defective mutants (K689R or K719R) were immunoprecipitated from HeLa cells treated or not with 10 μM MG132 for 2h. The immuno-precipitated proteins were visualised by Western blot using specific antibodies. The neddylation-defective CUL2 variants are similarly defective in interacting with endogenous UBXN7.

It was previously shown that UBXN7 can interact, albeit less efficiently, with the other cullins CUL1, CUL3 and CUL4 (Alexandru et al., 2008). Since neddylation is a common feature among cullins, treatment with the neddylation inhibitor MLN4924 prevented not only UBXN7 interaction with CUL2, but also with CUL1, CUL3 and CUL4A (data not shown; experiment performed by Gabriela Alexandru).

3.2.4 The UIM of UBXN7 is required to engage the NEDD8 modification on cullins

The data presented so far suggest that the neddylation on CUL2 is required for the interaction with UBXN7. Next, we wanted to explore which of the UBXN7 domains are required for this interaction. There are four signature domains present within UBXN7. The N-terminus of UBXN7 harbours an UBA domain, followed by a UAS domain, a UIM and a UBX domain at the C-terminus.

To investigate which of these domains were required for UBXN7 interaction with CUL2, we compared the ubiquitin- and CUL2-binding capability of several UBXN7 variants, including wild type, a point mutant in the UBX domain (P459G), and truncation mutants lacking either the UBA, UAS, UIM or UBX domains (Figure 3.5A and B, performed by Gabriela Alexandru).

Figure 3.5A shows that UBA or UIM truncation mutants are partially defective in ubiquitin binding (Figure 3.5A, compare lanes 1, 2 and 4). Although both UBA and UIM contribute to ubiquitin binding, only the UIM truncation is strongly reduced in CUL2-binding (Figure 3.5B, compare lanes 1 and 4). Thus the UIM of UBXN7 is required for its interaction with CUL2. Consistent with the reduced binding of UBXN7 ΔUIM to CUL2, overexpression of this mutant failed to cause an up-shift of CUL2 to its neddylated form (Figure 3.5B, compare lanes 8 and 11).

The truncation of the UAS domain did not alter UBXN7 interaction with ubiquitin or CUL2 compared to wild type UBXN7 (Figure 3.5A/B, compare lanes 1 and 3). As previously shown by Alexandru et al., the truncation of the UBX domain completely disrupted the binding to ubiquitylated substrates. Similar results were obtained with the P459G mutant that introduces a conformational re-arrangement of the UBX domain resulting in defective p97 binding. The defect in binding to p97 or ubiquitinated substrates did not affect UBXN7 interaction with CUL2, confirming that this interaction does not depend on its binding to p97 or ubiquitin.

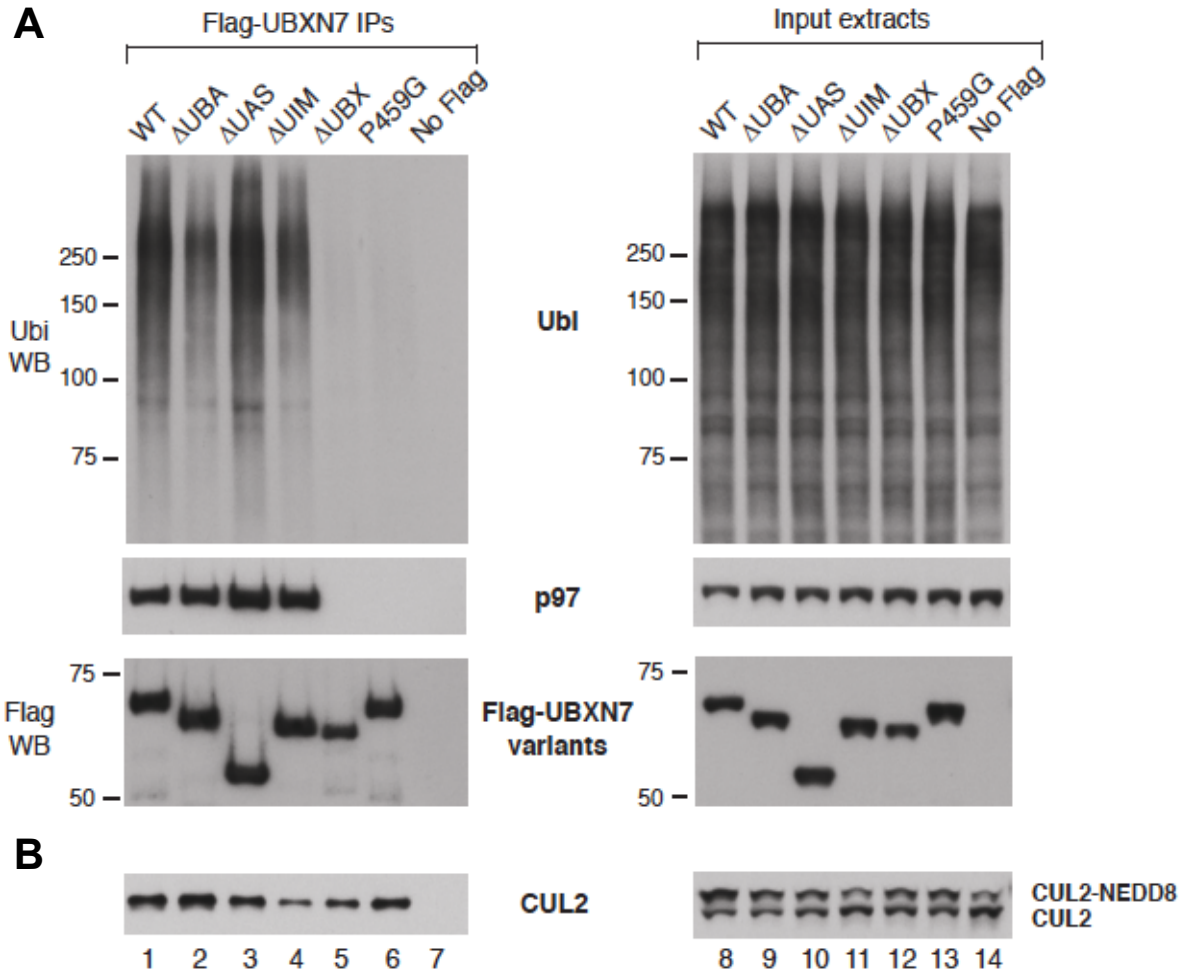

Figure 3.5: The UIM of UBXN7 is required for CUL2 binding

Flag-UBXN7 wild type and various mutants were immunoprecipitated from HeLa cells and immunoprecipitated proteins visualised by Western blot using specific antibodies.
(A) The UBA or UIM deletion caused a reduction in ubiquitin binding to UBXN7, whereas the UBX mutants were severely impaired in their ubiquitin binding (left panel).
(B) Flag-UBXN7 ΔUIM was the only mutant that caused a strong reduction in CUL2 binding to UBXN7 (left panel) and abolished the CUL2 up-shift caused by UBXN7 overexpression (right panel).

The UIM was identified as the CUL2 interaction site. The sequence alignment of UBXN7 UIM with various described UIMs confirmed that UBXN7 contains the conserved residues characteristic for a UIM (L290, A293, S297 and E300) (Figure 3.6, dark purple). These residues were also shown to be important for UIM interaction with ubiquitin (Bilodeau et al., 2002, Hirano et al., 2006). Notably, the hydrophobic patch in ubiquitin, that is required for its interaction with UIMs, is conserved in NEDD8. To

exclude the possibility that truncation of the whole UIM causes defect in binding to CUL2 due to protein misfolding, we generated two point mutants in the conserved residues, substituting Ala293 with glutamine, or Ser297 with either alanine or histidine.

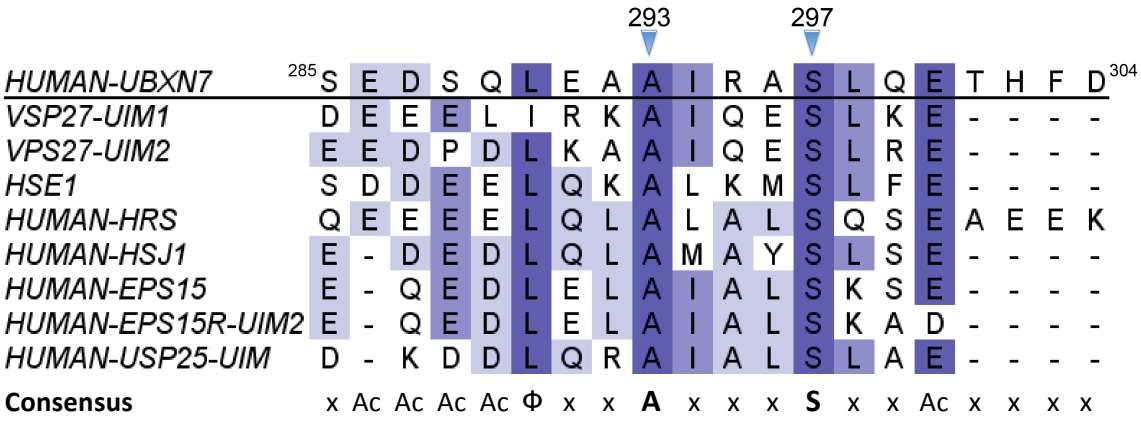

Figure 3.6: The UIM of UBXN7 contains the conserved residues characteristic for a UIM

The sequence alignment of UBXN7 UIM with various described UIMs confirmed that the UIM of UBXN7 contains the conserved residues characteristic for a UIM. Conserved amino acids of the UIM domain are indicated below the alignment, where Φ represents a large hydrophobic residue (typically Leu), Ac represents an acidic residue (Glu, Asp), and X represents residues that are less well conserved. The sequence alignment was performed using Jalview.

To analyse their binding to CUL2, I performed immunoprecipitations of Flag-UBXN7 wild type, ΔUIM, and both point mutants. The residue S297 changed either to alanine or histidine caused a defect in binding to neddylated-CUL2 similar to the truncation of the whole UIM (Figure 3.7, compare lanes 3 with 4/5). The mutant Flag-UBXN7 A293Q was also defective in its binding, but slightly less pronounced than the ΔUIM or the S297A/H mutant (Figure 3.7, compare lane 3 and 6). The p97 binding was not affected by any of these mutations.

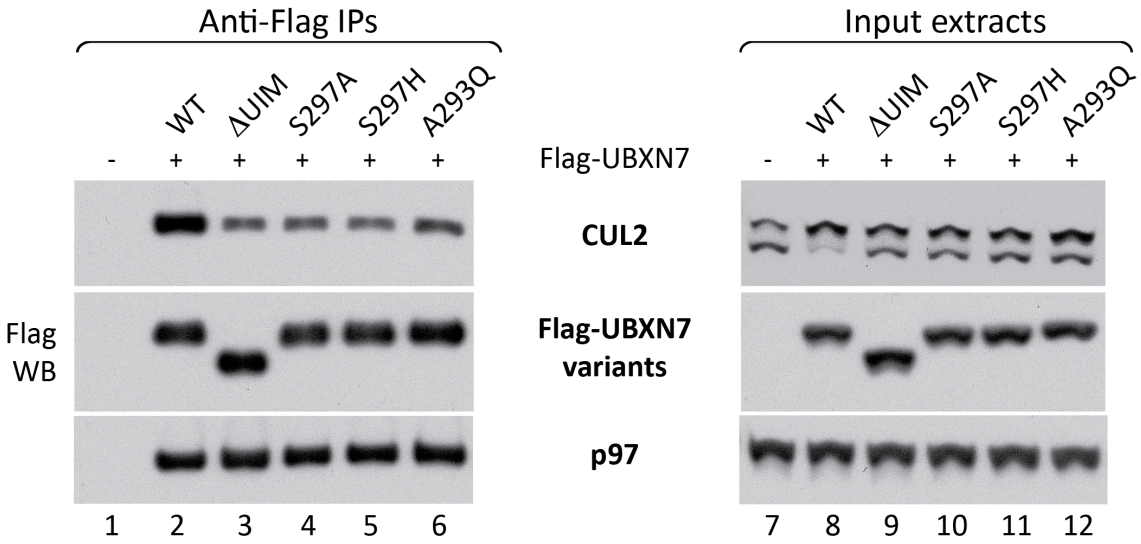

Figure 3.7: UIM-defective mutants of UBXN7 show reduced binding to neddylated-CUL2

HeLa cells were transfected with the indicated variants of Flag-UBXN7 and immunoprecipitated using anti-Flag beads. The lysate inputs (right) and the immunoprecipitates (left) were analysed by Western blot and the indicated proteins were detected using specific antibodies. The overexpression of the UIM-defective mutants did not cause the up-shift of CUL2 to its neddylated form and showed reduced binding to neddylated CUL2 compared to Flag-UBXN7 wild type.

To further substantiate the ability of the UBXN7 UIM to interact with NEDD8 rather than ubiquitin, we performed *in vitro* binding assays using NEDD8- or ubiquitin-agarose.

Wild type UBXN7 was pulled-down efficiently with both types of beads (Figure 3.8). Deletion of the UIM caused a clear reduction in NEDD8 binding and had no effect on ubiquitin-binding. The UBA deletion abolished ubiquitin binding and caused some reduction in NEDD8 binding as well.

These data strongly support the notion that the UIM of UBXN7 is specialised in recognising NEDD8 and can directly engage the NEDD8 modification on cullins.

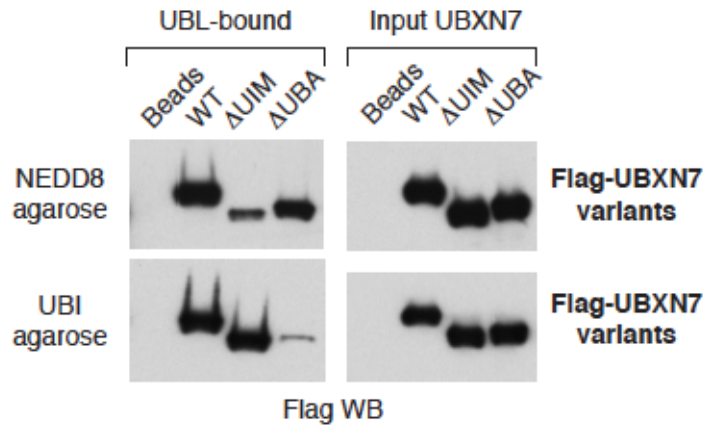

Figure 3.8: The UIM of UBXN7 directly recognises NEDD8

NEDD8- or ubiquitin-agarose beads were incubated with the indicated recombinant variants of UBXN7. The truncation of the UIM exclusively reduces UBXN7 binding to NEDD8 while deletion of the UBA domain abolishes the interaction with ubiquitin.

3.2.5 UBXN7 interacts with cullin-RING complexes in vitro

To check whether UBXN7 could interact with cullin complexes *in vitro*, Flag-UBXN7 was incubated with either unmodified or neddylated CUL2 and then immunoprecipitated using anti-Flag beads (performed by Gabriela Alexandru).

Figure 3.9A shows that wild type UBXN7 could interact efficiently with CUL2 irrespective of its neddylated status. A UBXN7 variant lacking the UIM was equally proficient in interacting with both forms (Figure 3.9B). Therefore, under these conditions, UBXN7 interaction with CUL2 does not appear to depend strictly on either UIM or NEDD8.

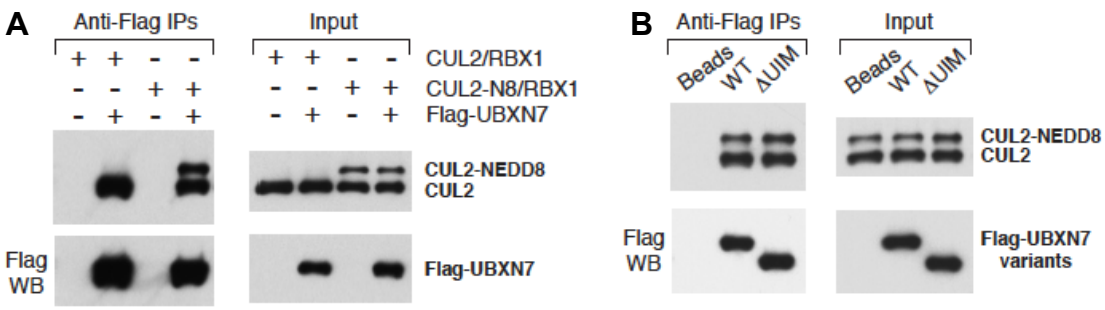

Figure 3.9: Wild type UBXN7 interacts with CUL2 irrespective of its neddylated status *in vitro*
A) Bacterially-expressed Flag-UBXN7 was pre-incubated with full-length CUL2 either unmodified or partially neddylated and then immunoprecipitated using anti-Flag beads. Wild-type UBXN7 efficiently pulls-down CUL2 irrespective of its modification status.
B) Wild-type or UIM-deleted Flag-UBXN7 was incubated with a mixture of neddylated and non-neddylated CUL2 and then immunoprecipitated using anti-Flag beads. The in vitro interaction of UBXN7 with full-length CUL2 is not affected by UIM deletion.

3.2.6 UBXN7 overexpression causes HIF1α accumulation in a UIM-dependent manner

The data provided so far suggest that the UIM in UBXN7, as well as the neddylation on CUL2 are required to mediate interaction between the two proteins. Furthermore, the overexpression of UBXN7 causes an up-shift of CUL2 to its neddylated form, indicating that UBXN7 might affect CUL2 neddylation.

To investigate whether overexpression of Flag-UBXN7 wild type or the UIM mutant has an effect on CRL2 substrates, we decided to look more closely at the levels of the hypoxia-inducible factor 1-alpha (HIF1α). HIF1α is constitutively degraded by the CRL2 complex under normoxia (Ivan and Kaelin, 2001) and, furthermore, was shown to co-immunoprecipitate with UBXN7 (Alexandru et al., 2008).

Figure 3.10 shows that overexpression of the wild type UBXN7 caused a significant accumulation of HIF1α especially in its non-ubiquitylated form (compare lanes 6 and 7), suggesting that the CUL2-mediated HIF1α ubiquitylation might be hampered. Most importantly, this defect was dependent on the UIM, as HIF1α levels in cells overexpressing a UIM-deleted or mutated version of UBXN7 (S297A and S297H) were similar to untransfected cells (Figure 3.10, compare lane 6 and 8-10). Furthermore, wild type UBXN7 interacted with HIF1α having various degrees of ubiquitylation, while

UIM-defective UBXN7 (UIM deletion or point mutation at Ser297) only interacted with slow-migrating, poly-ubiquitylated HIF1α (Figure 3.10, compare lanes 2 with 3–5).

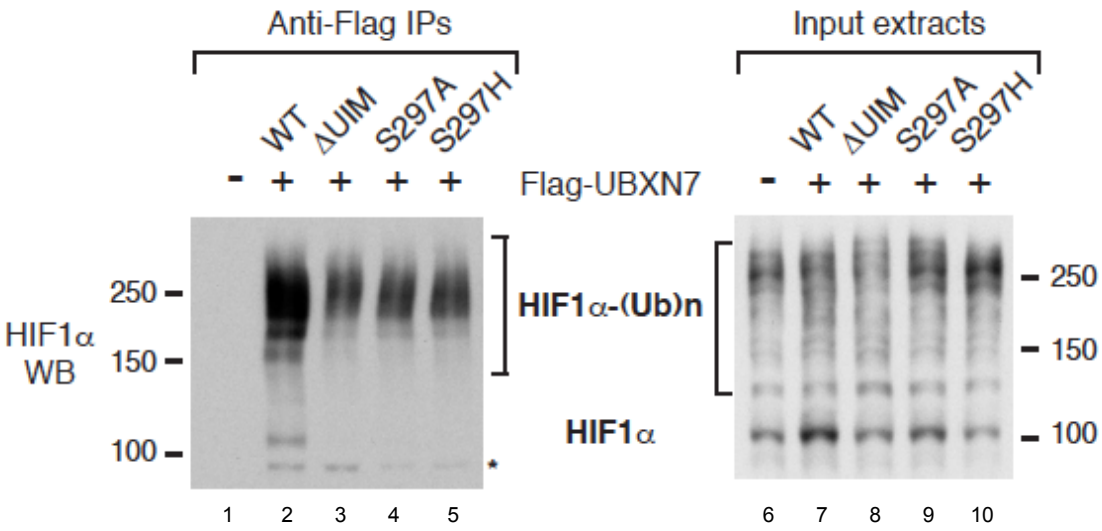

Figure 3.10: UBXN7 overexpression causes HIF1α accumulation in a UIM-dependent manner
Experiment in figure 3.8 blotted for HIF1α. The lysate inputs (*right*) and the immunoprecipitates (*left*) were analysed by Western blot.

3.2.7 Overexpression of another UIM-containing protein, PSMD4, does not alter HIF1α levels

The UIM of UBXN7 is required for its binding to neddylated CUL2, and the overexpression of wild type UBXN7 leads to the accumulation of the CRL2 substrate HIF1α. Besides UBXN7, there are other ubiquitin receptors harbouring UIMs.

To investigate whether the overexpression of any other UIM-containing ubiquitin receptor causes accumulation of HIF1α, the proteasome subunit PSMD4 (UIM-containing protein) was overexpressed in HeLa cells (Figure 3.11, lane 3). Notably, the two UIMs of PSMD4 contain the conserved residues characteristic for a UIM, including the alanine and serine residues that caused a reduced binding of neddylated-CUL2 when mutated in the UIM of UBXN7.

The comparison of HIF1α levels in Flag-UBXN7- or Flag-PSMD4-expressing cells showed that UBXN7 seems to be specific in its ability to cause UIM-dependent accumulation of HIF1α, as overexpression of the UIM-containing ubiquitin receptor PSMD4 had no effect on HIF1α levels (Figure 3.11, lanes 2 and 3).

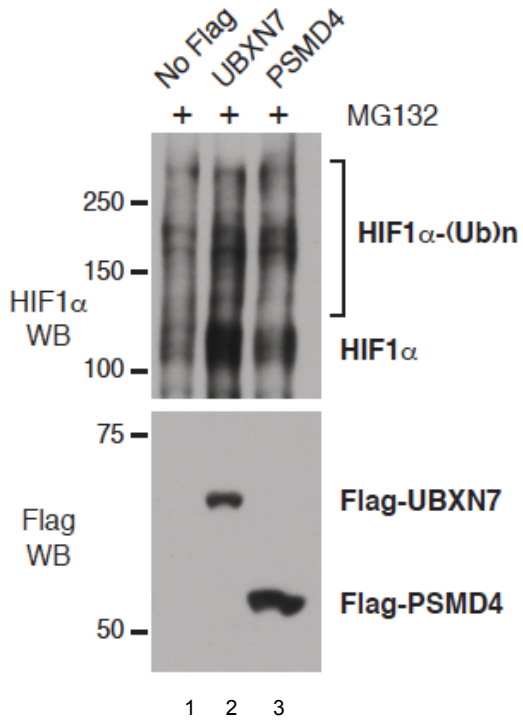

Figure 3.11: UBXN7 is specific in its ability to cause UIM-dependent accumulation of HIF1α
Protein extracts from Flag-UBXN7 and Flag-PSMD4 overexpressing HeLa cells were analysed by Western blot. The indicated proteins were detected using specific antibodies.

3.2.8 Long ubiquitin chains on HIF1α cause reduced ubiquitin receptor selectivity

Wild type UBXN7 binds non-ubiquitylated, and various degrees of poly-ubiquitylated HIF1α, whereas UIM-defective UBXN7 only interacts with its slow-migrating, poly-ubiquitylated form (Figure 3.10). This ΔUIM interaction with ubiquitylated HIF1α is likely to be mediated via its UBA domain. This is consistent with the fact that other UBA–UBX proteins can also interact, albeit inefficiently, with HIF1α carrying long ubiquitin chains (Alexandru et al., 2008).

The degradation of UBA–UBX protein substrates depends on p97. To investigate if HIF1α can be degraded by other ubiquitin receptors that are p97 independent, Flag-RAD23B immunoprecipitates were analysed for HIF1α binding. RAD23B (RAD23-like protein B) is an UBA domain-containing ubiquitin receptor, and is involved in ubiquitin-dependent proteolysis as well as nucleotide excision repair (Hiyama et al., 1999, Glockzin et al., 2003, Yokoi et al., 2000). Furthermore, RAD23B is nuclear localised (van der Spek et al., 1996), similar to Flag-UBXN7, which localises exclusively in the nucleus in HeLa cells (Figure 3.12).

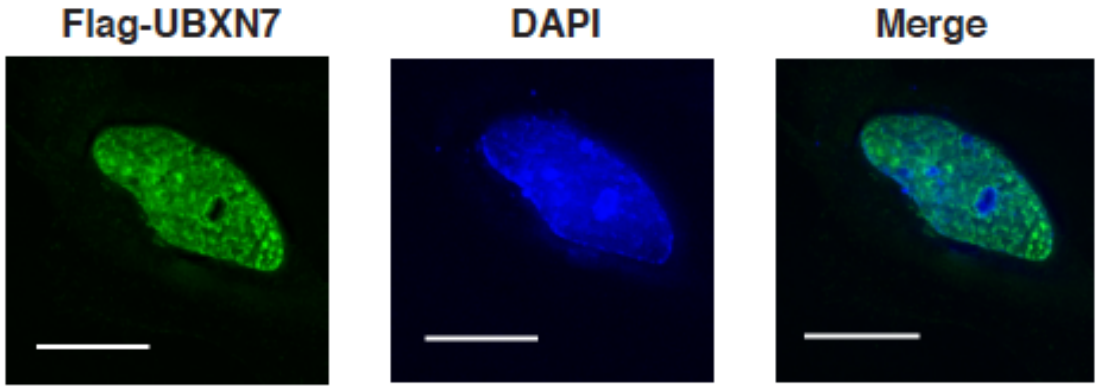

Figure 3.12: Flag-UBXN7 localises into the nucleus of HeLa cells
HeLa cells were transfected with wild-type Flag-UBXN7 and its subcellular localisation was analysed by immunofluorescence microscopy. The DNA was stained with DAPI (blue). Flag-UBXN7 was detected using mouse anti-Flag antibodies and a FITC-conjugated secondary (green). Images were obtained with a DeltaVision Spectris microscope. The scale bar represents 15 μm.

To check whether RAD23B can also interact with HIF1α, I performed immunoprecipitations with Flag-RAD23B and Flag-UBXN7.

Like the UBA–UBX proteins, RAD23B was able to co-immunoprecipitate only HIF1α carrying longer ubiquitin chains (Figure 3.13, compare lanes 2 and 3) and its overexpression failed to cause accumulation of unmodified HIF1α, as observed upon UBXN7 overexpression (Figure 3.13, compare lanes 5 and 6).

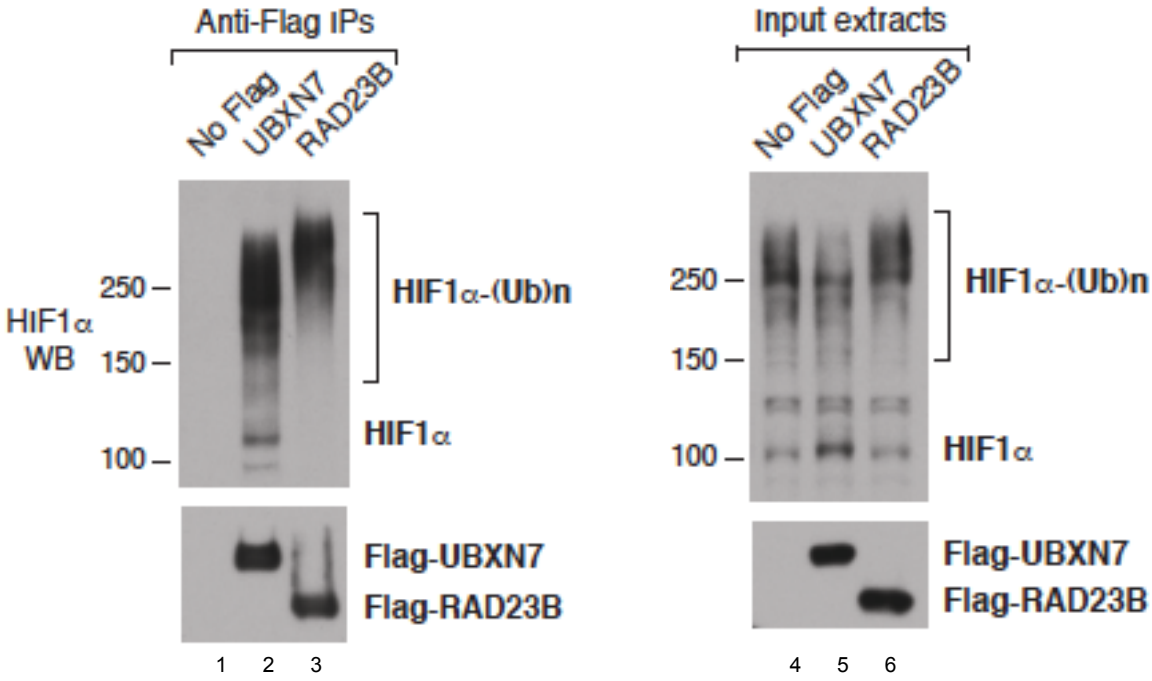

Figure 3.13: Long ubiquitin-chains on HIF1α cause reduced ubiquitin-receptor selectivity
Hela cells were transfected with either Flag-UBXN7 or Flag-RAD23B, both of which are nuclear UBA domain-containing proteins. The Flag-tagged proteins were immunoprecipitated using anti-Flag beads and the lysate inputs (*right*), as well as the immunoprecipitates (*left*) were analysed by Western blot. The indicated proteins were detected using specific antibodies.

Hence, as the ubiquitin chains get longer, the substrate appears less selective in its interaction with ubiquitin receptors. These results suggest that poly-ubiquitylated HIF1α might be less selective in its interaction with ubiquitin receptors and that UBXN7 may compete with receptors like RAD23B for the binding to poly-ubiquitylated HIF1α in the nucleus. However, its ability to cause accumulation of non-ubiquitylated HIF1α, which might be a consequence of its inhibitory effect on CUL2, seems to be specific for UBXN7.

3.3 Discussion

3.3.1 UBXN7 interaction with cullins is independent of the ubiquitylated substrate

Multiple lines of evidence indicate that the UBXN7 interaction with cullins is not mediated by its ubiquitylated targets bound to the UBA domain.

1) The inhibition of the ubiquitin-E1 strongly reduces ubiquitin binding to UBXN7 but has no affect on CUL2 binding to UBXN7.

2) The interaction between UBXN7 and HIF1α/VHL is clearly enhanced after proteasome inhibition, whereas UBXN7 interaction with the core CRL2 complex is stable.

3) The truncation of the UBA domain reduces ubiquitin binding to UBXN7, but it does not affect the interaction with CUL2.

3.3.2 UBXN7 binds the NEDD8 modification on CUL2 via its UIM

The data illustrate that UBXN7 binds the neddylated form of CUL2 by directly engaging the NEDD8 modification. Hence, the neddylation-defective CUL2 mutants are defective in UBXN7 binding, and the chemical inhibition of NEDD8-E1 abolished the UBXN7 interaction with multiple cullins.

Furthermore, we found that the binding of UBXN7 to the neddylated form of CUL2 is mediated through its UIM. The UIM and UBA domains recognize ubiquitin through a hydrophobic surface (formed by Leu8, Ile44, His68 and Val70) on ubiquitin, which is conserved in NEDD8. Therefore, in principle, both UIM and UBA domains could have served as docking site for neddylated cullin. However, the UBXN7 mutant lacking the UBA domain interacts with neddylated CUL2 similar to the wild type, ruling out its

involvement in cullin-binding. In contrast, UBXN7 lacking the UIM or carrying point mutations therein is strongly defective in cullin-binding.

The *in vitro* assays supports that the UIM contributes to the direct binding of UBXN7 to neddylated CUL2. UBXN7 variant lacking the UIM becomes defective in binding to NEDD8 – but not ubiquitin–agarose. Furthermore, this experiment illustrated that the UIM recognizes the NEDD8 modification *per se* rather than the neddylated conformation of cullins.

However, our *in vitro* assays also show that UBXN7 can interact with non-neddylated cullins, suggesting that UIM-NEDD8 may not be the only link between UBXN7 and CRLs. We used a simplified CRL complex containing only cullin and RBX1. Hence, the structural arrangement might expose contributing binding sites that are normally only accessible upon neddylation. Thereby, the strict requirement for neddylation that we observed for the native form of CUL2 present in cell extracts might be revoked.

We therefore propose that UBXN7 binds the NEDD8 modification on cullins, and that additional sites in UBXN7 and the CRLs contribute to stabilize the binding.

At the same time as our paper, den Besten et al. (2012) published a paper on UBXN7 also describing (consistent with our data) that UBXN7 interacts with neddylated cullins via its UIM. By studying more closely the UIM–NEDD8 interaction, den Besten et al. demonstrated that UBXN7's UIM could be swapped with the second UIM of proteasome subunit PSMD4 with no effect on UBXN7-CRL association *in vitro*.

However, our data show that overexpression of the PSMD4 does not cause an accumulation of the CRL2 substrate HIF1α in cell extracts, as seen upon UBXN7 overexpression (further discussed below). Therefore, although one of the UIMs of PSMD4 is able to bind neddylated cullins in the context of UBXN7 *in vitro*, it does not

bestow on PSMD4 the ability to affect CRL substrate levels, as shown with UBXN7 *in vivo*. These results indicate that the NEDD8 specificity of the UBXN7 UIM, as well as its flanking regions, contribute to the interaction between UBXN7 and the neddylated cullins.

3.3.3 UBXN7 sequesters the CRL2 complex in its neddylated form in a UIM-dependent manner

The UBXN7 overexpression causes the accumulation of neddylated CUL2, suggesting that UBXN7 binding sequesters CUL2 in its neddylated form. Furthermore, UBXN7 binding reduces the processivity of the CRL2 ubiquitin ligase, since UBXN7 overexpression leads to the accumulation of the CRL2 substrate HIF1α, mainly in its non-ubiquitylated form. These data suggest that UBXN7 is not only an ubiquitin-binding adaptor for p97 as described by Alexandru et al., but it may also embody a novel mechanism of CRL inhibition. This is in agreement with previous observations that UBXN7 silencing by siRNA causes a reduction in HIF1α levels, not HIF1α accumulation (Alexandru et al., 2008).

The regulatory effect on the CRL2 complex activity is UIM dependent. UIM-defective UBXN7 mutants do not shift the balance towards neddylated-CUL2 or cause HIF1α accumulation. Based on these observations, it is tempting to propose that, by sequestering CUL2 in its neddylated form, UBXN7 might sterically hinder the transition of the CRL2 complex to an open conformation and thereby mitigate the positive effect of NEDD8 on the CRL E3 activity.

Furthermore, Emberley et al. (2012) showed that UBXN7 strongly inhibits deneddylation of CUL1–RBX1 through CSN, *in vitro*. Together with the observed accumulation of NEDD8-conjugated CUL2 upon UBXN7 overexpression *in vivo*, this

could suggest that UBXN7 binding to neddylated-CUL2 not only sequesters CUL2 in its neddylated state but also shields CUL2 from CSN; thus preventing NEDD8-deconjugation (Emberley et al., 2012).

However, the data obtained by den Besten in yeast, point to a positive role for the UBXN7 orthologue Ubx5 in the UV-induced degradation of polyubiquitylated Rbp1 (large subunit of RNA polymerase II). While upon UV-treatment, Rpb1 was rapidly degraded in the wild type strain, its degradation was delayed in the ubx5uimΔ mutant, and further impaired in an ubx5Δ background (den Besten et al., 2012). Therefore, the knockout of the UBXN7 orthologue Ubx5 has the opposite effect on the CRL2 substrate, as observed upon UBXN7 silencing in mammalian cells (Alexandru et al., 2008). The paper by den Besten et al. did not show the effect on Rbp1 upon Ubx5 overexpression. This conflicting result might suggest that UBXN7's function depends on the substrate. HIF1α is a transcription factor that is soluble under normoxia conditions, and poly-ubiquitinated-HIF1α might be targeted for degradation by p97-independent pathways. In contrast, the RNA polymerase subunit Rpb1 is part of a 12-subunit complex that is bound to DNA, and its degradation is induced only upon UV treatment. Therefore, the p97 recruitment through Ubx5 might be essential for the Rpb1 extraction prior to its degradation.

3.3.4 UBXN7 recruits p97 to nuclear HIF1α

The data presented here show that ubiquitin-receptor selectivity is compromised when HIF1α carries long ubiquitin chains. However, upon UBXN7 binding to neddylated cullins, the CRL processivity is reduced, resulting in non-ubiquitylated and short ubiquitin chains on HIF1α. Hence, we suggest that reduced CRL processivity would

favour p97 recruitment to the UBX-domain of UBXN7 rather than recruitment of alternative ubiquitin receptors, such as RAD23B, to a fast-growing ubiquitin chain. The binding of UBXN7 to the neddylated CRLs would be ideally poised to modulate substrate ubiquitylation and to shift the balance towards p97 recruitment.

To recruit p97 to the CRL substrates could be particularly important in the nucleus, where HIF1α forms complexes with HIF1β and associates with the promoters of its target genes (Jiang et al., 1996). Among the various ubiquitin receptors, p97 uniquely provides the segregase activity to dissociate nuclear HIF1α from its protein partner and/or from chromatin prior to its degradation. Endogenous HIF1α is found in the nuclei of normoxic cells from normal and tumour tissues (Stroka et al., 2001) and poly-ubiquitylated HIF1α, as well as VHL/ubiquitinated-HIF1α complexes, are found solely in the nuclear compartment of normoxic HeLa cells (Groulx and Lee, 2002). That UBXN7 and p97 target specifically the nuclear pool of HIF1α is further supported by our finding that Flag-UBXN7 localises in the nucleus of HeLa cells under normoxia.

Chapter 4

4. The p97-cofactor UBXN8 has an inhibitory effect on the Fanconi anaemia proteins FANCD2 and FANCI

4.1 Introduction

The UBX-only protein UBXN8 is an ER membrane protein that binds p97 via its UBX domain. UBXN8 is required for ER-associated degradation of misfolded proteins by tethering p97 at the ER membrane (Madsen et al., 2011). Furthermore, a recent publication introduced *UBXN8* as a target gene for HBV (hepatitis B virus) integration and showed that its overexpression in hepatocellular carcinoma cells induces a delay in the G1/S transition via a p53/p21$^{WAF1/CIP1}$ – dependent mechanism (Li et al., 2014).

Our identification of the FA proteins FANCD2 and FANCI in Flag-UBXN8 immunoprecipitates (unpublished results by Gabriela Alexandru) suggests a new function of UBXN8 in the DNA damage response. This may link UBXN8 to the genetic disease FA, which is caused by mutations in at least 15 FA genes, resulting in defective DNA crosslink repair and predisposition to cancer. DNA interstrand crosslinks (ICL) covalently link both strands of the helix thereby blocking DNA replication and transcription (Scharer, 2005, German et al., 1987). Because the FA pathway plays a major role in removing these crosslinks, FA proteins are involved in a novel DNA repair mechanism required for maintaining genomic stability and preventing cancer (Kee and D'Andrea, 2010). A better understanding of the molecular details and the regulation of the FA pathway can therefore help to improve or develop therapies for FA patients as well as non-FA cancer patients.

This chapter of my thesis describes the identification of the p97-cofactor UBXN8 as new interaction partner of the FA proteins FANCD2 and FANCI and sheds light on the functional relevance of these interactions.

4.2 Results

PART I - Identification of the key FA proteins FANCD2 and FANCI as UBXN8 binding partners

4.2.1. Analysis of Flag-UBXN8 immunoprecipitates by mass spectrometry identified FANCD2 and FANCI as UBXN8 interaction partners

The initial mass spectrometry (MS) analysis of Flag-UBXN8 immunoprecipitates was performed by my supervisor Gabriela Alexandru and identified the FA proteins FANCD2 and FANCI as potential UBXN8 interaction partners. These interactions implicate UBXN8 in the FA pathway and raise the question whether UBXN8 has a broader role in DNA damage response. Therefore, to identify novel UBXN8 interactions that might help us to address this question, we carried out MS analyses of Flag-UBXN8 immunoprecipitates from HeLa cells treated or not with the DNA damaging agent hydroxyurea (HU). As an inhibitor of ribonucleotide reductase, HU inhibits replication and activates several DNA repair pathways. Immunoprecipitates from cells that were not transfected with Flag-UBXN8 were used as negative control.

The MS analysis of Flag-UBXN8 immunoprecipitates identified numerous potential binding-partners, however the qualitative comparison between non-damaged and DNA-damaged cells did not reveal significant differences. The proteins identified were

grouped based on their function and at least two of these groups might be particularly relevant for the role of UBXN8 in mammalian cells: proteins involved in DNA damage response (Table 4.1) and proteins required for nuclear import/export (Table 4.2).

In the DNA repair category, besides FANCD2 and FANCI, we identified proteins required for: DSB repair (FIGNL1, RIF1, BRAT1) (Yuan and Chen, 2013, Kumar and Cheok, 2014, Aglipay et al., 2006), DNA damage resistance by regulating the ATM/ATR abundance (TTT-complex: TELO2, TTI1, TTI2) (Hurov et al., 2010) and p53 activation upon DNA damage (ATM-dependent phosphatase PPM1G) (Khoronenkova et al., 2012); as well as proteins that are phosphorylated upon DNA-damage (Table 4.1).

Table 4.1: Identified proteins which are involved in DNA damage response

Protein Name	Mass [kDa]	No. of peptides identified		Sequence coverage [%]		Protein function
		-	+ HU	-	+ HU	
FANCD2	166.5	10 (19)	3 (5)	9	2.7	**Interstrand crosslink repair (ICL)**
FANCI	149.3	6 (11)	6 (7)	6.1	6.7	
BRAT1	88.1	2 (3)	3 (4)	3.6	5.7	**DNA double-strand break repair**
RIF1	274.5	1 (2)	2 (3)	0.5	1.2	
FIGNL1	74	7 (12)	10 (18)	14.5	20.8	
TELO2	91.7	7 (12)	7 (13)	13.6	14.8	**Telo2, TTI1, and TTI2 form the TTT complex that is required for DNA damage resistance by regulating the ATM/ATR abundance (Hurov et al., 2010)**
TTI1	122	4 (7)	6 (9)	6.1	9.4	
TTI2	56.9	4 (6)	2 (4)	9.3	5.1	
PPM1G	59.2	6 (12)	7 (13)	13	17.8	**ATM-dependent protein phosphatase that down-regulates USP7 in response to DNA damage, resulting in p53 activation (Khoronenkova et al., 2012)**
CLPTM1L	62.2	2 (4)	4 (6)	7.2	11.7	**Enhance cisplatin-mediated apoptosis upon decreased CLPTM1L level (James et al., 2012)**
SAAL1	53.5	7 (11)	6 (10)	22.7	16.8	**Function unknown, phosphorylated upon DNA damage**
NCAPD2	157.1	2 (3)	-	2.1	-	**NCAPD2 is part of the condensin complex; involved in chromosome assembly and segregation; phosphorylated upon DNA damage**

The column "No. of peptides identified" shows the number of unique peptides and the total number of peptides is indicated in parenthesis, which takes into account that some peptides were identified multiple times. *Light grey*: identifications with only one unique peptide.

Table 4.2 indicates proteins required for protein transport to/from the nucleus, including several importins, exportins, and nuclear pore complex components. The number of peptides identified for each import/export protein is significantly high and suggests that UBXN8 might play a role in nuclear import/export.

Table 4.2: Identified proteins involved in nuclear transport

Protein Name	Mass [kDa]	No. of identified peptides		Sequence coverage [%]		Protein function
		-	+ HU	-	+ HU	
KPNB1	91.2	29 (55)	27 (49)	36.3	31.6	**NUCLEAR IMPORT** Importins that mediate the nuclear import of proteins bearing a nuclear localization signal (NLS).
KPNB2	102.4	17 (29)	17 (29)	26.5	33	
IPO4	118.7	3(5)	2 (4)	2.9	1.9	
IPO5	123.7	16 (27)	20 (34)	21.6	24.6	
IP07	119.5	11 (19)	13 (23)	14.5	15.7	
IPO8	119.9	6 (12)	9 (17)	8.7	11.9	
IPO9	116	17 (29)	21 (34)	19.6	26	
IPO11	112.5	-	2 (2)	-	2.5	
IPO13	108.2	9 (17)	10 (18)	12.9	15.5	
XPO1	123.4	18 (28)	15 (25)	21	17.7	**NUCLEAR EXPORT** Exportins that mediate the nuclear export of proteins bearing a nuclear export signal (NES).
XPO2	110.4	20 (32)	22 (35)	23.4	26.6	
XPO4	130.1	12 (22)	11 (21)	14.2	12.9	
NUP43	42.1	2 (3)	1 (1)	8.4	4.5	**NUCLEAR PORE COMPLEX (NPC) PROTEINS** NUP43, NUP85 and NUP160 are part of the NUP107-160 complex which is required for the assembly of a functional NPC.
NUP85	75	5 (8)	3 (3)	15.8	6.7	
NUP160	162.1	18 (31)	1 2 (21)	16.5	11.8	
MVP	99.3	12 (20)	11 (17)	20.9	18.8	
RAN	12.2	2 (4)	1 (1)	8.9	5.1	GTP-binding nuclear protein Ran required for nuclear import and for RNA export
RanBP1	23.3	3 (4)	3 (5)	15.4	14.4	Increases GTP hydrolysis by RanGAP1

The column "No. of peptides identified" shows the number of unique peptides and the total number of peptides is indicated in parenthesis, which takes into account that some peptides were identified multiple times. *Light grey*: identifications with only one unique peptide.

The identification of other DNA damage-related proteins supports the assumption that UBXN8 might have a broader role in the DNA damage response.

4.2.2 Membrane-anchored isoforms of UBXN8 interact with FANCD2 and FANCI

To confirm the interaction between Flag-UBXN8 and the FA proteins FANCD2 and FANCI by Western blot, Flag-immunoprecipitations from Flag-UBXN8 transfected U2OS cells were performed. There are three predicted UBXN8 isoforms, based on alternative splicing: isoform 1 as full-length UBXN8, isoform 2 that lacks a region between the coiled-coil and the UBX-domain, and isoform 3 that lacks the transmembrane domain. We therefore decided to perform Flag-immunoprecipitation with each splice variant of UBXN8 to investigate which one of them co-immunoprecipitates FANCD2 and FANCI.

The immunoprecipitation of full-length Flag-UBXN8 confirmed its interaction with FANCD2 and FANCI (Figure 4.1, lane 2). Furthermore, comparing the binding ability of all three UBXN8 isoforms, only the membrane-anchored isoforms of UBXN8 (1 and 2) co-immunoprecipitated the endogenous FA proteins (Figure 4.1, lanes 2 and 3). UBXN8 isoform 1 appeared to interact best with FANCD2 and FANCI, while isoform 2 only showed a weak interaction to both proteins.

Transmembrane domains consist of amino acids carrying hydrophobic side chains that allow their insertion in the hydrophobic layers of the cell membrane (Borgese and Fasana, 2011). In the case of UBXN8, it is therefore unlikely that its (embedded) transmembrane domain mediates the interaction with soluble FANCD2 and FANCI. Therefore, our results rather suggest that the membrane localisation of UBXN8 is important for its interaction with both FA proteins.

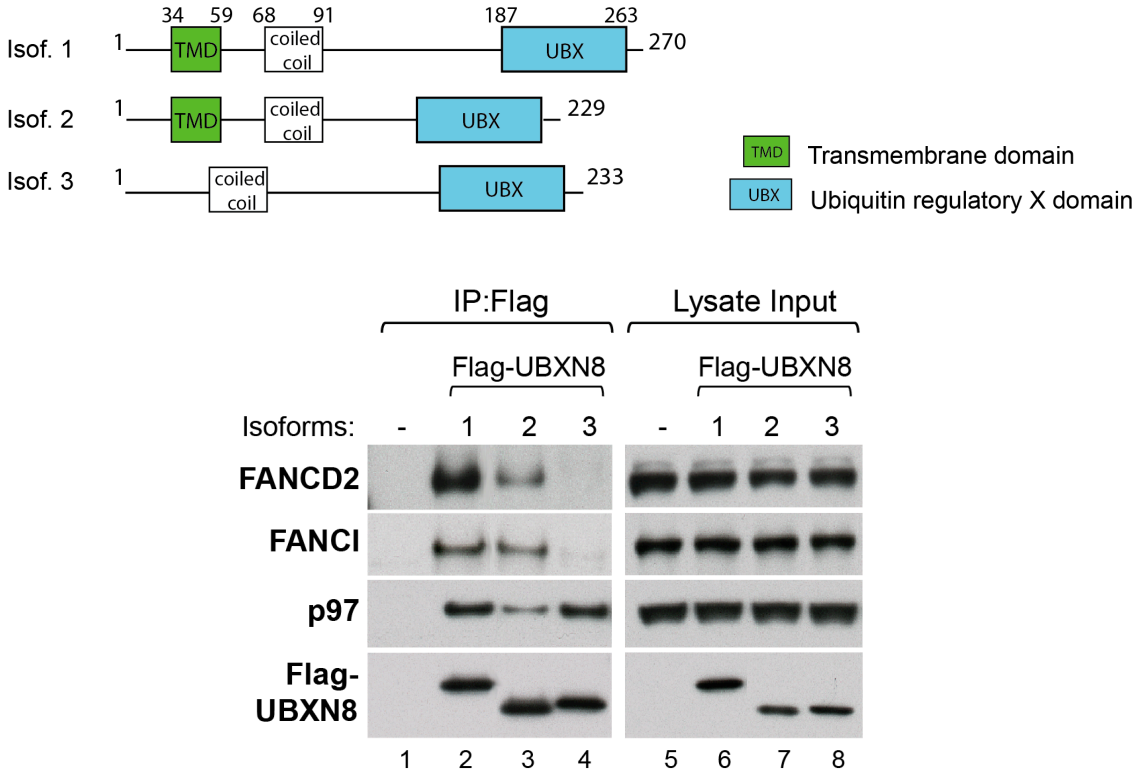

Figure 4. 1: Membrane-anchored isoforms of UBXN8 interact with FANCD2 and FANCI
U2OS cells were transfected with the three predicted Flag-tagged UBXN8 isoforms (1–3, *top*), with isoform 1 being full-length UBXN8. Flag-tagged UBXN8 was immunoprecipitated using anti-Flag beads and the indicated proteins detected by Western blot. Cells expressing no Flag-tagged protein were used as negative control. *Left*: Flag-IP; *right*: Lysate Input

The subcellular localisation of the three UBXN8 isoforms was analysed in HeLa cells using immunofluorescence microscopy (Figure 4.2). The images obtained confirmed the ER localisation of full-length Flag-UBXN8 as described by Madsen et al. (2012). Notably, I also observed a distinct staining of Flag-UBXN8 at the nuclear envelope, which will be further addressed in the next section. Isoform 2 showed the same subcellular localisation as isoform 1, whereas isoform 3 showed a diffused staining all over the cell.

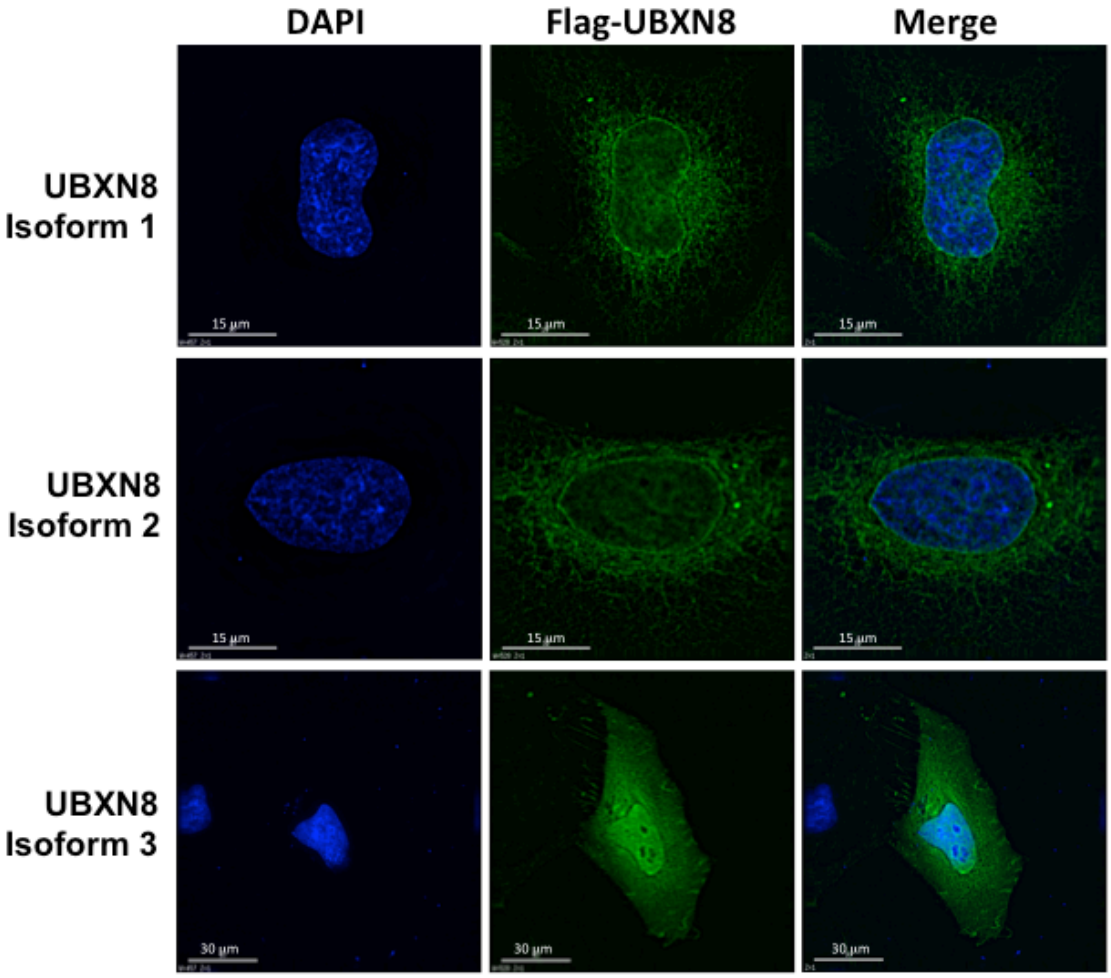

Figure 4.2: Membrane-anchored isoforms of Flag-tagged UBXN8 localise at the ER and around the nucleus

HeLa cells were transfected with Flag-tagged UBXN8 isoform 1–3 and processed for immunostaining after 24 h. Flag-tagged proteins were detected with an anti-Flag antibody (*green*) and the nuclei stained using DAPI (*blue*). The scale bars represent 15 µm.

4.2.3 UBXN8 is anchored in the inner nuclear membrane

The immunofluorescence staining of Flag-UBXN8 showed that a fraction of Flag-UBXN8 distinctly localised at the nuclear envelope.

The FA proteins FANCD2 and FANCI are mainly nuclear localised (Boisvert et al., 2013, Colnaghi et al., 2011), which made us wonder whether a fraction of UBXN8 might actually localise at the inner nuclear membrane and this could be the site where UBXN8 interacts with the FA proteins. To address this hypothesis, I performed

immunofluorescence microscopy with tetracycline-inducible U2OS cells expressing Flag-UBXN8, to compare the UBXN8 localisation with that of lamin B1, an inner nuclear envelope marker.

The images were taken with a DeltaVision deconvolution microscope and processed using the visualising and analysing software softWoRx. The image shown in Figure 4.3 shows a mid-section of a U2OS cell co-immunostained for Flag-UBXN8 (green) and lamin B1 (red). The intensity line profile shows the pixel intensity values of both channels along the drawn line (across nucleus). The overlap of the intensity peaks at the indicated regions, suggest co-localisation of Flag-UBXN8 and lamin B1 at the nuclear envelope (indicated with arrows).

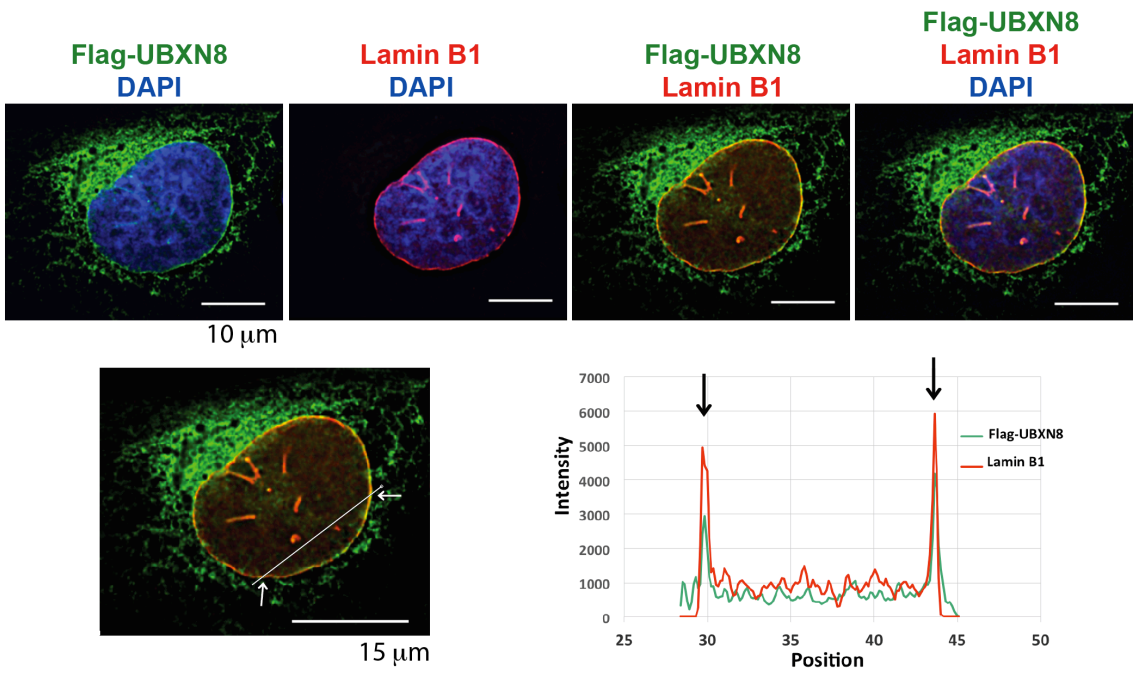

Figure 4.3: Flag-UBXN8 co-localises with lamin B1 using a conventional deconvolution microscope

A) Tetracycline-inducible U2OS cells expressing Flag-UBXN8 were co-immunostained for lamin B1 (red) and Flag-UBXN8 (green). DNA was counterstained with DAPI (blue). The images were taken with a DeltaVision deconvolution microscope and processed using the software softWoRx. The scale bars represent 10 µm.

B) The intensity line profile shows the pixel intensity values of the red and green channels along the line across the nucleus. The line profile shows co-localisation of Flag-UBXN8 and lamin B1 at the nuclear envelope. The scale bar represents 15 µm.

One of the limitations of the DeltaVision deconvolution microscope is its low resolution relative to the scale of subcellular structures. This means that objects closer together than 200–350 nm cannot be resolved, and appear to be merged into one (Schermelleh et al., 2008).

Therefore, the slides were also analysed using the OMX, a super resolution microscope. The OMX provides images with twice the resolution of conventional light microscopy by implementing three-dimensional structured illumination technology (3D-SIM) (Schermelleh et al., 2008). Schermelleh et al. demonstrated the potential of 3D-SIM to resolve subtle differences of epitope localisations within the nuclear pore complex (NPC). The multicolor imaging of the nuclear periphery with 3D-SIM makes it possible to differentiate between Nup proteins that are located in the centre and the cytoplasmic side of the NPC (Nup62, Nup214 or Nup358) and Nup proteins that are located on the nucleoplasmic side of the NPC (Nup153). The latter show a pore signal in the same plane as the lamin B signal (Schermelleh et al., 2008).

The resolution achieved with OMX structured illumination microscopy should be therefore high enough to determine whether membrane-bound UBXN8 faces into the nucleoplasm.

The experiment was performed as described before, and images were taken with the help of Markus Posch in the light microscopy facility in the College of Life Sciences, Dundee. The softWoRx tools for OMX image processing were used to reconstruct and align structured illumination images.

The image in figure 4.4 shows a mid-section of a U2OS cell co-immunostained for Flag-UBXN8 (green) and lamin B1 (red). The single dots (green) representing Flag-UBXN8 lie in the same plane as the lamin B1 signal, thus confirming that UBXN8 is anchored at the inner nuclear membrane (Figure 4.4, a and b). The localisation of

UBXN8 to the inner nuclear envelope supports the hypothesis that the interaction between UBXN8 and FANCD2/I occurs at this location.

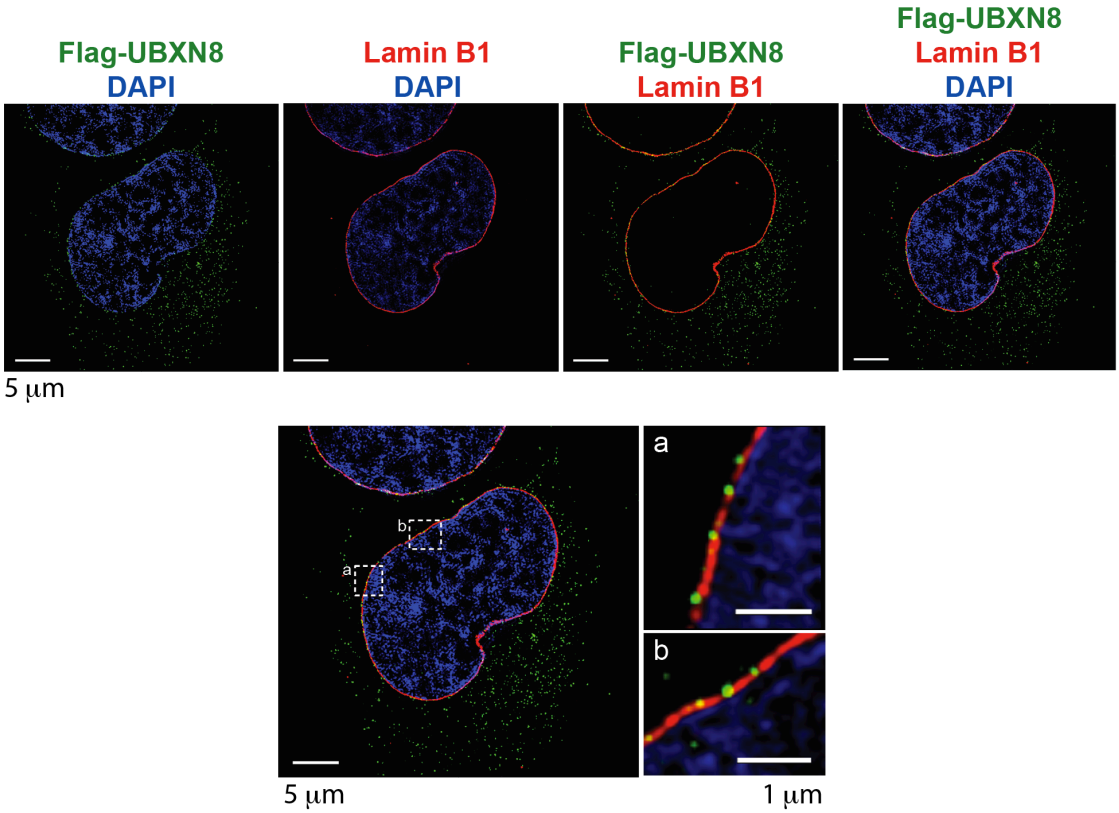

Figure 4.4: Flag-UBXN8 localises at the inner nuclear membrane

Tetracycline-inducible U2OS cells expressing Flag-UBXN8 were co-immunostained for lamin B1 (red) and Flag-UBXN8 (green). DNA was counterstained with DAPI (blue). The images were taken with the Dundee OMX microscope implementing three-dimensional structured illumination (3D-SIM). The softWoRx tools for OMX image processing were used to reconstruct and align structured illumination images. The scale bars in the upper panel of images represent 5 μm. The scale bars in the zoomed in images represent 1 μm.

To actually address whether UBXN8 co-localises with FANCD2 and FANCI, I performed immunofluorescence microscopy with U2OS cells, tetracycline-inducible for Flag-UBXN8. The cells were stained for Flag-UBXN8 and endogenous FANCD2. However, the strong signal of overexpressed Flag-UBXN8 and the weak signal of FANCD2 did not allow a reliable analysis for co-localisation. Furthermore, the signal for endogenous FANCD2 was too weak to analyse samples by OMX microscopy.

PART II - Interaction studies between UBXN8 and FANCD2/I

4.2.4 FANCD2 and FANCI are released from UBXN8 upon DNA damage

As shown in section 4.2.2, full-length Flag-UBXN8 co-immunoprecipitated both FA proteins in the absence of DNA damage. In the presence of DNA damage, FANCD2 and FANCI are localised at the DNA damage site to facilitate DNA repair (Smogorzewska et al., 2007).

Therefore, I wanted to know whether the presence of DNA damage has any effect on the interaction between UBXN8 and the FA proteins. The experiment was performed by immunoprecipitating Flag-UBXN8 from tetracycline-inducible Flag-UBXN8 U2OS cells that were either untreated or treated with DNA damage agent. Since the FA pathway is activated mainly through ICLs, the DNA damage was caused using the ICL inducing agent cisplatin. To allow the extraction of DNA-bound FANCD2 and FANCI, the cells were lysed in the presence of the endonuclease benzonase that degrades all forms of DNA and RNA.

The results show that, in the absence of DNA damage, Flag-UBXN8 co-immunoprecipitated FANCD2 and FANCI (Figure 4.5, lane 3). However, upon DNA damage, these interactions were clearly reduced compared, to non-treatment conditions (Figure 4.5, compare lanes 3 and 4). This suggests that the FA proteins are released, at least in part, from membrane-anchored UBXN8 upon their activation in response to DNA damage. Furthermore, comparing the extracts before and after the immunoprecipitation revealed only a small change in FANCD2 and FANCI levels, indicating that only a fraction of the FA proteins interacted with Flag-UBXN8 (Figure 4.5, compare lanes 7 and 8 with 9 and 10). The interaction between Flag-UBXN8 and p97 did not change upon DNA damage (Figure 4.5, compare lanes 3 and 4).

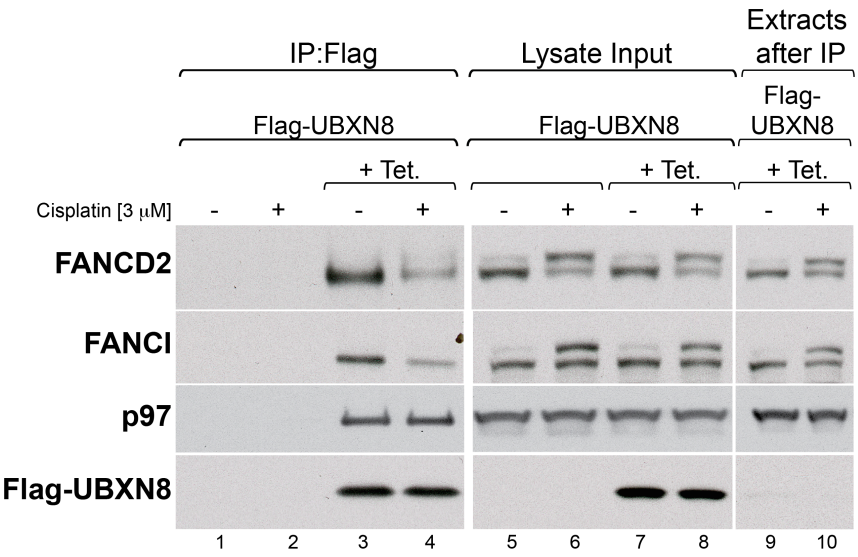

Figure 4.5: Upon DNA damage, FANCI and FANCD2 get released from wild type UBXN8
Flag-UBXN8 was immunoprecipitated from tetracycline-inducible U2OS cells expressing full-length Flag-UBXN8 and were untreated or treated with 3 μM cisplatin for 24h. The expression was induced by adding 0.5 μg/ml tetracycline. Uninduced U2OS cells were used as control. Flag-tagged proteins were immunoprecipitated with anti-Flag beads. Co-immunoprecipitated proteins were detected with specific antibodies. (*left*: IP, *right*: Lysate Input/Extracts after IP)

4.2.5 Endogenous FANCD2 co-immunoprecipitates endogenous UBXN8

The analysis of Flag-UBXN8 immunoprecipitates by mass spectrometry and Western blot showed that overexpressed Flag-UBXN8 co-immunoprecipitated endogenous FANCD2 and FANCI. To exclude the possibility that UBXN8 interaction with FA proteins is an artefact, due to protein overexpression, the interactions between the endogenous proteins were further analysed.

For this purpose, we raised two rabbit anti-UBXN8 polyclonal antibodies (called R2823 and R2824) against the full-length protein. Both UBXN8 antibodies detect denatured UBXN8 in Western blots (Figure 4.6). It should be mentioned that, in the protein extracts of UBXN8-silenced cells, only one band for UBXN8 disappeared, indicating that only one isoform exists in HeLa cells.

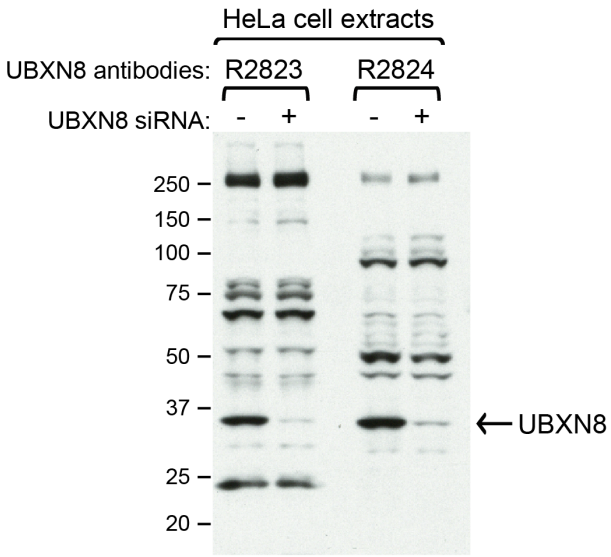

Figure 4.6: Both UBXN8 antibodies detect endogenous UBXN8 by Western blot
Western blot with cell extracts [20 µg/lane] from wild type or UBXN8-depleted HeLa cells. Total cell extracts were immunoblotted with two different purified anti-UBXN8 antibodies (R2823 and R2824). Binding of the primary antibody was detected using peroxidase-conjugated goat anti-rabbit IgG antibody followed by enhanced chemiluminescence.

However, in immunoprecipitations both UBXN8 antibodies showed cross-reactions with several other proteins, including FANCD2 and p97. Consequently, neither of the two UBXN8 antibodies could be used to study the interaction between the endogenous proteins.

Therefore, I decided to use the sheep anti-FANCD2 antibody (S099D) provided by the DSTT to study the interaction between the endogenous proteins.

I immunoprecipitated endogenous FANCD2 from U2OS cells untreated or treated with cisplatin using the anti-FANCD2 antibody. The cell lysates were incubated first with the antibody, followed by the incubation of the antibody–lysate mix with protein A-Sepharose beads. Cell lysates incubated with protein A-Sepharose in the absence of the FANCD2 antibodies were used as control (Figure 4.7).

The immunoprecipitation of endogenous FANCD2 shows that FANCD2 interacts mainly with modified FANCI (Figure 4.7, lanes 2 and 3), and that this interaction dramatically increased upon DNA damage. By comparing the ‘lysate input’ and the ‘extracts after IP’, the unmodified fraction of FANCI seems mostly unaffected (Figure

4.7, lanes 6 and 8). Indeed, FANCD2 co-immunoprecipitates only a small amount of unmodified FANCI, and the binding did not change in the presence or absence of DNA damage (indicated with arrow). These results suggest that FANCD2 interacts mainly with modified FANCI (even in the absence of DNA damage) and that unmodified FANCI, except for a small portion, does not interact with FANCD2.

Furthermore, UBXN8 was detected in endogenous FANCD2 immunoprecipitates, confirming the interaction between FANCD2 and UBXN8 at endogenous levels (Figure 4.7, lanes 2 and 3). Consistent with the data obtained by Flag-UBXN8 immunoprecipitation, endogenous FANCD2 showed decreased binding to UBXN8 upon DNA damage, compared to non-damage conditions.

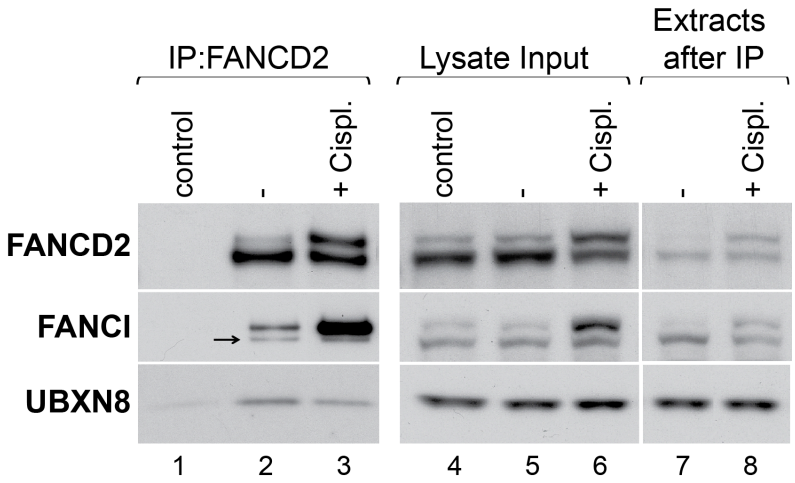

Figure 4.7: Endogenous FANCD2 co-immunoprecipitates endogenous UBXN8
Endogenous FANCD2 was immunoprecipitated from U2OS cells untreated or treated with 3 μM cisplatin. The immunoprecipitation was performed using anti-FANCD2 antibodies and protein A-Sepharose beads. Naked protein A-Sepharose beads incubated with extract were used as negative control. Co-immunoprecipitated proteins were detected with specific antibodies. (*left*: IP, *right*: Lysate Input and Extract after IP)

To show that the reduced binding of UBXN8 to FANCD2 is due to the mono-ubiquitylation/activation of FANCD2 upon DNA damage, I performed an endogenous FANCD2 immunoprecipitation with UBE2T-silenced U2OS cells untreated or treated

with cisplatin. UBE2T is the E2 enzyme that, together with the E3 ligase FANCL facilitates the mono-ubiquitylation of FANCD2 and FANCI in response to DNA damage (Longerich et al., 2009, Alpi et al., 2008, Zhang et al., 2008). By silencing UBE2T, the activation of FANCD2 in the presence of ICLs should be abolished and, therefore, the release from UBXN8 impeded. Cells transfected with Luciferase siRNA were used as negative control, and FANCD2-silenced cells were used to analyse non-specific binding of the FANCD2 antibody to UBXN8.

Figure 4.8 shows that silencing of the E2 enzyme, UBE2T strongly reduced the mono-ubiquitylation of FANCD2 and FANCI upon DNA damage (compare lanes 12 with 14). Furthermore, in UBE2T-silenced cells, the binding between FANCD2 and UBXN8 remained unchanged with or without DNA damage (Figure 4.8, lanes 5 and 6). This result supports the possibility that the activation/mono-ubiquitylation of FANCD2 (and FANCI) reduces the FANCD2-binding to UBXN8. However, the immunoprecipitation of Flag-UBXN8 from wild type vs. UBE2T-silenced cells in the presence and absence of DNA damage would clarify, whether the activation of FANCD2 and FANCI causes their release from membrane-anchored UBXN8.

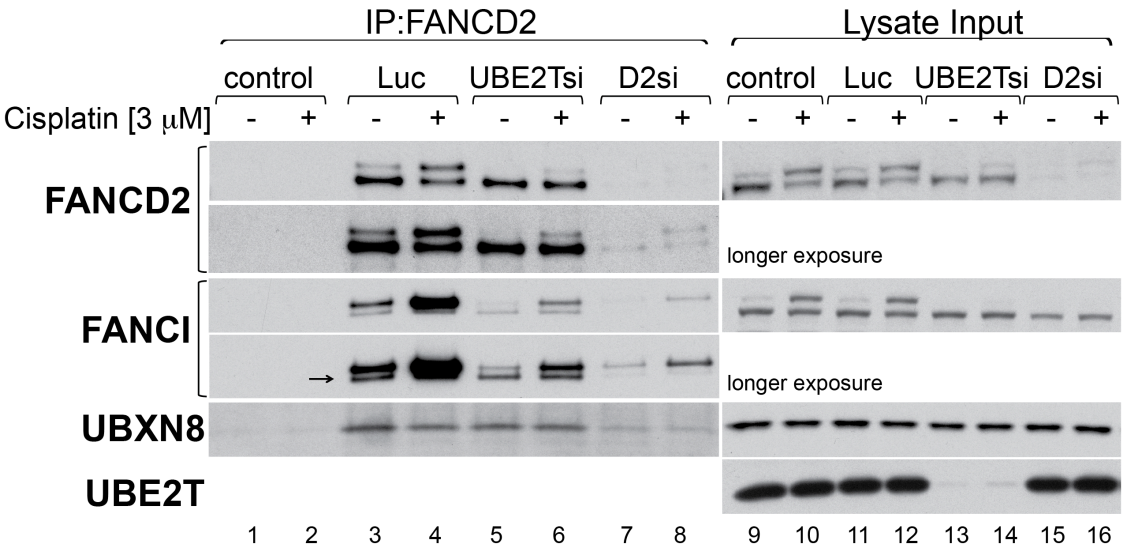

Figure 4.8: Preventing FANCD2 activation upon DNA damage inhibits its release from UBXN8
Endogenous FANCD2 was immunoprecipitated from U2OS cells that were depleted for UBE2T or FANCD2 and either untreated or treated with 3 μM cisplatin. Cells transfected with Luciferase siRNA were used as control. The immunoprecipitations were performed using anti-FANCD2 antibodies and protein A-Sepharose beads. Naked protein A-Sepharose beads incubated with extract or anti-FANCD2 antibody/beads incubated with FANCD2-silenced cells were used as negative control. Co-immunoprecipitated proteins were detected with specific antibodies. (*left*: IP, *right*: Lysate Input and Extract after IP)

4.2.6 Release from DNA damage does not increase the binding between FANCD2 and UBXN8

Flag-UBXN8 and endogenous FANCD2 immunoprecipitations showed that only a small fraction of UBXN8 interacts with FANCD2 and FANCI.

The microscopy images obtained with the OMX indicate that only a small fraction of UBXN8 is localised to the inner nuclear membrane. If this is the actual site of interaction between UBXN8 and FANCD2/I, the small amount of nuclear UBXN8 would be only able to bind a small pool of the FA proteins.

Furthermore, the immunoprecipitations of endogenous FANCD2 showed that FANCD2 interacts mainly with modified FANCI, and that this interaction dramatically increased upon DNA damage (Figure 4.7, lanes 2 and 3). Although the majority of non-ubiquitylated FANCI is not bound to FANCD2, I also observed a minor fraction of it in FANCD2 immunoprecipitates (Figure 4.7, lane 2 [arrow]). Since Flag-UBXN8 co-immunoprecipitates only a small fraction of non-ubiquitylated FANCD2 and FANCI (Figure 4.5, compare lanes 7 with 9), I wondered if UBXN8 binds non-ubiquitylated FANCD2/I heterodimers. This could be another reason why the interaction between UBXN8 and FANCD2/I only involves small fractions of the proteins.

After the execution of DNA repair, FANCD2 and FANCI are de-ubiquitylated and dissociate from chromatin, which might increase the pool of non-ubiquitylated FANCD2/I heterodimers. Therefore, to test this assumption and to see whether this

leads to an increase in UBXN8 binding, I performed a FANCD2 immunoprecipitation from U2OS cells that were released from DNA damage.

The time window for the release experiment was chosen based on live cell imaging with U2OS cells stably expressing GFP-FANCD2 that revealed clear reduction in foci between 24h and 48h after release (Figure 4.9). Within the first 24h after release, the FANCD2/I dimer formation did not show significant changes.

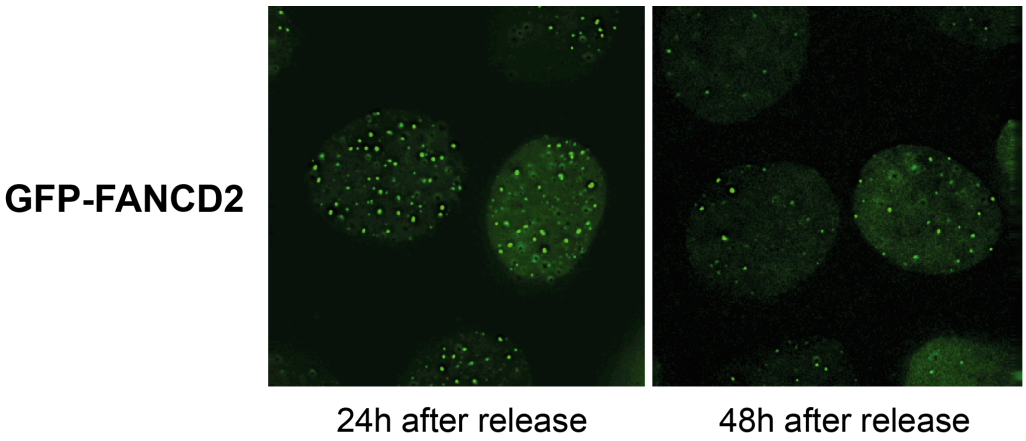

Figure 4.9: Foci formation of GFP-FANCD2 is clearly reduced 48h after the release from DNA damage
Tetracycline-inducible U2OS cells expressing GFP-FANCD2 were released from cisplatin treatment [3 μM, 24h]. During the release, the reduction in number of foci was monitored via live cell imaging using a Delta Vision microscope.

Furthermore, the cell cycle progression upon DNA damage release was analysed by FACS. The treatment with cisplatin for 24h arrested cells in S-phase, the cell cycle stage in which the replication and repair of DNA takes place (Figure 4.10). Twenty-four hours after release from DNA damage, the cells are mostly in G2. The G2/M arrest is described in the literature and prevents the cells' progression into mitosis before DNA repair is completed (Stark and Taylor, 2004). Forty-eight hours after release, the cells partially progress to G1- and S-phase, suggesting that they overcame the induced DNA damage and re-entered the cell cycle.

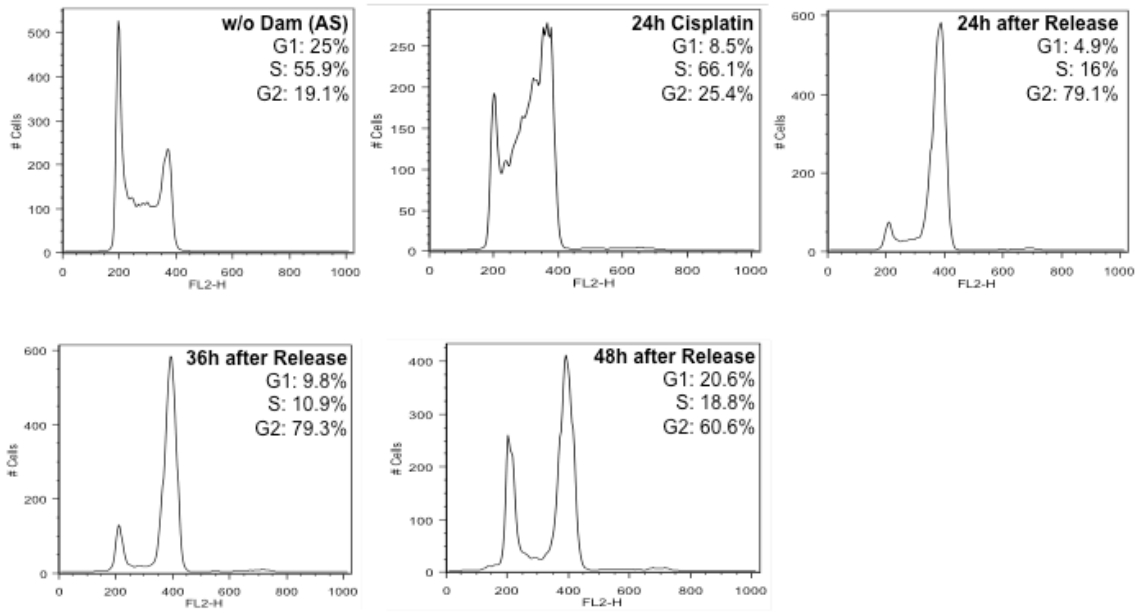

Figure 4.10: U2OS cells partially re-enter the cell cycle 48h after DNA damage release

U2OS cells were treated with 3 μM cisplatin. Fresh medium was added 24h after cisplatin treatment to allow DNA repair and cell cycle progression. Cells were harvested before, and at the indicated time points after DNA damage. The cells were stained with propidium iodide and their cell cycle stages analysed by FACS. For each time point, the FACS profile and the percentage of cells in the different cell cycle stages are shown.

For the release experiment, FANCD2 was immunoprecipitated from U2OS cells that had been treated for 24h with cisplatin and then lysed at 24h, 36h and 48h after release. The immunoprecipitates were analysed by Western blot to monitor changes in the FANCD2/I dimer upon release, and its interaction with UBXN8.

The results of the FANCD2 immunoprecipitation are shown in Figure 4.11. The cell lysates prepared at the time points 24h, 36h and 48h after release from DNA damage showed gradually reducing levels of modified FANCD2 and FANCI (Figure 4.11, lanes 8–10). Accordingly, the levels of co-immunoprecipitated modified FANCI decreased as well (lanes 2–4) but did not reach the low level of FANCD2/I interaction observed under non-treatment conditions (Figure 4.11, compare lanes 4 and 5).

Interestingly, the reduction in FANCI co-immunoprecipitated with FANCD2 correlates with an increased interaction with p97, reaching its peak 36h after release (lane 3). As

mentioned in the introduction, p97 is reported to be involved in the DNA damage response, by dissociating chromatin-bound proteins (Dantuma and Hoppe, 2012). Therefore, it is tempting to speculate that p97 might be required for FANCD2/I dimer dissociation from chromatin.

Probing the FANCD2 immunoprecipitates for UBXN8 with the R2823 antibody led to the detection of two protein species that strongly accumulated upon release, but migrated higher than expected (Figure 4.11, lanes 3 and 4). These could be modified forms of UBXN8, given that ubiquitylation and phosphorylation sites for UBXN8 were found in previous proteome analyses (Daub et al., 2008, Dephoure et al., 2008, Kim et al., 2011). However, the R2824 antibody showed a better detection of UBXN8, but did not detect these slower migrating bands to the same extent, indicating that these bands were recognised non-specifically by the R2823 UBXN8 antibody.

The release from DNA damage caused a reduction in FANCD2 binding to modified FANCI, but the binding to unmodified FANCI remained low. Therefore, the initial hypothesis that release from DNA damage may lead to an increased pool of soluble, unmodified dimer was not confirmed.

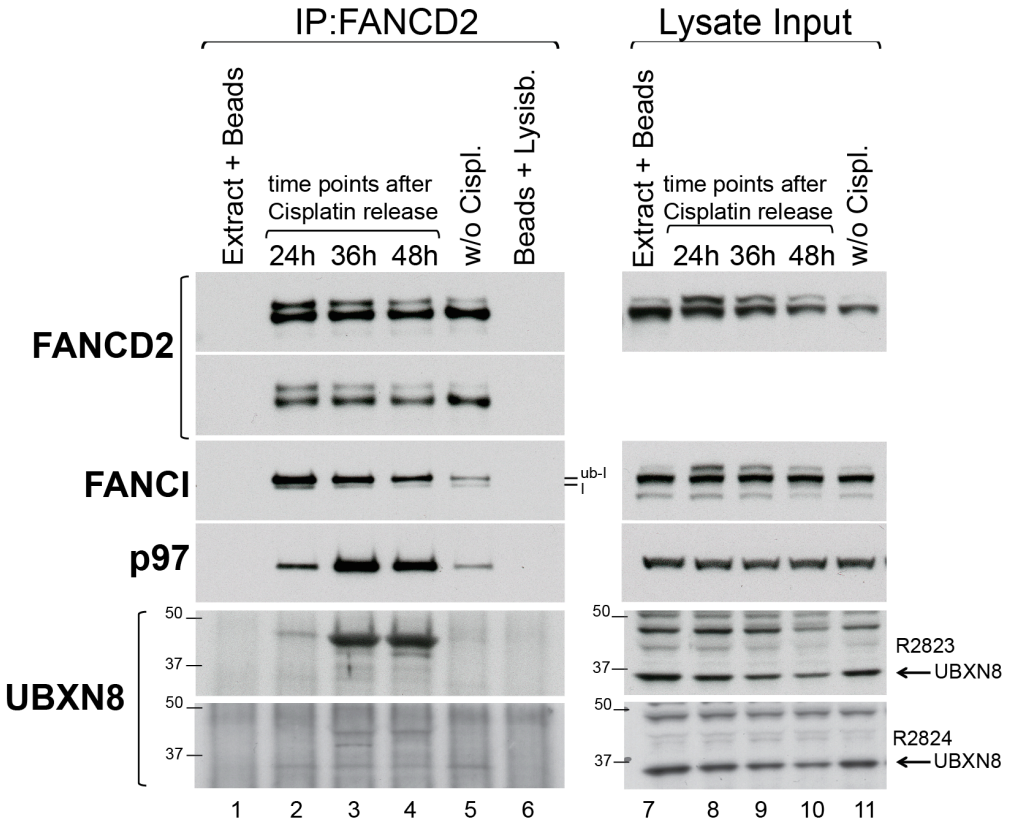

Figure 4.11: FANCD2/I dimer dissociation correlates with increased p97-binding after release from DNA damage

Endogenous FANCD2 was immunoprecipitated from U2OS cells that were treated with 3 μM cisplatin for 24h, released by adding fresh media and harvested at the indicated time points. Cells were lysed in the presence of 500U/ml benzonase. The immunoprecipitation was performed using anti-FANCD2 antibodies and protein A-Sepharose beads. Naked protein A-Sepharose beads incubated with extract or lysis buffer/antibody were used as negative controls. Co-immunoprecipitated proteins were detected with specific antibodies. Endogenous UBXN8 was detected using the UBXN8 antibodies R2823 or R2824. (*left*: IP, *right:* Lysate Input)

To investigate whether the observed co-immunoprecipitation of p97 depends on UBXN8, the time course experiment was repeated with UBXN8-silenced U2OS cells. Figure 4.12 shows that silencing of UBXN8 did not change the increase binding of p97 to FANCD2 upon DNA damage release (lanes 2 and 3). The bands detected between 37 kDa and 50 kDa did not disappear in UBXN8-silenced cells (lanes 6 and 7), confirming that this band did not represent modified UBXN8. UBXN8 detection with the R2824 antibody revealed a slight increase in UBXN8 binding 36h after release (Figure 4.12, compare lanes 2 and 4).

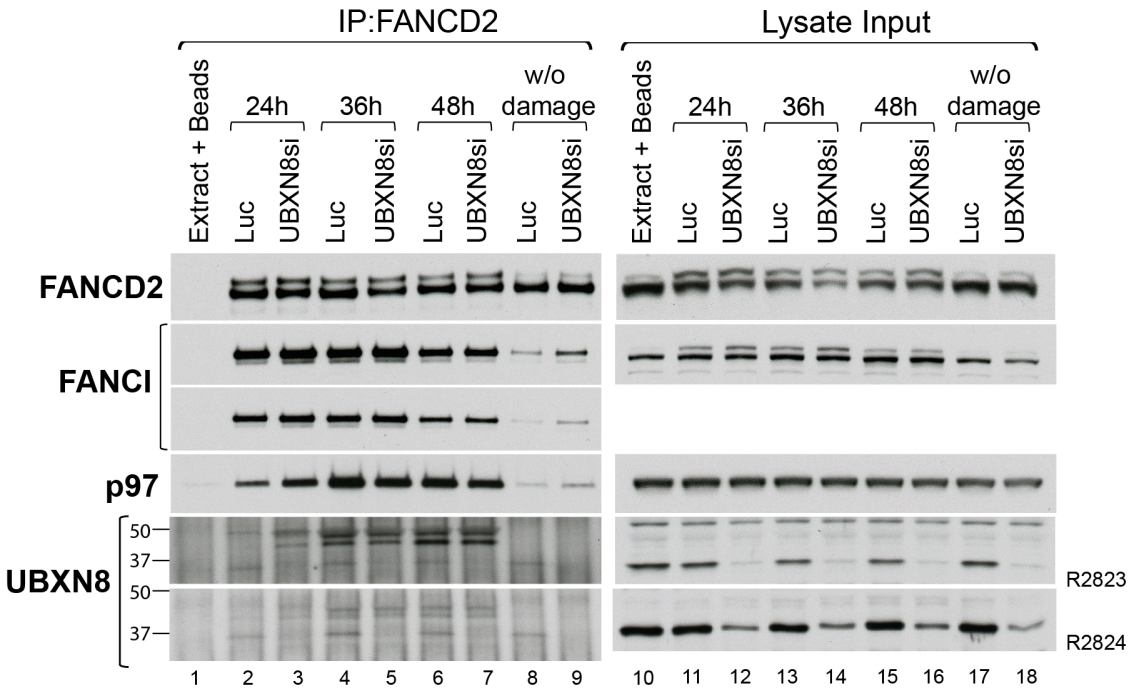

Figure 4.12: FANCD2 co-immunoprecipitates p97 independently from UBXN8

Endogenous FANCD2 was immunoprecipitated from U2OS cells silenced or not for UBXN8 that were treated with 3 μM cisplatin for 24h, released by adding fresh media and harvested to the indicated time points. Cells were lysed in the presence of 500U/ml benzonase. The immunoprecipitation was performed using anti-FANCD2 antibodies and protein A-Sepharose beads. Naked protein A-Sepharose beads incubated with extract or lysis buffer/antibody were used as control. Co-immunoprecipitated proteins were detected with specific antibodies. Endogenous UBXN8 was detected using two different UBXN8 antibodies: R2823 and R2824 (*left*: IP, *right*: Lysate Input and Extract after IP)

The silver staining of the FANCD2-immunoprecipitates showed a dramatic increase in co-immunoprecipitated proteins after 36h–48h after release from DNA damage. Therefore, I decided to analyse bands that changed more dramatically after release by MS (Figure 4.13). The MS analysis identified mainly cytoskeletal proteins, including alpha- and beta-actin that were assigned to the band cut around 40 kDa, which we initially thought to be modified-UBXN8. Filamin A and actin, that build crosslinked actin filaments, are reported to be required for DSB repair as well as recovery from DNA damage-induced G_2 arrest (Andrin et al., 2012, Meng et al., 2004). However, it is not obvious why cytoskeletal proteins are so abundant in FANCD2 co-immunoprecipitates upon DNA damage release.

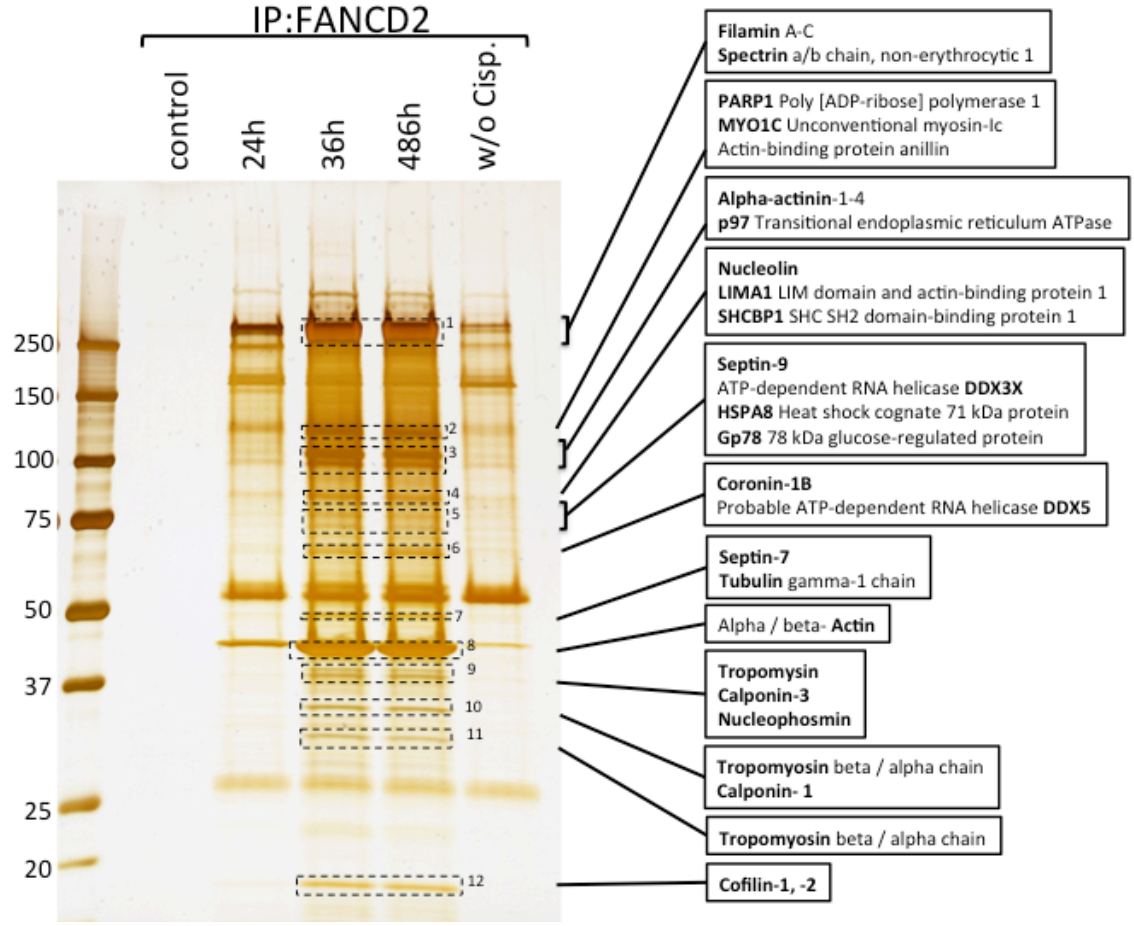

Figure 4.13: FANCD2 binds to multiple cytoskeletal proteins after release from DNA damage
Endogenous FANCD2 was immunoprecipitated from U2OS cells that were treated with 3 μM cisplatin for 24h, released by adding fresh media and harvested at the indicated time points. Cells were lysed in the presence of 500U/ml benzonase. The immunoprecipitations were performed using anti-FANCD2 antibodies and protein A-Sepharose beads. Naked protein A-Sepharose beads incubated with extract were used as control. The proteins in the immunoprecipitates were separated by gel electrophoresis and protein bands were visualized by silver staining. The indicated bands were cut, the proteins in the gel digested, and identified by mass spectrometry. The most abundant protein hits identified in each band are listed in the boxes on the right.

4.2.7 Flag-FANCI immunoprecipitations to study how changes in the FANCD2/I dimer formation affect the interaction to UBXN8

Ishiai et al. showed that six key serine residues are important phosphorylation sites in chicken FANCI and are required for the mono-ubiquitylation of FANCD2 and the activation of the FA pathway (Ishiai et al., 2008). They described a sextuple phospho-mimicking serine to aspartate (Dx6) mutant, and a phospho-dead serine to alanine (Ax6)

mutant of chicken FANCI, and showed that the phospho-mimicking mutant induces constitutive mono-ubiquitylation and foci formation of FANCI and FANCD2. Conversely, the phospho-dead mutant largely abrogated the mono-ubiquitylation and foci formation of both FA proteins, resulting in loss of the DNA repair function.

Based on these data, I attempted an alternative approach to study the interaction between UBXN8 and the heterodimer FANCD2/I. I aimed to artificially increase the FANCD2/I dimer formation in cells, to study how this affects the interaction to UBXN8.

4.2.7.1 Quadruple Flag-FANCI phospho-mimicking mutant constitutively activates FANCD2 and induces dimer formation with FANCD2 in the absence of DNA damage

To investigate whether constitutive dimer formation of FANCD2/I changes the binding to UBXN8, I used human sextuple FANCI phospho-mutants (Dx6 and Ax6) equivalent to the chicken ones described by Ishiai et al. In addition, I included a quadruple mutant of human FANCI that harboured only four of the six mutations (Figure 4.14).

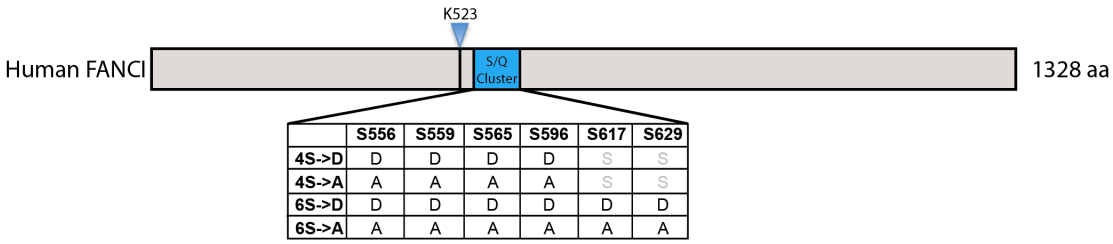

	S556	S559	S565	S596	S617	S629
4S->D	D	D	D	D	S	S
4S->A	A	A	A	A	S	S
6S->D	D	D	D	D	D	D
6S->A	A	A	A	A	A	A

Figure 4.14: S/Q cluster in human FANCI

Schematic representation of human FANCI highlighting a S/Q cluster close to the ubiquitylation site K523. The table shows the quadruple and sextuple phopho-mimicking and phospho-dead mutant used for the experiments described in figure 4.15.

In contrast to the data described for chicken FANCI by Ishiai et al, the sextuple phospho-mimicking mutant in human FANCI failed to constitutively activate FANCD2 (Figure 4.15, lanes 14 and 17) and failed to induce dimer formation in mammalian cells (lanes 2 and 5). Interestingly, these effects were, however, induced by the quadruple phospho-mimicking mutant of human FANCI that we created. This version of FANCI increased the levels of mono-ubiquitylated FANCD2 similarly to that observed upon DNA damage (compare lanes 15 and 21). In the absence of DNA damage, this mutant co-immunoprecipitated high FANCD2 levels comparable to that observed for wild type FANCI after DNA damage (lanes 3 and 8). In contrast, the quadruple phospho-dead mutant did not show any binding to mono-ubiquitylated FANCD2 either with, or without, DNA damage (lanes 4 and 10). However, I found that endogenous UBXN8 bound to wild type and mutant Flag-FANCI with similar efficiency.

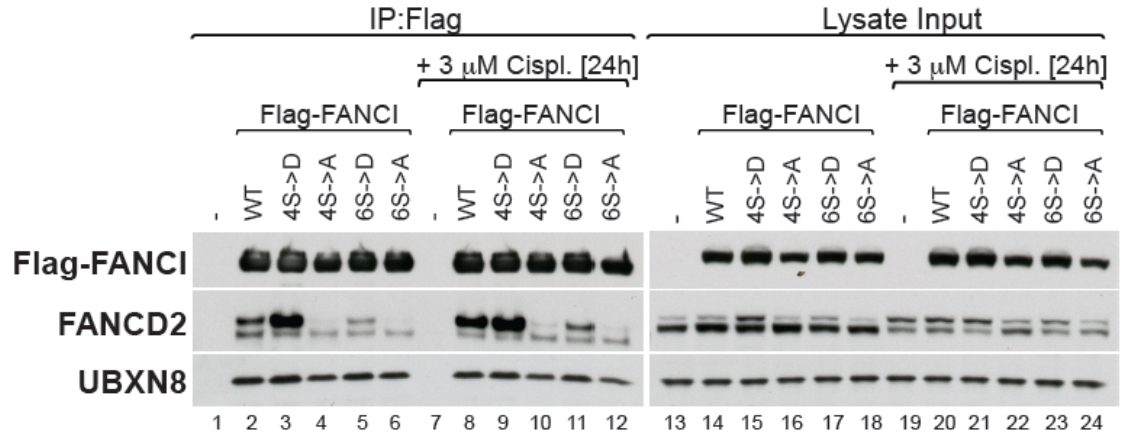

Figure 4.15: Phospho-mimicking mutations in FANCI induce FANCD2/I dimer formation in the absence of DNA damage

U2OS cells were transfected for 24h with wild type Flag-FANCI or the quadruple [S556A/D, S559A/D, S565A/D, S596A/D] or sextuple [S556A/D, S559A/D, S565A/D, S596A/D, S617A/D, S629A/D] Flag-FANCI phospho-mutants, which were either phospho-mimicking or phospho-dead mutants. The cells were untreated or treated with 3 μM cisplatin (24h) and the Flag-tagged proteins were immunoprecipitated with anti-Flag beads. All indicated proteins were detected with specific antibodies. Cells expressing no Flag-tagged protein were used as negative control. (*left*: IP, *right*: Lysate Input)

I took advantage of the fact that I could only extract chromatin-bound proteins by using benzonase, which degrades all forms of DNA and RNA. By performing the protein extraction with or without benzonase, I found that most of the co-immunoprecipitated modified FANCD2 was only extracted with benzonase, suggesting that modified FANCD2 was DNA-bound (Figure 4.16A, right panel). This indicates that the ectopically formed FANCD2/I dimer binds to the DNA even though DNA damage was not induced. Hence, the artificially induced dimer of FANCD2/I did not lead to an increase of dimer that was not bound to the DNA. It is likely that DNA-bound FANCD2/I is not accessible to interact with UBXN8 that is anchored at the nuclear membrane. The reduced UBXN8 interaction with FANCD2 and FANCI upon DNA damage supports this idea.

The dimer with unmodified FANCD2 was extracted equally well either with or without benzonase, suggesting that it is not bound to the DNA. This pool of FANCD2/I dimer is soluble and could therefore be accessible for UBXN8 for interaction.

In FANCI, the conserved lysine residue K523 was shown to be the site of mono-ubiquitylation (Smogorzewska et al., 2007). The mutation K523R in human FANCI that prevents its mono-ubiquitylation strongly reduced the interaction with modified FANCD2 but did not affect its binding to unmodified FANCD2 (Figure 4.16A, compare lanes 6 and 7). In DT40 cells, the mono-ubiquitylation of chicken FANCI was described to be largely dispensable for FANCD2 binding and mono-ubiquitylation (Ishiai et al., 2008). However, studies in mammalian cells suggested that FANCD2/I mono-ubiquitylation might stabilise the ID complex formation (Joo et al., 2011, Rego et al., 2012). The K523R mutation, in combination with the 4SD mutations, could not restore the FANCI interaction with modified FANCD2 to the wild type FANCI level (Figure 4.16B, compare lanes 9 and 11). This suggests that the ubiquitylation of FANCI is

essential for the dimer formation with modified FANCD2. Furthermore, the dimer containing unmodified FANCD2 was extracted equally well in the presence and absence of benzonase, indicating that the ubiquitylation of FANCI might be required to stabilise the FANCD2/I dimer on the chromatin.

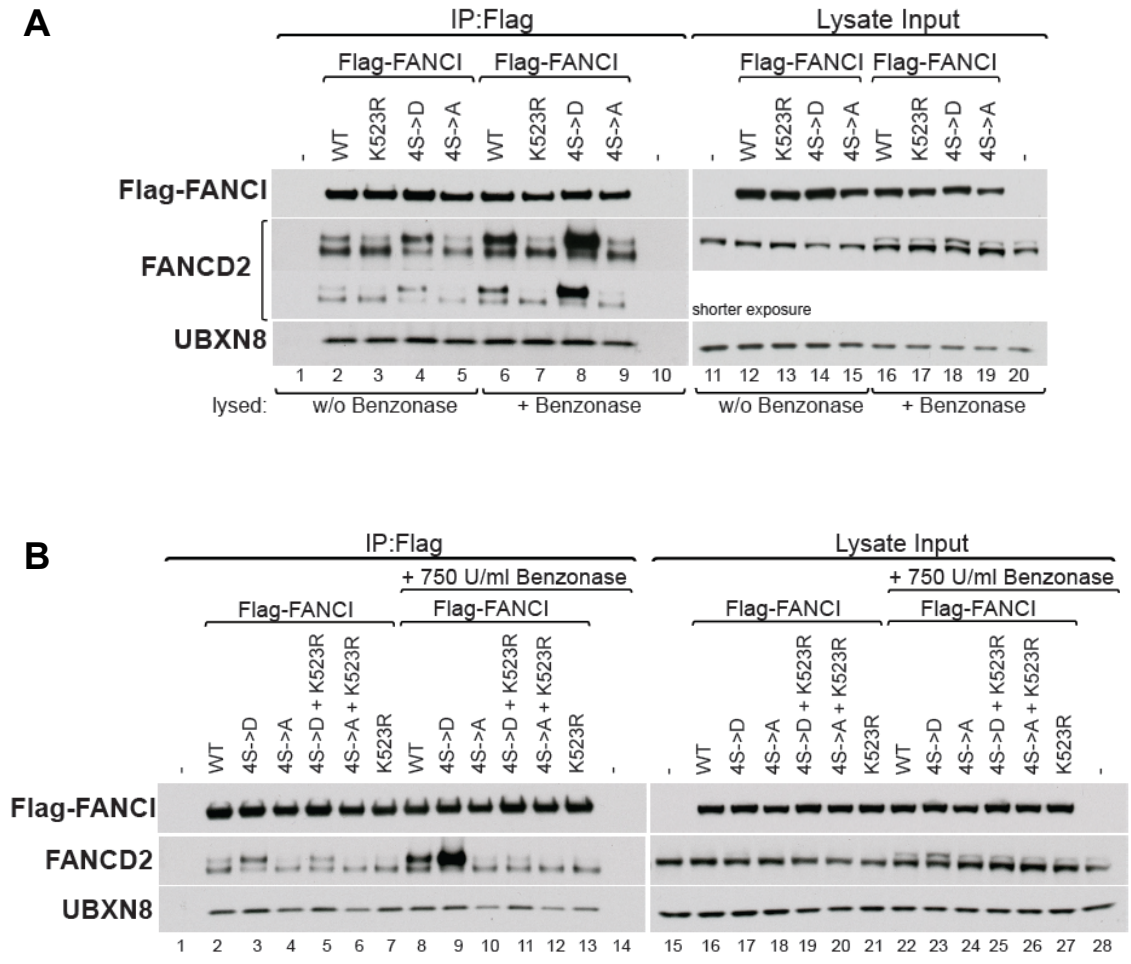

Figure 4.16: Ectopically formed FANCD2/I dimer binds to the DNA in the absence of DNA damage

A) U2OS cells were transfected for 24h with wild type Flag-FANCI or the quadruple [S556A/D, S559A/D, S565A/D, S596A/D] Flag-FANCI phospho-mutants, which were either phospho-mimicking or phospho-dead. The cells were lysed in the presence or absence of benzonase, and Flag-tagged proteins were immunoprecipitated using anti-Flag beads. All indicated proteins were detected with specific antibodies. Cells expressing no Flag-tagged protein were used as negative control.

B) Same experimental setup as described in A, including the Flag-FANCI phospho-mimicking or phospho-dead mutant, with the additional K523R mutation.

4.2.7.2 Attempt to increase the soluble pool of FANCD2/I dimer using a DNA-binding deficient quadruple Flag-FANCI phospho-mimicking mutant

We generated the quadruple mutant with two additional amino acid changes (K898E and K980E) at putative DNA binding region of FANCI (Joo et al., 2011), in an attempt to increase the dimers that are not targeted to the DNA.

Figure 4.17 shows the Flag-FANCI immunoprecipitations performed in the presence and absence of benzonase. As described before, the overexpression of the quadruple phospho-mimicking mutant (4SD) led to increased dimer formation (Figure 4.17, compare lanes 6 and 7). The DNA binding mutations (2KE) had a negative effect on dimerization both alone and in combination with 4SD (Figure 4.17, compare lanes 6 with 8 and 7 with 9). However, when comparing the results with and without benzonase, it appears that the 2KE mutants are still able to bind the DNA. We therefore cannot determine whether the defect in dimerization is due to partially defective DNA binding, or if the 2KE mutations directly affect dimerization.

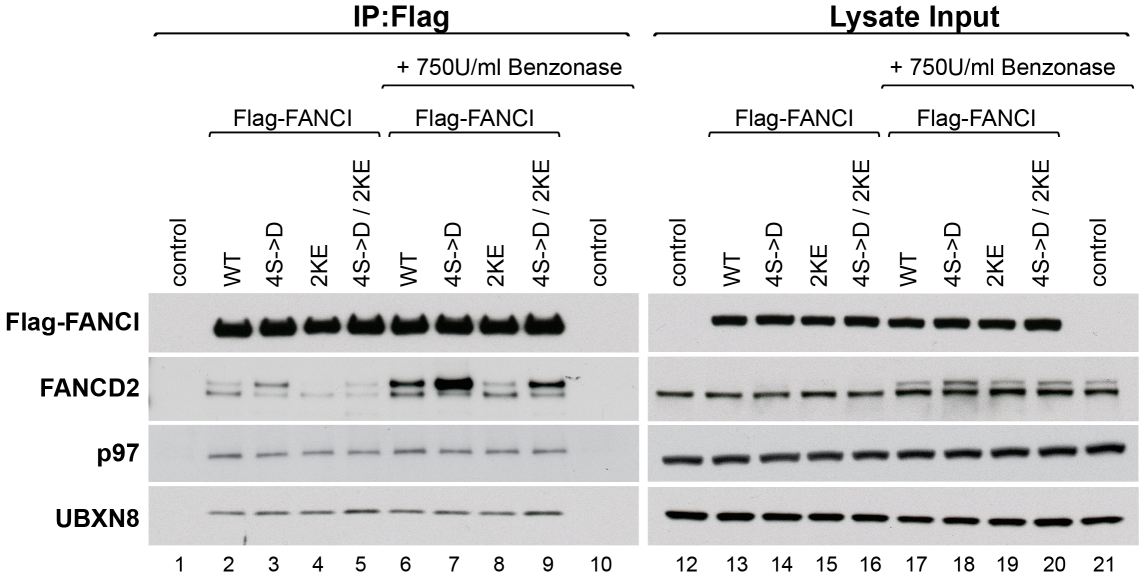

Figure 4.17: The DNA binding mutations (K898/K980) had a negative effect on FANCD2/I dimerization

U2OS cells were transiently transfected with wild type or different mutants of Flag-FANCI [4SD = S556D, S559D, S565D, S596D; 2KE = K898E K980E; 4SD/2KE: 4SD + 2KE]. The pellet was divided into two tubes and the cells lysed in the presence or absence of 750U/ml

benzonase. Flag-tagged proteins were immunoprecipitated with anti-Flag beads. Co-immunoprecipitated proteins were detected with specific antibodies. Cells expressing no Flag-tagged protein were used as negative control. (*top*: IP, *bottom*: Lysate Input)

Taken together, the results obtained with the quadruple Flag-FANCI mutants show that phosphorylation of the four serine residues S556D, S559D, S565D, S596D in human FANCI constitutively activate FANCD2 and induce FANCD2/I dimer formation in the absence of DNA damage. However, this artificially induced dimer was targeted to chromatin even in the absence of DNA damage. The additional mutations at putative DNA binding regions of FANCI caused a defect in FANCD2/I dimerization and therefore did not increase the soluble pool of FANCD2/I dimer. The increase in DNA-bound dimer did not change UBXN8 binding to FANCI.

4.2.8 Small changes in UBXN8 levels after release from double-thymidine block

To analyse if UBXN8 levels are cell cycle regulated, cells were arrested in S-phase using a double thymidine block. After thymidine release, the cells were harvested at two-hour intervals for the next 18h (Figure 4.18). To monitor the cell cycle stages, a small fraction of cells were stained with propidium iodide and analysed by FACS. The rest of the cells were used to prepare protein extracts, which were analysed by Western blot. The detection of the phosphorylation of serine 10 in histone H3 was used as a mitosis marker.

The FA proteins FANCD2 and FANCI showed a strong mono-ubiquitylation, due to the thymidine treatment, that gradually decreased after release as cells progressed through the cell cycle, and was not re-induced when cells re-entered S-phase (Figure 4.18). The increased levels of mono-ubiquitylated FANCD2 and FANCI were caused by thymidine, which is described to induce DNA damage response (Bolderson et al., 2004). The total FANCD2 and FANCI levels in the cells seemed not to change during

the cell cycle. The increased levels of mono-ubiquitylated FANCD2 and FANCI after thymidine treatment are accompanied by reduced UBXN8 levels compared to asynchronised cells, or cells harvested at later time points (10–18h). This could suggest that UBXN8 levels are reduced upon DNA damage to allow the additional release/activation of repair proteins. Under non-damage conditions, normal UBXN8 levels might be required to capture these proteins at the membrane. The p97 level did not change throughout the cell cycle.

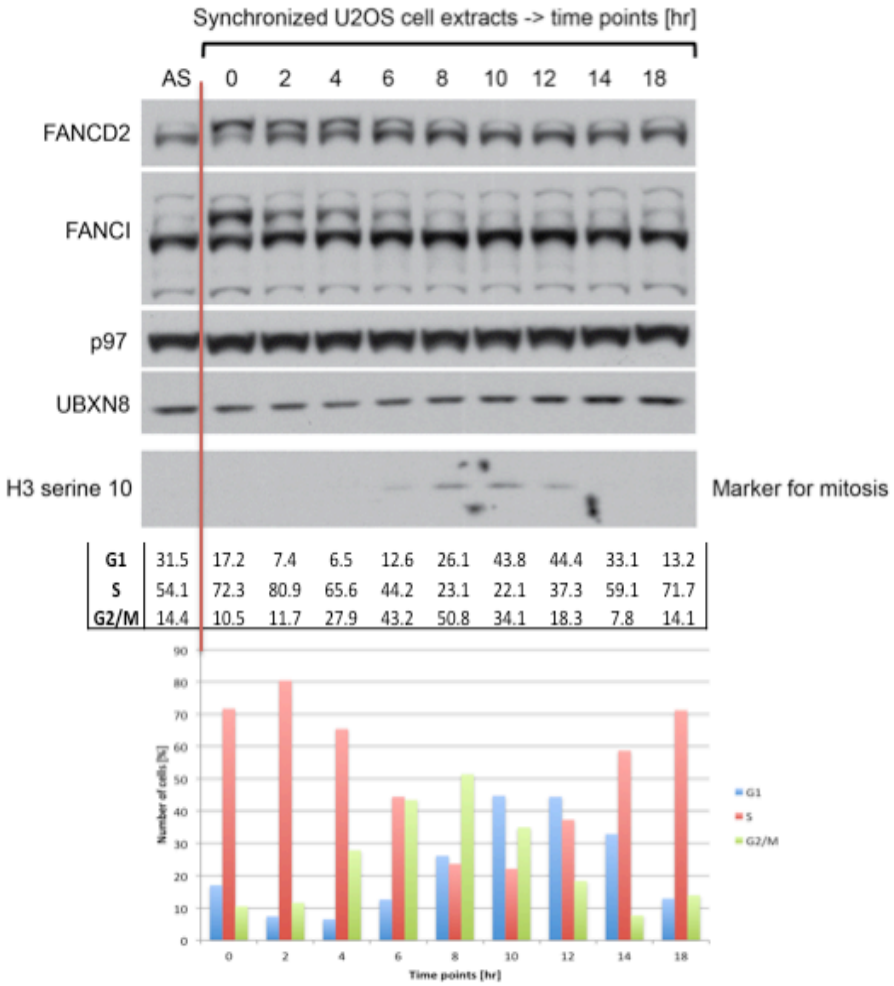

Figure 4.18: UBXN8 shows cell cycle dependent regulation

U2OS cells were arrested in S-phase by using a double thymidine block. After releasing the cells from the arrest, cells were harvested at different time points for the next 18 hours. A small cell-fraction was stained with propidium iodide and analysed by FACS. The rest of the cells were used to prepare protein extracts. Phosphorylation of serine 10 in histone H3 was used as a mitotic marker.

Top: Western blot with protein extracts isolated from synchronized U2OS cells at different cell cycle stages.
Bottom: FACS analysis of the synchronized U2OS cells. The percentages of cells in the different cell cycle stages are indicated.

4.2.9 Increased UBXN8 and FANCD2 interaction in cell populations with the highest percentage of cells in S-phase

To address whether the interaction between UBXN8 and both FA proteins, FANCD2 and FANCI, is cell cycle regulated, endogenous FANCD2 was immunoprecipitated from U2OS cells that were either arrested in G1-phase via serum starvation or in mitosis via nocodazole treatment (Figure 4.19). The optimisation for S-phase arrest with a drug that does not induce FANCD2/I activation/mono-ubiquitylation (as e.g. observed with thymidine) was still in progress while writing this thesis.

The FANCD2 immunoprecipitations from asynchronised U2OS cells with the largest percentage of cells in S-phase might show the highest UBXN8/FANCD2 interaction. (Figure 4.19, compare lanes 2 with 3 and 4). This correlates with increased UBXN8 levels in the lysate input compared to G1 and mitosis-arrested cells (Figure 4.19, compare lane 6 with lanes 7 or 8). This suggests that UBXN8 levels are higher during S-phase under non-damage conditions, compared to those in G1 and mitosis.

During mitosis, only the interaction between unmodified FANCD2 and FANCI was detected (Figure 4.19, lane 4). Interestingly, the mitotic arrest led to the detection of two bands for UBXN8 in the extracts (Figure 4.19, lane 8), corresponding to full-length UBXN8 and a slower migrating form that could be phosphorylated UBXN8. Indeed, phosphorylation sites were identified for UBXN8 in phospho-proteome analyses of mitotic cells (Daub et al., 2008, Dephoure et al., 2008, Kim et al., 2011). FANCD2 co-immunoprecipitated both forms of UBXN8. Furthermore, the binding pattern of UBXN8 to FANCD2 mimicked the binding of FANCD2 to unmodified FANCI, and

could indicate that UBXN8 binds unmodified dimer. However, it is also possible that UBXN8 was co-immunoprecipitated with monomeric FANCD2.

The cells arrested in G1 showed a decreased interaction between FANCD2 and FANCI, as well as FANCD2 and UBXN8 compared to asynchronous cells (Figure 4.19, compare lanes 2 and 3).

A

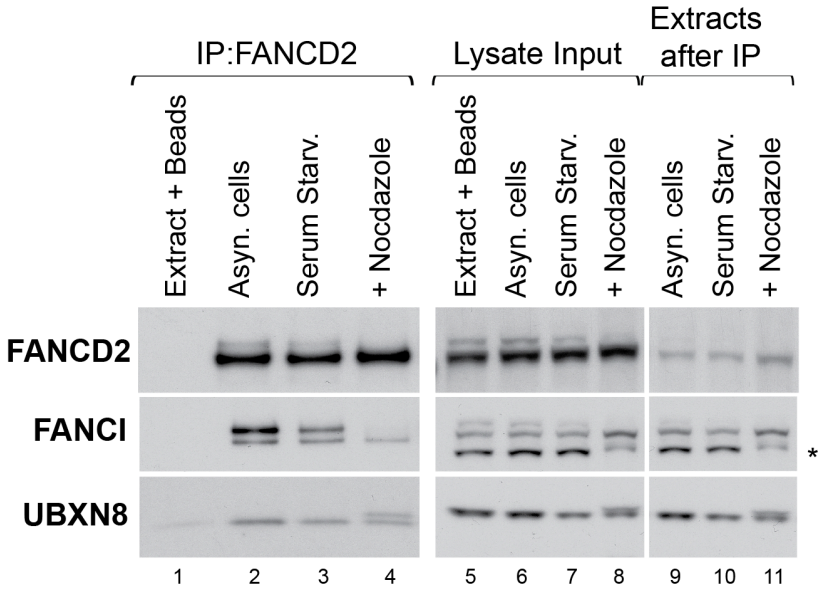

B

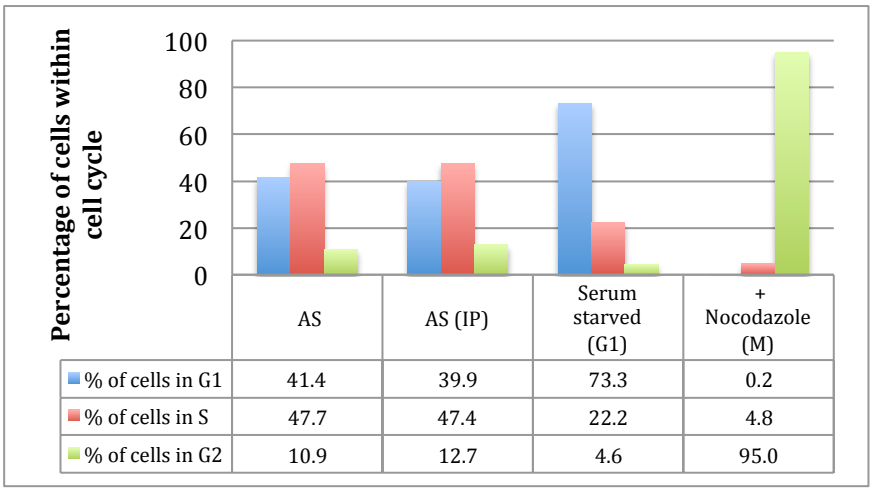

	AS	AS (IP)	Serum starved (G1)	+ Nocodazole (M)
% of cells in G1	41.4	39.9	73.3	0.2
% of cells in S	47.7	47.4	22.2	4.8
% of cells in G2	10.9	12.7	4.6	95.0

Figure 4.19: Increased UBXN8 and FANCD2 interaction in cell populations with the highest percentage of cells in S-phase

FANCD2 was immunoprecipitated from U2OS that were either arrested in G1-phase via serum starvation, or mitosis via nocodazole treatment. Asynchronised cells (AS) were used as control.

A) Immunoprecipitates and lysate inputs were analysed by Western blot using specific antibodies.

B) FACS analysis of the described samples.

4.2.10 Coiled-coil domain in UBXN8 is required for the interaction with FANCD2 and FANCI

The transmembrane domain of UBXN8 is required for its membrane localization, while the UBX domain is required for its interaction with p97. Besides these two domains, UBXN8 harbours a predicted coiled-coil domain located close to the transmembrane domain. Coiled-coil domains are described as protein–protein interaction domains (Hu, 2000) and I speculated whether it is required for FANCD2 and FANCI binding.

I performed Flag-immunoprecipitations from U2OS cells transfected with wild type and Flag-UBXN8 Δ67–91 (Δcoil), lacking the coiled-coil domain. Interestingly, both FA proteins showed reduced binding to Flag-UBXN8 Δcoil, compared to wild type UBXN8 (Figure 4.20), suggesting that the coiled-coil domain is required for UBXN8 interaction with FANCD2 and FANCI. In contrast, binding to p97 was not affected.

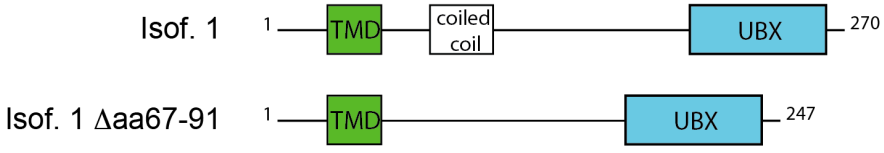

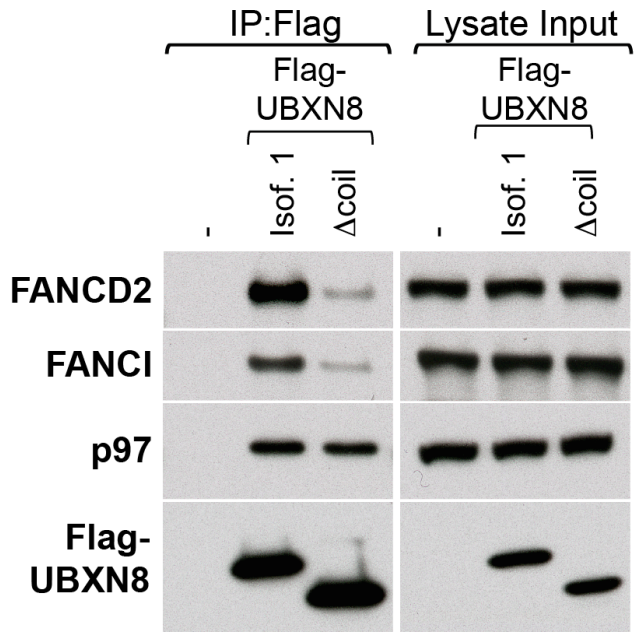

Figure 4.20: The coiled-coil domain of UBXN8 is required for the binding to FANCD2 and FANCI
U2OS cells were transfected with either wild type Flag-UBXN8 or Flag-UBXN8 Δ67–91 (Δcoil) and the Flag-tagged proteins were immunoprecipitated using anti-Flag beads. The immunoprecipitates were analysed by Western blot using specific antibodies.

To exclude the possibility that the reduced interaction was due to protein mislocalisation, I performed immunofluorescence microscopy with Flag-UBXN8 Δcoil-transfected U2OS cells.

Figure 4.21 shows that Flag-UBXN8 Δcoil, localized at the ER membrane and at the nuclear envelope, as described for wild type Flag-UBXN8. The reduced binding of Flag-UBXN8 Δcoil to FANCD2 and FANCI was therefore not due to changes in the subcellular localisation of UBXN8.

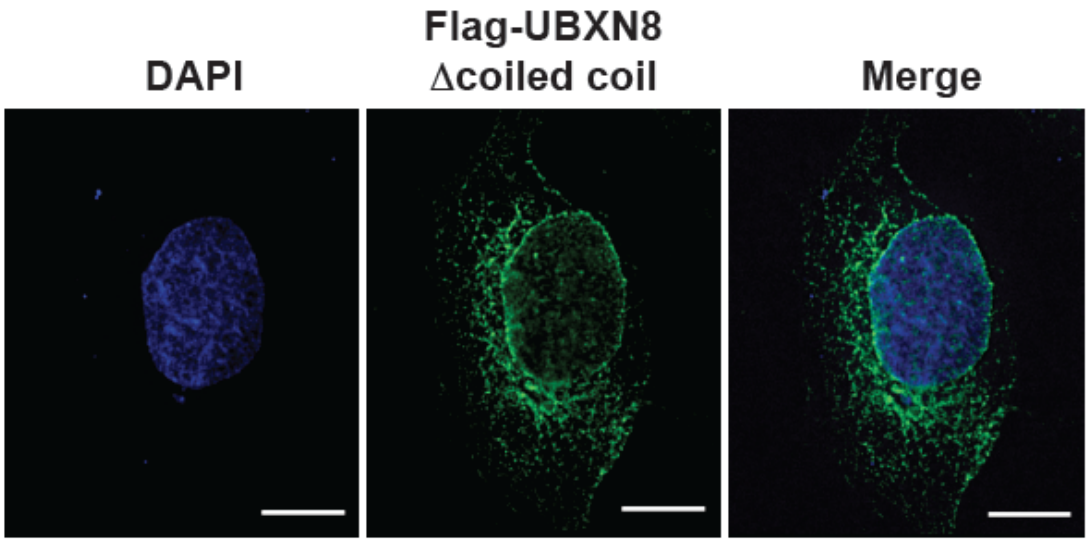

Figure 4.21: The truncation of the coiled-coil domain in UBXN8 did not change its subcellular localization to the ER membrane and the nuclear envelope
U2OS cells were transfected with Flag-tagged UBXN8 Δcoil and after 24h were processed for immunostaining. Flag-tagged proteins were detected with a anti-Flag antibody (*green*) and the nuclei stained using DAPI (*blue*). The scale bar represents 10 μm.

4.2.11 UBXN8 forms homodimers independent from its coiled-coil domain

Size-exclusion chromatography (SEC) with bacterially-expressed and purified Flag-UBXN8 aa67–270 (truncated transmembrane domain) was performed using a Superdex 75 column (performed by Dr. R. Sundaramoorthy/Prof. T. Hughes laboratory). The analysis was done in reference to two protein standards, BSA (MW 66 kDa) and the DNA binding domain (DBD) of *S. cerevisiae* Chd1 (MW 25 kDa). The estimated theoretical molecular mass of Flag-UBXN8 (aa67–270) is approximately 24kDa. Therefore, the elution profile should be closer to ScChd1 DBD than to BSA. Interestingly, the elution profile of Flag-UBXN8 was closer to BSA than to ScChd1 DBD (Figure 4.22), suggesting that Flag-UBXN8 forms a higher oligomer, possibly a dimer.

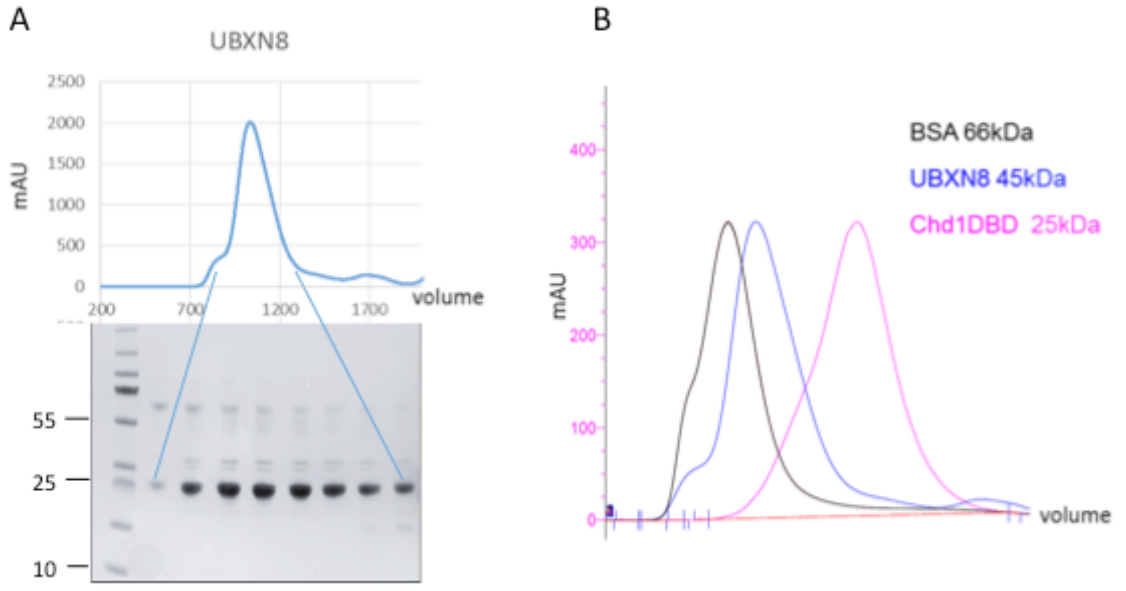

Figure 4.22: UBXN8 forms a higher oligomer *in vitro*

Gel filtration analysis with recombinant Flag-UBXN8 (performed by Dr. R. Sundaramoorthy). The gel filtration analysis was performed in reference to two protein standards, BSA (MW 66 kDa) and the DNA binding domain (DBD) of *S. cerevisiae* Chd1 (MW 25 kDa).

A) Gel filtration profile of bacterially-expressed and purified Flag-UBXN8 aa67–270. The fractions of the peak were run on a SDS-PAGE gel and stained with coomassie.

B) Gel filtration profile of Flag-UBXN8 (blue) along with the two protein standards BSA (black) and Chd1 DBD (pink).

To determine the molecular weight of the Flag-UBXN8 oligomeric form, gel-filtration chromatography coupled to multi-angle light scattering (SEC-MALS) was performed. The molecular weight estimated using SEC-MALS was 49 kDa (Figure 4.23), suggesting that *in vitro* purified UBXN8 forms homodimer in solution.

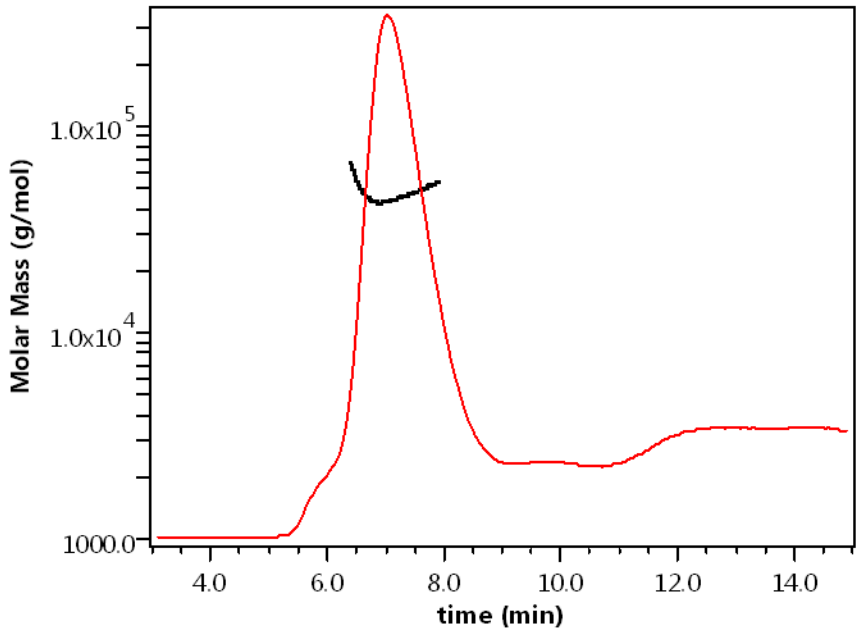

Figure 4.23: UBXN8 forms homodimer *in vitro*
SEC–MALS analysis of Flag-UBXN8. The elution profile of Flag-UBXN8 is drawn in red and the molar mass over elution peaks is shown in black. The molecular weight estimated using SEC-MALS was 49 kDa, suggesting that *in vitro* purified UBXN8 forms homodimers.

To check, whether UBXN8 forms homodimer in cells, and whether this dimerization depends on its coiled-coil domain, I performed Flag-immunoprecipitations from U2OS cells co-transfected with wild type HA-UBXN8 and one of the following Flag-UBXN8 variants: wild type Flag-UBXN8, truncated Flag-UBXN8 Δcoil that lacks the coiled-coil domain, or the mutant Flag-UBXN8 P238G that is defective in p97 binding. The latter is used as control to exclude the possibility that HA-UBXN8 co-immunoprecipitates due to binding to the same p97 hexamer.

Figure 4.24 shows that wild type Flag-UBXN8 as well as Flag-UBXN8 Δcoil co-immunoprecipitated HA-UBXN8 (lane 2 and 3), and that reduced p97 binding did not affect this binding (lane 4). Hence, these results indicate that UBXN8 forms oligomers in cells, most likely dimers, but that its coiled-coil domain does not mediate this interaction.

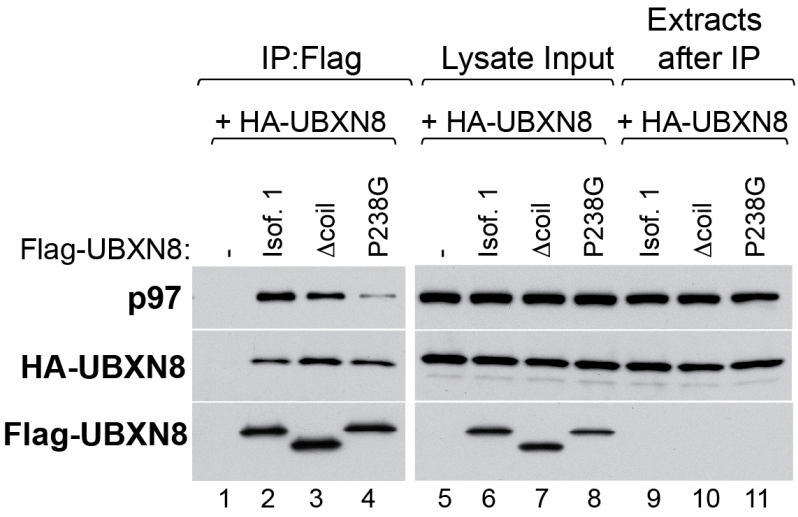

Figure 4.24: UBXN8 forms homodimer independently from its coiled-coil domain *in vivo*
Flag-immunoprecipitations were performed from U2OS cells co-transfected with wild type HA-UBXN8 and either wild-type Flag-UBXN8, truncated Flag-UBXN8 Δcoil or the mutant Flag-UBXN8 P238G that is defected in p97-binding. Flag-tagged proteins were immunoprecipitated using anti-Flag beads, and the immunoprecipitates were analysed by Western blot using specific antibodies.

4.2.12 UBXN8 interacts with monomeric FANCD2 and FANCI in vitro

To study whether the interaction between UBXN8 and the FA proteins is direct, I performed *in vitro* binding assays using recombinant human Flag-UBXN8 (without the transmembrane domain) and murine FANCD2 and FANCI (provided by Michael Hodskinson/KJ Patel laboratory).

The *in vitro* binding assays were done by incubation of Flag-UBXN8 with increasing amounts of monomeric FANCD2 or FANCI. Flag-UBXN8 was immunoprecipitated using anti-Flag beads.

Figure 4.25 shows that Flag-UBXN8 incubated with monomeric FANCD2 or FANCI can bind either FA protein independently from each other (Figure 4.24). Furthermore, the interaction occurs even when there is ten times less monomeric FANCD2 or FANCI (Figure 4.24A/B, lane 3), suggesting a stable complex formation between UBXN8 and the two FA proteins. Furthermore, Flag-UBXN8 interacts with increasing amounts of FANCD2 or FANCI, up to a 1:1 ratio, indicating that one molecule of Flag-UBXN8 can bind one molecule of FANCD2 or FANCI. This means that, for dimeric Flag-UBXN8, one dimer harbours binding sites for two molecules of the FA proteins (Figure 4.25). Furthermore, UBXN8 shows no specific binding preferences for either FANCD2 or FANCI, since it co-immunoprecipitated both with similar efficiency.

Taken together, UBXN8 can bind either FA proteins, FANCD2 or FANCI, independently from each other.

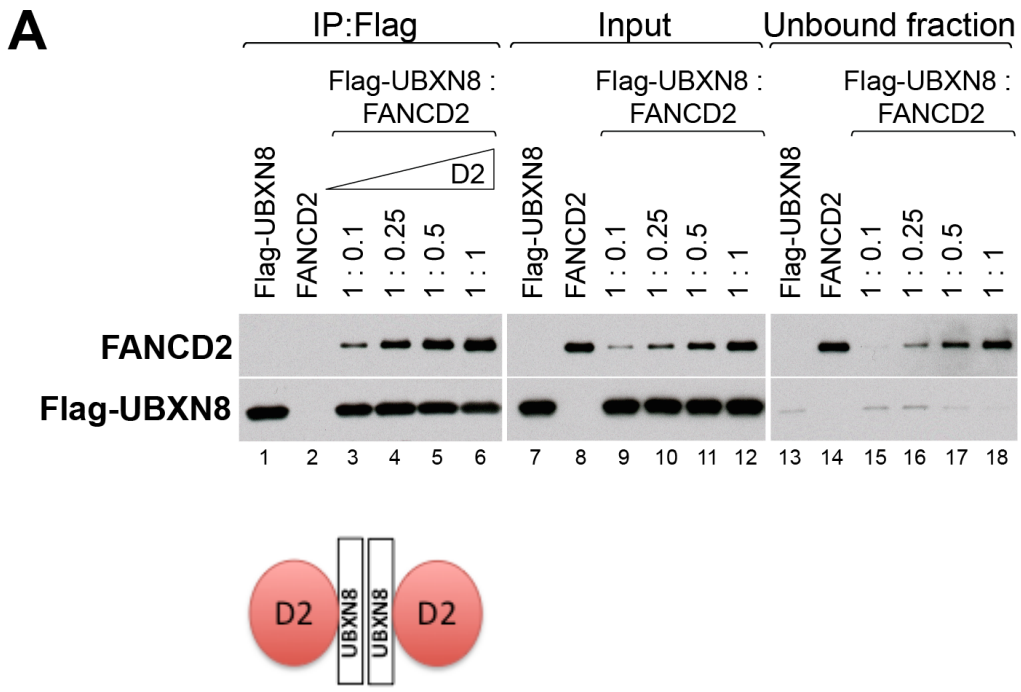

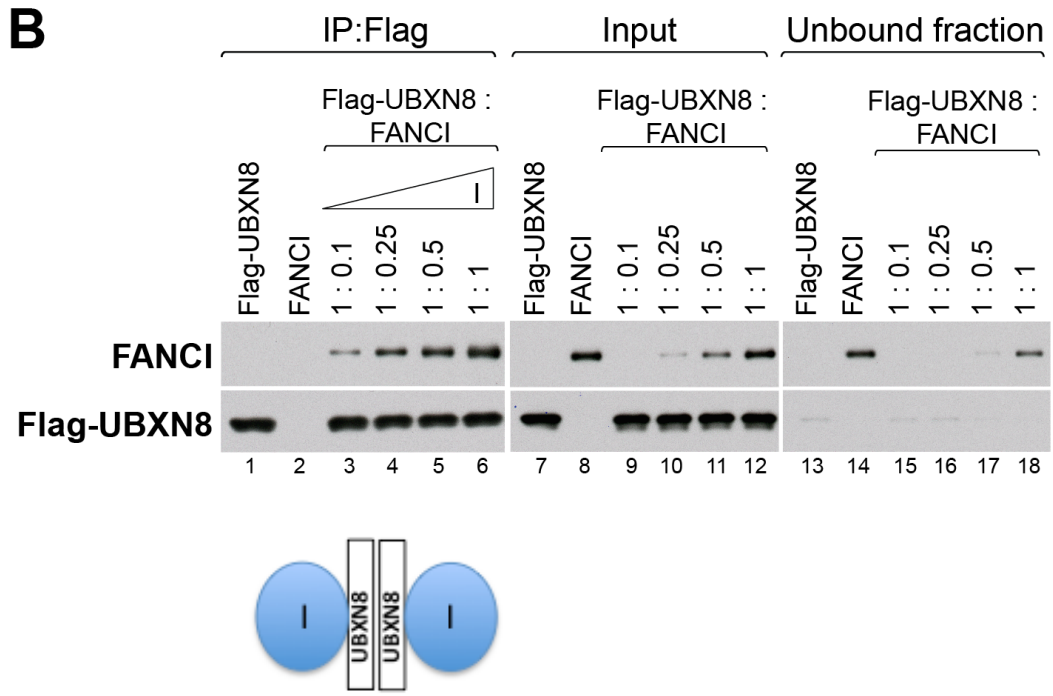

Figure 4.25: UBXN8 binds monomeric FANCD2 or FANCI independently

The *in vitro* binding assays were performed by incubating Flag-UBXN8 with increasing amounts of monomeric FANCD2 (A) or FANCI (B). Flag-UBXN8 was immunoprecipitated using anti-Flag beads. The indicated proteins were detected by Western blot using specific antibodies. The cartoons below the Western blots show the binding scenarios between dimeric UBXN8 and monomeric FANCD2 or FANCI.

4.2.13 Investigating the role of p97 in the interaction between UBXN8 and the FA proteins FANCD2 and FANCI

The experiments described in section 4.2.6 revealed that upon release from DNA damage, the FANCI interaction with FANCD2 was reduced, which correlated with an increased in binding to p97. The ATPase p97 is described to be involved in the DNA damage response by extracting chromatin-bound proteins (Dantuma and Hoppe, 2012). Therefore, it is tempting to speculate that p97 might be required for FANCD2/I dimer dissociation from chromatin. Although, the increased p97 binding to FANCD2 upon DNA damage release was UBXN8 independent, I wanted to know whether p97 regulates the interaction between UBXN8 and the FA proteins.

4.2.13.1 Preventing the UBXN8/p97 interaction causes an increased FANCI binding to UBXN8 under non-damage conditions

To investigate if p97 regulates the interaction between UBXN8 and the two FA proteins, U2OS cells were transfected with either wild type Flag-UBXN8 or the mutant Flag-UBXN8 P238G. As shown in figure 4.24 (Section 4.2.11), the P238G mutation in the FPR motif nearly abolishes the interaction between UBXN8 and p97.

The results of the Flag-immunoprecipitations show that the P238G mutant interacts with FANCI more strongly than wild type UBXN8 (Figure 4.26). In contrast, FANCD2 binds wild type and mutant UBXN8 to a similar extent. Hence, p97 seemed to be especially required for the release of FANCI from UBXN8.

Furthermore, the results suggest two scenarios: either that p97 dissociates monomeric FANCI from UBXN8, or that p97 dissociates the FANCD2/I dimers while bound to UBXN8.

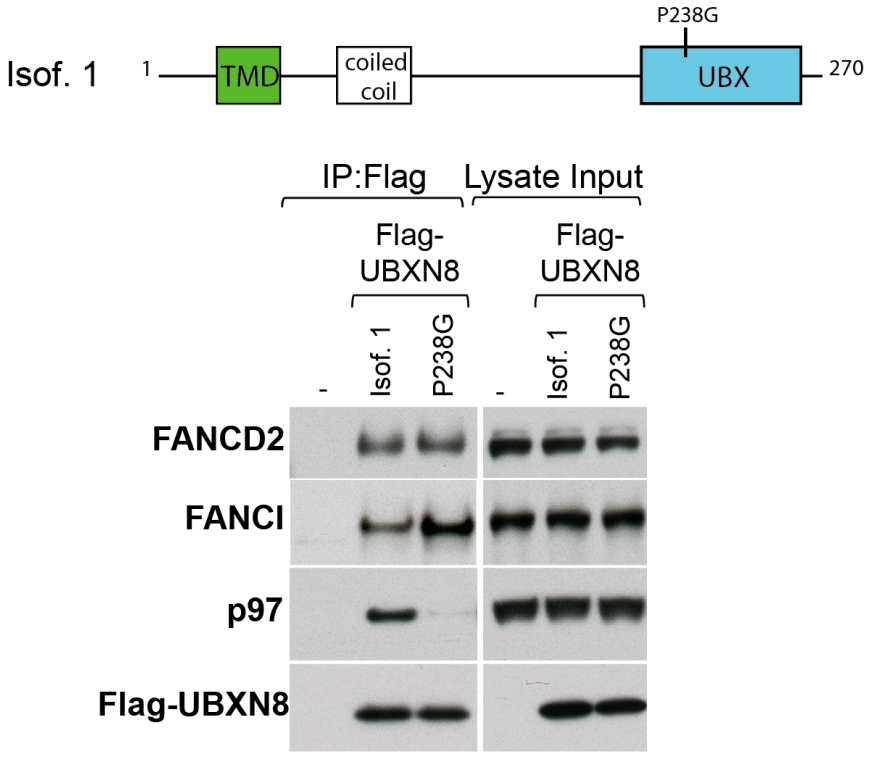

Figure 4.26: p97-binding is required for dissociation of FANCI from UBXN8

U2OS cells were transfected with Flag-UBXN8 wild type or the P238G mutant and grown for 24h. Flag-tagged proteins were immunoprecipitated with anti-Flag beads. All indicated proteins were detected with specific antibodies. Cells expressing no Flag-tagged protein were used as negative control. (*left*: IP, *right*: Lysate Input)

4.2.13.2 Preventing the UBXN8/p97 interaction causes an impaired FANCI release from the mutant Flag-UBXN8 P238G upon DNA damage

The immunoprecipitation of wild-type Flag-UBXN8 and its mutant P238G indicated that preventing the UBXN8/p97 interaction caused an increased FANCI binding to UBXN8.

The experiments described in section 4.2.4 show that FANCD2 and FANCI are released from UBXN8 upon DNA damage. To investigate whether the P238G mutant affects FANCD2 and FANCI release after DNA damage, the experiment was repeated with U2OS cells stably expressing wild type Flag-UBXN8 or the P238G mutant under a tetracycline-inducible promoter in the presence or absence of DNA damage. For this experiment, tetracycline-inducible cells were used instead of transfection, because transfection in combination with cisplatin treatment reduced cell viability (data not shown).

Figure 4.27A shows that FANCD2 and FANCI were released from wild type UBXN8 upon DNA damage. The FANCI release from the UBXN8 mutant was impaired compared to wild type Flag-UBXN8 (compare Figure 4.27A, lanes 3 and 4 with 4.27B, lanes 3 and 4). This suggests that p97 binding to UBXN8 is particularly important for FANCI release upon DNA damage.

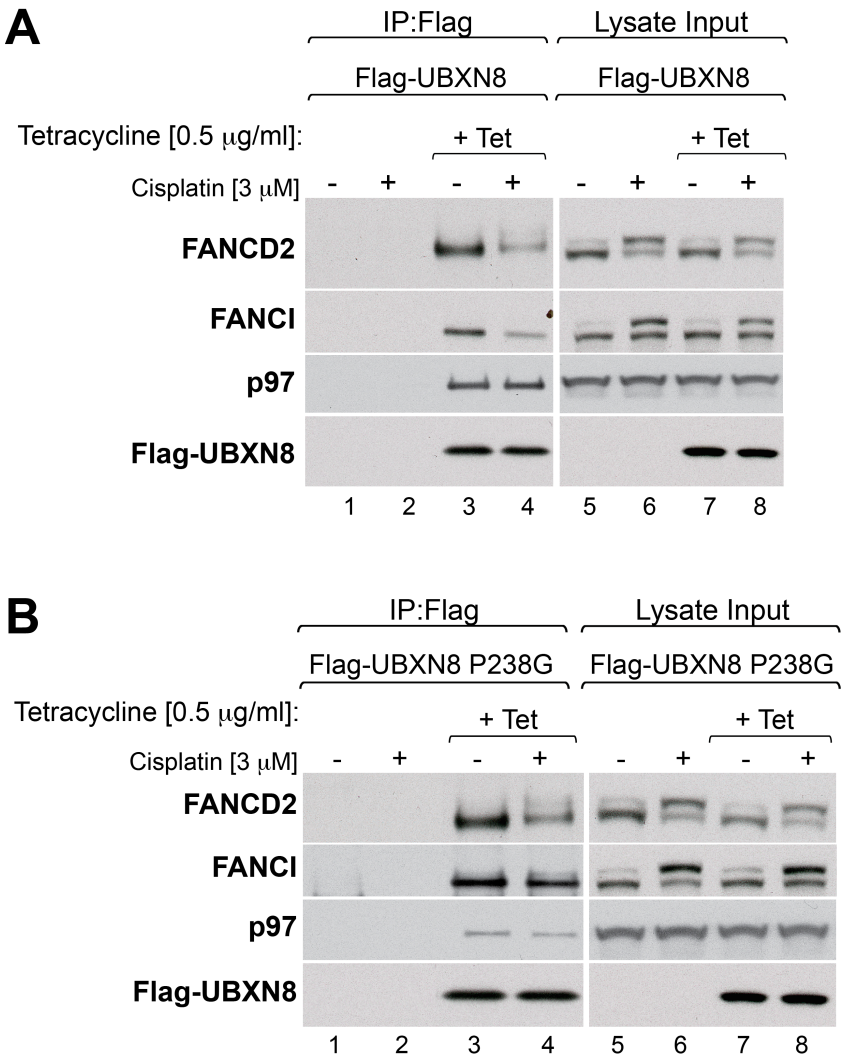

Figure 4.27: Upon DNA damage, the release of FANCI from Flag-UBXN8 P238G is impaired
Wild type Flag-UBXN8 or the P238G mutant were immunoprecipitated from tetracycline-inducible U2OS cells and were either untreated or treated with 3 μM cisplatin (24h). The expression was induced by adding 0.5 μg/ml tetracycline to the cells. Uninduced U2OS cells were used as control. Flag-tagged proteins were immunoprecipitated with anti-Flag beads. Co-immunoprecipitated proteins were detected with specific antibodies (*left*: IP, *right*: Lysate Input).

PART III – The role of UBXN8 in regulating the DNA damage response and the FA proteins FANCD2 and FANCI

The data presented so far, illustrate that UBXN8 interacts with FANCD2 and FANCI and that both FA proteins are partially released from UBXN8 upon DNA damage. Furthermore, *in vitro* binding assays with the recombinant proteins show that UBXN8 can directly interact with FANCD2 and FANCI. However, since UBXN8 can form

homodimers it may also interact with FANCD2/I heterodimers. Super resolution microscopy showed that a small fraction of Flag-UBXN8 localises at the inner nuclear membrane, which suggests that UBXN8 interaction with FANCD2 and FANCI may occur at the inner nuclear membrane.

The experiments in the following section address the role of UBXN8 in regulating the activation and the interaction of the FA proteins FANCD2 and FANCI.

4.2.14 UBXN8 depletion increases U2OS cell resistance to ICL-inducing reagents

In order to understand whether UBXN8 affects the DNA damage response to ICL, I performed clonogenic survival assays with wild type and UBXN8-depleted cells upon treatment with mitomycin C (MMC) or cisplatin (Figure 4.28). These agents induce ICL that are recognized and repaired by the FA pathway.

For the clonogenic survival assay, U2OS cells were transfected with siRNA (UBXN8 ♯1 and ♯2) specifically targeting UBXN8. Luciferase siRNA was used as a negative control. The depletion of FAN1, a DNA repair nuclease recruited to DNA damage sites by mono-ubiquitylated FANCD2, was used as positive control (MacKay et al., 2010). After 48h of siRNA treatment, the cells were seeded at low density and treated with varying drug concentrations. Twenty-four hours after treatment, the medium was changed to drug-free medium and cells were grown for a further eight days to allow colony formation of the surviving cells.

The clonogenic survival assays with MMC and cisplatin were repeated in three independent experiments, each performed in triplicate. The results of the assays show that UBXN8 silencing caused increased cell survival compared to luciferase siRNA transfected cells (Figure 4.28). Thus, UBXN8 silencing increases resistance to ICL-

inducing agents compared to control cells. These results suggest that UBXN8 acts as a negative regulator of the DNA damage response.

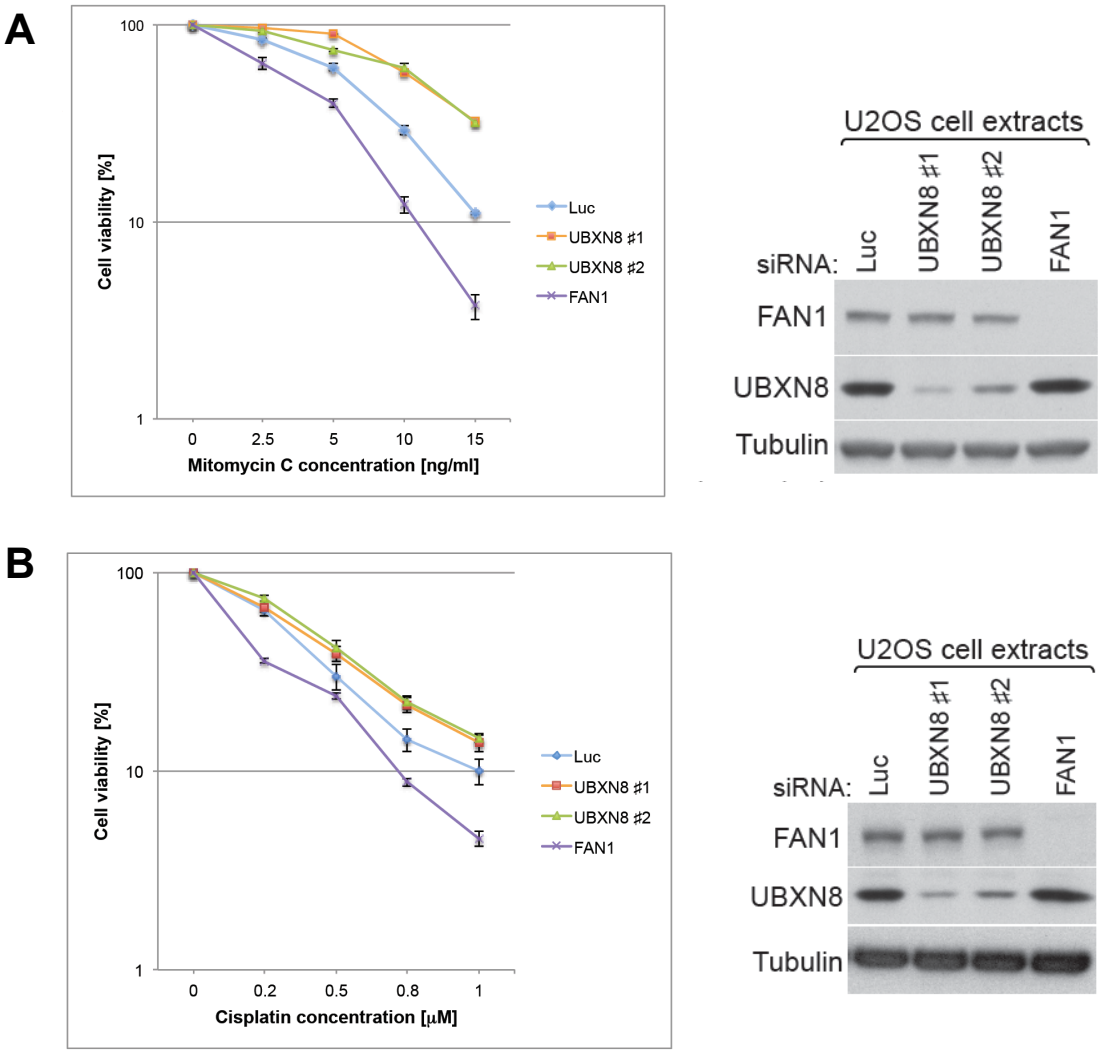

Figure 4.28: UBXN8 depletion causes an increasd cell resistance to ICL-inducing agents

A) U2OS cells, transfected with indicated siRNAs, were seeded at low density and were treated for 24 h with different concentration of mitomycin (A) or cisplatin (B). The medium was changed to drug-free medium 24h after treatment and the cells were grown for a further eight days to allow colony formation of surviving cells. Cell survival was assessed by a colorimetric assay using Giemsa stain. Colonies with more than 50 cells were counted. For each siRNA-treated sample, cell viability of untreated cells was set as 100%. Each data point indicates the mean value ± standard deviation.

Only small fractions of silenced cells were used for the clonogenic survival assay, and the remainder of the cells were harvested and cell extracts were prepared. The extracts were analysed by Western blot using specific antibodies to confirm the successful silencing of the proteins (right panels).

4.2.15 UBXN8 silencing causes an increase in FANCD2 and FANCI mono-ubiquitylation

To analyse whether depletion of UBXN8 alters FANCD2 and/or FANCI levels or their mono-ubiquitylation in the presence and absence of DNA damage, total cell extracts were prepared from U2OS cells treated with two different UBXN8 siRNA oligonucleotides (#1 and #2) (Figure 4.29). After 48 h siRNA treatment, the cells were incubated for additional 24h with cisplatin and were harvested after 0, 12, 16, 20 and 24 hours. Cells transfected with luciferase siRNA (Luc) were used as a negative control. The changes in FANCD2 and FANCI levels were quantified using the *LI-COR* imaging system/software.

UBXN8 silencing of UBXN8 was efficient with both UBXN8 siRNAs (Figure 4.29). The depletion of UBXN8 caused a reduction in the levels of non-ubiquitylated FANCD2 and FANCI throughout the time course, compared to control cells treated with luciferase siRNA. This was accompanied by a slight increase in the ubiquitylated form of FANCD2 and FANCI compared to control cells (Figure 4.29, compare Luc with UBXN8si #1 and #2 for each time point). However, the decrease in the levels of the non-ubiquitylated FA proteins was not equivalent to the increase in their ubiquitylated form. This is likely due to an incomplete extraction of DNA-bound modified FANCD2 and FANCI.

The results were confirmed in three independent experiments. The band intensities of the lower (non-ubiquitylated) and upper (mono-ubiquitylated) bands of FANCD2 and FANCI were quantified for each time point and the ratio of ubiquitylated (Ub) /non-ubiquitylated (non-Ub) was calculated. The mean value for the ratios from all three experiments was plotted, and the standard deviation is shown as error bars (Figure 29B).

Furthermore, the calculation of the p-value (indicated with stars) confirmed that the obtained results are statistically significant.

Taken together, these results suggest that depletion of UBXN8 affects the modification state of FANCD2 and FANCI, by increasing the ratio of ubiquitylated over non-ubiquitylated FANCD2 and FANCI in the presence and absence of DNA damage.

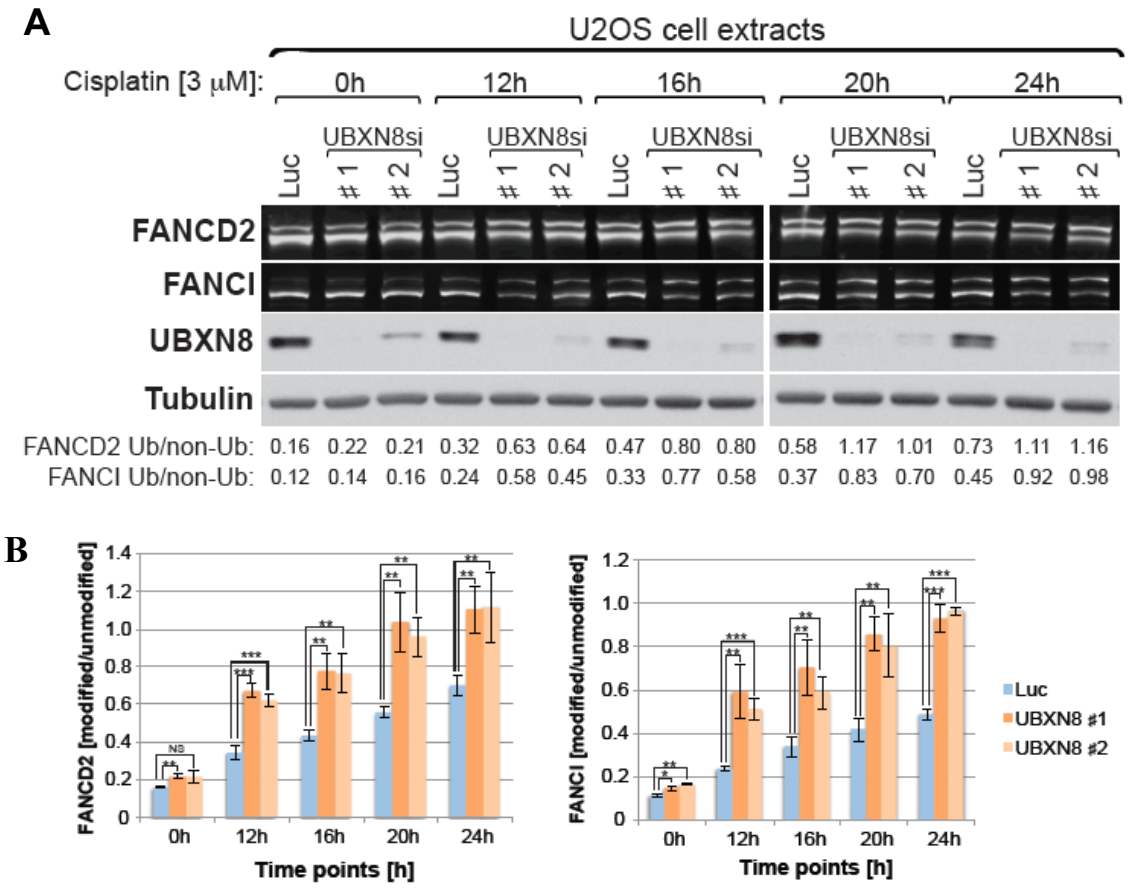

Figure 4.29: UBXN8 silencing causes an increase in the ratio of modified/unmodified FANCD2 and FANCI

Total cell extracts were prepared from U2OS cells treated with two different UBXN8 siRNA oligonucleotides (#1 and #2). Luciferase siRNA (Luc) was used as negative control. After 48h siRNA treatment, 3 μM cisplatin was added for an additional 24h. Cells were harvested at the indicated time points and protein extracts were prepared.

A) The protein extracts were analysed by Western blot using specific antibodies. The detection of FANCD2 and FANCI was performed with a fluorophore-conjugated secondary antibody and the bands were visualized using the *LI-COR* imaging system. The intensities of the upper (Ub) and lower (non-Ub) bands for FANCD2 and FANCI were quantified. Ub/non-Ub indicates the ratio of the mono-ubiquitylated over non-ubiquitylated FANCD2 and FANCI. Tubulin is shown as loading control.

(B) The Ub/non-Ub ratios from three independent experiments were combined and the mean value for each time point was plotted. The error bars indicate the standard deviations. The

asterisks indicate the statistical significance of the mean differences as calculated by t-test: * = statistically significant ($p < 0.05$), ** = very statistically significant ($p < 0.01$, *** = extremely statistically significant ($p < 0.001$), NS = not significant ($p > 0.05$)

4.2.16 UBXN8 silencing increases FANCD2/I dimer formation

UBXN8 silencing increases the shift of both FA proteins from their non-ubiquitylated to their mono-ubiquitylated state. The modification of FANCD2 requires FANCI and suggests that mono-ubiquitylation requires their prior dimerization (Sato et al., 2012b). Therefore, I wanted to analyse whether the increase in modified FA proteins upon UBXN8 silencing had any effect on FANCD2/I dimerization under normal and DNA damage conditions.

To address this question, I immunoprecipitated endogenous FANCD2 from wild type and UBXN8-silenced U2OS cells, using anti-FANCD2 antibodies. The silencing of UBXN8 was performed with two oligonucleotides (♯1 and ♯2) as before.

Figure 4.30A shows that UBXN8 silencing increased the FANCD2/I dimer formation both under normal conditions (compare lanes 2 with 3 and 4), and upon DNA damage (compare lanes 5 with 6 and 7). The levels of FANCD2 and FANCI in the immunoprecipitates were quantified using the *LI-COR* imaging system/software. FANCI levels were normalised to account for minor differences in the amount of FANCD2 immunoprecipitated. The value for luciferase was set at one, and the values for the UBXN8 silencing were reported relative to it. This allows comparison of the data from three independent experiments. The mean value of the three independent experiments was plotted (Figure 4.30B). The standard deviation is shown as error bars. Furthermore, the calculated p-values indicate that the results were statistically significant.

The results show that the upshift of FANCD2 and FANCI caused by UBXN8 silencing in the extracts correlates with an increased dimer formation between the two FA proteins. Although, the increase of modified FANCD2 and FANCI was not very marked in the extracts, as discussed in section 4.2.15, the extracts of the IPs clearly showed that the decrease of the non-ubiquitylated FA proteins upon UBXN8 silencing causes an up-shift to their mono-ubiquitylated state (Figure 30A, see Lysate Inputs). The better extraction of the FA proteins in this case could be due to lysis in a larger volume that allows the continuous rotation during cell lysis, resulting in better access of benzonase to DNA.

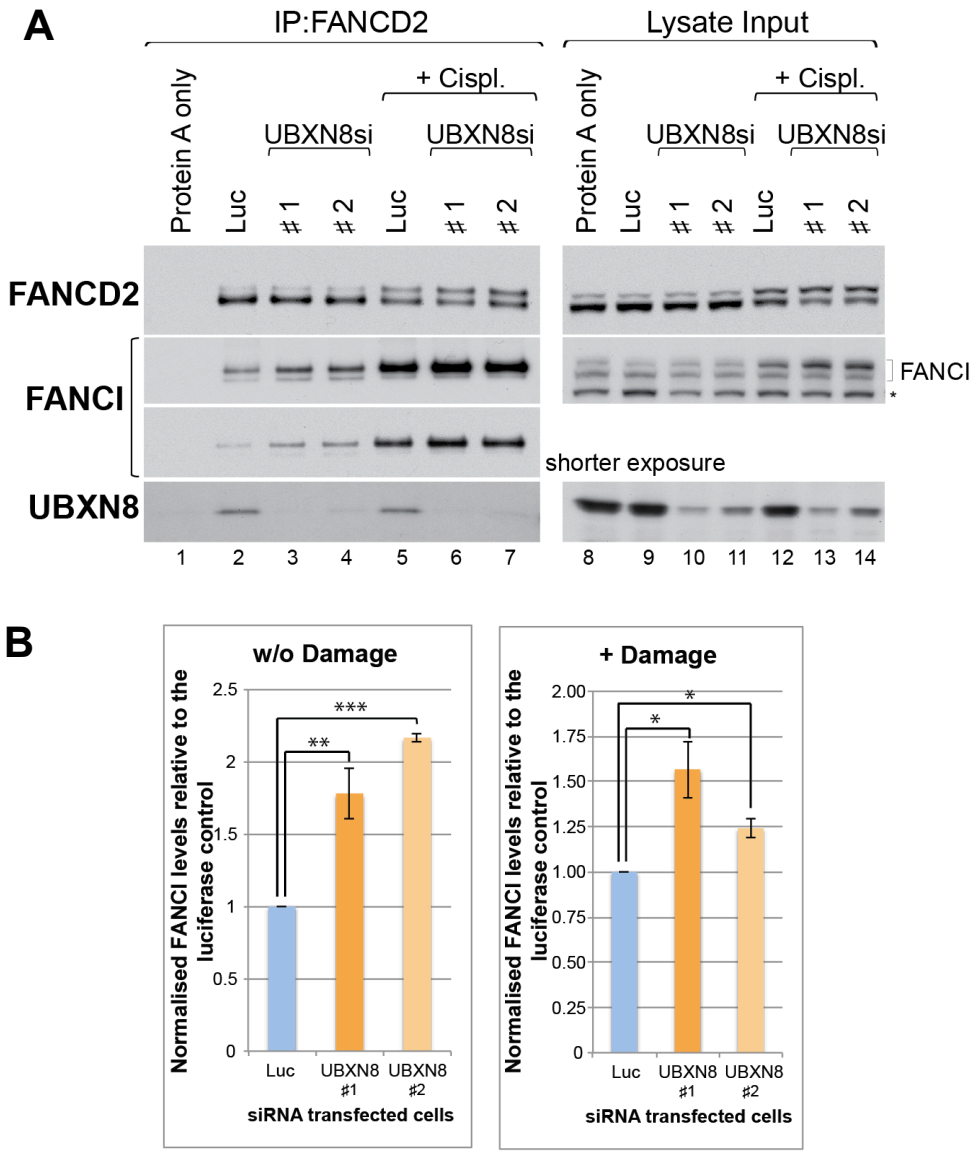

Figure 4.30: UBXN8 silencing increases FANCD2/I dimer formation under normal and DNA-damage conditions

A) Endogenous FANCD2 was immunoprecipitated from U2OS cells that were depleted for UBXN8 using two independent oligonucleotides (♯1 and ♯2) and untreated or treated with 3 μM cisplatin [24h]. The immunoprecipitations were performed using anti-FANCD2 antibodies and protein A-Sepharose beads. Naked protein A-Sepharose beads incubated with extract were used as control. The immunoprecipitates and lysate inputs were analysed by Western blot using the indicated antibodies. The asterisk marks an unspecific band detected by the FANCI antibodies (*left*: IP, *right*: Lysate Input).

B) The detection of FANCD2 and FANCI in the immunoprecipitates was also performed with the *LI-COR* imaging system using fluorophore-conjugated secondary antibodies. The bands were quantified and the normalized FANCI levels relative to the luciferase control were calculated. The graphs shown in B represent the mean value of 'normalized FANCI levels relative to the Luciferase control' from three independent experiments. The error bars represent the standard deviation. The asterisks indicate the statistical significances of the means as calculated by t-test: * = statistically significant ($p < 0.05$), ** = very statistically significant ($p < 0.01$), *** = extremely statistically significant ($p < 0.001$)

4.2.16.1 UBXN8 silencing does not alter cell cycle progression

The FA proteins FANCD2 and FANCI are mono-ubiquitylated/activated during S-phase, resulting in their dimerization and localisation to ICL (Taniguchi et al., 2002, Smogorzewska et al., 2007). Therefore, to exclude the possibility that the increased dimer formation of FANCD2/I observed upon UBXN8 silencing is due to a defect in S-phase progression, the samples of the immunoprecipitations discussed above were analysed by FACS.

The FACS profiles of this analysis are shown in figure 4.31 and revealed that the changes observed in FANCD2 and FANCI dimer formation, upon UBXN8 silencing, were not due to altered cell cycle progression.

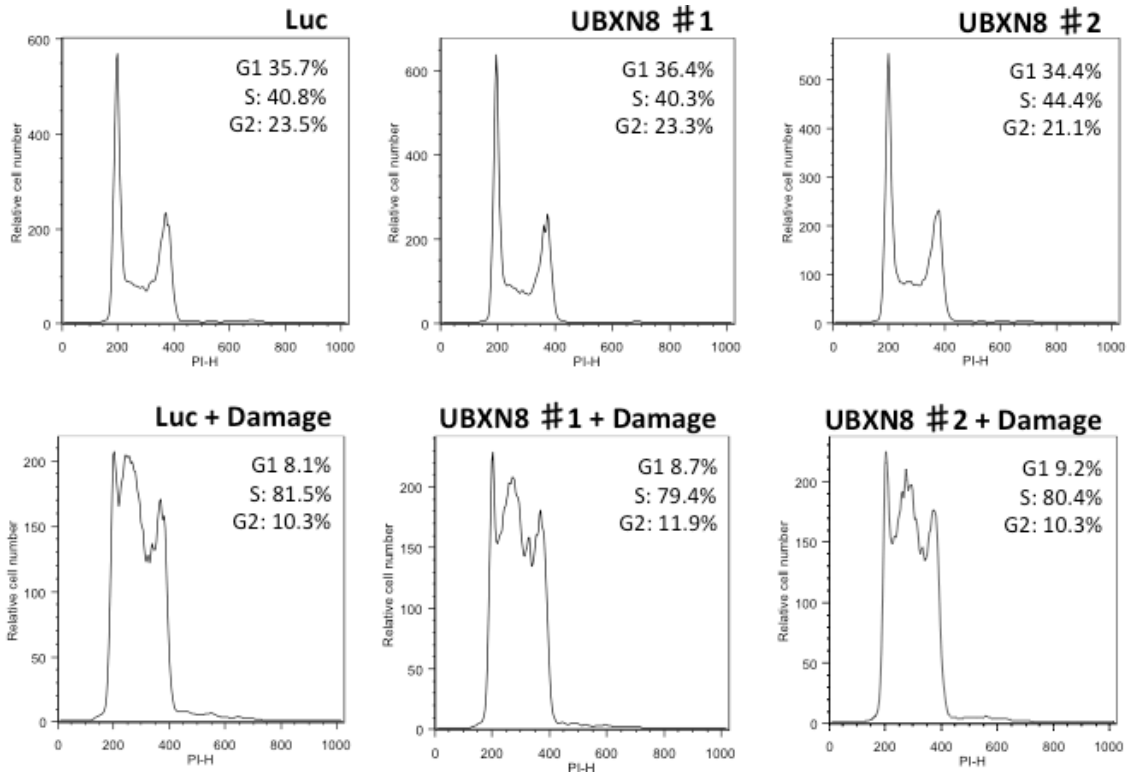

Figure 4.31: UBXN8 silencing did not alter cell cycle progression

FACS analysis with the samples of the endogenous FANCD2 immunoprecipitation described in figure 4.30. The percentage of cells for the different cell cycle stages is shown.

4.2.17 UBXN8 silencing increases FANCD2 foci formation

FANCD2 and FANCI are mono-ubiquitylated in response to DNA damage, resulting in their localisation to nuclear foci at the DNA damage sites (Smogorzewska et al., 2007). Furthermore, *in vitro* experiments show that mono-ubiquitylation of the FANCD2/I dimer is stimulated by DNA (Longerich et al., 2014).

To address whether the excess FANCD2/I dimers observed upon UBXN8 silencing affects foci formation, I performed immunofluorescence microscopy with wild type and UBXN8 silenced U2OS cells in the presence and absence of DNA damage. The cells were stained for endogenous FANCD2. To reduce background staining, the soluble nuclear proteins were pre-extracted prior to staining. The number of FANCD2 foci per

cell was determined using the analysis software Imaris. For each condition, approximately 100 cells were analysed.

The results of the immunofluorescence experiment are shown in figure 4.32. The distribution plots created represent the percentage of cells that correspond to each foci number interval (Figure 4.32).

Under non-treatment conditions, approximately 74% of cells treated with luciferase siRNA had below 40 foci per cell, while the majority of UBXN8-silenced cells had more than 40 foci per cell (60% for UBXN8 ♯1 and 69% for UBXN8 ♯2; Figure 4.32A). The validation of the number of foci upon DNA damage showed that approximately 60% of cells treated with luciferase siRNA had below 110 foci per cell, while the UBXN8 silenced cells had more than 110 foci per cell (app. 66% for UBXN8 ♯1 or UBXN8 ♯2; Figure 4.32B). These results suggest that U2OS cells silenced for UBXN8 have more foci per cell, both under normal conditions and upon DNA damage, than control cells. Furthermore, the results obtained without damage suggest that the ectopically formed dimer caused by UBXN8 silencing localises to chromatin even in the absence of ICLs.

Since I did not have antibodies for endogenous UBXN8 that work for microscopy, cells were harvested to confirm the UBXN8 silencing by Western blot (Figure 4.32C). The extracts in figure 4.32C show that the UBXN8 silencing was very efficient; therefore it is safe to assume that UBXN8 was depleted in most of the cells.

The results obtained suggest that the availability of more FANCD2/I dimer that can be targeted to the DNA damage sites might explain the increased resistance of UBXN8-silenced cells to ICL-inducing agents, compared to control cells.

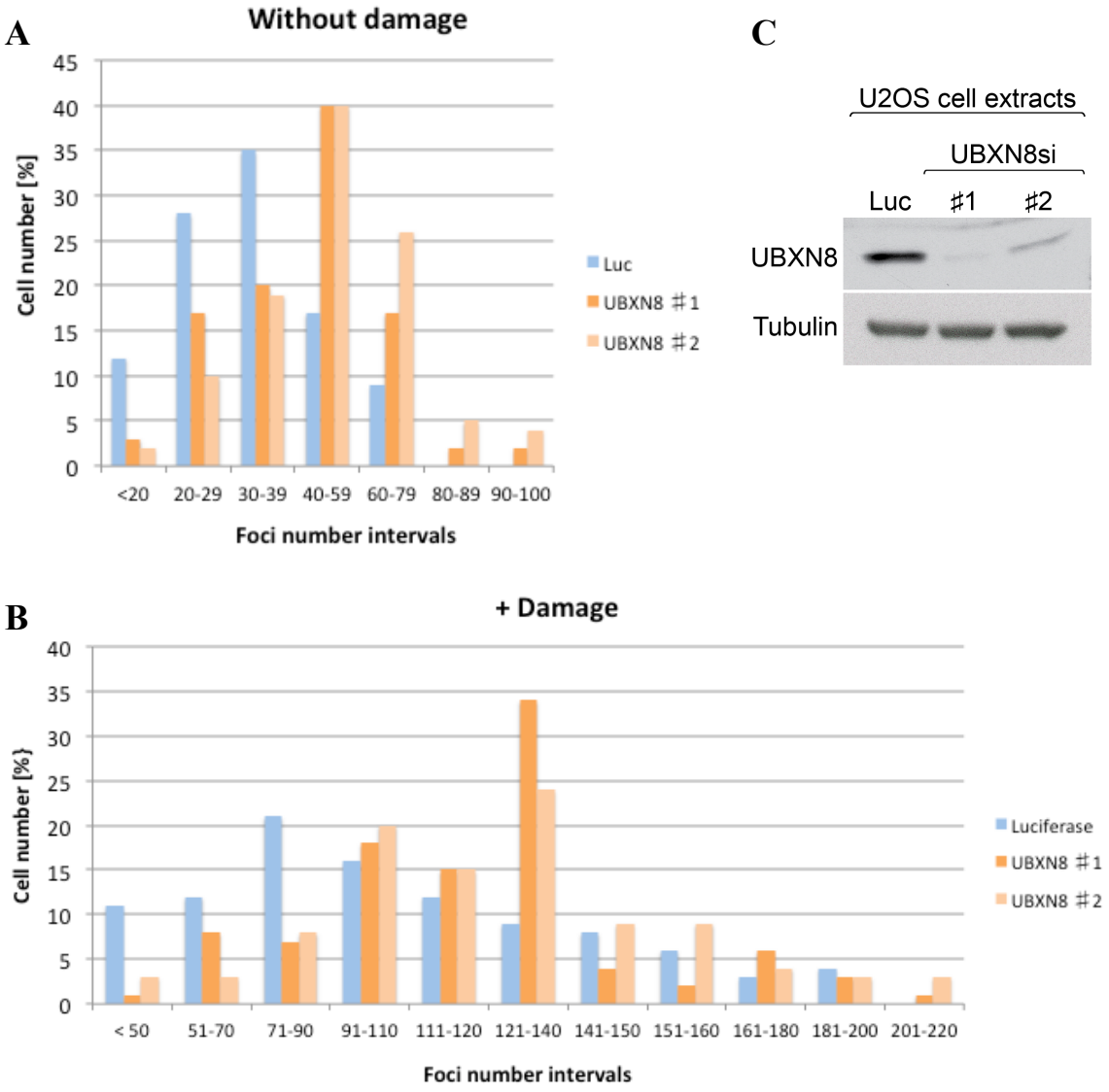

Figure 4.32: UBXN8 silencing stimulates FANCD2 foci formation

U2OS cells were seeded on coverslips and were silenced for UBXN8 using two different siRNA oligonucleotides (#1 and #2). The silencing was performed for 72h. To induce ICLs, cells were treated with 3 μM cisplatin for 24h, added after 48h of siRNA transfection. Luciferase siRNA (Luc) transfected cells were used as negative control.

To analyse the FANCD2 foci number, non-chromatin bound proteins were pre-extracted and the cells were fixed and stained for endogenous FANCD2 using a specific anti-FANCD2 antibody. The images were taken with a DeltaVision deconvolution microscope (100x lens) and the number of foci in each cell determined using the Imaris software. For each condition, approximately 100 cells were analysed.

A-B) Graphs show the percentage of cells for each foci number interval.

C) To show that the silencing was successful, cell were seeded into additional wells without coverslips and treated as described. The extracts were then analysed by Western blot using the indicated antibodies.

4.2.18 UBXN8 overexpression causes an increase in the level of unmodified FANCI

UBXN8 silencing results in increased levels of modified FANCD2 and FANCI, which correlates with increased FANCD2/I dimer and FANCD2 foci formation in the presence and absence of DNA damage. Therefore, I wanted to know whether UBXN8 overexpression might have the opposite effect.

The FANCD2 and FANCI levels were analysed in total cell extracts obtained from U2OS cells expressing Flag-UBXN8 from a tetracycline-inducible promoter (Figure 4.33). As negative control, I used tetracycline-inducible U2OS cells with integrated empty vector and tetracycline-inducible U2OS cells expressing Flag-VAPB. Like UBXN8, VAPB is an ER protein and was included to help assess non-specific changes due to protein overexpression. After 12h of induction/overexpression, cells were incubated for additional 12h with cisplatin and were harvested at 0, 4, 8 and 12 hours (Figure 4.33). A shorter cisplatin treatment was chosen, since the upshift to mono-ubiquitylated FANCD2 and FANCI reaches its plateau at 12 hours of treatment. Furthermore, the Flag-UBXN8 levels decreased dramatically after 24h induction/12h of DNA damage (Figure 4.33). However, the decrease of Flag-UBXN8 was not due to the DNA damage, since it was also observed under normal conditions (data not shown). The Western blots for FANCD2 and FANCI were developed and quantified using the *LI-COR* imaging system/software, as before.

Figure 4.33A shows that Flag-UBXN8 overexpression led to increased levels of unmodified FANCI in the extracts collected at the indicated time points. The increased levels of unmodified FANCI were accompanied by a slight decrease in the ubiquitylated form, compared to control cells. Hence, the results obtained for FANCI upon UBXN8 overexpression show the opposite effect to that observed upon UBXN8 silencing. The combined quantification of three independent experiments and the calculation of the p-

values illustrate that these changes are statistically significant (Figure 4.33B). UBXN8 overexpression also caused slightly reduced levels of mono-ubiquitylated-FANCD2 compared to control cells, but the changes observed are not statistically significant, except for the 4h time point (Figure 4.33A). This might indicate a stronger regulation of UBXN8 on FANCI than FANCD2. The tetracycline-inducible Flag-VAPB cells did not show changes in the FANCD2 or FANCI modifications compared to control cells.

These results suggest that Flag-UBXN8 overexpression affects mainly FANCI, by shifting the balance from mono-ubiquitylated to non-ubiquitylated FANCI under normal and DNA damage conditions.

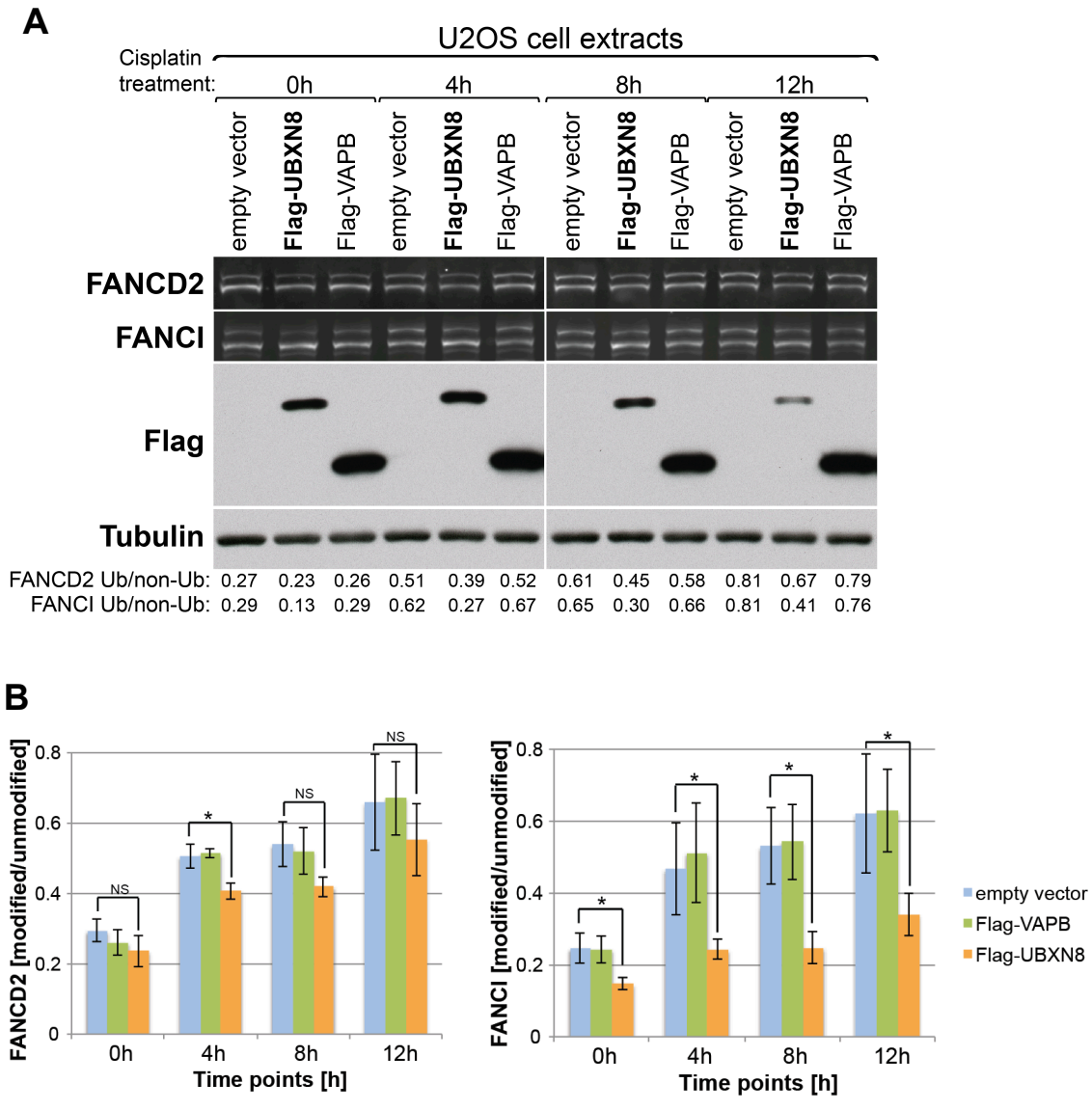

Figure 4.33: UBXN8 overexpression causes a decrease in the levels of modified FANCI

Total cell extracts were prepared from tetracycline-inducible U2OS cells expressing either Flag-UBXN8 or Flag-VAPB. VAPB as well as U2OS cells with integrated empty vector were used as negative controls. After 12h induction with 0.5 μg/ml tetracycline, cells were treated with 3 μM cisplatin for an additional 12h. Cells were harvested at the indicated time points and protein extracts were prepared.

A) The protein extracts were analysed by Western blot using specific antibodies. The detection of FANCD2 and FANCI was performed with a fluorophore-conjugated secondary antibody and the bands were visualized using the *LI-COR* imaging system. The intensities of the upper (Ub) and lower (non-Ub) bands for FANCD2 and FANCI were quantified. Ub/non-Ub indicates the ratio of the mono-ubiquitylated to non-ubiquitylated forms of FANCD2 and FANCI. Tubulin is shown as loading control.

(B) The Ub/non-Ub ratios of three independent experiments were combined and the mean values were plotted for each time point. The error bars represent the standard deviation of the means. The asterisks indicate the statistical significances of the differences as calculated by t-test: * = statistically significant ($p < 0.05$), NS = not significant ($p > 0.05$)

4.2.19 UBXN8 overexpression decreases FANCD2/I dimer formation

The analysis of cell extracts obtained from Flag-UBXN8 overexpressing cells showed increased levels of unmodified FANCI. To investigate whether this results in changes in FANCD2/I dimer formation, I performed immunoprecipitation of endogenous FANCD2 from U2OS cells expressing Flag-UBXN8 from a tetracycline-inducible promoter, under normal and DNA damage conditions.

Figure 4.34A shows the endogenous FANCD2 immunoprecipitation from undamaged cells. Upon Flag-UBXN8 overexpression, the lysate inputs show reduced levels of modified FANCD2 and FANCI (compare lanes 10 and 11), which correlates with a slight decrease in FANCD2/I dimer formation in the immunoprecipitates, compared to that in the control cells (compare lanes 4 and 5). The levels of FANCD2 and FANCI in the immunoprecipitates were quantified and the FANCI levels normalised, as previously described, to account for minor differences in the amount of FANCD2 immunoprecipitated. The experiment was performed twice, and the mean value of the two experiments was plotted in Figure 4.34A (right panel). The calculated p-values show that the changes observed between Flag-UBXN8 overexpressing cells and control

cells in the absence of DNA damage were statistically significant. Although Flag-VAPB overexpression did not change FANCD2 and FANCI modifications in the cell extracts, FANCD2/I dimer formation was moderately reduced in Flag-VAPB overexpressing cells compared to control cells. Therefore, taking the changes due to overexpression into account, the clear reduction in dimer formation observed upon Flag-UBXN8 overexpression might actually be less pronounced than indicated. However, it must be noted that the expression levels of Flag-VAPB are much higher compared to Flag-UBXN8 (compare levels in the anti-Flag Western blot).

The FACS profiles of this analysis are shown in figure 4.34B and revealed that the changes observed in FANCD2/I dimer formation upon UBXN8 overexpression were not due to altered cell cycle progression.

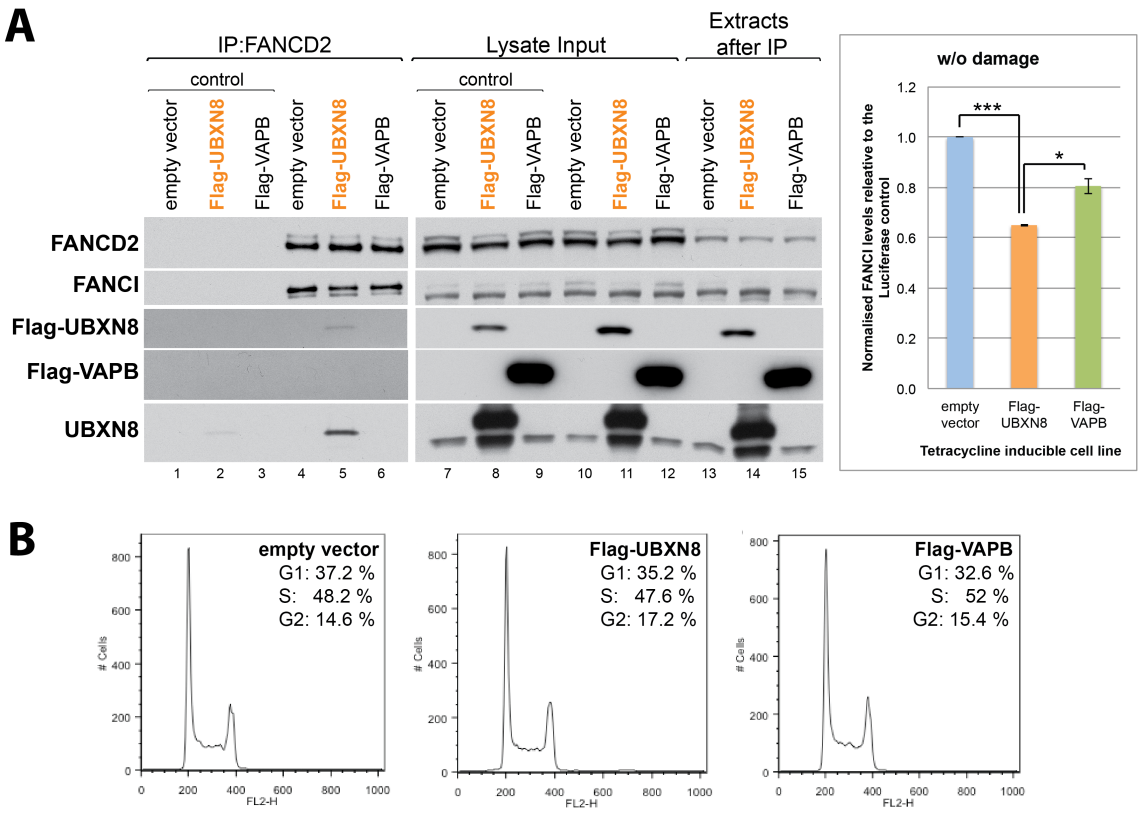

Figure 4.34: UBXN8 overexpression causes a decrease in FANCD2/FANCI dimer formation in the absence of DNA damage

A) Endogenous FANCD2 was immunoprecipitated from tetracycline-inducible U2OS cells expressing either Flag-UBXN8 or Flag-VAPB. VAPB as well as U2OS cells with integrated empty vector were used as negative controls. Immunoprecipitations were performed 24h after induction using anti-FANCD2 antibodies and protein A-Sepharose beads. Naked protein A-Sepharose beads incubated with extracts from tetracycline-induced cells were used as a negative control. The immunoprecipitates and lysate inputs were analysed by Western blot using the indicated antibodies (*left*).

The detection of FANCD2 and FANCI in the immunoprecipitates was additionally performed with the *LI-COR* imaging system using fluorophore-conjugated secondary antibodies. The bands were quantified and the FANCI levels normalized relative to the luciferase control. The graphs shown in the right panel represent the means of 'normalized FANCI levels relative to the luciferase control' from two independent experiments. The error bars represent the standard deviation. The asterisks indicate the statistical significances in means as calculated by t-test: * = statistically significant ($p < 0.05$), ** = very statistically significant ($p < 0.01$) (*right*).

B) Samples discussed in panel A were analysed by FACS. The FACS profiles as well as the percentage of cells for the different cell cycle stages are shown for each condition.

Figure 4.35A shows the endogenous FANCD2 immunoprecipitation from DNA damaged U2OS cells. Similarly to the results obtained without DNA damage, Flag-UBXN8 overexpression caused a decrease in FANCD2/I dimer formation compared to control cells. The corrections of FANCI levels to account for minor differences in the levels of immunoprecipitated FANCD2 were performed as described (Figure 4.35A, right panel). In contrast, the overexpression of Flag-VAPB (again much higher expression levels than with Flag-UBXN8) did not change the FANCD2/I dimer formation compared to control cells.

The FACS profiles of this analysis are shown in figure 4.35B, and confirmed that the changes observed in FANCD2/I dimer formation upon DNA damage in the presence of UBXN8 overexpression were not due to altered cell cycle progression.

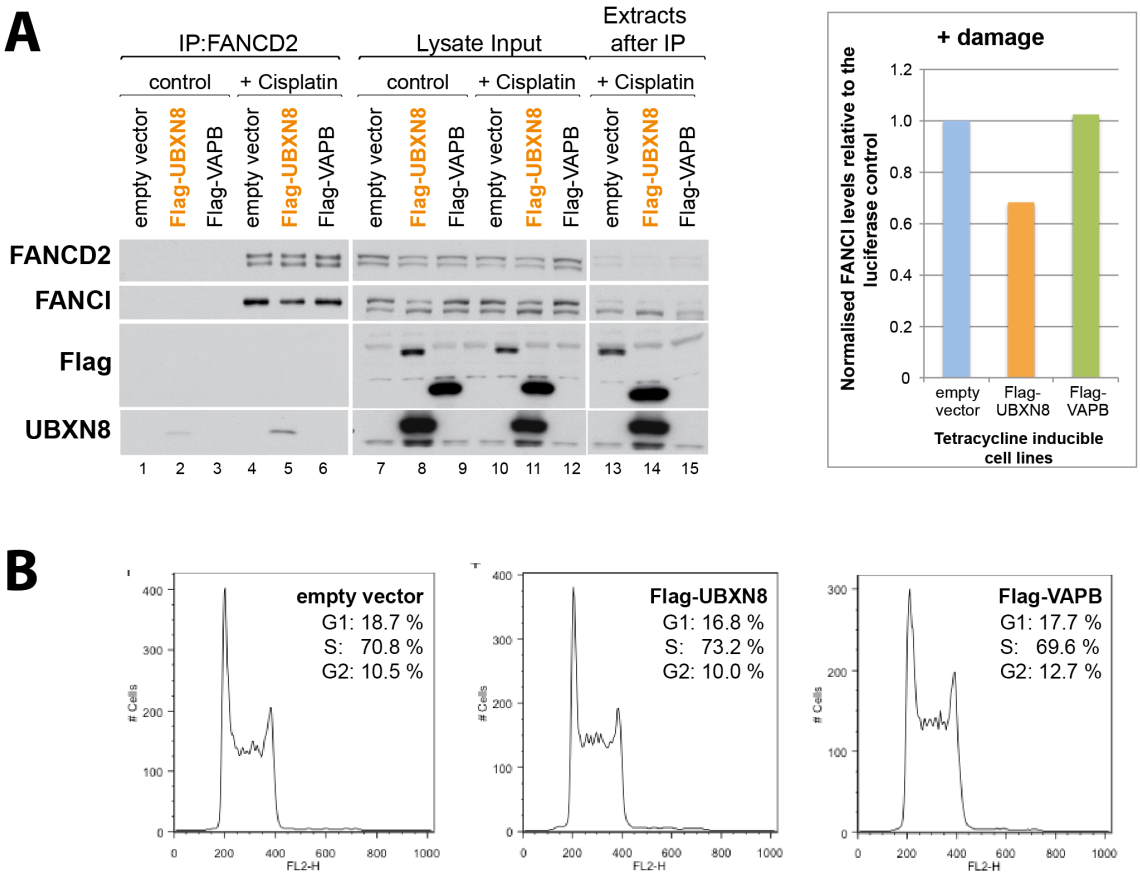

Figure 4.35: UBXN8 overexpression causes a decrease in FANCD2/I dimer formation in the presence of DNA damage

A) Endogenous FANCD2 was immunoprecipitated from tetracycline-inducible U2OS cells expressing either Flag-UBXN8 or Flag-VAPB. VAPB as well as U2OS cell with integrated empty vector were used as negative controls. After 12h induction with 0.5 µg/ml tetracycline, the cells were treated with 3 µM cisplatin for an additional 24h. To maintain Flag-UBXN8 levels, the cells were reinduced with 0.5 µg/ml tetracycline after 12h cisplatin treatment. Immunoprecipitations were performed 24h after DNA damage using anti-FANCD2 antibodies and protein A-Sepharose beads. Naked protein A-Sepharose beads incubated with extract from tetracycline-induce cells were used as a control. The immunoprecipitates and lysate inputs were analysed by Western blot using the indicated antibodies (*left*).

The detection of FANCD2 and FANCI in the immunoprecipitates was additionally performed with the *LI-COR* imaging system using fluorophore-conjugated secondary antibodies. The bands were quantified and the normalized FANCI levels relative to the luciferase control were plotted.

B) Samples discussed in panel A were analysed by FACS. The FACS profiles as well as the percentage of cells for the different cell cycle stages are shown for each condition.

Taken together, UBXN8 silencing shifted the balance of FANCD2 and FANCI from their non-ubiquitylated to their mono-ubiquitylated state, and this correlates with increased FANCD2/I dimer and FANCD2 foci formation. The results obtained with Flag-UBXN8 overexpression showed the opposite effect by reducing FANCI mono-

ubiquitylation and FANCD2/I dimer formation. Hence, these results indicate that UBXN8 controls the balance between modified and unmodified FANCD2 and FANCI in the presence and absence of DNA damage.

4.2.20 UBXN8 reduces FANCD2/I mono-ubiquitylation in vitro

The experiments discussed in the previous section indicate that UBXN8 has a negative regulatory effect on the mono-ubiquitylation of FANCD2 and FANCI.

To investigate whether UBXN8 directly affects the FANCD2/I mono-ubiquitylation, I performed *in vitro* ubiquitylation assays with recombinant proteins. Jennifer Miles, from Helen Walden's laboratory, provided the protocol as well as the protein preparations of *Xenopus laevis* FANCD2 and *Xenopus tropicalis* FANCL (E3 ligase).

For the ubiquitylation assay, FANCD2 and FANCI were used either individually or mixed together in equimolar ratios to form dimers (Figure 4.36). These were incubated with UBE1 as E1, UBE2T as E2, FANCL as E3 and HA-ubiquitin. Parallel reactions were performed with an up to 20-fold excess of human Flag-UBXN8 (without the transmembrane domain) over substrates, and corresponded to a 2.5 times excess of FANCL (Figure 4.36).

Figure 4.36 shows the HA-ubiquitin blots of the experiments. Interestingly, the mono-ubiquitylation of FANCD2 and FANCI, both individually and as part of a dimer, was gradually reduced upon incubation with increasing amounts of Flag-UBXN8. This indicates that UBXN8 might directly inhibit the mono-ubiquitylation of FANCD2 and FANCI in their monomeric state or in the FANCD2/I heterodimer.

An inhibitory effect of wild-type Flag-UBXN8 on FANCD2 and FANCI mono-ubiquitylation *in vitro* is consistent with my data showing that UBXN8 overexpression

reduces FANCI mono-ubiquitylation in cells, while UBXN8 silencing causes an increase in the level of FANCD2 and FANCI modifications.

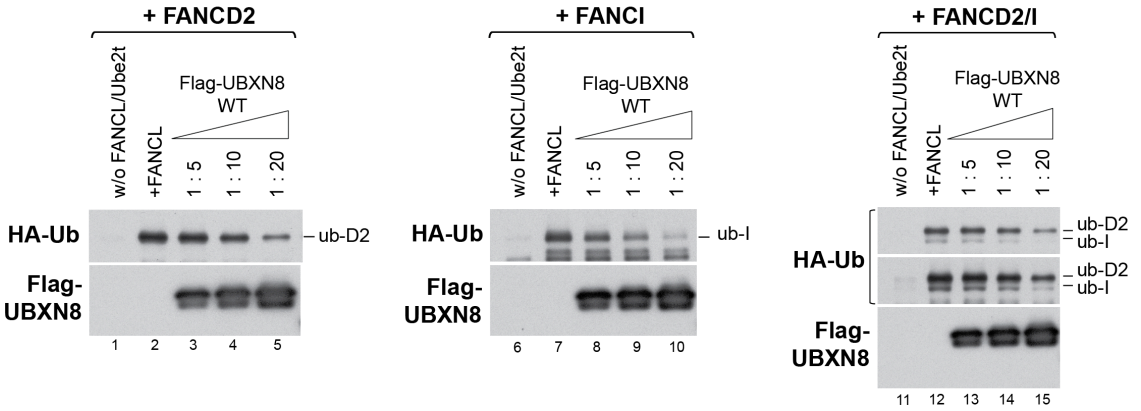

Figure 4.36: UBXN8 reduces the mono-ubiquitylation of monomeric and dimeric FANCD2/I *in vitro*

The *in vitro* ubiquitylation assays were performed by incubating *X. laevis* FANCD2 and FANCI were used either individually or mixed together in equimolar ratios to form dimers. These were incubated with human UBE1 as E1, human UBE2T as E2, *X. tropicalis* FANCL as E3 and HA-ubiquitin. Parallel reactions were performed with up to 20 fold excess of human Flag-UBXN8 (without the transmembrane domain) over substrates and corresponded to 2.5 times excess to FANCL FANCD2 and FANCI either individually or mixed together in equimolar ratios with the E3 ligase FANCL. Parallel reactions were performed with increasing molar ratios of human Flag-UBXN8 wild type. The reactions were incubated for 1.5h at 26°C and were stopped by adding SDS buffer. The mono-ubiquitylations of FANCD2 and FANCI were analysed by Western blot using anti-HA antibodies to detect HA-ubiquitin. Flag-UBXN8 was detected using anti-Flag antibodies. The molar ratios of UBXN8 to the FA protein substrates are indicated.

Interestingly, performing the ubiquitylation assays with the FANCD2/I mixtures containing the phospho-mimicking mutant FANCI 4SD (described in section 4.2.7.1) completely abolished the mono-ubiquitylation of FANCD2 and FANCI (Figure 4.37). This was surprising, since the overexpression of this mutant in cells induced the mono-ubiquitylation of FANCD2 in the absence of DNA damage. A possible explanation for this result could be that FANCD2 and the phospho-mimicking mutant of FANCI form such a tight dimer that it prevents the ubiquitylation of the proteins *in vitro*. The structure of the FANCD2/I dimer shows that the ubiquitylation sites are embedded within the interface between the FA proteins and that it requires a conformational

change of the dimer to allow modification with ubiquitin (Joo et al., 2011). In cells, this could be facilitated through binding to DNA, which is shown to stimulate mono-ubiquitylation on FANCD2 and FANCI within the dimer (Longerich et al., 2014). Additionally, the experiment with the FANCI 4SD mutant shows that by merely incubating FANCD2 and FANCI together, they can form heterodimers in our reactions. Otherwise, if FANCD2 exists as monomer it would be mono-ubiquitylated.

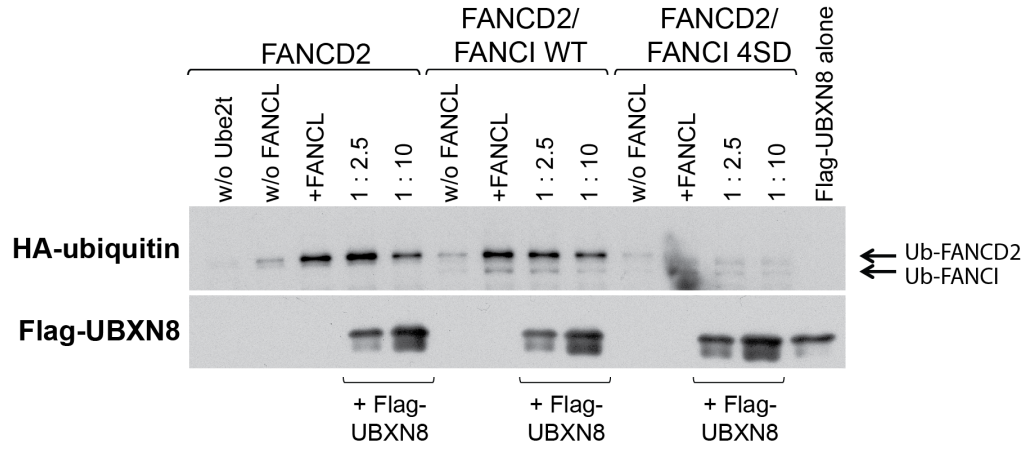

Figure 4.37: Phospho-mimicking FANCI abolishes the mono-ubiquitylation of FANCD2 *in vitro*

The *in vitro* ubiquitylation assays were performed by incubating *X. laevis* FANCD2 with wild type FANCI or its phospho-mimicking mutant (4SD), in equimolar ratios, to form dimers. For the ubiquitylation reaction, I used UBE1 as E1, UBE2T as E2, FANCL as E3 and HA-ubiquitin. Parallel reactions were performed with up to 20-fold excess human Flag-UBXN8 over substrates. The reactions were incubated for 1.5h at 26°C and were stopped by adding SDS buffer. The mono-ubiquitylation of FANCD2 and FANCI was analysed by Western blot using anti-HA antibodies. Flag-UBXN8 was detected using anti-Flag antibodies. The molar ratios of UBXN8 to the FA protein substrates are indicated.

4.6 Discussion

The UBX-only protein UBXN8 is an ER membrane protein that binds p97 via its UBX domain. UBXN8 is required for ER-associated degradation of misfolded proteins by tethering p97 at the ER membrane (Madsen et al., 2011). Furthermore, a recent publication introduced *UBXN8* as a target gene for HBV integration, and implicated UBXN8 as a new tumour suppressor candidate (Li et al., 2014).

The analysis of Flag-UBXN8 immunoprecipitates by MS identified several DNA damage-related proteins as potential UBXN8 interaction partners, including FANCD2 and FANCI (ICL repair), BRAT1, RIF1, and the three components of the TTT complex Telo2, TTI1 and TTI2 (DSB repair). These interactions raised the possibility that UBXN8 has a broader role in the DNA damage response.

The identification of the two key FA proteins, FANCD2 and FANCI, in Flag-UBXN8 immunoprecipitates may link UBXN8 to the rare genetic disease FA that is caused by defects in the ICL repair. Therefore, the aim of this project was to investigate the interaction between UBXN8 and the FA proteins FANCD2 and FANCI, to shed light on the functional relevance of these interactions, as well as to gain a better understanding of the role of UBXN8 in the DNA damage response.

4.6.1 UBXN8 captures unmodified FANCD2 and FANCI away from the DNA

I showed that full-length UBXN8 interacts with non-ubiquitylated FANCD2 and FANCI, and that both proteins are released from UBXN8 in the presence of DNA damage. This suggests that UBXN8 binds both FA proteins in their inactive state in the absence of DNA damage. These interactions were confirmed between the endogenous proteins. Furthermore, *in vitro* binding assays showed that UBXN8 can bind both FA proteins, FANCD2 and FANCI directly and independently from each other. However, I

was unable to clarify whether UBXN8 can also interact with heterodimeric FANCD2 and FANCI. A SEC-MALS (Size-exclusion chromatography and multi angle light scattering) experiment with recombinant Flag-UBXN8 and co-purified FANCD2/I heterodimer might answer this question, and is currently in progress.

The immunoprecipitations with each of the Flag-UBXN8 isoforms show that only the membrane-anchored isoforms 1 and 2 interact with FANCD2 and FANCI, suggesting that the membrane localization of UBXN8 is important for its interaction with both FA proteins. Furthermore, the *in vitro* binding assays performed with Flag-UBXN8 lacking the transmembrane domain showed a stable complex formation between UBXN8 and monomeric FANCD2 or FANCI, implicating that the transmembrane region is not required for the interaction.

The subcellular localization of UBXN8 was analysed in HeLa cells using immunofluorescence microscopy. The images obtained confirmed the ER localisation of full-length Flag-UBXN8 as described by Madsen et al. (2012). Furthermore, I observed that a fraction of Flag-UBXN8 distinctly localised at the nuclear envelope. By using OMX structured illumination microscopy, I showed that a small fraction of UBXN8 localises inside the nucleus to the inner nuclear membrane. Because FANCD2 and FANCI are mainly nuclear-localised (Smogorzewska et al., 2007, Garcia-Higuera et al., 2001), the inner nuclear membrane could be the actual site of interaction between UBXN8 and both FA proteins. The small fraction of nuclear localised UBXN8 would only be able to bind a small pool of FANCD2 and FANCI, and could explain why only minor fractions of these proteins interact.

However, my first attempts to show co-localisation between UBXN8 and FANCD2 using microscopy were not successful and require further improvement of the experimental setup. Alternatively, Flag-UBXN8 immunoprecipitation or size

fractionation (using SEC) from nuclear cell fractions could be performed to investigate whether UBXN8 interacts with FANCD2 and FANCI in the nucleus.

4.6.2 The coiled-coil domain in UBXN8 is required for the interaction with FANCD2 and FANCI

Full-length UBXN8 contains a transmembrane domain at the N-terminus, followed by a predicted coiled-coil region, and a UBX domain at the C-terminus. It has been shown that the transmembrane domain anchors UBXN8 at the ER membrane, while the UBX domain mediates its interaction with the N-terminus of p97 (Madsen et al., 2011).

Coiled-coil domains are, in general, described as mediating protein-protein interactions. However, the function of the predicted coiled-coil region in UBXN8 was unknown.

My results show that UBXN8 forms a homodimer *in vitro*, and in cells, independent from its coiled-coil domain. However, the truncation of this region nearly abolished UBXN8 binding to FANCD2 and FANCI, suggesting that the coiled-coil domain in UBXN8 is required for the interaction with both FA proteins. The reduced binding of Flag-UBXN8 Δcoiled-coil to FANCD2 and FANCI was not due to changes in the subcellular localisation of UBXN8, since this mutant still localises at the ER membrane and the nuclear envelope, as is wild type UBXN8.

It is true that also UBXN8 isoform 2, which lacks a region between the coiled-coil and UBX domain, showed a clear reduction in FANCD2 binding and a small reduction in its interaction with FANCI compared to wild-type UBXN8. Therefore, it is possible that residues within the missing region of isoform 2 contribute to the binding of FANCD2 and FANCI.

The determination of the minimal region or residues of the interaction interface between UBXN8 and the FA proteins FANCD2 and FANCI would require the crystal structure of the UBXN8–FANCD2 and/or –FANCI complex.

The finding that UBXN8 binds FANCD2 and FANCI via its coiled-coil domain supports the notion that UBX-only proteins, because of their lack of the UBA domain, bind their substrates more specifically in an ubiquitin-independent manner. Hence, UBXN8 only interacts with non-ubiquitylated FANCD2 and FANCI; their ubiquitylation is not necessary for the interaction with UBXN8.

4.6.3 UBXN8 prevents ectopic activation of FANCD2 and FANCI

The clonogenic survival assays showed that UBXN8 silencing caused increased resistance to the ICL-inducing agents MMC or cisplatin compared to control cells. These results suggest that UBXN8 is a negative regulator of the DNA damage response.

The mono-ubiquitylation of FANCD2 and FANCI is considered to be the essential step in the activation of the FA pathway. The results presented in this thesis give multiple lines of evidence that UBXN8 negatively regulates the activation of FANCD2 and FANCI, namely:

(1) The silencing of UBXN8 in U2OS cells caused an increase in the levels of FANCD2 and FANCI mono-ubiquitylation under normal and DNA damage conditions. Consistent with the increase in FANCD2 and FANCI mono-ubiquitylation in UBXN8-depleted cells, I also observed an increase in FANCD2/I dimer formation between the mono-ubiquitylated proteins, as well as an increase in the FANCD2 foci formation under normal and DNA damage conditions.

(2) The overexpression of UBXN8 led to the opposite effect compared to UBXN8 silencing. UBXN8 overexpression caused a reduction in the levels of FANCI mono-

ubiquitylation and the FANCD2/I dimer formation in the presence and absence of DNA damage.

(3) The *in vitro* ubiquitylation assays showed that UBXN8 reduces FANCD2 and FANCI mono-ubiquitylation in their monomeric state as well as in the context of the FANCD2/I dimer. This result suggests an inhibitory effect of UBXN8 on FANCD2 and FANCI mono-ubiquitylation *in vitro* and is consistent with the data showing that UBXN8 overexpression reduces FANCI mono-ubiquitylation in cells, while UBXN8 silencing causes an increase in the level of FANCD2 and FANCI modification.

The structure of the murine ID complex revealed that the ubiquitylation site Lys561 and Lys523 in FANCD2 and FANCI, respectively, are embedded within the interface of the ID complex. Therefore, it was suggested that the ubiquitylation of both FA proteins either happens on the monomeric proteins before their dimerization, or that the ID complex has to undergo a conformational change to allow the access of the E3 ligase to the lysine residues. Although it is still controversial whether FANCD2 and FANCI dimerize before DNA-binding or on the chromatin, recent findings support the notion that dimerization is required for DNA binding and mono-ubiquitylation. For example, the DNA binding activity of FANCI is important for the mono-ubiquitylation of FANCD2 within the ID complex *in vitro*. This suggests that FANCD2 and FANCI have to form a heterodimer for efficient DNA binding and consequently this is prior to FANCD2 mono-ubiquitylation (Longerich et al., 2014). Furthermore, it has been shown that DNA stimulates the mono-ubiquitylation of FANCD2 and FANCI *in vitro*, suggesting that DNA binding occurs prior to the ubiquitylation of the FA proteins (Sato et al., 2012b, Longerich et al., 2014).

Taking these findings into account, the results obtained upon UBXN8 silencing could suggest the following scenario (Figure 4.38):

UBXN8 tethers FANCD2 and FANCI at the membrane (most likely at the nuclear membrane) to prevent their binding to DNA and to keep them in their inactive (unmodified) state.

Several studies indicate that proteins at the nuclear periphery contribute to genome stability (Nagai et al., 2011, Misteli and Soutoglou, 2009). This has been investigated mainly in yeast and it was shown that certain types of DNA damage, such as persistent DSBs or collapsed replication forks, are recruited to the nuclear pores or sites along the inner nuclear envelope to be repaired by an alternative type of recombination repair (Nagai et al., 2008, Palancade et al., 2007, Kalocsay et al., 2009). Although the MS analysis of Flag-UBXN8 immunoprecipitates identified nucleoporins, such as Nup43, Nup85 and Nup160 as potential UBXN8 interaction partners, my data does not indicate that the DNA repair machinery localises to membrane-anchored UBXN8. Further, UBXN8 shows reduced FANCD2 and FANCI binding upon DNA damage, and does not interact with the mono-ubiquitylated form of FANCD2 and FANCI, which according to my data seems to represent the active and chromatin-bound state of both FA proteins. Hence, UBXN8 seems not to bind chromatin-associated FANCD2 and FANCI. This suggests that UBXN8 does not positively co-operate with FANCD2 and FANCI in DNA damage repair. It also has to be mentioned, that DSBs in mammalian cells seem to undergo no or limited motion in the nuclear space, therefore canonical HR events seem to occur preferentially in intranuclear foci, and are not sequestered to the nuclear periphery (Misteli and Soutoglou, 2009, Soutoglou et al., 2007, Oza et al., 2009). This further negate the possibility that UBXN8 interaction with FANCD2 and

FANCI at the membrane is to facilitate the repair of damaged DNA near the nuclear periphery.

Therefore, the silencing of UBXN8 would consequently result in an increased pool of free/soluble FANCD2 and FANCI. Because I was unable to clarify whether UBXN8 binds monomeric and/or heterodimeric FANCD2/I, UBXN8 silencing might either increase the monomeric pool and/or the heterodimeric pool of FANCD2/I. Nonetheless, the free FANCD2 and FANCI are recruited to the DNA, where they get activated through mono-ubiquitylation, independently of DNA damage. Hence, the increased dimer formation and mono-ubiquitylation of FANCD2 and FANCI observed upon UBXN8 depletion might be a consequence of the increased amount of DNA localised FANCD2/I.

The inhibitory effect of wild type UBXN8 on FANCD2 and FANCI mono-ubiquitylation observed *in vitro* suggests that the binding of UBXN8 to the FA proteins prevents their mono-ubiquitylation. It has been shown that FANCL, similar to FANCD2 and FANCI, is mainly nuclear localised and not chromatin bound in the absence of DNA damage (Tremblay et al., 2008). Furthermore, the core complex that includes FANCL is constitutively assembled and stable throughout the cell cycle (Alpi et al., 2007). Therefore, the specific binding of UBXN8 to FANCD2 and FANCI might represent an additional mechanism to prevent FANCD2 and FANCI mono-ubiquitylation away from the DNA.

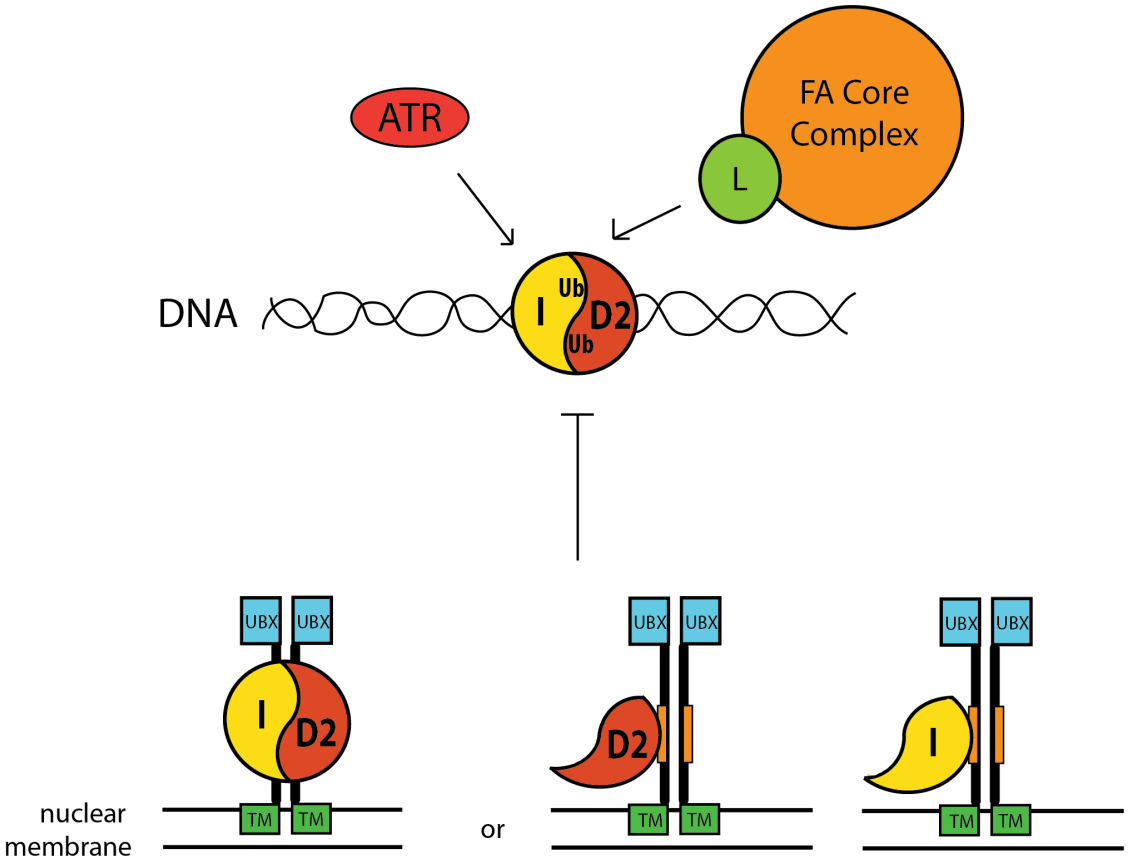

Figure 4.38: UBXN8 prevents the ectopic activation of FANCD2 and FANCI

Proposed model: UBXN8 homodimers capture monomeric FANCD2 (D2) and FANCI (I) or the ID complex at the nuclear membrane. This consequently keeps both proteins away from the DNA and prevents their ectopic dimerization and mono-ubiquitylation. This may be particularly important in the absence of DNA damage, when unrestricted activation of the FA pathway likely has deleterious effects for the cell.
TM: transmembrane domain, UBX: Regulatory X domain, coiled-coil domain (orange), D2: FANCD2, I: FANCI, L: FANCL, Ub: ubiquitin.

In the presence of DNA damage, the increased amounts of active/mono-ubiquitylated FANCD2 and FANCI in UBXN8-silenced cells might have a positive effect and could explain the increased resistance to ICL-inducing reagents. That an increase in mono-ubiquitylated and DNA-bound FANCD2 might be an advantage in the presence of DNA damage was also described for USP1-silenced cancer cells. Similar to the UBXN8 silenced cells, USP1 silencing increased FANCD2 mono-ubiquitylation and its chromatin-association (Nijman et al., 2005). Upon DNA damage, the silencing of USP1

in HEK293 cells caused reduced MMC-induced chromosomal aberrations and provided relative resistance compared to control cells. It was therefore suggested that the increased levels of FANCD2 mono-ubiquitylation might protect cells from ICL-induced DNA damage (Nijman et al., 2005). However, it must be mentioned that *USP1* knockdown in chicken DT40 cells, as well as *Usp1*$^{-/-}$ mouse embryonic fibroblasts, show an increased FANCD2 mono-ubiquitylation and chromatin-association, but cells are hypersensitive to DNA damaging agents (Kim et al., 2009, Oestergaard et al., 2007). The reason for the contradicting observation could be that silencing of USP1 with siRNA does not lead to complete depletion of USP1 as a knockout does. Therefore, de-ubiquitylation of FANCD2 is not completely abolished in USP1-silenced cells.

In the absence of DNA damage ectopic activation of FANCD2 and FANCI and the possible recruitment of downstream factors, such as the endonucleases FAN1 and SLX4 through mono-ubiquitylated FANCD2 could cause an increase in mutation frequency and genome instability. Therefore, it will be important to test whether silencing of UBXN8 causes reduced cell viability in the absence of DNA damage. If this were the case, it would show the importance of UBXN8 in maintaining genome integrity by regulating the availability of DNA-targeted FANCD2 and FANCI.

Furthermore, the inhibitory effect of UBXN8 would be in line with numerous other mechanisms that control the FA pathway activity to ensure its activation only when it is required. Other control mechanisms are for example: the ATR-dependent phosphorylation of FANCI and FANCD2 that restricts the activation of the FA pathway to S-phase (Andreassen et al., 2004, Pichierri and Rosselli, 2004, Ishiai et al., 2008); the phosphorylation of FANCA, FANCE and FANCG that are important for the activation of the FA pathway (Collins et al., 2009, Wang et al., 2007, Mi et al., 2004); the

phosphorylation of FANCM is regulated during cell cycle and restricts the recruitment of the core complex to the DNA in S-phase (Kim et al., 2008); the de-ubiquitylation of FANCD2 and FANCI by USP1/UAF1 inactivates the FA pathway (Nijman et al., 2005). The presence of these control mechanism also suggests that the unrestricted activation of the FA pathway likely has deleterious effects for the cell. However, whether unscheduled activation of the FA pathway causes DNA damage is not known.

4.6.4 Reduced UBXN8 levels allow increased FANCD2/I availability upon DNA damage

The double-thymidine block used for S-phase arrest caused a strong mono-ubiquitylation of FANCD2 and FANCI that gradually decreased after release as cells progressed through the cell cycle. The increased levels of mono-ubiquitylated FANCD2 and FANCI were caused by thymidine, which is described to induce DNA damage response (Bolderson et al., 2004). Interestingly, the increased levels of mono-ubiquitylated FANCD2 and FANCI after the release from thymidine are accompanied by reduced UBXN8 levels compared to asynchronous cells, or cells harvested at later time points (10–18h) that have similar cell cycle distributions. The time points (12-18h) in which cells re-entered S-phase did not re-induce increased mono-ubiquitylation of FANCD2 and FANCI, while UBXN8 levels gradually increase to the levels observed with asynchronous cells. This result suggests that UBXN8 levels might be reduced upon DNA damage to allow the activation of repair proteins such as FANCD2 and FANCI. The reduction of UBXN8 levels would release the inhibitory effect that it has upon FANCD2 and FANCI in the absence of damage.

Furthermore, under non-damaged conditions, cell populations with a larger percentage of cells in S-phase show higher UBXN8 levels compared to G1 or mitosis-arrested cell

populations. The activation of the FA pathway is restricted to S-phase, which is ensured by several control mechanisms (Andreassen et al., 2004, Qiao et al., 2004, Wang et al., 2007, Ishiai et al., 2008). Therefore, during S-phase and in the absence of DNA damage, increased UBXN8 levels might allow a tighter control of FANCD2 and FANCI to prevent their localisation to DNA, and consequent ectopic activation.

4.6.5 Phosphorylation of four serine residues in FANCI causes ectopic activation of FANCD2

The main upstream regulator of the FA pathway is ATR that coordinates the DNA damage response in S-phase. Although ATR phosphorylates several components of the FA core complex, its most relevant target in the FA pathway is FANCI.

Ishiai et al. have shown that six key serine residues are important phosphorylation sites in chicken FANCI and are required for the mono-ubiquitylation of FANCD2 and the activation of the FA pathway (Ishiai et al., 2008). To investigate whether constitutive dimer formation of FANCD2/I changes the binding to UBXN8, I used the human, chicken equivalent, sextuple FANCI phospho-mutants (Dx6 and Ax6), as well as a quadruple mutant of human FANCI that harboured only four of the six mutations.

The results obtained with the sextuple mutant in human FANCI failed to induce FANCD2 mono-ubiquitylayion and FANCD2/I foci formation, suggesting that there are differences in the importants of various phosphorylation sites between human and chicken FANCI. Interestingly, I identified the quadruple phospho-mimicking mutant (S556D, S559D, S565D, S596D) in human FANCI that constitutively activate FANCD2 and strongly induce FANCD2/I dimer formation in the absence of DNA damage. In contrast, the quadruple phospho-dead mutant did not show any binding to mono-ubiquitylated FANCD2 with or without DNA damage. The equivalent of the

quadruple mutant was not tested by Ishiai et al, therefore it is unclear whether these phospho-mimicking mutations at the equivalent residues in chicken FANCI would cause the same effect as seen with human FANCI. Furthermore, only the first two serine residues S556D and S559D have been shown to be phosphorylated in cells (Mu et al., 2007) and it would be interesting to see whether the phosphorylation of these two residues is enough to cause the phenotype observed with the quadruple mutant. Preliminary data indicate that these two residues (S556D/S559D) as well as the first three residues (S556D/S559D/S565D) induce FANCD2 mono-ubiquitylation similar to the quadruple phospho-mimicking FANCI mutant, however both mutants show reduced binding to mono-ubiquitylated FANCD2.

The majority of the FANCD2/FANCI 4SD dimer was only extracted by lysing the cells with benzonase, suggesting that this artificially induced dimer was targeted to chromatin even in the absence of DNA damage. Hence, the artificially induced dimer of FANCD2/I 4SD did not lead to an increase in dimer that was not DNA-bound. The mutations in FANCI did not affect its binding to endogenous UBXN8 that bound to wild type and mutant Flag-FANCI with similar efficiency. It is likely that DNA-bound FANCD2/I is not accessible to interact with UBXN8, which is anchored at the nuclear membrane. The reduced UBXN8 interaction with FANCD2 and FANCI upon DNA damage supports this idea. To prevent binding to the DNA, I created additional mutations (K898E and K980E) at putative DNA binding regions of FANCI. However, these mutations caused a defect in FANCD2/I dimerization and therefore did not increase the soluble pool of FANCD2/I dimer.

The model I propose suggests that UBXN8 acts as a negative regulator by capturing FANCD2 and FANCI at the membrane to prevent ectopic activation particularly in the absence of DNA damage (Figure 4.38).

Studying the localisation of the sextuple phospho-mimicking GFP-chFANCI mutant in DT40 *fanci* cells, Ishiai et al. has shown that the phospho-mimicking-mutant (Dx6) drastically increases FANCD2/I foci formation on chromatin in the absence of DNA damage. These foci only partially localised with γH2AX or RAD51 foci, suggesting that these are not DNA damage foci (Ishiai et al., 2008).

The ectopic activation of the FA pathway induced by the phospho-mimicking FANCI 4SD mutant represents another example of how important it is to control the unrestricted activation of the FA pathway. Furthermore, it supports the notion, that a negative regulator such as UBXN8 might be required to prevent the FANCD2 and FANCI localisation to DNA and their ectopic activation in the absence of DNA damage. It would be interesting to investigate whether the overexpression of Flag-UBXN8 could suppress the FANCD2 mono-ubiquitylation and foci formation induced by the phospho-mimicking FANCI 4SD mutant.

4.6.6 p97 and its dual function in the FA pathway

The *in vitro* binding assays have shown that UBXN8 can bind FANCD2 and FANCI in the absence of p97, suggesting that binding between these proteins is not mediated by p97. However, preventing p97 interaction with UBXN8 through the P238G mutation in the FPR motif within the UBX domain caused an increased UBXN8 binding to FANCI compared to the wild type. This effect was not observed with FANCD2 that binds wild type and mutant UBXN8 to the same extent. Furthermore, I showed that FANCD2 and

FANCI get released from Flag-UBXN8 upon DNA damage and that the FANCI release was impaired in the case of the P238G mutant compared to the wild type.

These results suggest the p97 regulates the binding between UBXN8 and FANCI, by mediating its release from UBXN8. This might be particularly important upon DNA damage – the time in which FANCD2 and FANCI are activated and localise to DNA lesions to facilitate DNA repair.

The *in vitro* binding assays have shown that UBXN8 can bind monomeric FANCD2 or FANCI. However, since UBXN8 forms homodimers both *in vitro* and in cells, it theoretically has two binding sites and could bind the heterodimer FANCD2/I as well. Therefore, the results obtained with the P238G mutant suggest two scenarios of how p97 regulates the binding of FANCI: (1) UBXN8 binds monomeric FANCD2 and FANCI, and p97 dissociates monomeric FANCI from UBXN8, or (2) UBXN8 binds the heterodimer FANCD2/I and p97 dissociates FANCI from FANCD2 that remains bound to UBXN8. Both scenarios take into consideration that the binding of UBXN8 to FANCD2 is regulated in a p97-independent manner.

The regulatory function of p97 could be studied further using a p97 inhibitor such as ML240 or ML241. This would allow the inhibition of p97 ATPase activity in a shorter period (Chou et al., 2013) and might reduce the side effects, such as cell cycle arrest and decreased cell viability, observed with siRNA treatment.

Interestingly, upon release from DNA damage FANCI interaction with FANCD2 gradually declined over time, while the binding to p97 drastically increased. Recent publications have shown that p97 and its cofactor NPL4-UFD1 are recruited to DNA damage sites to extract substrate proteins, such as L3MBTL1 (Acs et al., 2011) or the TLS polymerase Pol η (Davis et al., 2012) to allow the proper assembly of downstream

signalling factors, including Rad51, BRCA1 and 53BP1 (Acs et al., 2011, Meerang et al., 2011). Therefore, it is tempting to speculate that p97 might be required for FANCD2/I dimer dissociation from chromatin, or the dissociation of the heterodimer itself when DNA repair is complete. The increased p97-binding to FANCD2 upon release from DNA damage was UBXN8-independent, because UBXN8 silencing did not affect the increase in p97-binding. Therefore, p97 might have a dual function in the FA pathway: (1) regulating the interaction between UBXN8 and FANCI and (2) dissociating the heterodimer FANCD2/I from chromatin or from each other upon completion of DNA repair.

5. References

ACS, K., LUIJSTERBURG, M. S., ACKERMANN, L., SALOMONS, F. A., HOPPE, T. & DANTUMA, N. P. 2011. The AAA-ATPase VCP/p97 promotes 53BP1 recruitment by removing L3MBTL1 from DNA double-strand breaks. *Nature structural & molecular biology,* 18**,** 1345-50.

AGLIPAY, J. A., MARTIN, S. A., TAWARA, H., LEE, S. W. & OUCHI, T. 2006. ATM activation by ionizing radiation requires BRCA1-associated BAAT1. *J. Biol. Chem.,* 281**,** 9710-8.

ALEXANDRU, G., GRAUMANN, J., SMITH, G. T., KOLAWA, N. J., FANG, R. & DESHAIES, R. J. 2008. UBXD7 binds multiple ubiquitin ligases and implicates p97 in HIF1alpha turnover. *Cell,* 134**,** 804-16.

ALPI, A., LANGEVIN, F., MOSEDALE, G., MACHIDA, Y. J., DUTTA, A. & PATEL, K. J. 2007. UBE2T, the Fanconi anemia core complex, and FANCD2 are recruited independently to chromatin: a basis for the regulation of FANCD2 monoubiquitination. *Molecular and cellular biology,* 27**,** 8421-30.

ALPI, A. F., PACE, P. E., BABU, M. M. & PATEL, K. J. 2008. Mechanistic insight into site-restricted monoubiquitination of FANCD2 by Ube2t, FANCL, and FANCI. *Mol. Cell,* 32**,** 767-77.

ALTOMARE, D. A., MENGES, C. W., PEI, J., ZHANG, L., SKELE-STUMP, K. L., CARBONE, M., KANE, A. B. & TESTA, J. R. 2009. Activated TNF-alpha/NF-kappaB signaling via down-regulation of Fas-associated factor 1 in asbestos-induced mesotheliomas from Arf knockout mice. *Proceedings of the National Academy of Sciences of the United States of America,* 106**,** 3420-5.

ANDREASSEN, P. R., D'ANDREA, A. D. & TANIGUCHI, T. 2004. ATR couples FANCD2 monoubiquitination to the DNA-damage response. *Genes & development,* 18**,** 1958-63.

ANDRIN, C., MCDONALD, D., ATTWOOD, K. M., RODRIGUE, A., GHOSH, S., MIRZAYANS, R., MASSON, J. Y., DELLAIRE, G. & HENDZEL, M. J. 2012. A requirement for polymerized actin in DNA double-strand break repair. *Nucleus,* 3**,** 384-95.

ARGANI, P., ANTONESCU, C. R., ILLEI, P. B., LUI, M. Y., TIMMONS, C. F., NEWBURY, R., REUTER, V. E., GARVIN, A. J., PEREZ-ATAYDE, A. R., FLETCHER, J. A., BECKWITH, J. B., BRIDGE, J. A. & LADANYI, M. 2001. Primary renal neoplasms with the ASPL-TFE3 gene fusion of alveolar soft part

sarcoma: a distinctive tumor entity previously included among renal cell carcinomas of children and adolescents. *The American journal of pathology,* 159**,** 179-92.

AUERBACH, A. D. 2009. Fanconi anemia and its diagnosis. *Mutation research,* 668**,** 4-10.

AUERBACH, A. D. & WOLMAN, S. R. 1976. Susceptibility of Fanconi's anaemia fibroblasts to chromosome damage by carcinogens. *Nature,* 261**,** 494-6.

BAKKER, S. T., DE WINTER, J. P. & TE RIELE, H. 2013. Learning from a paradox: recent insights into Fanconi anaemia through studying mouse models. *Disease models & mechanisms,* 6**,** 40-7.

BANDAU, S., KNEBEL, A., GAGE, Z. O., WOOD, N. T. & ALEXANDRU, G. 2012. UBXN7 docks on neddylated cullin complexes using its UIM motif and causes HIF1alpha accumulation. *BMC biology,* 10**,** 36.

BILODEAU, P. S., URBANOWSKI, J. L., WINISTORFER, S. C. & PIPER, R. C. 2002. The Vps27p Hse1p complex binds ubiquitin and mediates endosomal protein sorting. *Nature cell biology,* 4**,** 534-9.

BJORLING-POULSEN, M., SEITZ, G., GUERRA, B. & ISSINGER, O. G. 2003. The pro-apoptotic FAS-associated factor 1 is specifically reduced in human gastric carcinomas. *International journal of oncology,* 23**,** 1015-23.

BLOOM, J., AMADOR, V., BARTOLINI, F., DEMARTINO, G. & PAGANO, M. 2003. Proteasome-mediated degradation of p21 via N-terminal ubiquitinylation. *Cell,* 115**,** 71-82.

BOH, B. K., SMITH, P. G. & HAGEN, T. 2011. Neddylation-induced conformational control regulates cullin RING ligase activity in vivo. *Journal of molecular biology,* 409**,** 136-45.

BOISVERT, R. A., REGO, M. A., AZZINARO, P. A., MAURO, M. & HOWLETT, N. G. 2013. Coordinate nuclear targeting of the FANCD2 and FANCI proteins via a FANCD2 nuclear localization signal. *PloS one,* 8**,** e81387.

BOLDERSON, E., SCORAH, J., HELLEDAY, T., SMYTHE, C. & MEUTH, M. 2004. ATM is required for the cellular response to thymidine induced replication fork stress. *Human molecular genetics,* 13**,** 2937-45.

BORGESE, N. & FASANA, E. 2011. Targeting pathways of C-tail-anchored proteins. *Biochimica et biophysica acta,* 1808**,** 937-46.

BOSU, D. R. & KIPREOS, E. T. 2008. Cullin-RING ubiquitin ligases: global regulation and activation cycles. *Cell division,* 3**,** 7.

BROWNELL, J. E., SINTCHAK, M. D., GAVIN, J. M., LIAO, H., BRUZZESE, F. J., BUMP, N. J., SOUCY, T. A., MILHOLLEN, M. A., YANG, X., BURKHARDT, A. L., MA, J., LOKE, H. K., LINGARAJ, T., WU, D., HAMMAN, K. B., SPELMAN, J. J., CULLIS, C. A., LANGSTON, S. P., VYSKOCIL, S., SELLS, T. B., MALLENDER, W. D., VISIERS, I., LI, P., CLAIBORNE, C. F., ROLFE, M., BOLEN, J. B. & DICK, L. R. 2010. Substrate-assisted inhibition of ubiquitin-like protein-activating enzymes: the NEDD8 E1 inhibitor MLN4924 forms a NEDD8-AMP mimetic in situ. *Molecular cell,* 37**,** 102-11.

BUCHBERGER, A. 2002. From UBA to UBX: new words in the ubiquitin vocabulary. *Trends in cell biology,* 12**,** 216-21.

CARIM-TODD, L., ESCARCELLER, M., ESTIVILL, X. & SUMOY, L. 2001. Identification and characterization of UBXD1, a novel UBX domain-containing gene on human chromosome 19p13, and its mouse ortholog. *Biochim. Biophys. Acta.,* 1517**,** 298-301.

CHOU, T. F., LI, K., FRANKOWSKI, K. J., SCHOENEN, F. J. & DESHAIES, R. J. 2013. Structure-activity relationship study reveals ML240 and ML241 as potent and selective inhibitors of p97 ATPase. *ChemMedChem,* 8**,** 297-312.

CICCIA, A., LING, C., COULTHARD, R., YAN, Z., XUE, Y., MEETEI, A. R., LAGHMANI EL, H., JOENJE, H., MCDONALD, N., DE WINTER, J. P., WANG, W. & WEST, S. C. 2007. Identification of FAAP24, a Fanconi anemia core complex protein that interacts with FANCM. *Molecular cell,* 25**,** 331-43.

CIMPRICH, K. A. & CORTEZ, D. 2008. ATR: an essential regulator of genome integrity. *Nature reviews. Molecular cell biology,* 9**,** 616-27.

COHN, M. A., KOWAL, P., YANG, K., HAAS, W., HUANG, T. T., GYGI, S. P. & D'ANDREA, A. D. 2007. A UAF1-containing multisubunit protein complex regulates the Fanconi anemia pathway. *Molecular cell,* 28**,** 786-97.

COLE, A. R., LEWIS, L. P. & WALDEN, H. 2010. The structure of the catalytic subunit FANCL of the Fanconi anemia core complex. *Nature structural & molecular biology,* 17**,** 294-8.

COLLINS, N. B., WILSON, J. B., BUSH, T., THOMASHEVSKI, A., ROBERTS, K. J., JONES, N. J. & KUPFER, G. M. 2009. ATR-dependent phosphorylation of FANCA on serine 1449 after DNA damage is important for FA pathway function. *Blood,* 113**,** 2181-90.

COLLIS, S. J., BARBER, L. J., WARD, J. D., MARTIN, J. S. & BOULTON, S. J. 2006. C. elegans FANCD2 responds to replication stress and functions in interstrand cross-link repair. *DNA repair,* 5**,** 1398-406.

COLLIS, S. J., CICCIA, A., DEANS, A. J., HOREJSI, Z., MARTIN, J. S., MASLEN, S. L., SKEHEL, J. M., ELLEDGE, S. J., WEST, S. C. & BOULTON, S. J. 2008. FANCM and FAAP24 function in ATR-mediated checkpoint signaling independently of the Fanconi anemia core complex. *Molecular cell,* 32**,** 313-24.

COLNAGHI, L., JONES, M. J., COTTO-RIOS, X. M., SCHINDLER, D., HANENBERG, H. & HUANG, T. T. 2011. Patient-derived C-terminal mutation of FANCI causes protein mislocalization and reveals putative EDGE motif function in DNA repair. *Blood,* 117**,** 2247-56.

COPE, G. A., SUH, G. S., ARAVIND, L., SCHWARZ, S. E., ZIPURSKY, S. L., KOONIN, E. V. & DESHAIES, R. J. 2002. Role of predicted metalloprotease motif of Jab1/Csn5 in cleavage of Nedd8 from Cul1. *Science,* 298**,** 608-11.

DAI, R. M., CHEN, E., LONGO, D. L., GORBEA, C. M. & LI, C. C. 1998. Involvement of valosin-containing protein, an ATPase Co-purified with IkappaBalpha and 26 S proteasome, in ubiquitin-proteasome-mediated degradation of IkappaBalpha. *The Journal of biological chemistry,* 273**,** 3562-73.

DANTUMA, N. P. & HOPPE, T. 2012. Growing sphere of influence: Cdc48/p97 orchestrates ubiquitin-dependent extraction from chromatin. *Trends in cell biology,* 22**,** 483-91.

DAUB, H., OLSEN, J. V., BAIRLEIN, M., GNAD, F., OPPERMANN, F. S., KORNER, R., GREFF, Z., KERI, G., STEMMANN, O. & MANN, M. 2008. Kinase-selective enrichment enables quantitative phosphoproteomics of the kinome across the cell cycle. *Molecular cell,* 31**,** 438-48.

DAVIS, E. J., LACHAUD, C., APPLETON, P., MACARTNEY, T. J., NATHKE, I. & ROUSE, J. 2012. DVC1 (C1orf124) recruits the p97 protein segregase to sites of DNA damage. *Nature structural & molecular biology,* 19**,** 1093-100.

DEANS, A. J. & WEST, S. C. 2009. FANCM connects the genome instability disorders Bloom's Syndrome and Fanconi Anemia. *Molecular cell,* 36**,** 943-53.

DELABARRE, B. & BRUNGER, A. T. 2005. Nucleotide dependent motion and mechanism of action of p97/VCP. *Journal of molecular biology,* 347**,** 437-52.

DEN BESTEN, W., VERMA, R., KLEIGER, G., OANIA, R. S. & DESHAIES, R. J. 2012. NEDD8 links cullin-RING ubiquitin ligase function to the p97 pathway. *Nature structural & molecular biology,* 19**,** 511-6, S1.

DEPHOURE, N., ZHOU, C., VILLEN, J., BEAUSOLEIL, S. A., BAKALARSKI, C. E., ELLEDGE, S. J. & GYGI, S. P. 2008. A quantitative atlas of mitotic phosphorylation. *Proceedings of the National Academy of Sciences of the United States of America,* 105**,** 10762-7.

DESHAIES, R. J. & JOAZEIRO, C. A. 2009. RING domain E3 ubiquitin ligases. *Annual review of biochemistry,* 78**,** 399-434.

DREVENY, I., KONDO, H., UCHIYAMA, K., SHAW, A., ZHANG, X. & FREEMONT, P. S. 2004. Structural basis of the interaction between the AAA ATPase p97/VCP and its adaptor protein p47. *The EMBO journal,* 23**,** 1030-9.

DUDA, D. M., BORG, L. A., SCOTT, D. C., HUNT, H. W., HAMMEL, M. & SCHULMAN, B. A. 2008. Structural insights into NEDD8 activation of cullin-RING ligases: conformational control of conjugation. *Cell,* 134**,** 995-1006.

EL-DEIRY, W. S., HARPER, J. W., O'CONNOR, P. M., VELCULESCU, V. E., CANMAN, C. E., JACKMAN, J., PIETENPOL, J. A., BURRELL, M., HILL, D. E., WANG, Y. & ET AL. 1994. WAF1/CIP1 is induced in p53-mediated G1 arrest and apoptosis. *Cancer research,* 54**,** 1169-74.

EMBERLEY, E. D., MOSADEGHI, R. & DESHAIES, R. J. 2012. Deconjugation of Nedd8 from Cul1 is directly regulated by Skp1-F-box and substrate, and the COP9 signalosome inhibits deneddylated SCF by a noncatalytic mechanism. *The Journal of biological chemistry,* 287**,** 29679-89.

ENCHEV, R. I., SCOTT, D. C., DA FONSECA, P. C., SCHREIBER, A., MONDA, J. K., SCHULMAN, B. A., PETER, M. & MORRIS, E. P. 2012. Structural basis for a reciprocal regulation between SCF and CSN. *Cell reports,* 2**,** 616-27.

FANG, S., FERRONE, M., YANG, C., JENSEN, J. P., TIWARI, S. & WEISSMAN, A. M. 2001. The tumor autocrine motility factor receptor, gp78, is a ubiquitin protein ligase implicated in degradation from the endoplasmic reticulum. *Proceedings of the National Academy of Sciences of the United States of America,* 98**,** 14422-7.

FEKAIRI, S., SCAGLIONE, S., CHAHWAN, C., TAYLOR, E. R., TISSIER, A., COULON, S., DONG, M. Q., RUSE, C., YATES, J. R., 3RD, RUSSELL, P., FUCHS, R. P., MCGOWAN, C. H. & GAILLARD, P. H. 2009. Human SLX4 is a Holliday junction resolvase subunit that binds multiple DNA repair/recombination endonucleases. *Cell,* 138**,** 78-89.

FERNANDEZ-SAIZ, V. & BUCHBERGER, A. 2010. Imbalances in p97 co-factor interactions in human proteinopathy. *EMBO reports,* 11**,** 479-85.

FORNER, A., LLOVET, J. M. & BRUIX, J. 2012. Hepatocellular carcinoma. *Lancet,* 379**,** 1245-55.

FRENCH, C. A., MASSON, J. Y., GRIFFIN, C. S., O'REGAN, P., WEST, S. C. & THACKER, J. 2002. Role of mammalian RAD51L2 (RAD51C) in recombination and genetic stability. *The Journal of biological chemistry,* 277**,** 19322-30.

GARCIA-HIGUERA, I., TANIGUCHI, T., GANESAN, S., MEYN, M. S., TIMMERS, C., HEJNA, J., GROMPE, M. & D'ANDREA, A. D. 2001. Interaction of the Fanconi anemia proteins and BRCA1 in a common pathway. *Mol. Cell,* 7**,** 249-62.

GARTEL, A. L. & RADHAKRISHNAN, S. K. 2005. Lost in transcription: p21 repression, mechanisms, and consequences. *Cancer research,* 65**,** 3980-5.

GERMAN, J., SCHONBERG, S., CASKIE, S., WARBURTON, D., FALK, C. & RAY, J. H. 1987. A test for Fanconi's anemia. *Blood,* 69**,** 1637-41.

GLOCKZIN, S., OGI, F. X., HENGSTERMANN, A., SCHEFFNER, M. & BLATTNER, C. 2003. Involvement of the DNA repair protein hHR23 in p53 degradation. *Molecular and cellular biology,* 23**,** 8960-9.

GOLDENBERG, S. J., CASCIO, T. C., SHUMWAY, S. D., GARBUTT, K. C., LIU, J., XIONG, Y. & ZHENG, N. 2004. Structure of the Cand1-Cul1-Roc1 complex reveals regulatory mechanisms for the assembly of the multisubunit cullin-dependent ubiquitin ligases. *Cell,* 119**,** 517-28.

GROULX, I. & LEE, S. 2002. Oxygen-dependent ubiquitination and degradation of hypoxia-inducible factor requires nuclear-cytoplasmic trafficking of the von Hippel-Lindau tumor suppressor protein. *Molecular and cellular biology,* 22**,** 5319-36.

GUETTINGER, S., LAURELL, E. & KUTAY, U. 2009. Orchestrating nuclear envelope disassembly and reassembly during mitosis. *Nature reviews. Molecular cell biology,* 10**,** 178-91.

HAINES, D. S. 2010a. p97-containing complexes in proliferation control and cancer: emerging culprits or guilt by association? *Genes Cancer,* 1**,** 753-763.

HAINES, D. S. 2010b. p97-containing complexes in proliferation control and cancer: emerging culprits or guilt by association? *Genes & cancer,* 1**,** 753-763.

HALAWANI, D., LEBLANC, A. C., ROUILLER, I., MICHNICK, S. W., SERVANT, M. J. & LATTERICH, M. 2009. Hereditary inclusion body myopathy-linked p97/VCP mutations in the NH2 domain and the D1 ring modulate p97/VCP ATPase activity and D2 ring conformation. *Molecular and cellular biology,* 29**,** 4484-94.

HANADA, K., BUDZOWSKA, M., MODESTI, M., MAAS, A., WYMAN, C., ESSERS, J. & KANAAR, R. 2006. The structure-specific endonuclease Mus81-Eme1 promotes conversion of interstrand DNA crosslinks into double-strands breaks. *The EMBO journal,* 25**,** 4921-32.

HEO, J. M., LIVNAT-LEVANON, N., TAYLOR, E. B., JONES, K. T., DEPHOURE, N., RING, J., XIE, J., BRODSKY, J. L., MADEO, F., GYGI, S. P., ASHRAFI, K., GLICKMAN, M. H. & RUTTER, J. 2010. A stress-responsive system for mitochondrial protein degradation. *Molecular cell,* 40**,** 465-80.

HETZER, M., MEYER, H. H., WALTHER, T. C., BILBAO-CORTES, D., WARREN, G. & MATTAJ, I. W. 2001. Distinct AAA-ATPase p97 complexes function in discrete steps of nuclear assembly. *Nature cell biology,* 3**,** 1086-91.

HICKE, L., SCHUBERT, H. L. & HILL, C. P. 2005. Ubiquitin-binding domains. *Nature reviews. Molecular cell biology,* 6**,** 610-21.

HIRANO, S., KAWASAKI, M., URA, H., KATO, R., RAIBORG, C., STENMARK, H. & WAKATSUKI, S. 2006. Double-sided ubiquitin binding of Hrs-UIM in endosomal protein sorting. *Nature structural & molecular biology,* 13**,** 272-7.

HIYAMA, H., YOKOI, M., MASUTANI, C., SUGASAWA, K., MAEKAWA, T., TANAKA, K., HOEIJMAKERS, J. H. & HANAOKA, F. 1999. Interaction of hHR23 with S5a. The ubiquitin-like domain of hHR23 mediates interaction with S5a subunit of 26 S proteasome. *The Journal of biological chemistry,* 274**,** 28019-25.

HO, G. P., MARGOSSIAN, S., TANIGUCHI, T. & D'ANDREA, A. D. 2006. Phosphorylation of FANCD2 on two novel sites is required for mitomycin C resistance. *Molecular and cellular biology,* 26**,** 7005-15.

HO, T. V., GUAINAZZI, A., DERKUNT, S. B., ENOIU, M. & SCHARER, O. D. 2011. Structure-dependent bypass of DNA interstrand crosslinks by translesion synthesis polymerases. *Nucleic acids research,* 39**,** 7455-64.

HODSON, C., PURKISS, A., MILES, J. A. & WALDEN, H. 2014. Structure of the human FANCL RING-Ube2T complex reveals determinants of cognate E3-E2 selection. *Structure,* 22**,** 337-44.

HU, J. C. 2000. A guided tour in protein interaction space: coiled coils from the yeast proteome. *Proceedings of the National Academy of Sciences of the United States of America,* 97**,** 12935-6.

HUANG, T. T., NIJMAN, S. M., MIRCHANDANI, K. D., GALARDY, P. J., COHN, M. A., HAAS, W., GYGI, S. P., PLOEGH, H. L., BERNARDS, R. & D'ANDREA, A. D. 2006. Regulation of monoubiquitinated PCNA by DUB autocleavage. *Nature cell biology,* 8**,** 339-47.

HUEN, M. S., GRANT, R., MANKE, I., MINN, K., YU, X., YAFFE, M. B. & CHEN, J. 2007. RNF8 transduces the DNA-damage signal via histone ubiquitylation and checkpoint protein assembly. *Cell,* 131**,** 901-14.

HUROV, K. E., COTTA-RAMUSINO, C. & ELLEDGE, S. J. 2010. A genetic screen identifies the Triple T complex required for DNA damage signaling and ATM and ATR stability. *Genes & development,* 24**,** 1939-50.

HUYTON, T., PYE, V. E., BRIGGS, L. C., FLYNN, T. C., BEURON, F., KONDO, H., MA, J., ZHANG, X. & FREEMONT, P. S. 2003. The crystal structure of murine p97/VCP at 3.6A. *Journal of structural biology,* 144**,** 337-48.

ISHIAI, M., KITAO, H., SMOGORZEWSKA, A., TOMIDA, J., KINOMURA, A., UCHIDA, E., SABERI, A., KINOSHITA, E., KINOSHITA-KIKUTA, E., KOIKE, T., TASHIRO, S., ELLEDGE, S. J. & TAKATA, M. 2008. FANCI phosphorylation functions as a molecular switch to turn on the Fanconi anemia pathway. *Nature structural & molecular biology,* 15**,** 1138-46.

IVAN, M. & KAELIN, W. G., JR. 2001. The von Hippel-Lindau tumor suppressor protein. *Current opinion in genetics & development,* 11**,** 27-34.

JENSEN, R. B., CARREIRA, A. & KOWALCZYKOWSKI, S. C. 2010. Purified human BRCA2 stimulates RAD51-mediated recombination. *Nature,* 467**,** 678-83.

JENTSCH, S. & RUMPF, S. 2007. Cdc48 (p97): a "molecular gearbox" in the ubiquitin pathway? *Trends in biochemical sciences,* 32**,** 6-11.

JIANG, B. H., RUE, E., WANG, G. L., ROE, R. & SEMENZA, G. L. 1996. Dimerization, DNA binding, and transactivation properties of hypoxia-inducible factor 1. *The Journal of biological chemistry,* 271**,** 17771-8.

JOHNSON, J. O., MANDRIOLI, J., BENATAR, M., ABRAMZON, Y., VAN DEERLIN, V. M., TROJANOWSKI, J. Q., GIBBS, J. R., BRUNETTI, M., GRONKA, S., WUU, J., DING, J., MCCLUSKEY, L., MARTINEZ-LAGE, M., FALCONE, D., HERNANDEZ, D. G., AREPALLI, S., CHONG, S., SCHYMICK, J. C., ROTHSTEIN, J., LANDI, F., WANG, Y. D., CALVO, A., MORA, G., SABATELLI, M., MONSURRO, M. R., BATTISTINI, S., SALVI, F., SPATARO, R., SOLA, P., BORGHERO, G., GALASSI, G., SCHOLZ, S. W., TAYLOR, J. P., RESTAGNO, G., CHIO, A. & TRAYNOR, B. J. 2010. Exome sequencing reveals VCP mutations as a cause of familial ALS. *Neuron,* 68**,** 857-64.

JOO, W., XU, G., PERSKY, N. S., SMOGORZEWSKA, A., RUDGE, D. G., BUZOVETSKY, O., ELLEDGE, S. J. & PAVLETICH, N. P. 2011. Structure of the FANCI-FANCD2 complex: insights into the Fanconi anemia DNA repair pathway. *Science,* 333**,** 312-6.

JU, J. S., FUENTEALBA, R. A., MILLER, S. E., JACKSON, E., PIWNICA-WORMS, D., BALOH, R. H. & WEIHL, C. C. 2009. Valosin-containing protein (VCP) is required for autophagy and is disrupted in VCP disease. *The Journal of cell biology,* 187**,** 875-88.

KALOCSAY, M., HILLER, N. J. & JENTSCH, S. 2009. Chromosome-wide Rad51 spreading and SUMO-H2A.Z-dependent chromosome fixation in response to a persistent DNA double-strand break. *Molecular cell,* 33**,** 335-43.

KAMURA, T., KOEPP, D. M., CONRAD, M. N., SKOWYRA, D., MORELAND, R. J., ILIOPOULOS, O., LANE, W. S., KAELIN, W. G., JR., ELLEDGE, S. J., CONAWAY, R. C., HARPER, J. W. & CONAWAY, J. W. 1999. Rbx1, a component of the VHL tumor suppressor complex and SCF ubiquitin ligase. *Science,* 284**,** 657-61.

KAMURA, T., SATO, S., IWAI, K., CZYZYK-KRZESKA, M., CONAWAY, R. C. & CONAWAY, J. W. 2000. Activation of HIF1alpha ubiquitination by a reconstituted von Hippel-Lindau (VHL) tumor suppressor complex. *Proceedings of the National Academy of Sciences of the United States of America,* 97**,** 10430-5.

KARIN, M. & BEN-NERIAH, Y. 2000. Phosphorylation meets ubiquitination: the control of NF-[kappa]B activity. *Annual review of immunology,* 18**,** 621-63.

KEE, Y. & D'ANDREA, A. D. 2010. Expanded roles of the Fanconi anemia pathway in preserving genomic stability. *Genes Dev.,* 24**,** 1680-94.

KEE, Y. & D'ANDREA, A. D. 2012. Molecular pathogenesis and clinical management of Fanconi anemia. *The Journal of clinical investigation,* 122**,** 3799-806.

KERN, S. E., KINZLER, K. W., BRUSKIN, A., JAROSZ, D., FRIEDMAN, P., PRIVES, C. & VOGELSTEIN, B. 1991. Identification of p53 as a sequence-specific DNA-binding protein. *Science,* 252**,** 1708-11.

KHORONENKOVA, S. V., DIANOVA, II, TERNETTE, N., KESSLER, B. M., PARSONS, J. L. & DIANOV, G. L. 2012. ATM-dependent downregulation of USP7/HAUSP by PPM1G activates p53 response to DNA damage. *Molecular cell,* 45**,** 801-13.

KIKKERT, M., DOOLMAN, R., DAI, M., AVNER, R., HASSINK, G., VAN VOORDEN, S., THANEDAR, S., ROITELMAN, J., CHAU, V. & WIERTZ, E. 2004. Human HRD1 is an E3 ubiquitin ligase involved in degradation of proteins from the endoplasmic reticulum. *The Journal of biological chemistry,* 279**,** 3525-34.

KIM, H. & D'ANDREA, A. D. 2012. Regulation of DNA cross-link repair by the Fanconi anemia/BRCA pathway. *Genes & development,* 26**,** 1393-408.

KIM, H., ZHANG, H., MENG, D., RUSSELL, G., LEE, J. N. & YE, J. 2013. UAS domain of Ubxd8 and FAF1 polymerizes upon interaction with long-chain unsaturated fatty acids. *Journal of lipid research,* 54**,** 2144-52.

KIM, J. M., KEE, Y., GURTAN, A. & D'ANDREA, A. D. 2008. Cell cycle-dependent chromatin loading of the Fanconi anemia core complex by FANCM/FAAP24. *Blood,* 111**,** 5215-22.

KIM, J. M., PARMAR, K., HUANG, M., WEINSTOCK, D. M., RUIT, C. A., KUTOK, J. L. & D'ANDREA, A. D. 2009. Inactivation of murine Usp1 results in genomic instability and a Fanconi anemia phenotype. *Developmental cell,* 16**,** 314-20.

KIM, W., BENNETT, E. J., HUTTLIN, E. L., GUO, A., LI, J., POSSEMATO, A., SOWA, M. E., RAD, R., RUSH, J., COMB, M. J., HARPER, J. W. & GYGI, S. P. 2011. Systematic and quantitative assessment of the ubiquitin-modified proteome. *Molecular Cell,* 44**,** 325-40.

KITAO, H. & TAKATA, M. 2011. Fanconi anemia: a disorder defective in the DNA damage response. *Int. J. Hematol.,* 93**,** 417-24.

KONDO, H., RABOUILLE, C., NEWMAN, R., LEVINE, T. P., PAPPIN, D., FREEMONT, P. & WARREN, G. 1997. p47 is a cofactor for p97-mediated membrane fusion. *Nature,* 388**,** 75-8.

KREJCI, L., ALTMANNOVA, V., SPIREK, M. & ZHAO, X. 2012. Homologous recombination and its regulation. *Nucleic acids research,* 40**,** 5795-818.

KUMAR, R. & CHEOK, C. F. 2014. RIF1: A novel regulatory factor for DNA replication and DNA damage response signaling. *DNA repair,* 15**,** 54-9.

KURODA, N., MIKAMI, S., PAN, C. C., COHEN, R. J., HES, O., MICHAL, M., NAGASHIMA, Y., TANAKA, Y., INOUE, K., SHUIN, T. & LEE, G. H. 2012. Review of renal carcinoma associated with Xp11.2 translocations/TFE3 gene fusions with focus on pathobiological aspect. *Histology and histopathology,* 27**,** 133-40.

KURZ, T., CHOU, Y. C., WILLEMS, A. R., MEYER-SCHALLER, N., HECHT, M. L., TYERS, M., PETER, M. & SICHERI, F. 2008. Dcn1 functions as a scaffold-type E3 ligase for cullin neddylation. *Molecular cell,* 29**,** 23-35.

KURZ, T., OZLU, N., RUDOLF, F., O'ROURKE, S. M., LUKE, B., HOFMANN, K., HYMAN, A. A., BOWERMAN, B. & PETER, M. 2005. The conserved protein DCN-1/Dcn1p is required for cullin neddylation in C. elegans and S. cerevisiae. *Nature,* 435**,** 1257-61.

LADANYI, M., LUI, M. Y., ANTONESCU, C. R., KRAUSE-BOEHM, A., MEINDL, A., ARGANI, P., HEALEY, J. H., UEDA, T., YOSHIKAWA, H., MELONI-EHRIG, A., SORENSEN, P. H., MERTENS, F., MANDAHL, N., VAN DEN BERGHE, H., SCIOT, R., DAL CIN, P. & BRIDGE, J. 2001. The der(17)t(X;17)(p11;q25) of human alveolar soft part sarcoma fuses the TFE3 transcription factor gene to ASPL, a novel gene at 17q25. *Oncogene,* 20**,** 48-57.

LEE, H., ALPI, A. F., PARK, M. S., ROSE, A. & KOO, H. S. 2013. C. elegans ring finger protein RNF-113 is involved in interstrand DNA crosslink repair and interacts with a RAD51C homolog. *PloS one,* 8**,** e60071.

LI, X., ZHANG, J., YANG, Z., KANG, J., JIANG, S., ZHANG, T., CHEN, T., LI, M., LV, Q., CHEN, X., MCCRAE, M. A., ZHUANG, H. & LU, F. 2014. The function of targeted host genes determines the oncogenicity of HBV integration in hepatocellular carcinoma. *Journal of hepatology*.

LIANG, J., YIN, C., DOONG, H., FANG, S., PETERHOFF, C., NIXON, R. A. & MONTEIRO, M. J. 2006. Characterization of erasin (UBXD2): a new ER protein that promotes ER-associated protein degradation. *Journal of cell science,* 119**,** 4011-24.

LITMAN, R., PENG, M., JIN, Z., ZHANG, F., ZHANG, J., POWELL, S., ANDREASSEN, P. R. & CANTOR, S. B. 2005. BACH1 is critical for homologous recombination and appears to be the Fanconi anemia gene product FANCJ. *Cancer cell,* 8**,** 255-65.

LIU, J., FURUKAWA, M., MATSUMOTO, T. & XIONG, Y. 2002. NEDD8 modification of CUL1 dissociates p120(CAND1), an inhibitor of CUL1-SKP1 binding and SCF ligases. *Molecular cell,* 10**,** 1511-8.

LIU, Y., TARSOUNAS, M., O'REGAN, P. & WEST, S. C. 2007. Role of RAD51C and XRCC3 in genetic recombination and DNA repair. *The Journal of biological chemistry,* 282**,** 1973-9.

LIU, Y. & YE, Y. 2012. Roles of p97-associated deubiquitinases in protein quality control at the endoplasmic reticulum. *Current protein & peptide science,* 13**,** 436-46.

LONGERICH, S., KWON, Y., TSAI, M. S., HLAING, A. S., KUPFER, G. M. & SUNG, P. 2014. Regulation of FANCD2 and FANCI monoubiquitination by their interaction and by DNA. *Nucleic acids research*.

LONGERICH, S., SAN FILIPPO, J., LIU, D. & SUNG, P. 2009. FANCI binds branched DNA and is monoubiquitinated by UBE2T-FANCL. *The Journal of biological chemistry,* 284**,** 23182-6.

LYAPINA, S., COPE, G., SHEVCHENKO, A., SERINO, G., TSUGE, T., ZHOU, C., WOLF, D. A., WEI, N. & DESHAIES, R. J. 2001. Promotion of NEDD-CUL1 conjugate cleavage by COP9 signalosome. *Science,* 292**,** 1382-5.

MACHIDA, Y. J., MACHIDA, Y., CHEN, Y., GURTAN, A. M., KUPFER, G. M., D'ANDREA, A. D. & DUTTA, A. 2006. UBE2T is the E2 in the Fanconi anemia pathway and undergoes negative autoregulation. *Mol. Cell,* 23**,** 589-96.

MACKAY, C., DECLAIS, A. C., LUNDIN, C., AGOSTINHO, A., DEANS, A. J., MACARTNEY, T. J., HOFMANN, K., GARTNER, A., WEST, S. C., HELLEDAY, T., LILLEY, D. M. & ROUSE, J. 2010. Identification of KIAA1018/FAN1, a DNA repair nuclease recruited to DNA damage by monoubiquitinated FANCD2. *Cell,* 142**,** 65-76.

MADSEN, L., KRIEGENBURG, F., VALA, A., BEST, D., PRAG, S., HOFMANN, K., SEEGER, M., ADAMS, I. R. & HARTMANN-PETERSEN, R. 2011. The tissue-specific Rep8/UBXD6 tethers p97 to the endoplasmic reticulum membrane for degradation of misfolded proteins. *PloS one,* 6**,** e25061.

MADSEN, L., SEEGER, M., SEMPLE, C. A. & HARTMANN-PETERSEN, R. 2009. New ATPase regulators--p97 goes to the PUB. *The international journal of biochemistry & cell biology,* 41**,** 2380-8.

MAILAND, N., BEKKER-JENSEN, S., FAUSTRUP, H., MELANDER, F., BARTEK, J., LUKAS, C. & LUKAS, J. 2007. RNF8 ubiquitylates histones at DNA double-strand breaks and promotes assembly of repair proteins. *Cell,* 131**,** 887-900.

MAREK, L. R. & BALE, A. E. 2006. Drosophila homologs of FANCD2 and FANCL function in DNA repair. *DNA repair,* 5**,** 1317-26.

MAXWELL, P. H., WIESENER, M. S., CHANG, G. W., CLIFFORD, S. C., VAUX, E. C., COCKMAN, M. E., WYKOFF, C. C., PUGH, C. W., MAHER, E. R. & RATCLIFFE, P. J. 1999. The tumour suppressor protein VHL targets hypoxia-inducible factors for oxygen-dependent proteolysis. *Nature,* 399**,** 271-5.

MEERANG, M., RITZ, D., PALIWAL, S., GARAJOVA, Z., BOSSHARD, M., MAILAND, N., JANSCAK, P., HUBSCHER, U., MEYER, H. & RAMADAN, K. 2011. The ubiquitin-selective segregase VCP/p97 orchestrates the response to DNA double-strand breaks. *Nature cell biology,* 13**,** 1376-82.

MENG, X., YUAN, Y., MAESTAS, A. & SHEN, Z. 2004. Recovery from DNA damage-induced G2 arrest requires actin-binding protein filamin-A/actin-binding protein 280. *The Journal of biological chemistry,* 279**,** 6098-105.

MEYER, H. H., WANG, Y. & WARREN, G. 2002. Direct binding of ubiquitin conjugates by the mammalian p97 adaptor complexes, p47 and Ufd1-Npl4. *The EMBO journal,* 21**,** 5645-52.

MI, J., QIAO, F., WILSON, J. B., HIGH, A. A., SCHROEDER, M. J., STUKENBERG, P. T., MOSS, A., SHABANOWITZ, J., HUNT, D. F., JONES, N. J. & KUPFER, G. M. 2004. FANCG is phosphorylated at serines 383 and 387 during mitosis. *Molecular and cellular biology,* 24**,** 8576-85.

MISTELI, T. & SOUTOGLOU, E. 2009. The emerging role of nuclear architecture in DNA repair and genome maintenance. *Nature reviews. Molecular cell biology,* 10**,** 243-54.

MIZUSHIMA, N. 2007. Autophagy: process and function. *Genes & development,* 21**,** 2861-73.

MOLDOVAN, G. L. & D'ANDREA, A. D. 2009. How the fanconi anemia pathway guards the genome. *Annu. Rev. Genet.,* 43**,** 223-49.

MU, J. J., WANG, Y., LUO, H., LENG, M., ZHANG, J., YANG, T., BESUSSO, D., JUNG, S. Y. & QIN, J. 2007. A proteomic analysis of ataxia telangiectasia-mutated (ATM)/ATM-Rad3-related (ATR) substrates identifies the ubiquitin-proteasome system as a regulator for DNA damage checkpoints. *The Journal of biological chemistry,* 282**,** 17330-4.

NAGAI, S., DAVOODI, N. & GASSER, S. M. 2011. Nuclear organization in genome stability: SUMO connections. *Cell research,* 21**,** 474-85.

NAGAI, S., DUBRANA, K., TSAI-PFLUGFELDER, M., DAVIDSON, M. B., ROBERTS, T. M., BROWN, G. W., VARELA, E., HEDIGER, F., GASSER, S. M. & KROGAN, N. J. 2008. Functional targeting of DNA damage to a nuclear pore-associated SUMO-dependent ubiquitin ligase. *Science,* 322**,** 597-602.

NARENDRA, D., TANAKA, A., SUEN, D. F. & YOULE, R. J. 2008. Parkin is recruited selectively to impaired mitochondria and promotes their autophagy. *The Journal of cell biology,* 183**,** 795-803.

NIEDERNHOFER, L. J., DANIELS, J. S., ROUZER, C. A., GREENE, R. E. & MARNETT, L. J. 2003. Malondialdehyde, a product of lipid peroxidation, is mutagenic in human cells. *The Journal of biological chemistry,* 278**,** 31426-33.

NIEDERNHOFER, L. J., ODIJK, H., BUDZOWSKA, M., VAN DRUNEN, E., MAAS, A., THEIL, A. F., DE WIT, J., JASPERS, N. G., BEVERLOO, H. B., HOEIJMAKERS, J. H. & KANAAR, R. 2004. The structure-specific endonuclease Ercc1-Xpf is required to resolve DNA interstrand cross-link-induced double-strand breaks. *Molecular and cellular biology,* 24**,** 5776-87.

NIJMAN, S. M., HUANG, T. T., DIRAC, A. M., BRUMMELKAMP, T. R., KERKHOVEN, R. M., D'ANDREA, A. D. & BERNARDS, R. 2005. The deubiquitinating enzyme USP1 regulates the Fanconi anemia pathway. *Molecular cell,* 17**,** 331-9.

NIWA, H., EWENS, C. A., TSANG, C., YEUNG, H. O., ZHANG, X. & FREEMONT, P. S. 2012. The role of the N-domain in the ATPase activity of the mammalian AAA ATPase p97/VCP. *The Journal of biological chemistry,* 287**,** 8561-70.

NOLL, D. M., MASON, T. M. & MILLER, P. S. 2006. Formation and repair of interstrand cross-links in DNA. *Chemical reviews,* 106**,** 277-301.

OESTERGAARD, V. H., LANGEVIN, F., KUIKEN, H. J., PACE, P., NIEDZWIEDZ, W., SIMPSON, L. J., OHZEKI, M., TAKATA, M., SALE, J. E. & PATEL, K. J. 2007. Deubiquitination of FANCD2 is required for DNA crosslink repair. *Molecular cell,* 28**,** 798-809.

OGURA, T., WHITEHEART, S. W. & WILKINSON, A. J. 2004. Conserved arginine residues implicated in ATP hydrolysis, nucleotide-sensing, and inter-subunit interactions in AAA and AAA+ ATPases. *Journal of structural biology,* 146**,** 106-12.

OLZMANN, J. A., RICHTER, C. M. & KOPITO, R. R. 2013. Spatial regulation of UBXD8 and p97/VCP controls ATGL-mediated lipid droplet turnover. *Proceedings of the National Academy of Sciences of the United States of America,* 110**,** 1345-50.

OSAKA, F., KAWASAKI, H., AIDA, N., SAEKI, M., CHIBA, T., KAWASHIMA, S., TANAKA, K. & KATO, S. 1998. A new NEDD8-ligating system for cullin-4A. *Genes & development,* 12**,** 2263-8.

OVED, S., MOSESSON, Y., ZWANG, Y., SANTONICO, E., SHTIEGMAN, K., MARMOR, M. D., KOCHUPURAKKAL, B. S., KATZ, M., LAVI, S., CESARENI, G. & YARDEN, Y. 2006. Conjugation to Nedd8 instigates ubiquitylation and down-regulation of activated receptor tyrosine kinases. *The Journal of biological chemistry,* 281**,** 21640-51.

OZA, P., JASPERSEN, S. L., MIELE, A., DEKKER, J. & PETERSON, C. L. 2009. Mechanisms that regulate localization of a DNA double-strand break to the nuclear periphery. *Genes & development,* 23**,** 912-27.

PALANCADE, B., LIU, X., GARCIA-RUBIO, M., AGUILERA, A., ZHAO, X. & DOYE, V. 2007. Nucleoporins prevent DNA damage accumulation by modulating Ulp1-dependent sumoylation processes. *Molecular biology of the cell,* 18**,** 2912-23.

PAN, Z. Q., KENTSIS, A., DIAS, D. C., YAMOAH, K. & WU, K. 2004. Nedd8 on cullin: building an expressway to protein destruction. *Oncogene,* 23**,** 1985-97.

PARK, S., ISAACSON, R., KIM, H. T., SILVER, P. A. & WAGNER, G. 2005. Ufd1 exhibits the AAA-ATPase fold with two distinct ubiquitin interaction sites. *Structure,* 13**,** 995-1005.

PATEL, K. J. & JOENJE, H. 2007. Fanconi anemia and DNA replication repair. *DNA repair,* 6**,** 885-90.

PETROSKI, M. D. & DESHAIES, R. J. 2005. Mechanism of lysine 48-linked ubiquitin-chain synthesis by the cullin-RING ubiquitin-ligase complex SCF-Cdc34. *Cell,* 123**,** 1107-20.

PHAN, V. T., DING, V. W., LI, F., CHALKLEY, R. J., BURLINGAME, A. & MCCORMICK, F. 2010. The RasGAP proteins Ira2 and neurofibromin are negatively regulated by Gpb1 in yeast and ETEA in humans. *Molecular and cellular biology,* 30**,** 2264-79.

PICHIERRI, P. & ROSSELLI, F. 2004. The DNA crosslink-induced S-phase checkpoint depends on ATR-CHK1 and ATR-NBS1-FANCD2 pathways. *The EMBO journal,* 23**,** 1178-87.

PIERCE, N. W., LEE, J. E., LIU, X., SWEREDOSKI, M. J., GRAHAM, R. L., LARIMORE, E. A., ROME, M., ZHENG, N., CLURMAN, B. E., HESS, S., SHAN, S. O. & DESHAIES, R. J. 2013. Cand1 promotes assembly of new SCF complexes through dynamic exchange of F box proteins. *Cell,* 153**,** 206-15.

QIAO, F., MI, J., WILSON, J. B., ZHI, G., BUCHEIMER, N. R., JONES, N. J. & KUPFER, G. M. 2004. Phosphorylation of fanconi anemia (FA) complementation group G protein, FANCG, at serine 7 is important for function of the FA pathway. *The Journal of biological chemistry,* 279**,** 46035-45.

RAASI, S. & WOLF, D. H. 2007. Ubiquitin receptors and ERAD: a network of pathways to the proteasome. *Seminars in cell & developmental biology,* 18**,** 780-91.

RAMADAN, K. 2012. p97/VCP- and Lys48-linked polyubiquitination form a new signaling pathway in DNA damage response. *Cell cycle,* 11**,** 1062-9.

RAMADAN, K., BRUDERER, R., SPIGA, F. M., POPP, O., BAUR, T., GOTTA, M. & MEYER, H. H. 2007. Cdc48/p97 promotes reformation of the nucleus by extracting the kinase Aurora B from chromatin. *Nature,* 450**,** 1258-62.

REGO, M. A., KOLLING, F. W. T., VUONO, E. A., MAURO, M. & HOWLETT, N. G. 2012. Regulation of the Fanconi anemia pathway by a CUE ubiquitin-binding domain in the FANCD2 protein. *Blood,* 120**,** 2109-17.

RESNITZKY, D. & REED, S. I. 1995. Different roles for cyclins D1 and E in regulation of the G1-to-S transition. *Molecular and cellular biology,* 15**,** 3463-9.

SAHA, A. & DESHAIES, R. J. 2008. Multimodal activation of the ubiquitin ligase SCF by Nedd8 conjugation. *Molecular cell,* 32**,** 21-31.

SALVAT, C., ACQUAVIVA, C., SCHEFFNER, M., ROBBINS, I., PIECHACZYK, M. & JARIEL-ENCONTRE, I. 2000. Molecular characterization of the thermosensitive E1 ubiquitin-activating enzyme cell mutant A31N-ts20. Requirements upon different levels of E1 for the ubiquitination/degradation of the various protein substrates in vivo. *European journal of biochemistry / FEBS,* 267**,** 3712-22.

SATO, K., SUNDARAMOORTHY, E., RAJENDRA, E., HATTORI, H., JEYASEKHARAN, A. D., AYOUB, N., SCHIESS, R., AEBERSOLD, R., NISHIKAWA, H., SEDUKHINA, A. S., WADA, H., OHTA, T. & VENKITARAMAN, A. R. 2012a. A DNA-damage selective role for BRCA1 E3 ligase in claspin ubiquitylation, CHK1 activation, and DNA repair. *Current biology : CB,* 22**,** 1659-66.

SATO, K., TODA, K., ISHIAI, M., TAKATA, M. & KURUMIZAKA, H. 2012b. DNA robustly stimulates FANCD2 monoubiquitylation in the complex with FANCI. *Nucleic acids research,* 40**,** 4553-61.

SCHARER, O. D. 2005. DNA interstrand crosslinks: natural and drug-induced DNA adducts that induce unique cellular responses. *Chembiochem.,* 6**,** 27-32.

SCHERMELLEH, L., CARLTON, P. M., HAASE, S., SHAO, L., WINOTO, L., KNER, P., BURKE, B., CARDOSO, M. C., AGARD, D. A., GUSTAFSSON, M. G., LEONHARDT, H. & SEDAT, J. W. 2008. Subdiffraction multicolor imaging of the nuclear periphery with 3D structured illumination microscopy. *Science,* 320**,** 1332-6.

SCHUBERTH, C. & BUCHBERGER, A. 2008. UBX domain proteins: major regulators of the AAA ATPase Cdc48/p97. *Cell Mol. Life Sci.,* 65**,** 2360-71.

SCHWAB, R. A., BLACKFORD, A. N. & NIEDZWIEDZ, W. 2010. ATR activation and replication fork restart are defective in FANCM-deficient cells. *The EMBO journal,* 29**,** 806-18.

SCOTT, D. C., MONDA, J. K., GRACE, C. R., DUDA, D. M., KRIWACKI, R. W., KURZ, T. & SCHULMAN, B. A. 2010. A dual E3 mechanism for Rub1 ligation to Cdc53. *Molecular cell,* 39**,** 784-96.

SHAFRITZ, D. A., SHOUVAL, D., SHERMAN, H. I., HADZIYANNIS, S. J. & KEW, M. C. 1981. Integration of hepatitis B virus DNA into the genome of liver cells in chronic liver disease and hepatocellular carcinoma. Studies in percutaneous liver biopsies and post-mortem tissue specimens. *The New England journal of medicine,* 305**,** 1067-73.

SHIGECHI, T., TOMIDA, J., SATO, K., KOBAYASHI, M., EYKELENBOOM, J. K., PESSINA, F., ZHANG, Y., UCHIDA, E., ISHIAI, M., LOWNDES, N. F., YAMAMOTO, K., KURUMIZAKA, H., MAEHARA, Y. & TAKATA, M. 2012. ATR-ATRIP kinase complex triggers activation of the Fanconi anemia DNA repair pathway. *Cancer research,* 72**,** 1149-56.

SINGH, T. R., SARO, D., ALI, A. M., ZHENG, X. F., DU, C. H., KILLEN, M. W., SACHPATZIDIS, A., WAHENGBAM, K., PIERCE, A. J., XIONG, Y., SUNG, P. & MEETEI, A. R. 2010. MHF1-MHF2, a histone-fold-containing protein complex, participates in the Fanconi anemia pathway via FANCM. *Molecular cell,* 37**,** 879-86.

SMOGORZEWSKA, A., MATSUOKA, S., VINCIGUERRA, P., MCDONALD, E. R., 3RD, HUROV, K. E., LUO, J., BALLIF, B. A., GYGI, S. P., HOFMANN, K., D'ANDREA, A. D. & ELLEDGE, S. J. 2007. Identification of the FANCI protein, a monoubiquitinated FANCD2 paralog required for DNA repair. *Cell,* 129**,** 289-301.

SOMMERS, J. A., RAWTANI, N., GUPTA, R., BUGREEV, D. V., MAZIN, A. V., CANTOR, S. B. & BROSH, R. M., JR. 2009. FANCJ uses its motor ATPase to destabilize protein-DNA complexes, unwind triplexes, and inhibit RAD51 strand exchange. *The Journal of biological chemistry,* 284**,** 7505-17.

SONG, C., WANG, Q. & LI, C. C. 2003. ATPase activity of p97-valosin-containing protein (VCP). D2 mediates the major enzyme activity, and D1 contributes to the heat-induced activity. *The Journal of biological chemistry,* 278**,** 3648-55.

SOUTOGLOU, E., DORN, J. F., SENGUPTA, K., JASIN, M., NUSSENZWEIG, A., RIED, T., DANUSER, G. & MISTELI, T. 2007. Positional stability of single double-strand breaks in mammalian cells. *Nature cell biology,* 9**,** 675-82.

STARK, G. R. & TAYLOR, W. R. 2004. Analyzing the G2/M checkpoint. *Methods in molecular biology,* 280**,** 51-82.

STEBBINS, C. E., KAELIN, W. G., JR. & PAVLETICH, N. P. 1999. Structure of the VHL-ElonginC-ElonginB complex: implications for VHL tumor suppressor function. *Science,* 284**,** 455-61.

STROKA, D. M., BURKHARDT, T., DESBAILLETS, I., WENGER, R. H., NEIL, D. A., BAUER, C., GASSMANN, M. & CANDINAS, D. 2001. HIF-1 is expressed in normoxic tissue and displays an organ-specific regulation under systemic

hypoxia. *FASEB journal : official publication of the Federation of American Societies for Experimental Biology,* 15**,** 2445-53.

SUBRAMANYAM, S., JONES, W. T., SPIES, M. & SPIES, M. A. 2013. Contributions of the RAD51 N-terminal domain to BRCA2-RAD51 interaction. *Nucleic acids research,* 41**,** 9020-32.

TANAKA, T., KAWASHIMA, H., YEH, E. T. & KAMITANI, T. 2003. Regulation of the NEDD8 conjugation system by a splicing variant, NUB1L. *The Journal of biological chemistry,* 278**,** 32905-13.

TANG, W. K., LI, D., LI, C. C., ESSER, L., DAI, R., GUO, L. & XIA, D. 2010. A novel ATP-dependent conformation in p97 N-D1 fragment revealed by crystal structures of disease-related mutants. *The EMBO journal,* 29**,** 2217-29.

TANIGUCHI, T., GARCIA-HIGUERA, I., ANDREASSEN, P. R., GREGORY, R. C., GROMPE, M. & D'ANDREA, A. D. 2002. S-phase-specific interaction of the Fanconi anemia protein, FANCD2, with BRCA1 and RAD51. *Blood,* 100**,** 2414-20.

TAYLOR, E. B. & RUTTER, J. 2011. Mitochondrial quality control by the ubiquitin-proteasome system. *Biochemical Society transactions,* 39**,** 1509-13.

TREMBLAY, C. S., HUANG, F. F., HABI, O., HUARD, C. C., GODIN, C., LEVESQUE, G. & CARREAU, M. 2008. HES1 is a novel interactor of the Fanconi anemia core complex. *Blood,* 112**,** 2062-70.

TRESSE, E., SALOMONS, F. A., VESA, J., BOTT, L. C., KIMONIS, V., YAO, T. P., DANTUMA, N. P. & TAYLOR, J. P. 2010. VCP/p97 is essential for maturation of ubiquitin-containing autophagosomes and this function is impaired by mutations that cause IBMPFD. *Autophagy,* 6**,** 217-27.

UCHIYAMA, K., JOKITALO, E., KANO, F., MURATA, M., ZHANG, X., CANAS, B., NEWMAN, R., RABOUILLE, C., PAPPIN, D., FREEMONT, P. & KONDO, H. 2002. VCIP135, a novel essential factor for p97/p47-mediated membrane fusion, is required for Golgi and ER assembly in vivo. *The Journal of cell biology,* 159**,** 855-66.

UCHIYAMA, K. & KONDO, H. 2005. p97/p47-Mediated biogenesis of Golgi and ER. *Journal of biochemistry,* 137**,** 115-9.

UCHIYAMA, K., TOTSUKAWA, G., PUHKA, M., KANEKO, Y., JOKITALO, E., DREVENY, I., BEURON, F., ZHANG, X., FREEMONT, P. & KONDO, H. 2006. p37 is a p97 adaptor required for Golgi and ER biogenesis in interphase and at the end of mitosis. *Developmental cell,* 11**,** 803-16.

VALLE, C. W., MIN, T., BODAS, M., MAZUR, S., BEGUM, S., TANG, D. & VIJ, N. 2011. Critical role of VCP/p97 in the pathogenesis and progression of non-small cell lung carcinoma. *PloS one,* 6**,** e29073.

VAN DER SPEK, P. J., EKER, A., RADEMAKERS, S., VISSER, C., SUGASAWA, K., MASUTANI, C., HANAOKA, F., BOOTSMA, D. & HOEIJMAKERS, J. H. 1996. XPC and human homologs of RAD23: intracellular localization and relationship to other nucleotide excision repair complexes. *Nucleic acids research,* 24**,** 2551-9.

VEMBAR, S. S. & BRODSKY, J. L. 2008. One step at a time: endoplasmic reticulum-associated degradation. *Nature reviews. Molecular cell biology,* 9**,** 944-57.

WADA, H., YEH, E. T. & KAMITANI, T. 1999. Identification of NEDD8-conjugation site in human cullin-2. *Biochemical and biophysical research communications,* 257**,** 100-5.

WANG, G. L., JIANG, B. H., RUE, E. A. & SEMENZA, G. L. 1995. Hypoxia-inducible factor 1 is a basic-helix-loop-helix-PAS heterodimer regulated by cellular O2 tension. *Proceedings of the National Academy of Sciences of the United States of America,* 92**,** 5510-4.

WANG, Q., SONG, C., YANG, X. & LI, C. C. 2003. D1 ring is stable and nucleotide-independent, whereas D2 ring undergoes major conformational changes during the ATPase cycle of p97-VCP. *The Journal of biological chemistry,* 278**,** 32784-93.

WANG, X., KENNEDY, R. D., RAY, K., STUCKERT, P., ELLENBERGER, T. & D'ANDREA, A. D. 2007. Chk1-mediated phosphorylation of FANCE is required for the Fanconi anemia/BRCA pathway. *Molecular and cellular biology,* 27**,** 3098-108.

WATERS, L. S., MINESINGER, B. K., WILTROUT, M. E., D'SOUZA, S., WOODRUFF, R. V. & WALKER, G. C. 2009. Eukaryotic translesion polymerases and their roles and regulation in DNA damage tolerance. *Microbiology and molecular biology reviews : MMBR,* 73**,** 134-54.

WATTS, G. D., WYMER, J., KOVACH, M. J., MEHTA, S. G., MUMM, S., DARVISH, D., PESTRONK, A., WHYTE, M. P. & KIMONIS, V. E. 2004. Inclusion body myopathy associated with Paget disease of bone and frontotemporal dementia is caused by mutant valosin-containing protein. *Nat. Genet.,* 36**,** 377-81.

WEIHL, C. C., DALAL, S., PESTRONK, A. & HANSON, P. I. 2006. Inclusion body myopathy-associated mutations in p97/VCP impair endoplasmic reticulum-associated degradation. *Human molecular genetics,* 15**,** 189-99.

WHITBY, F. G., XIA, G., PICKART, C. M. & HILL, C. P. 1998. Crystal structure of the human ubiquitin-like protein NEDD8 and interactions with ubiquitin pathway enzymes. *The Journal of biological chemistry,* 273**,** 34983-91.

WHITE, S. R. & LAURING, B. 2007. AAA+ ATPases: achieving diversity of function with conserved machinery. *Traffic,* 8**,** 1657-67.

WU, J. T., LIN, H. C., HU, Y. C. & CHIEN, C. T. 2005. Neddylation and deneddylation regulate Cul1 and Cul3 protein accumulation. *Nature cell biology,* 7**,** 1014-20.

WU, Y., SOMMERS, J. A., SUHASINI, A. N., LEONARD, T., DEAKYNE, J. S., MAZIN, A. V., SHIN-YA, K., KITAO, H. & BROSH, R. M., JR. 2010. Fanconi anemia group J mutation abolishes its DNA repair function by uncoupling DNA translocation from helicase activity or disruption of protein-DNA complexes. *Blood,* 116**,** 3780-91.

XIA, B., SHENG, Q., NAKANISHI, K., OHASHI, A., WU, J., CHRIST, N., LIU, X., JASIN, M., COUCH, F. J. & LIVINGSTON, D. M. 2006. Control of BRCA2 cellular and clinical functions by a nuclear partner, PALB2. *Molecular cell,* 22**,** 719-29.

XU, S., PENG, G., WANG, Y., FANG, S. & KARBOWSKI, M. 2011. The AAA-ATPase p97 is essential for outer mitochondrial membrane protein turnover. *Molecular biology of the cell,* 22**,** 291-300.

YAMABE, Y., ICHIKAWA, K., SUGAWARA, K., IMAMURA, O., SHIMAMOTO, A., SUZUKI, N., TOKUTAKE, Y., GOTO, M., SUGAWARA, M. & FURUICHI, Y. 1997. Cloning and characterization of Rep-8 (D8S2298E) in the human chromosome 8p11.2-p12. *Genomics,* 39**,** 198-204.

YAMAMOTO, K. N., KOBAYASHI, S., TSUDA, M., KURUMIZAKA, H., TAKATA, M., KONO, K., JIRICNY, J., TAKEDA, S. & HIROTA, K. 2011. Involvement of SLX4 in interstrand cross-link repair is regulated by the Fanconi anemia pathway. *Proceedings of the National Academy of Sciences of the United States of America,* 108**,** 6492-6.

YAMAMOTO, S., TOMITA, Y., HOSHIDA, Y., NAGANO, H., DONO, K., UMESHITA, K., SAKON, M., ISHIKAWA, O., OHIGASHI, H., NAKAMORI, S., MONDEN, M. & AOZASA, K. 2004. Increased expression of valosin-containing protein (p97) is associated with lymph node metastasis and prognosis of pancreatic ductal adenocarcinoma. *Annals of surgical oncology,* 11**,** 165-72.

YAMAMOTO, S., TOMITA, Y., NAKAMORI, S., HOSHIDA, Y., NAGANO, H., DONO, K., UMESHITA, K., SAKON, M., MONDEN, M. & AOZASA, K. 2003. Elevated expression of valosin-containing protein (p97) in hepatocellular carcinoma is correlated with increased incidence of tumor recurrence. *Journal of*

clinical oncology : official journal of the American Society of Clinical Oncology, 21**,** 447-52.

YAMAMOTO, S., TOMITA, Y., URUNO, T., HOSHIDA, Y., QIU, Y., IIZUKA, N., NAKAMICHI, I., MIYAUCHI, A. & AOZASA, K. 2005. Increased expression of valosin-containing protein (p97) is correlated with disease recurrence in follicular thyroid cancer. *Annals of surgical oncology,* 12**,** 925-34.

YAN, Z., DELANNOY, M., LING, C., DAEE, D., OSMAN, F., MUNIANDY, P. A., SHEN, X., OOSTRA, A. B., DU, H., STELTENPOOL, J., LIN, T., SCHUSTER, B., DECAILLET, C., STASIAK, A., STASIAK, A. Z., STONE, S., HOATLIN, M. E., SCHINDLER, D., WOODCOCK, C. L., JOENJE, H., SEN, R., DE WINTER, J. P., LI, L., SEIDMAN, M. M., WHITBY, M. C., MYUNG, K., CONSTANTINOU, A. & WANG, W. 2010. A histone-fold complex and FANCM form a conserved DNA-remodeling complex to maintain genome stability. *Molecular cell,* 37**,** 865-78.

YE, Y. 2006. Diverse functions with a common regulator: ubiquitin takes command of an AAA ATPase. *J. Struct. Biol.,* **156,** 29-40.

YE, Y., MEYER, H. H. & RAPOPORT, T. A. 2003. Function of the p97-Ufd1-Npl4 complex in retrotranslocation from the ER to the cytosol: dual recognition of nonubiquitinated polypeptide segments and polyubiquitin chains. *The Journal of cell biology,* 162**,** 71-84.

YEUNG, H. O., FORSTER, A., BEBEACUA, C., NIWA, H., EWENS, C., MCKEOWN, C., ZHANG, X. & FREEMONT, P. S. 2014. Inter-ring rotations of AAA ATPase p97 revealed by electron cryomicroscopy. *Open biology,* 4**,** 130142.

YEUNG, H. O., KLOPPSTECK, P., NIWA, H., ISAACSON, R. L., MATTHEWS, S., ZHANG, X. & FREEMONT, P. S. 2008. Insights into adaptor binding to the AAA protein p97. *Biochemical Society transactions,* 36**,** 62-7.

YOKOI, M., MASUTANI, C., MAEKAWA, T., SUGASAWA, K., OHKUMA, Y. & HANAOKA, F. 2000. The xeroderma pigmentosum group C protein complex XPC-HR23B plays an important role in the recruitment of transcription factor IIH to damaged DNA. *The Journal of biological chemistry,* 275**,** 9870-5.

YUAN, F., EL HOKAYEM, J., ZHOU, W. & ZHANG, Y. 2009. FANCI protein binds to DNA and interacts with FANCD2 to recognize branched structures. *The Journal of biological chemistry,* 284**,** 24443-52.

YUAN, J. & CHEN, J. 2013. FIGNL1-containing protein complex is required for efficient homologous recombination repair. *Proceedings of the National Academy of Sciences of the United States of America,* 110**,** 10640-5.

ZEMLA, A., THOMAS, Y., KEDZIORA, S., KNEBEL, A., WOOD, N. T., RABUT, G. & KURZ, T. 2013. CSN- and CAND1-dependent remodelling of the budding yeast SCF complex. *Nature communications,* 4**,** 1641.

ZHANG, J., ZHAO, D., WANG, H., LIN, C. J. & FEI, P. 2008. FANCD2 monoubiquitination provides a link between the HHR6 and FA-BRCA pathways. *Cell cycle,* 7**,** 407-13.

ZHANG, X., SHAW, A., BATES, P. A., NEWMAN, R. H., GOWEN, B., ORLOVA, E., GORMAN, M. A., KONDO, H., DOKURNO, P., LALLY, J., LEONARD, G., MEYER, H., VAN HEEL, M. & FREEMONT, P. S. 2000. Structure of the AAA ATPase p97. *Molecular cell,* 6**,** 1473-84.

ZHENG, J., YANG, X., HARRELL, J. M., RYZHIKOV, S., SHIM, E. H., LYKKE-ANDERSEN, K., WEI, N., SUN, H., KOBAYASHI, R. & ZHANG, H. 2002a. CAND1 binds to unneddylated CUL1 and regulates the formation of SCF ubiquitin E3 ligase complex. *Molecular cell,* 10**,** 1519-26.

ZHENG, N., SCHULMAN, B. A., SONG, L., MILLER, J. J., JEFFREY, P. D., WANG, P., CHU, C., KOEPP, D. M., ELLEDGE, S. J., PAGANO, M., CONAWAY, R. C., CONAWAY, J. W., HARPER, J. W. & PAVLETICH, N. P. 2002b. Structure of the Cul1-Rbx1-Skp1-F boxSkp2 SCF ubiquitin ligase complex. *Nature,* 416**,** 703-9.

ZHI, G., WILSON, J. B., CHEN, X., KRAUSE, D. S., XIAO, Y., JONES, N. J. & KUPFER, G. M. 2009. Fanconi anemia complementation group FANCD2 protein serine 331 phosphorylation is important for fanconi anemia pathway function and BRCA2 interaction. *Cancer research,* 69**,** 8775-83.

ZOU, L. & ELLEDGE, S. J. 2003. Sensing DNA damage through ATRIP recognition of RPA-ssDNA complexes. *Science,* 300**,** 1542-8.